CRANFIELD UNIVERSITY

Serhiy O. Korposh

DEVELOPMENT OF SENSITIVE ELEMENTS BASED ON PHOTOCHROMIC BACTERIORHODOPSIN FOR FIBRE OPTIC SENSORS

SCHOOL OF APPLIED SCIENCES

PhD THESIS

CRANFIELD UNIVERSITY

SCHOOL OF APPLIED SCIENCES

PhD THESIS

Academic Year 2006-2007

Serhiy O. Korposh

Development of sensitive elements based on photochromic bacteriorhodopsin for fibre optic sensors

Supervisor: Professor J.J. Ramsden

January 2007

This thesis is submitted in partial fulfilment of the requirements for the degree of Doctor of Philosophy

Abstract

This work focuses on the development of sensitive elements incorporating bacteriorhodopsin thin films for fibre optic sensors. The sensing principle is based on monitoring optical properties of the bacteriorhodopsin thin films during changes of environmental conditions.

The photochromic properties of the bR films change in response to the presence of different chemical species and this effect can be employed for the development of sensitive elements for optical sensors. For practical sensing applications, one can monitor changes (in the presence of chemical species) of the spectral and kinetic parameters of bR films incorporated into a matrix.

The main topic of this thesis is to study the possibility of using bacteriorhodopsin thin films for the construction of fibre-optic sensors for monitoring ammonia and humidity. The possibility to control sensitivity and selectivity of the sensor to the presence of ammonia and humidity by adding chemicals to the bR film and by employing different materials as a matrix for the creation of bR films is reported. The examples based on ammonia and relative humidity are used to show how using a broad range of different chemical additives bR can be sensitized to a wide spectrum of species, and thus possesses the potential to be a universal film material for optical sensors.

Acknowledgments

First of all I want to thank my wife, Lina, for her support, understanding and patience.

I would like also to express my gratitude to everyone who encouraged me in doing this work and let this work come to fruition. I would like to thank my supervisor Professor Jeremy Ramsden for his guidance through all my PhD research and for the opportunity created for me to do research in Japan. I want to say thank you to Dr. Y. P. Sharkan for his contribution into this work.

This all would not be possible if Professor Bill Batty did not make it happen. For that, I would like to thank him.

Contents

List of Figures

List of Tables

Notation

TIR	total internal reflection
c	speed of light in vacuum
v	speed of light in medium
θ_i	angle of incidence
θ_t	angle of refraction
θ_r	angle of reflection
n_1	refractive index of the incident medium
n_2	refractive index of the refractive medium
k_{i}	wave vectors of the incident wave
k_{t}	wave vectors of the refracted wave
k_{r}	wave vectors of the reflected wave
k_{ix}	projection of the wave vector onto X axis
k_{tx}	projection of the wave vector onto X axis
k_{rx}	projection of the wave vector onto X axis
R	reflectance
T	transmittance
θi_c	critical angle of incidence
θ_0	acceptance angle of the fibre
d	penetration depth of the evanescent wave into cladding
λ	wavelength of light
LD	lateral displacement
LD	laser diodes
LED	light emitting diode

FOS	fibre–optic sensors
IR	infrared spectral range
μm	micrometers (10^{-6} m)
CCD	charge–coupled device
AD	analogue–to–digital
S/N	signal–to–noise ratio
rH	relative humidity
nm	nanometre (10^{-9} meter)
ppm	part per million (10^{-6})
FWHM	full width half maximum
VOC	volatile organic compounds
α	light absorption coefficient of the sensitive element
NIR	near infrared
UV–Vis	ultraviolet visual spectral range
ppb	part per billion (10^{-9})
PCS	plastic cladded silica fibres
SPR	surface plasmon resonance
bR	bacteriorhodopsin
pm	purple membranes
GE	gelatin
PVA	polyvinyl alcohol
ΔA	absorbance changes
$\tau_{1/2}$	half–life
TEA	triethanolamine
DTMAB	dodecyltrimethyl ammonium bromide
FE-SEM	field emission scanning electron microscope

EDS	energy dispersive spectroscopy
AFM	atomic force microscope
BET	Brunauer– Emmet–Teller
BJH	Barret–Joyner–Halenda
SF	spectrophotometer
LS	probe light source
SH	sample holder
A	absorbance
S_λ	intensity transmitted through the sample at wavelength λ,
D_λ	dark intensity at wavelength λ
R_λ	reference intensity at wavelength λ
AL	actinic light source
PG	pressure gauges
L_1 and L_2	flow rates of the air passed through flask and carrier gas respectively
bR_{570}	ground state of the bR
M_{410}	excited state of the bR
S.R.	sensor response
pmf	purple membrane fragments
rpm	revolutions per minute
TEOS	tetraethoxysilane
TMOS	tetramethoxysilane
ΔA_{570}; ΔA_{410}	photo–induced absorbance changes of the bR at the wavelengths of 570 and 410 nm
LOD	limit of detection
t_{90}, t_{50}	response times

Introduction

Development of the chemical sensors able to operate in a continuous and reversible manner is an important requirement for many technological processes, as well as in medicine and ecological monitoring. Chemical sensors consist of a sensitive element and a transducer element. Almost all widely used chemical sensors are potentiometric and amperometric electrochemical devices. The measurement of electrochemical parameters, however, possesses several disadvantages such as the need for a reference electrode, limited time of operation and ambiguity of the indications. There are a number of laboratory based sensors techniques, such as chromatography and mass spectrometry, which are used with very high sensitivities for the detection of various environmental pollutants. The main disadvantages of these techniques are that they are expensive, need to use previously collected samples, are not portable and usually are time and energy consuming.

Development of fibre-optic sensors coated with selectively sensitive materials can overcome some of these disadvantages. Fibre-optic sensors are able to work in harsh environments, have immunity to strong electric and magnetic fields and create a number of possibilities for the design of different measurements systems.

The variety of different designs and measurement schemes of fibre-optic sensors provides the potential to create very sensitive and selective measurements techniques for the purpose of environmental monitoring. The key element of the fibre-optic sensors, in terms of selectivity and sensitivity, is the sensitive element. Current research in the field of optical fibre sensors is focused on the creation and development of new sensitive

elements which can expand the application area and increase the number and range of the analytes that can be measured by fibre-optic sensors.
The sensitive elements of fibre-optic sensors should be:

- transparent in the appropriate spectral range;
- change their optical properties under the influence of specific chemical species;
- fast in response and have wide dynamic range;
- reversible;
- selective;
- easy to immobilize onto glass/quartz/ plastic fibre;
- easily and cheaply manufactured.

The development and creation of the reactive materials characterized by high sensitivity and selectivity towards specific chemical species such as pollutants is a task of current importance.

The photochromic material - bacteriorhodopsin (bR) due to its ability to change photochromic optical properties as a response to the presence of chemical species and stimuli in the environment, will be considered in detail to demonstrate the possibility of employing it to provide a universal sensitive element for chemical optical sensors.

Chapter 1: Sensitive elements for fibre-optic sensors

This chapter will focus on the basic principles of the light propagation in a medium with high optical density embedded inside a less optically dense medium. The basic theory of the functioning and application of optical fibres is introduced. The principle of operation of fibre-optic sensors, their classification, advantages and recent achievements in the sensor technology are presented in this chapter. Examples of the extrinsic and intrinsic fibre-optic sensors and sensitive elements used to achieve a higher sensitivity and selectivity are given. The photochromic material bacteriorhodopsin is introduced and its structure, function, general and sensor based applications are analyzed in this chapter.

1.1 Theory of the fibre-optic sensors

1.1.1 Light propagation

Optical chemical measurements are well established nowadays. Using the light guiding properties of optical fibres can help to create optical sensor systems which will benefit from the advantages possessed by optical fibres such as geometric flexibility, electrical passiveness, environmental stability and well developed mass production.

The principle of light guiding in an optical fibre uses the property of total internal reflection (TIR); a process which can be explained from Snell's law.

Light incident at the interface between two slabs of dielectric material with different refractive indices will be partly reflected and partly transmitted as shown in Figure 1.1. This behaviour is controlled by the difference in the refractive indices of the two dielectric slabs. Refractive index is the ratio of the speed of light in a vacuum to the speed of light through the material:

$$n = \frac{c}{v}, \tag{1.1}$$

where c, speed of light in vacuum and v, speed of light in medium.

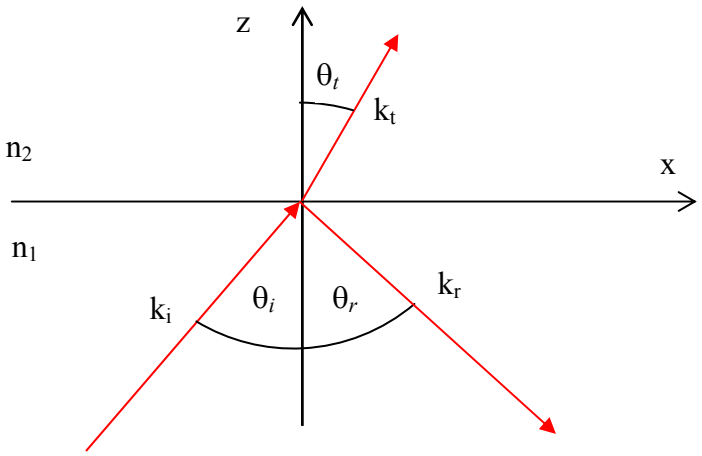

Figure 1.1: Reflection and refraction (transmission) at the interface of two dielectric media. θ_i, angle of incidence; θ_t, angle of refraction; θ_r, angle of reflection; n_1, refractive index of the incident medium; n_2, refractive index of the refractive medium; k_i, k_t, k_r, wave vectors of the incident, refracted and reflected wave respectively.

Light can behave as a particle and as a wave. To describe the nature of light it is necessary to use both the particle and wave theories of the propagation of electromagnetic radiation. Considering the electromagnetic nature of light, wave motion in a medium can be represented by Maxwell's equations of the electromagnetic field [1]. Taking into account boundary conditions:

$$k_{ix} = k_{tx} = k_{rx}$$
$$k_i \sin\theta_i = k_t \sin\theta_t = k_r \sin\theta_r \; k_i \,, \qquad (1.2)$$
$$k_i = (\frac{\omega}{c})n_1; k_t = (\frac{\omega}{c})n_2; k_r = (\frac{\omega}{c})n_1$$

where k_{ix}, k_{tx}, k_{rx} is the projection of the wave vector onto X axis; θ_i, angle of incidents; θ_t, angle of refraction, θ_r, angle of reflection; n_1, refractive index of the incident

medium; n_2, refractive index of the refractive medium; k_i, k_t, k_r, wave vectors of the incident, refracted (transmitted) and reflected light respectively.

This Equation 1.2 leads to *Snell's law* (Equation 1.3), formulated in the 17th century, which relates the sines of the angles of incidence and refraction at the interface between two optical media to the indexes of refraction of the two media. The mathematical expression of Snell's law is given by:

$$\sin\theta_i \cdot n_1 = \sin\theta_r \cdot n_2, \tag{1.3}$$

were θ_i, the angle of incidence; θ_r, the angle of refraction; n_1, refractive index of the incident medium; n_2, refractive index of the refractive medium.

The amplitudes of the reflected and refracted beams are described by Fresnel's equations and because the electromagnetic waves are transverse, there are separate coefficients in the directions perpendicular to and parallel to the surface of the dielectric [1]. In case of normal incidence of light (i.e. $\theta_i=90^o$) the reflection and transmission amplitude coefficients coincide for each of transverse electric (TE) and transverse magnetic (TM) radiation, giving:

$$R = \left(\frac{n_2 - n_1}{n_2 + n_1}\right)^2 \tag{1.4}$$

$$T = \frac{4n^2{}_1}{(n_2 + n_1)^2}, \tag{1.5}$$

where R and T are known as the reflectance and transmittance, respectively.

When light is propagated through a medium with a high optical density (refractive index n_1) to the boundary with a medium with a lower optical density (refractive index n_2) (i.e. $n_1 > n_2$) the light will be totally reflected at the interface between two media if the angle of incidence of the light θ_i is greater than some critical angle θi_c (Figure 1.2).

Ray 4 in Figure 1.2 is incident on the interface at an angle greater than the critical angle, and is totally reflected into the same medium from which it was propagated. Ray 4 obeys the law of reflection so that its angle of reflection is exactly equal to its angle of incidence.

This phenomenon of total internal reflection is exploited when designing light propagation in fibres by trapping the light in the fibre through successive internal reflections along the length of the fibre.

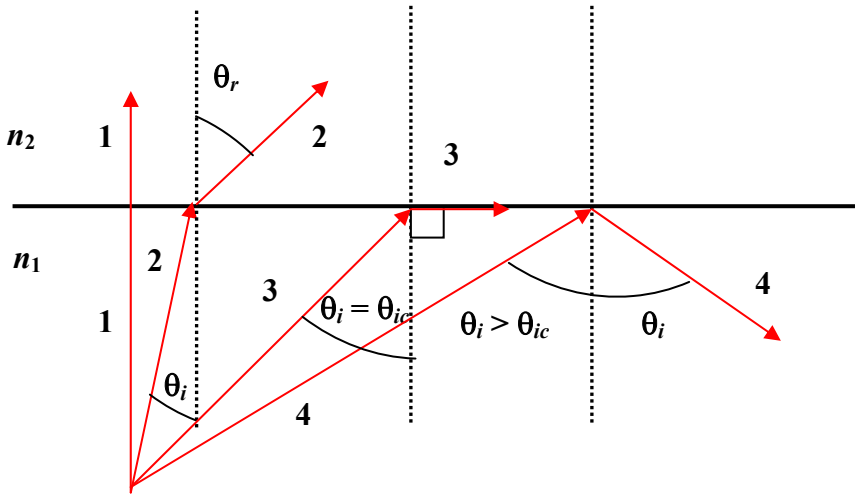

Figure 1.2: Critical angle and total internal reflection.

In Figure 1.2 total internal reflection (TIR) occurs if $\theta_i > \theta i_c$, or sin $\theta_i > n_2/n_1$. Using Snell's Equation 1.3 and referring to the ray 3 (Figure 1.2) the critical angle of incidence can be calculated:

$$n_1 \cdot \sin\theta_{ic} = n_2 \cdot \sin 90^0 , \tag{1.6}$$

where n_1, is the refractive index for the incident medium; θi_c, is the critical angle of incidence; n_2, is the refractive index for the medium of lower index; and $\theta_r = 90^o$, is the angle of refraction at the critical angle.

Then, since $\sin 90^o = 1$, the critical angle is obtained as:

$$\theta_{ic} = \sin^{-1}(\frac{n_2}{n_1}) , \tag{1.7}$$

where n_1, is the index for the incident medium; n_2, is the index for the medium of lower index; θi_c is the critical angle of incidence.

1.1.2 Optical fibre

An optical fibre is a cylindrical waveguide which consists of a core with refractive index n_1 surrounded by cladding with a lower refractive index n_2 and it propagates light along its axis using the TIR process (Figure 1.3). An optical fibre will guide only light which is incident on the cross-sectional face of the clad optical fibre within an acceptance cone which is described by acceptance angle of the fibre, θ_0 (Figure 1.3). It is also the minimum angle at which total internal reflection will occur and often is reported as a numerical aperture.

In order to calculate the acceptance angle θ_0 of the optical fibre with refractive index of core n_1, and refractive index of cladding n_2, Snell's law can be used in terms of the geometry shown in the Figure 1.2.

From Snell's law:

$$\sin\theta_c = \frac{\sin\theta_0}{n_1}, \tag{1.8}$$

since angles $\theta_c + \theta_i = 90^o$, the condition of total internal reflection is:

$$\sin\theta_0 < \sqrt{n^2{}_1 - n^2{}_2} \tag{1.9}$$

If the relative difference between the refractive indexes n_1 and n_2, defined as $\Delta = (n_1\text{-}n_2)/n_1$, is small, then Equation 1.9 can be written

$$\sin\theta_0 < \sqrt{(n_1 - n_2)(n_1 + n_2)} \tag{1.10}$$

since $n_1 \approx n_2$ Equation 1.8 can be written:

$$\sin\theta_0 < n_1\sqrt{2\Delta} \tag{1.11}$$

From Equation 1.6 the numerical aperture of the fibre is:

$$N.A. = \sin\theta_0 < \sqrt{(n^2{}_1 - n^2{}_2)} = n_1\sqrt{2\Delta} \tag{1.12}$$

The numerical aperture indicates that any light ray incident on the fibre face within the acceptance angle will undergo total internal reflection at the core-cladding face and remain confined in the fibre as it propagates along it.

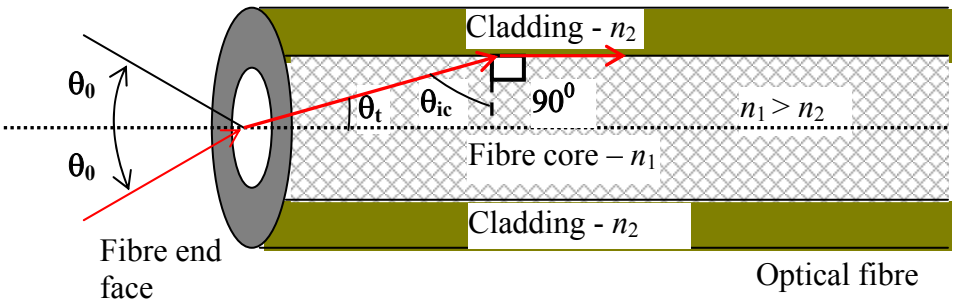

Figure 1.3: Acceptance angle of the clad optical fibre; n_1, the refractive index of the core; n_2, the refractive index of the cladding; θ_{ic}, critical angle; θ_0, acceptance angle.

In spite of TIR at the core-cladding interface some part of the light penetrates the cladding for a very short distance and so propagates in the cladding (Figure 1.4). This thin penetration of light into the cladding is called an *evanescent wave*. The amplitude of the evanescent wave exponentially decays in the Z direction (Figure 1.4). The energy flow of this evanescent wave is parallel to the surface of the core and propagates in the same direction as the main flow of energy within the core. The penetration depth of the evanescent wave into cladding is given by Equation 1.13.

$$d = \frac{\lambda}{2\pi\sqrt{n^2{}_1 \sin^2 \alpha - n^2{}_2}} \quad , \tag{1.13}$$

where n_1, refractive index of the core; n_2, refractive index of the cladding; α, incident angle; λ, wavelength of light.

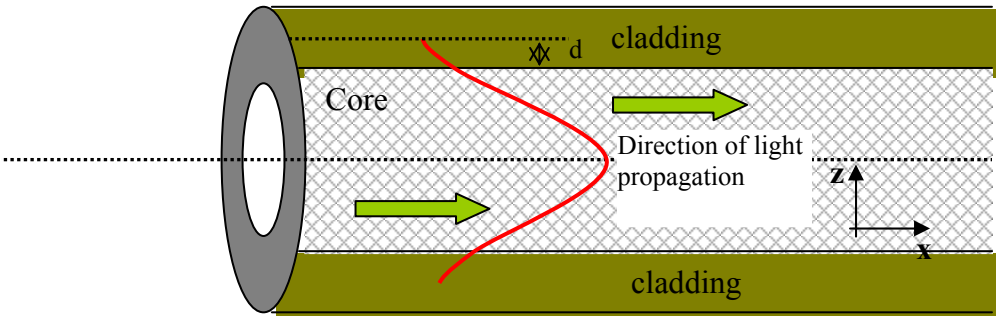

Figure 1.4: Propagation of evanescent wave in optical fibre; *d*, penetration depth.

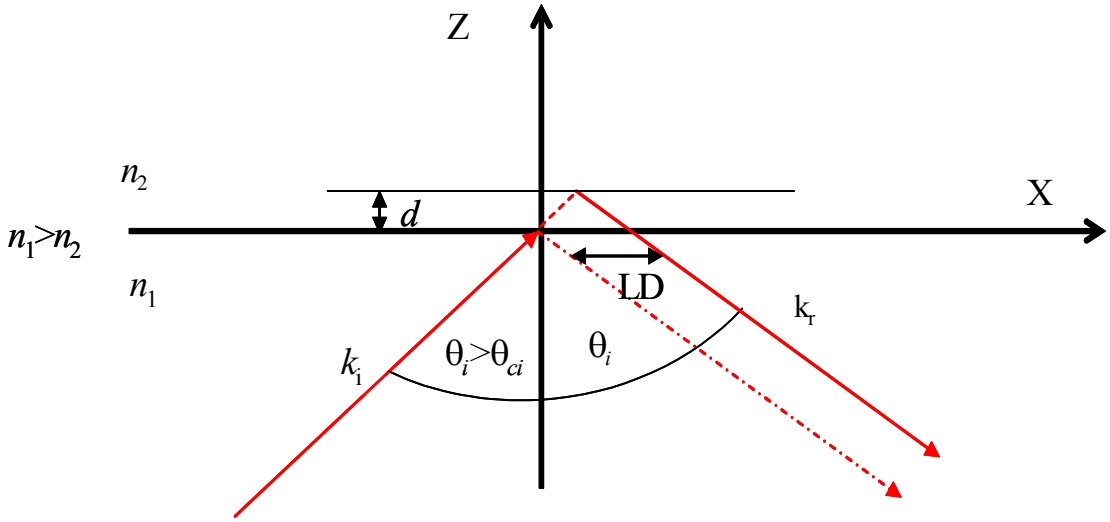

Figure 1.5: Lateral displacement of the totally reflected beam; *LD*, lateral displacement; *d*, penetration depth; n_1, refractive index of the incident medium; n_2, refractive index of the refractive medium; k_i, k_r, wave vectors of the incident and reflected waves respectively.

Along with the penetration of the light into the medium with lower refractive index the totally reflected beam experiences the lateral displacement (Figure 1.5). The phase of the reflected beam will be shifted with the respect to the phase of the incident beam (Equation 1.14) [1].

$$Z_s = (\frac{\lambda}{\pi \cdot n_1 \cdot \theta_z}) \cdot \sqrt{\frac{1}{\theta_a^2 - \theta_z^2}} \quad , \tag{1.14}$$

Where, n_1, the refractive index of the incident medium; λ, light wavelength in vacuum; $\theta_z = \pi/2 - \theta_i$; $\theta_a = \pi/2 - \theta_r$; θ_i, angle of incidence; θ_r, angle of refraction.

The phase shift Z_s in axial position is called a Goos-Haenchen shift; and makes the distance travelled by ray in propagating a distance *l* along the fibre shorter than it would be without the shift. The shift is very small unless the ray angle is close to the critical angle, in this case the evanescent wave penetrates very far into the cladding [1].

1.1.3 Modes in optical fibre

When ray theory (geometrical optics) is applied for the description of light propagation in an optical fibre it appears that any ray at the angle greater than the critical angle θ_{ic} will be guided. However, when the core radius of the optical fibre (or the quantity of Δ) becomes very small the ray theory based on geometrical optics is no longer valid and wave theory based on the Maxwell's equation should be applied [1], Figure 1.6. The electrical component of the monochromatic wave propagating in the *Z* direction can be express mathematically as:

$$E = E_0 \times \exp(-i \cdot \beta \cdot z), \tag{1.15}$$

where, E_0, amplitude of the electrical field; β, is the z component of the wave propagation constant $k=2\pi/\lambda$;

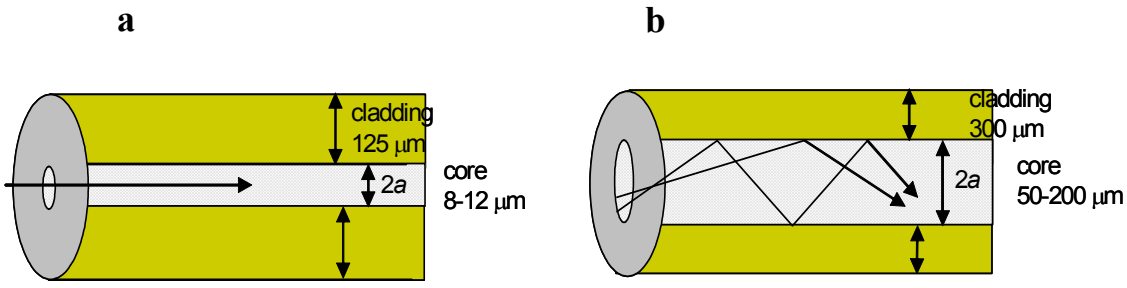

Figure 1.6: Types of optical fibre; a, single mode optical fibre; b, multimode optical fibre.

A mode is a spatial distribution of optical energy in one or more dimensions. For guided modes, β in Eq. 1.15 can assume only discrete values.

In wave theory by solving the Maxwell's equations subject to the boundary conditions at the interface between the core and the cladding the waveguide parameter (V) can be introduced:

$$V = \frac{2\pi}{\lambda} a \sqrt{n_1^2 - n_2^2}\,, \tag{1.16}$$

where, n_1, refractive index of the core; n_2, refractive index of the cladding; a, radius of the core; λ, wavelength of light.

The number of modes that can be supported in the optical fibre, depends on the: refractive indices Δ, core radius a, and on the wavelength λ.
It can be shown [1], that if V<2.4045, only one guided mode is possible and the fibre will be a *singlemode fibre*.

The order of the mode is equal to the number of the field zero across the optical fibre, Figure 1.7.

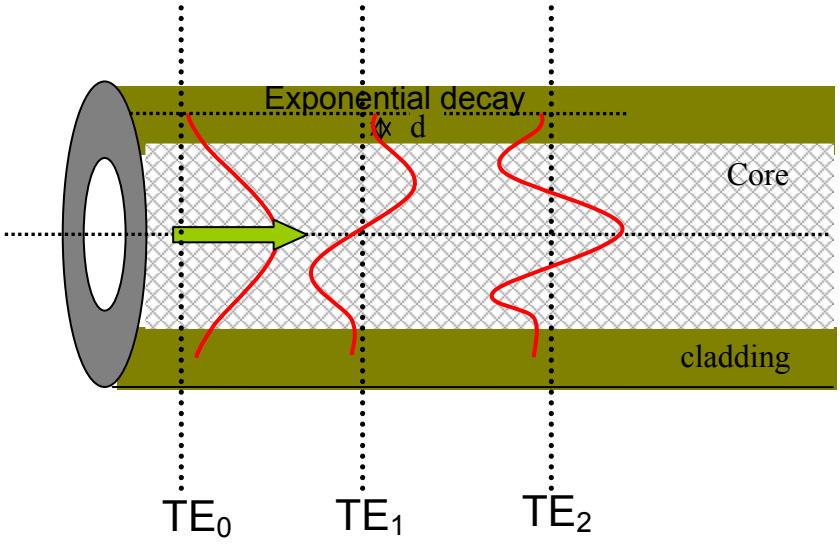

Figure 1.7: Number of modes; TE_0, fundamental mode; TE_1, first mode.

In addition to the guided modes the radiation modes (not trapped in the core), cladding modes (trapped in the cladding), and leaky (tunneling) modes (partly trapped in the core) exist in the optical fibre.

Single mode fibre is used for telecommunication purposes when low signal loss and high data bandwidth are required, because it does not suffer from modal dispersion in contrast to the multimode optical fibres. Modal dispersion is defined as the spreading of a pulse due to the time delay between lower-order modes and higher-order modes). The applications of singlemode and multimode fibres for sensor will be discussed in section 1.1.4.2.

1.1.4 Fibre optic sensors

Optical sensors detect the change of the optical parameters (refractive index, absorbance reflectance, fluorescence, etc.) of the measured medium, which usually depend on physicochemical parameters (chemical composition, temperature, etc.) of the investigated environment. By monitoring the interaction of light with a measured medium it is possible to detect and control the physicochemical parameters. In terms of practical application this is a very convenient method for creating optical sensors for remote monitoring using optical fibres. Fibre optic sensors possess several advantages over conventional sensor techniques [2–4]:

- they are not subject of the electromagnetic interference;
- no reference electrode is needed;
- they can offer a significant cost effectiveness;
- because optical fibres are made of glass they can survive harsh environment, tolerate high temperature and are biocompatible, which creates a possibility to use them within the human body;
- they can monitor a number of analytes using a several immobilized sensitive elements;
- they can be used for remote monitoring of the environment because of low-loss of signal that is property of light propagation in optical fibres.

A general scheme for the application of fibre-optic sensors is shown in the Figure 1.6 and consists of a light source coupled to the optical fibre which is used to guide light to and/or from the measurement zone, sensitive element or transducer, which provides the conversion of chemical

recognition step into an optical signal, photodetector and electronic systems used to display and process data into a human-interpretable form.

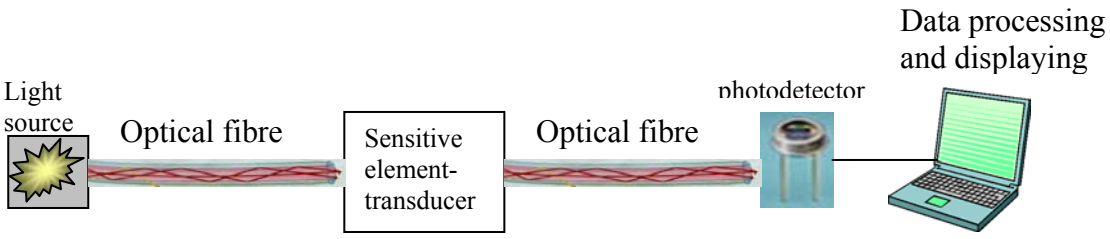

Figure 1.8: General scheme of the fibre-optic sensor.

1.1.4.1 Light sources

Choosing a proper light source suitable to the needs of optical sensing is a very important factor in the design of the effective optical chemical sensor systems. The general issues that should be considered include the wavelength of operation, stability, intensity, power consumption and lifetime of the desired system. The spectral output of the light source should be appropriate to wavelengths where the sensitive element has the maximal optical response. In general the light sources can be classified into the following groups: incandescent lamps, discharge lamp, lasers and semiconductor sources. All of these light sources have their own advantages and disadvantages and all are relatively successful when used for optical chemical sensors. The semiconductor sources which include laser diodes (LD) and light emitting diodes (LEDs) are attracting the most attention for fibre-optic sensors (FOS) applications because of their robustness, low power consumption, high stability and ability to cover almost all of the visible and IR spectral range [5].

1.1.4.2 Optical fibres

Recent developments in the field of telecommunication have led to the improvement and development in optical fibre technology. Depending on the sensing scheme requirements, one now can choose a variety of different optical fibres, from all-silica fibres used for visible and near-IR spectral range to fibres made from different glasses (fluoride glasses 0.5–5 μm, chalcogenide 1–6 μm and silver halide polycrystalline materials 3–15 μm) that are transparent in near-IR and mid-IR ranges and are suitable for application for direct spectroscopic absorption. Multimode optical fibres should be used if high intensity light is required and single mode optical fibres are used mostly for the interferometric sensors where phase change is measured.

1.1.4.3 Detectors

Depending on the spectral range required for the sensing element, a variety of different photo detectors are available. Silicon photodiodes are suitable in the visible spectral range and are low-cost detectors widely used in the intensity modulated measurements. For the IR spectral region the following are available for application as fibre optic sensing elements: pyro-electric detectors, PbS detectors in the 2 μm region, PbSe 3–5 μm, InSb detectors in the 5–7 μm region and HgCdTe detectors in the 5–14 μm region [5]. If very high gains are required, an avalanche photodiode can be used in conjunction with these sensing elements. The charge-coupled device (CCD) has largely become the type of detector used for FOS especially where spectral information is required. CCD detectors are naturally

integrating and therefore have an extensive dynamic range, only limited by the thermal current and the speed of the analogue-to-digital (AD) converter. The main advantages of CCD detectors are high number of pixels, high sensitivity and high speed. The main disadvantage is the lower signal-to–noise (S/N) ratio.

1.1.4.4 Data processing

Data processing can involve any electronic device that acquires information from the detector for further amplification, processing and displaying data as information in a form suitable for human understanding.

1.1.5 Fibre-optic sensor classification

There is no uniform approach for the classification of the FOS and nowadays with the current rapid progress in development it is almost impossible, even simply, to catalogue the range of the FOS systems [5]. Some authors [6, 7] classify FOS according to the modulation principle that is used, and thus intensity, wavelength, polarization, phase change or rate were used to distinguish the differences between different FOS. MacCraith [5] classified fibre-optic chemical sensors into two categories: direct spectroscopic sensors where the fibre acts as a simple light-guide and reagent-mediated sensors (optrodes), in which the specific chemistry is combined with the optical fibre. However, the most generally accepted method of classification of fibre-optic sensors is to group them into: intrinsic and extrinsic fibre-optic sensors [5].

Extrinsic fibre-optic sensors use the optical fibre to guide incoming and outgoing light to and from the site of measurement zone and their main

characteristic is that sensing takes place outside the fibre. In the intrinsic fibre-optic sensors the light is modulated inside the optical fibre by some environmentally induced interaction; the fibre serves as a sensitive element and sensing takes place in the optical fibre itself.
All of these fibre-optic sensors can be used for measurements of both physical and chemical parameters of the environment.

1.1.5.1 Extrinsic fibre-optic sensors

In this technique the probe light from the light source travels along an optical fibre to the reactive distal end of the optical fibre and reflected [8–10], scattered [11, 12], transmitted [13] or emitted light is detected by a photo detector either using second fibre (Figure 1.9) or by splitting the original fibre (Figure 1.10) [2, 8]. Extrinsic fibre-optic sensors have been used for measurements of the concentration of chemical species in the general environment [14, 15], pressure [10], temperature [10, 16], humidity [17] and refractive index [18].

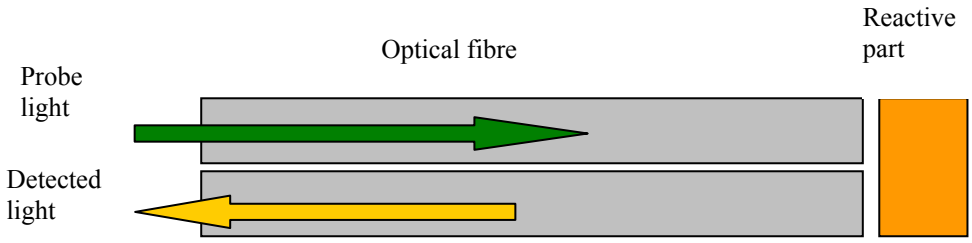

Figure 1.9: Extrinsic fibre-optic sensor with two optical fibres.

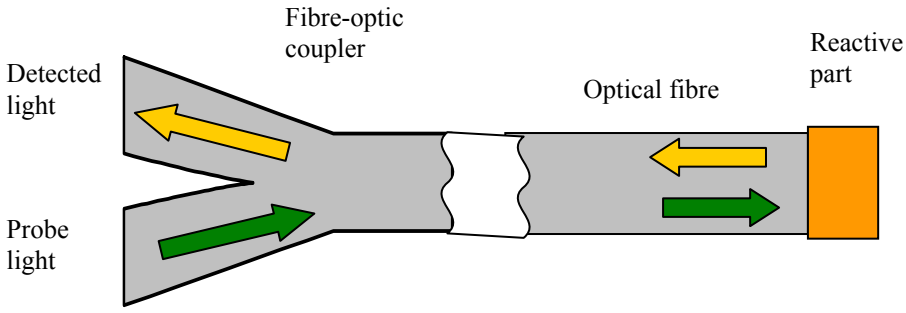

Figure 1.10: Extrinsic fibre-optic sensor with splitting of original optical fibre [5].

To achieve a selective optical response to a particular chemical component the appropriate wavelength source is chosen to that wavelength which is absorbed by this given chemical analyte [19, 20]. Alternatively, a selectively sensitive element [21, 22] is used that changes its optical properties under the influence induced by an introduced chemical species. Many different materials both of organic and inorganic origin have been used as sensitive elements of fibre-optic sensors to detect a range of different analytes.

For example, many different materials have been suggested as sensitive elements for the detection of ammonia vapours [13, 23–27]. Polyanilin has been proposed for the remote detection of gaseous ammonia using the change of the near infrared transmission behaviour of the polyanilin film when exposed to different concentrations of ammonia [13, 23]. Transmission of polyaniline films at 1300 nm changed by approximately 1% in response to gaseous ammonia levels rising from 0 to 6 ppm in an atmosphere with 50% relative humidity (rH) [13]. Sensors based on colour change induced in some dyes by ammonia vapour have been used for the creation of sensitive elements for fibre-optic sensors [24–26]. Cyanine dye

immobilized in a microporous glass thin film showed reversible ammonia sensitivity in the 5–100 ppm range in a period of less than 2 min [26]. Bromocresol Purple incorporated into thermoplastic polyurethane "Tecoflex", was used for monitoring of ammonia in the range from 0.03 to 1% observing a maximum variation of 6 dB at 600 nm [27]. A fluorescent fibre optic senor was constructed with hydroxypyrenetrisulfonic acid (HPTS) incorporated into inorganic sol-gel matrix. Using different coatings allowed pH, NH_3 and CO_2 to be monitored [28].

Fibre-optic ammonia sensors have been fabricated using electrochromic polymers where the light absorbance measured at 430 nm decreases with exposure to increasing ammonia concentration (0–100 ppm). Its working humidity range was from 50 up to 100% rH. However, reversibility of the proposed electrochromic polymer could not be achieved even by flushing the film with the dry air or HCl [29].

One of the most popular design schemes of the fibre-optic sensors is the so called "optrode", which uses the optical fibre distal end coated with a sensitive material or placed in contact with some reagent that serves as a sensitive element [9, 30] (Figure 1.11).

An example of the "optrode" is the reflectance fibre-optic sensors. Sensors of this type employ a thin film of zirconia (ZrO2) and poly(sodium-4-styrenesulfonate) salt deposited on the cleaved end of the standard telecom fibre using the electrostatic self-assembly method developed for ammonia detection (Figure 1.11) [9]. The principle of operation of the given sensor is based on the formation of a Fabry-Perot finesse on the cleaved end of the optical fibre and on the dependence of reflectance on the optical and geometric properties of the sensitive element. Finesse is defined as the ratio of free spectral range of the interferometer or etalon, to the full width at half maximum (FWHM) which is the width of the transmission peak at its

50% point. The periodic oscillations are due to an interferometric cavity formed by gradually increasing thickness at the end of the cleaved optical fibre (Figure 1.11).

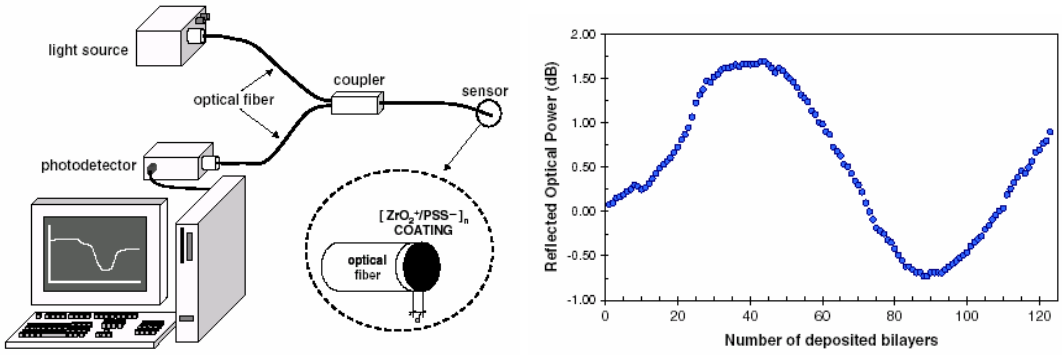

Figure 1.11: Experimental set-up and reflected optical power monitored when the $[ZrO^{+}_{2}/PSS^{-}]n$ coating is deposited on a standard multimode fibre [9].

Using Equation 1.17 which expresses the optical round-trip phase shift, Φ, it is possible to calculate the approximate thickness of the layers:

$$\phi = \frac{4\pi \cdot n \cdot d}{\lambda} \tag{1.17}$$

where n, refractive index of the coating at an optical wavelength of λ; and d, the total thickness of the coating.

The optimum structure for the sensitive element was a $[ZrO^{+}_{2}/PSS^{-}]_{10}$ that exhibited only 4% of cross-sensitivity to volatile organic compounds such as ethanol, acetone, dichloromethane with a recovery time less than 4 s and able to work at room temperature [9]. In addition, the sensitivity to humidity and temperature, in the 10–85% rH and 10–50 ^{o}C range respectively, was less than 2% [9].

A reflectance fibre-optic sensor based on a similar principle of operation (Figure 1.12) and using a film of syndiotactic polystyrene (sPS) in the nanoporous crystalline δ form has been used for the detection of chloroform in the vapour phase at partial pressures of between 0.2 and 5 Torr and for the measurements of the concentration of chloroform and toluene in water. The sensitivity of the proposed sensitive coating is very high but the selectivity is low and limited by host-guest interactions and by the size and shape of the detected molecule [31].

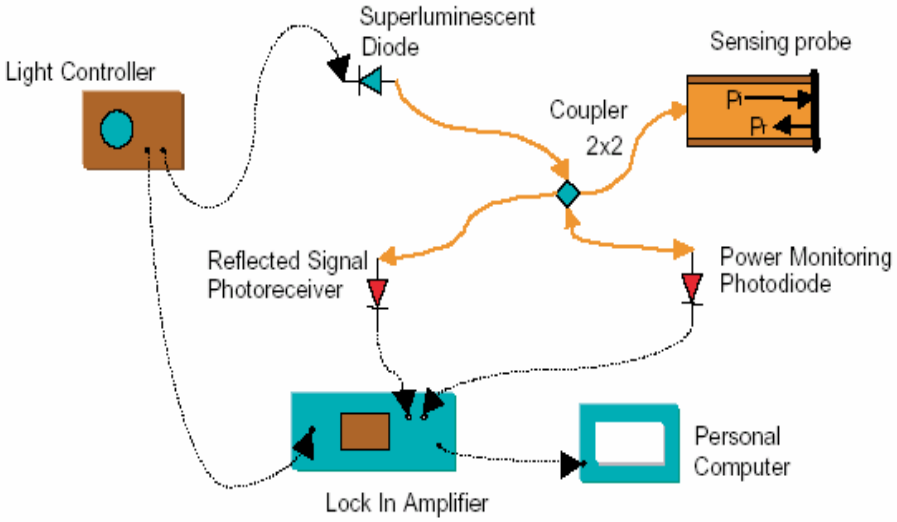

Figure 1.12: Optoelectronic set-up [31].

A Langmuir-Blodgett thin film of single-walled carbon nanotubes (SWCNTs) was used as a sensitive element for a single-mode fibre-optic sensor for measurement of volatile organic compounds [32].

Fibre-optic sensors can be used for luminescence measurements.

Polycyclic aromatic compounds present in commercially available epoxy glue were used as a temperature indicator in fibre-optic sensors. The monitoring of the change of the fluorescence intensity when the film was

exposed to a range of temperature from 25 ^{o}C up to 110 ^{o}C was used in this fibre-optic sensor [33].

Another type of luminescence fibre-optic sensor for detection of the calcium ions was developed by immobilization of calcium derivatives calcein acrylamide (CA) onto an optical fibre. The fluorescence of CA is pH-sensitive in the region pH 4–12 and also increases as a function of Ca^{2+} concentration at pH – 12 [34].

An inorganic palladium 10 nm thick film deposited onto glass substrate was used to detect the concentration of hydrogen with a detection limit of 500 ppm and corresponding response time of 130 s, while at 4% hydrogen concentrations the response time was 5 s at ambient temperatures [35].

It would be possible to measure simultaneously multiple pollutant parameters within the environment by bundling together optical fibres coated with different sensitive elements. An example of such sensor system would be an intensity type fibre-optic sensor which uses three different sensitive elements deposited onto an individual optical fibre for monitoring temperature, pH and concentration of calcium ions in the drinking water [36].

A VOC fibre-optic sensor has been developed that uses a vapochromic material which changes its colour when exposed to methanol and ethanol. The time responses of the sensor are different for methanol and ethanol and so the separate detection of these vapours is possible [37].

1.1.5.2 Intrinsic fibre-optic sensors

Intrinsic FOS use the fibre itself as a transducer; the behaviour of the light inside the fibre is modulated by some external effect. Different approaches exist for creation of intrinsic FOS, e.g. using the Bragg Gratings written

into the fibre core. By measuring the changes in the reflected light due to changes in the grating period it is possible to detect the effect caused by an external stimulus [38, 39]. Interferometric sensors can be made that use some external effect to cause a change in the optical path way or a phase difference in the interferometer caused by some external effect. All traditional interferometers such as Michelson, Mach Zehnder [40–43], Fizeau, Sagnac [44–47] and Fabry Perot [48–50] used for measuring of both chemical and physical parameters can be constructed utilizing optical fibres. The other type of intrinsic fibre-optic sensors is based on the evanescent wave absorption effect [51]. Employing different sensitive elements deposited onto the side of single-mode [52–54] and multimode [54] optical fibres allows the creation of an FOS with high sensitivity and selectivity.

The basic scheme of an intrinsic fibre-optic sensor based on evanescent waver absorption is shown on Figure 1.13.

Depending on the target analytes, a variety of different sensitive elements have been deposited on the side of an optical fibre.

For the creation of a pH sensor a porous silica film prepared by the sol-gel procedure was used as a sensitive element. The properties of the silica surface depend on the pH of the solution and the achieved sensitivity of the sensor was up to 0.66 dB/pH for the pH range of 7–10.5 [55].

Using a sol-gel film doped with a dye (e.g. coumarin, brilliant green, rhodamine 6G, and rhodamine B) [56–58] the dynamic range of the pH measurement can be increased to cover pH values from 2 up to 12. The sensor sensitivity was increased by decreasing the probe light wavelength, with the highest sensitivity being achieved at 400 nm [56].

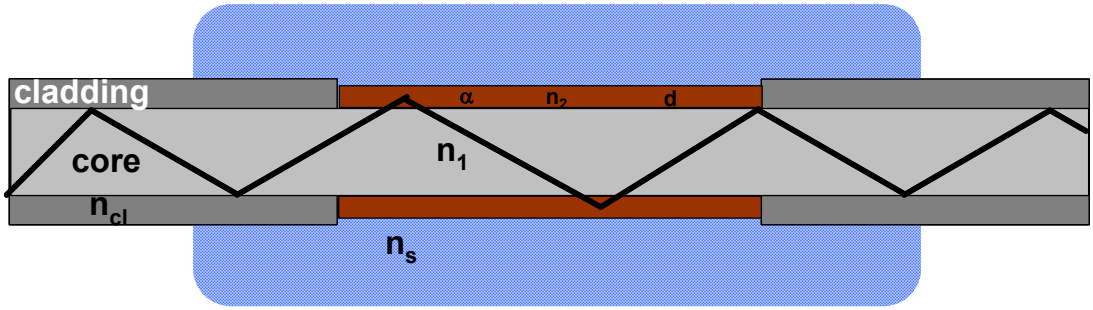

Figure 1.13: Basic scheme of the intrinsic FOS based on the evanescent wave absorption. n_1, refractive index of the core; n_{cl}, cladding refractive index; n_s, refractive index of the medium surrounded the optical fibre; n_2, refractive index of the sensitive element; d, thickness of the sensitive element; α, light absorption coefficient of the sensitive element.

A sensor element doped with polypyrrole was used as a sensitive element for nerve agent detection; using a 1,5 naphthalene disulphonic acid (NDSA) –doped polypyrrole coating produced by the *in situ* deposition technique a sensitivity of up to 26 ppm with a response time of a few seconds was achieved. Utilizing different deposition techniques and using different doping materials has produced fibre-optic sensors with different sensitivities and performances [59].

The transparency of an optical fibre depends on the fibre material and the wavelength of the probe light. Thus different fibres are appropriate for different spectral ranges; for the near infrared spectra (NIR) the chalcogenide [60, 61], for Mid-IR the silver halide [62, 63], and for the UV-Vis quartz [64] or plastic optical fibres [65] can be selected.

Chalcogenide glass fibres were used to perform remote infrared analysis of non-polar organic species in aqueous solution. This technique permits the observation of disruption induced in living mammalian cells by at least two different types of toxins and it is possible to distinguish between the effect

of a genotoxic agent (which damages nucleic acids) and a cytotoxic agent (which damages other cellular components) based on the cell's response to IR light [60].

For the detection of chemical species with very low concentration in water, chalcogenide fibres which had special chemical treatment were applied for evanescent wave absorption spectroscopy [61].

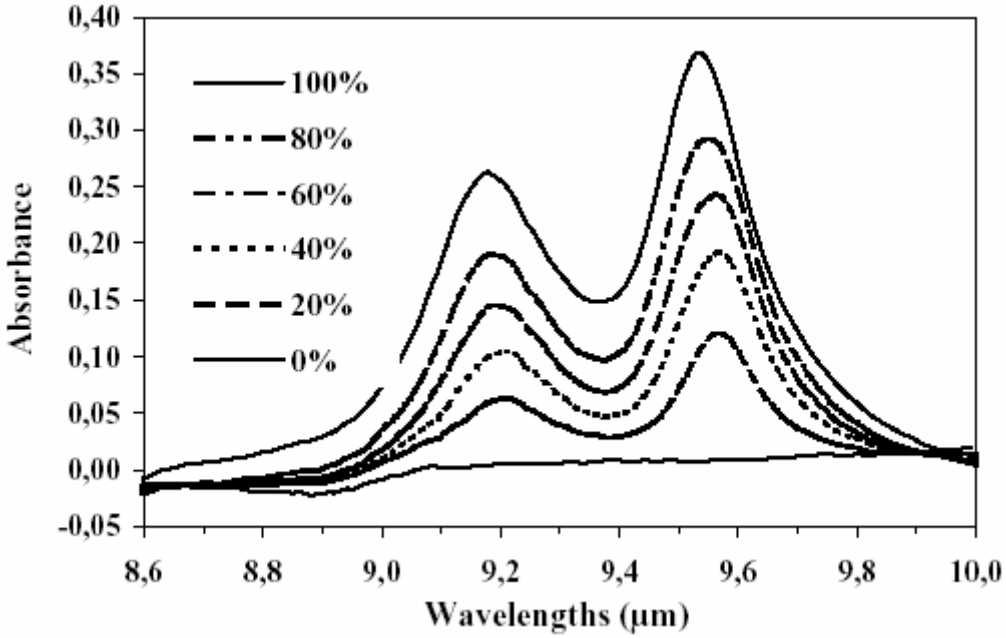

Figure 1.14: Absorbance spectrum of the different concentration of ethanol in water measured in the infrared spectral range 8.6–10 μm [61].

The concentration of chloroform and ethanol in water were measured using the variations of their absorbance in the infrared spectral range 8.6–10 μm (Figure 1.14). The lower limit of detection for ethanol concentration in water was approximately 0.5%, when the length of the sensing zone (removed cladding) was 3 cm [61].

A fibre-optic sensor consisting of a silver halide ($AgBr_xCl_{1-x}$) optical fibre coated with polyisobutylene (PIB) or Teflon was developed for the *in situ* monitoring of pesticides and chlorinated hydrocarbons in water for the spectral range 8.5–12 μm [62]. The sensitivity of this FOS was in the region of 100 ppb but it could be enhanced by increasing the interaction of the evanescent field with the investigated medium.

A mid-IR grating spectrometer operating in the wavelength range 8–12.5 μm was developed for the detection of chlorinated hydrocarbons with a detection limit of 900 ppb for tetrachloroethylene. The sensor was based on the detection of the characteristic absorption of chlorinated hydrocarbons in the polymer membrane coated onto the sensor silver halide fibre and the effects of the samples on the evanescent field of the guided light [63].

The most suitable fibres in the visual spectral range for the creation of intrinsic FOS based on the generation of an evanescent wave are the plastic cladded silica fibres (PCS); because the plastic cladding can be easily removed by mechanical stripping or by means of chemical etching. This FOS coated with an appropriate sensitive material could be used for the detection of chemical parameters and species [66–68].

The silica-silica type optical fibres have been used for the creation of high sensitivity refractive index sensors based on surface plasmon resonance [69–73].

Surface plasmon resonance (SPR) is a technique used for optical sensing. A surface plasmon is a wave which travels in a thin metal film when the film is excited by optical light, e.g. a photon is transformed into a surface plasmon. The changes induced in the SPR signals are proportional to the refractive index of the medium close to the sensor surface and so the signals are related to the amount and type of macromolecules bound to the

sensor surface. A SPR sensor used for the remote detection of gases was developed by deposition a 50 nm thick silver film by thermal evaporation onto the silica core of the optical fibre Figure 1.15 [69]. Self-assembled monolayers of long-chain alkanethiols were used in order to protect the silver from oxidation.

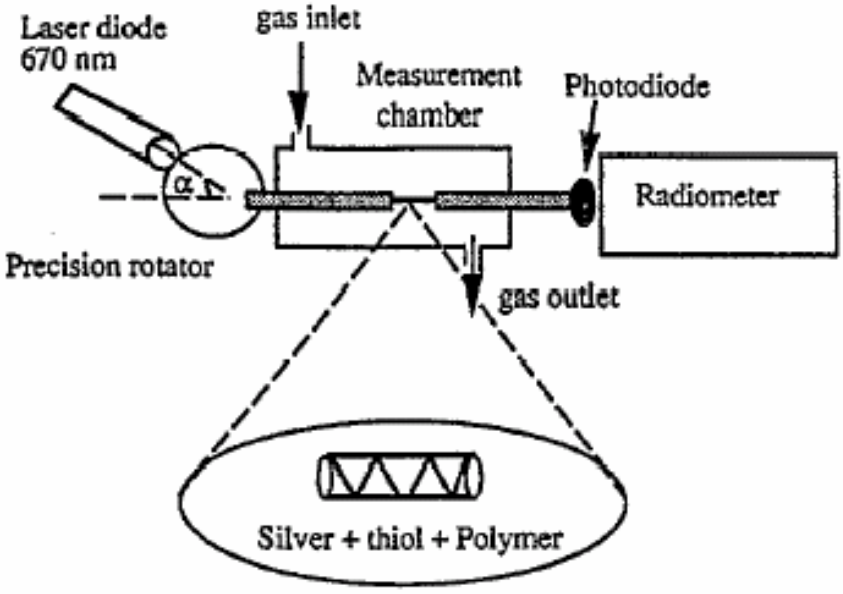

Figure 1.15: SPR sensor for the remote gas detection [69].

By choosing the angle of incidence of the light from the light source, see Figure 1.16, it was possible to vary the dynamic range of the measurement of refractive index of the sensor surface and thus to detect different gases. If the angle of incidence was fixed at 12^{o}, the optical power detected at the photodiode decreased continuously as the refractive index of a gas media with initial refractive indices of 1.362 was increased. Conversely, the optical power increased as the refractive index increased for media with an initial value of refractive index of 1.381.

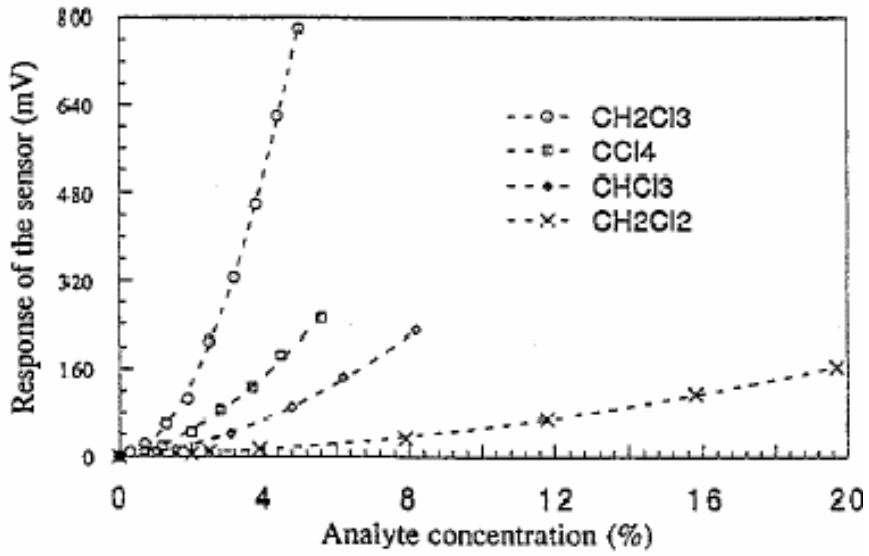

Figure 1.16: Sensor response to the concentration of different chlorinated hydrocarbons [69].

The detection limits for trichloroethylene, carbon tetrachloride, chloroform and methylene chloride utilizing this method were of 0.3%, 0.7%, 1% and 2% respectively, and both the response times and recovery times were less than 2 minutes [69].

The variety of different designs and measurement schemes of fibre-optic sensors provides the potential to create very sensitive and selective measurement techniques for the purpose of environmental monitoring. The key element of the FOS, in terms of selectivity and sensitivity, is the sensitive element. Current research in the field of optical fibre sensors is focusing on the creation and development of new sensitive elements which can expand an application area and increase the number and range of the analytes that can be measured by fibre-optic sensors.

The sensitive elements of fibre-optic sensors should be:

- transparent in the appropriate spectral range;
- change their optical properties under the influence of the specific chemical species;
- fast in response and have wide dynamic range;
- reversible;
- selective;
- easy to immobilize onto glass/quartz/ plastic fibre;
- easily and cheaply manufactured.

The development and creation of the reactive materials characterized by high sensitivity and selectivity towards specific chemical species such as pollutants is a task of current importance.

The photochromic material – bacteriorhodopsin (bR) due to its ability to change its photochromic optical properties as a response to the presence of different chemical species and stimuli in the environment, will be considered in detail to demonstrate the possibility of employing it to provide a universal sensitive element for chemical optical sensors.

1.2 Bacteriorhodopsin

1.2.1 Bacteriorhodopsin: structure and functions

For the last few decades biomolecules have attracted considerable research attention due to the possibility of utilizing them for bioelectronics and optoelectronics applications. Bacteriorhodopsin (bR) is a retinal-protein found in the bacterium *Halobacterium salinarum*. It exists in the form of a two-dimensional crystal incorporated into the bacterium cell membranes, which are called the purple membranes (pm) due to their intensive purple colour, Figure 1.17 [74]. The purple membrane consists of a bR protein and lipid assembly, usually in the ratio of 75 : 25. It has an irregular shape with a diameter of about 1.5 μm and constant thickness of about 5 nm Figure 1.18a and b, Figure 1.19 [75]. Bacteriorhodopsin plays a very important role in the membrane cell and its main function is to convert the energy of a received photon into chemical energy.

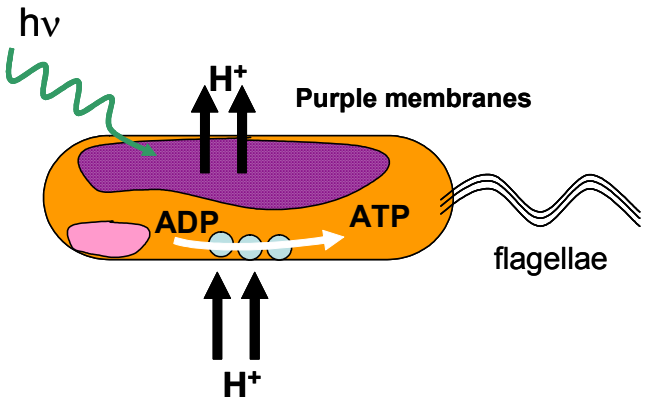

Figure 1.17: Purple membranes and two dimensional crystalline bR lattice [74].

Bacteriorhodopsin was discovered in the early 1970s by D. Oesterhelt and W. Stoeckenius [76]. Because bR has a relatively simple photosynthesis system it has attracted considerable research interest because of the possibility for using it in practical physical applications. Bacteriorhodopsin was one of the first trans-membrane proteins for which the amino acid sequences and structures were completely resolved [77, 78].

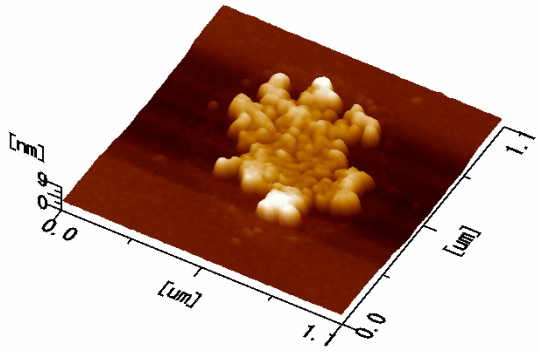

Figure 1.18 a: AFM image of the isolated purple membranes (taken on air at room temperature).

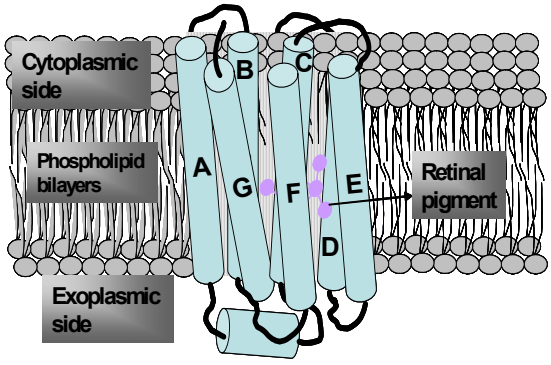

Figure 1.18 b: Schematic presentation of a single bR molecule in the membrane [75].

Bacteriorhodopsin consists of 248 amino acids which are arranged in seven α-helical (Figure 1.19) bundles inside the lipid membrane and retinal molecule that is covalently bound via a Schiff base to a conserved lysine (Lys-216) on helix G and uses light energy to pump protons across the membrane, thus forming a proton gradient [74, 79]. This gradient is used to synthesize ATP and to transport molecules across the membrane. The molecular function of bacteriorhodopsin is the pumping of protons, induced by actinic light, from the cytoplasmic membrane side to the extracellular side Figure 1.20 [80].

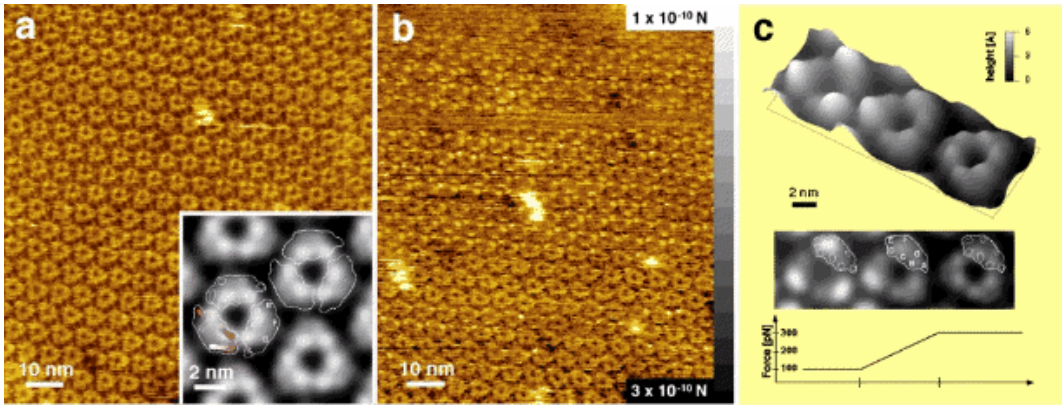

Figure 1.19: AFM image with a high resolution of the topography of the purple membrane containing bacteriorhodopsin and lipids [79].

Absorption of a light quantum by the retinal leads to a reversible colour change from purple to yellow due to protein conformational changes accompanied by a series of spectral changes of the protein called a photocycle. This process is characterized by displacements of the optical absorption bands [81] as demonstrated in Figure 1.21. The intermediate M_{412} is the longest lived intermediate and is the most interesting bR state when considering the functioning of the bR molecule. During the creation and decay of the M state the largest changes occur in the structure of bR molecule.

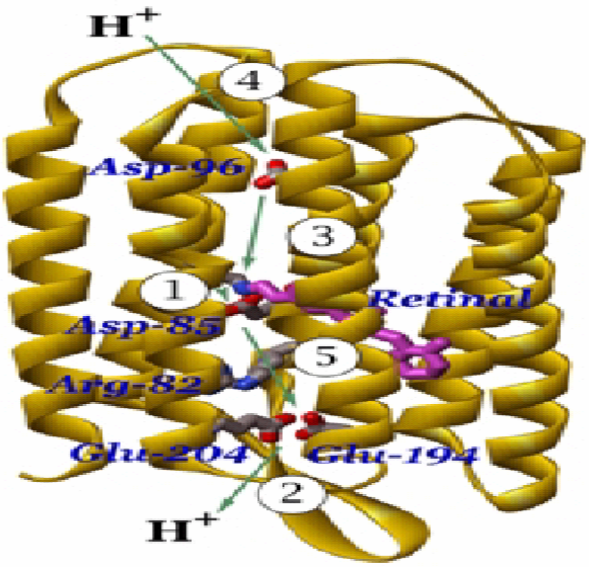

Figure 1.20: An overview of the seven-helical structure of bacteriorhodopsin. The all-trans retinal is shown in purple, important residues in blue. The path of proton translocation is shown with green arrows. Protonation/deprotonation steps follow one another as numbered: step 1, is protonation of *Asp-85* by the Schiff base; step 2, is proton release to the medium; step 3, is reprotonation of the Schiff base by Asp-96; step 4, is reprotonation of Asp-96; and step 5, is proton transfer from *Asp-85* to the proton release group [80].

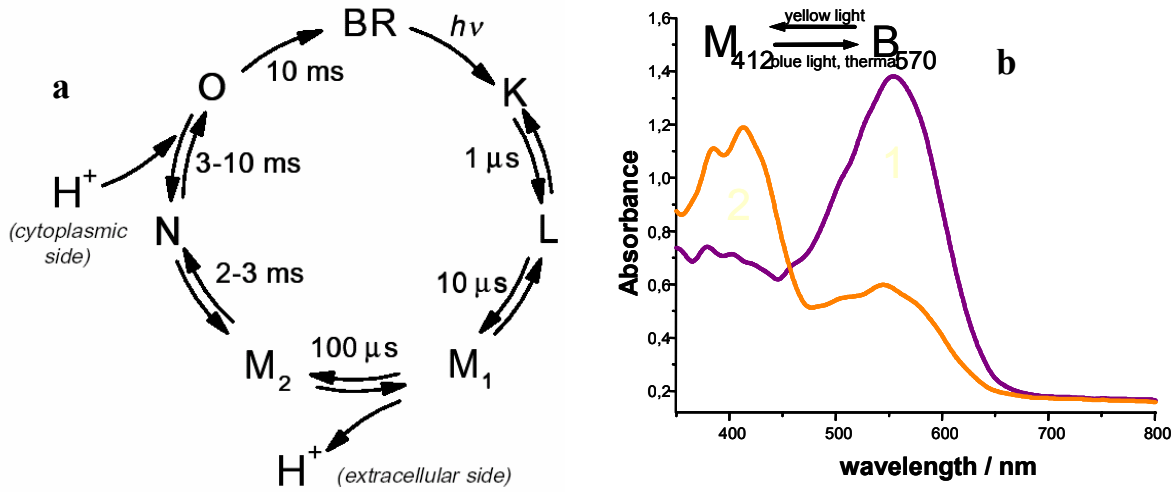

Figure 1.21: a, bacteriorhodopsin photocycle and photointermediates [81]; and b, absorption spectra of the bR_{570} in ground state and longest lived intermediate M_{412}.

The photocycle of the bR had been studied in detail with large numbers of publications each year about the features of the photocycle to provide a more detailed understanding of this reaction [82–84].

1.2.2 Application of bR

A wide range of practical applications have been found for bacteriorhodopsin due to its outstanding properties and its ability to survive in the harsh conditions in which *Halobacterium salinarum* lives [85]. These applications are based on the main functions of the bR molecule: charge separation, photochromic effect and charge transport [74]. The charge transport corresponds to the photoelectrical properties of the bR molecule and can be used for the creation of photon counters and photovoltaic converters [86], and artificial retinas [87–89]. The photochromic effect can be used for the creation of reversible holographic media [86, 90, 91], spatial light modulators [92, 93], associative memories, etc. [74]. These applications are considered as a main area where bR can compete with conventional devices. Additionally, it is possible to use bR within security inks [94], and for chemical and biological sensor [95].

1.2.3 Bacteriorhodopsin films

For most practical applications the bR is embedded into films because it is easier to work with such materials. Usually the polymer based matrices such as gelatin (GE) [96] and polyvinyl alcohol (PVA) [97] are used as matrices for the bR film preparation. These matrices allow mechanically stable films with the good optical quality to be manufactured. Several attempts have been made to incorporate bR into other matrices such as sol-

gel matrix [98, 99] and ployacrylamide [100]. However, the restriction that bR can not be used with organic solvents reduces to a great extent the chemical methods that can be applied [74]. For some applications highly orientated films are required and these films can be produced by means of the Langmuir-Blodgett (LB) method [101] or by electrostatic layer-by-layer adsorption [102].

1.2.4 Modification of the bR optical properties

The lifetime of the M intermediate in native bR protein is only a few milliseconds, which is too short for some optical measurement applications. Consequently, many attempts have been made to prolong the lifetime of the M intermediate state and to obtain the samples with the controlled optical properties [85].

The modification of the optical properties (time constant, colour change and reversibility) of bR can be achieved over a wide range by employing several approaches such as: changing the structural backbone of the protein, amino acid exchange [103], retinal analogues [104, 105], chemical modifications [103, 106–110], external field (temperature, electromagnetic field), and the environmental pH value [74].

The addition of some chemical additives with electronegative function groups can change the photochromic properties of the bR films. The interaction of these chemical additives with bR molecule can be complex and these film samples are called chemically modified bR films. By addition of arginine [107], crown ethers [109], tetraethylammonium chloride [111], guanidine hydrochloride [112], carbodiimide and amine derivatives [113] it is possible to prolong the lifetime of the M intermediate, while addition of sodium azide shows the opposite effect [114].

Z. Batori-Tarci et. al [115] studied the effect of chemical additives (Table 1.1) on the photochromic properties of the bR films. In order to study the influence of the chemical additives the absorbance changes (ΔA) at λ= 570 and 412 nm and half-life ($\tau_{1/2}$) of the intermediate M_{412} state were chosen as the measured parameters (Figure 1.22).

To measure the optical parameters a halogen lamp (250 W) with spectral filters was used as a probe light and an Nd-Yag laser (Surelite I-10, Continuum, pulse duration (6 ns, energy 10 mJ/cm^2) with the wavelength λ= 532 nm was used as actinic light (Figure 1.23).

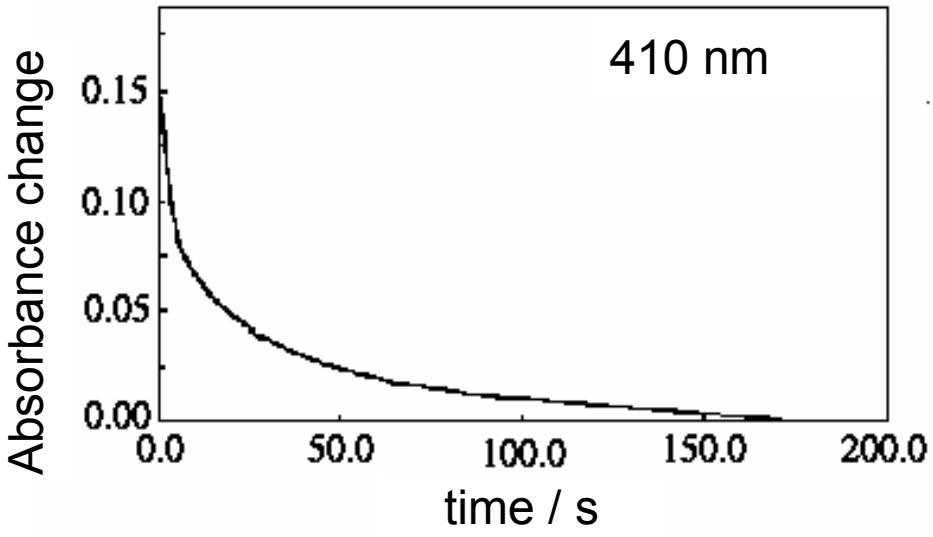

Figure 1.22: Absorption changes measured at 410 nm after turning off actinic light [115].

Table 1.1: Chemical additives used in bR films [115].

Name of chemical additives	Abbreviation	Formula
Triethanolamine (2,2',2''-nitrilotriethanol)	TEA	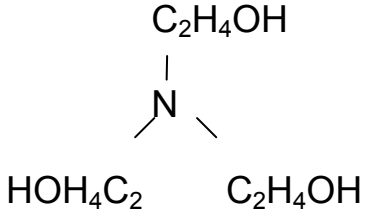
Tetrabutylammonium bromide	TBAB	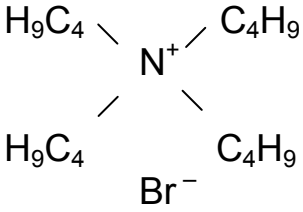
Ethylenediamine dihydrochloride	EDA	$H_2N\text{-}CH_2\text{-}CH_2\text{-}NH_2 \cdot 2HCl$
Dodecyltrimethyl ammonium bromide	DTMAB	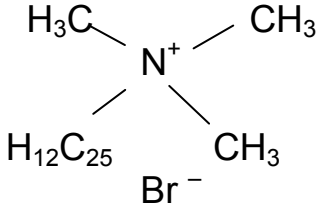
L- arginine hydrochloride	AGH	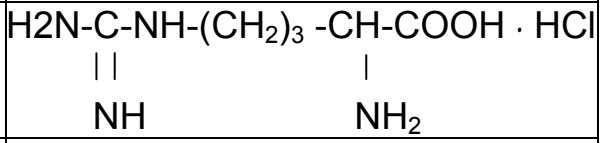
Phenyl-thiosemicarbazide	PTSC	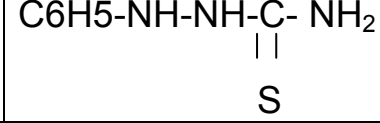
Thiourea	TU	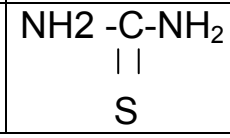

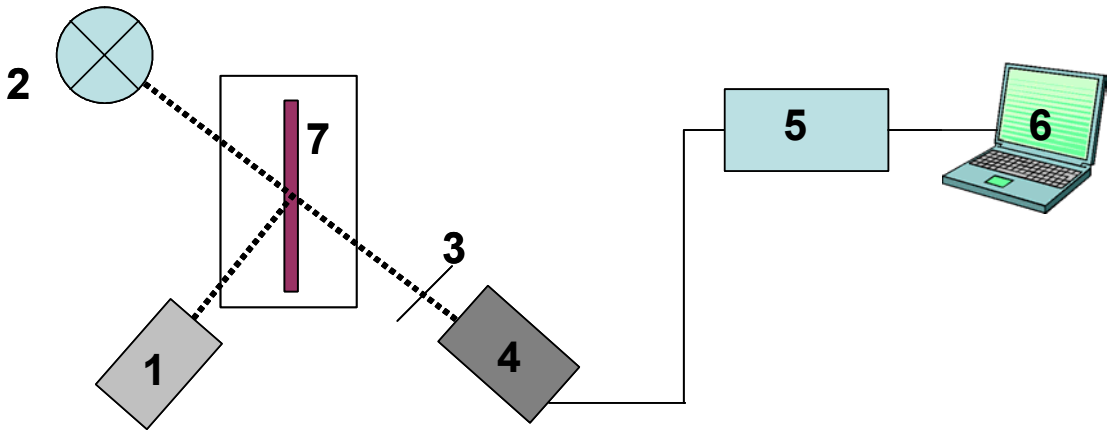

Figure 1.23: Set up for the measurement of the bR films optical parameters [115]. 1, Nd-YAG laser; 2, probe light; 3, spectral filters; 4, photomultiplier; 5, 6, data processing; 7, sample holder.

The chemical additives dramatically changed both the absorption changes and the lifetime of the intermediate M_{412}. For bR bound in a gelatin film without chemical additives the absorbance changes at λ=570 nm and 412 nm were 0.315 and 0.121 respectively, and the lifetime $\tau_{1/2}$ was 3 sec, while in the film with triethanolamine (TEA) and dodecyltrimethyl ammonium bromide (DTMAB) added the absorbance changes were 3 times bigger at 570 nm and 5 times bigger at 412 nm, and the decay rate of the intermediate M_{412} was 100 times slower. The optimal TEA/bR ratio at which the bR film possessed the biggest optical changes and the longest lifetime for the M_{412} state was found to be 250 bR/TEA ratio. Two bR mutants D96N (replacement of the Asp-96 by Asn-96) and E204Q (Glu-204 – Gln) with TEA added were used in order to study on which side of the membrane the TEA acted. Measured changes in the kinetics with and without TEA indicated that TEA probably acts on the extracellular side of the membrane [115].

1.2.5 Optical chemical sensors based on bR

One of the possible applications of the bR is for the creation of the sensitive elements for optical sensors. The influence on the optical properties of bR of the environmental parameters such as presence of different chemical species, pH value and other external effects leads to the possibility to monitor these parameters by registering the changes they induce in the bR optical properties. Numerous studies have been devoted to the investigation of the effects of the external media on the photochromic properties of bR films which are used for optical data-recording applications. For example, measuring humidity [116, 117], the concentration of solutions of local anaesthetics [118], detecting organic vapours [119], and ammonium ions and amines [120, 121]. All of these physical and chemical stimuli have demonstrable effects on the spectral and kinetic parameters of bR films. However, only a few of these studies considered the possibility of employing bR as a sensitive element for optical sensors [119–121].

Dehydration effects on the behaviours of the D96N mutant and wild-type bR films were studied in order to better understand the utilization limits of this material for application in optical recording. Decreasing of the relative humidity leads to a blue shift of adsorption maxima of the ground bR state along with the decreasing of absorption regardless of the nature of bR (Figure 1.24) [116].

Unlike the wild-type bR films, where decreasing the rH of the environment to 12% results in an approximate 200 fold increase in the lifetime of the M intermediate, the D96N mutant only exhibits a 17–20 fold increase in the lifetime of the M state Figure 1.25 [116].

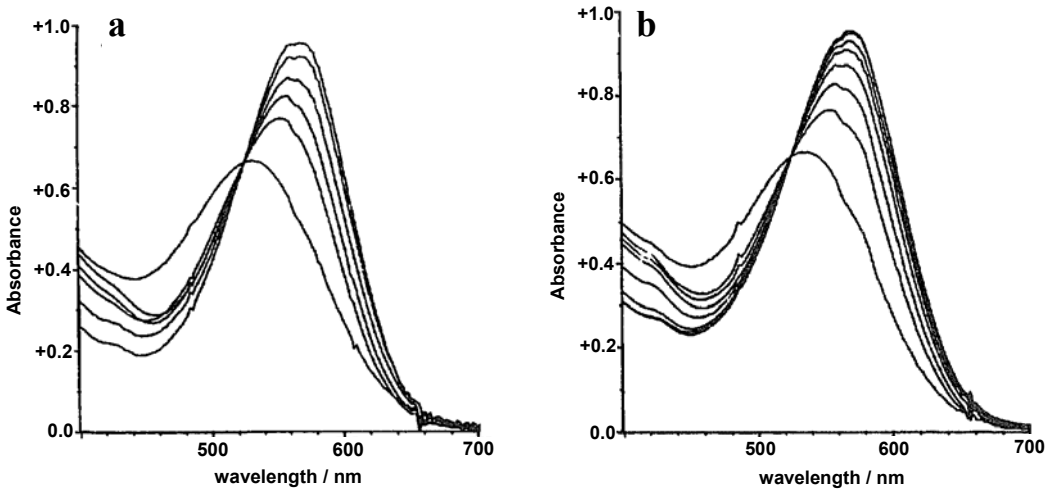

Figure 1.24: Dehydration-induced blue shift of the absorption maxima and decreasing of the absorption at decreasing relative humidity from 85 to 3% rH; a, wild-type bR; b, D96N mutant [116].

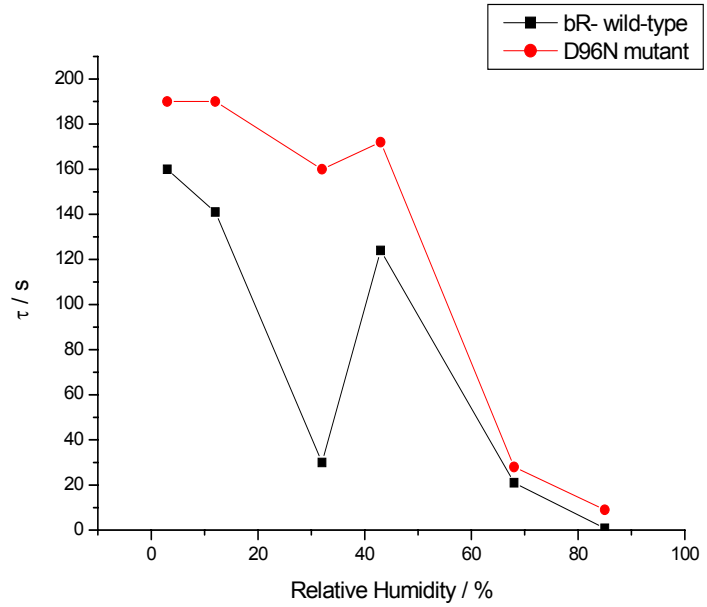

Figure 1.25: M state time constant vs. rH in D96N bR and wild-type bR films (adopted from table 1 in [116]).

These results indicate that D96N bR films, reported earlier as a suitable material for optical information-storage purposes, possess additional advantages. Additionally, the chemically modified D96N bR films have a bleaching efficiency close to unity and are independent of humidity over a wide rH range [116].

A bacteriorhodopsin solution was chosen as a model of a biomembrane in order to study the molecular mechanisms of anaesthesia at the atomic level and determine the quantitative relationship between different anaesthesia action modes and anaesthesia concentrations [118]. The dependence of the spectral changes on the anaesthetics concentration is shown in Figure 1.24 [118]. The decay time of the M intermediate was measured using the excitation wavelength 532 nm, and probing light with the wavelength of 375 nm, at which information about both M412 and M365 can be obtained. At the concentration where the bR567 was generated (low concentration conditions) the decay time became faster for intermediate M, while slower components appear at higher concentration [118].

According to the concentration of anaesthetics there are three distinctly different action modes. For low concentrations of anaesthetics, the absorption maximum shifts from the 569 nm to 567 nm and the decay time of the M state becomes fast. This state of bR is named bR567. For higher concentrations the absorption maxima shows a large blue shift to 480 nm, and intermediate M exists for longer and the bR loses its proton pump function; this state was named bR480. Furthermore several anaesthetics changed the λ_{max} to 380 nm; this was the 3rd mode and was named bR380 [118].

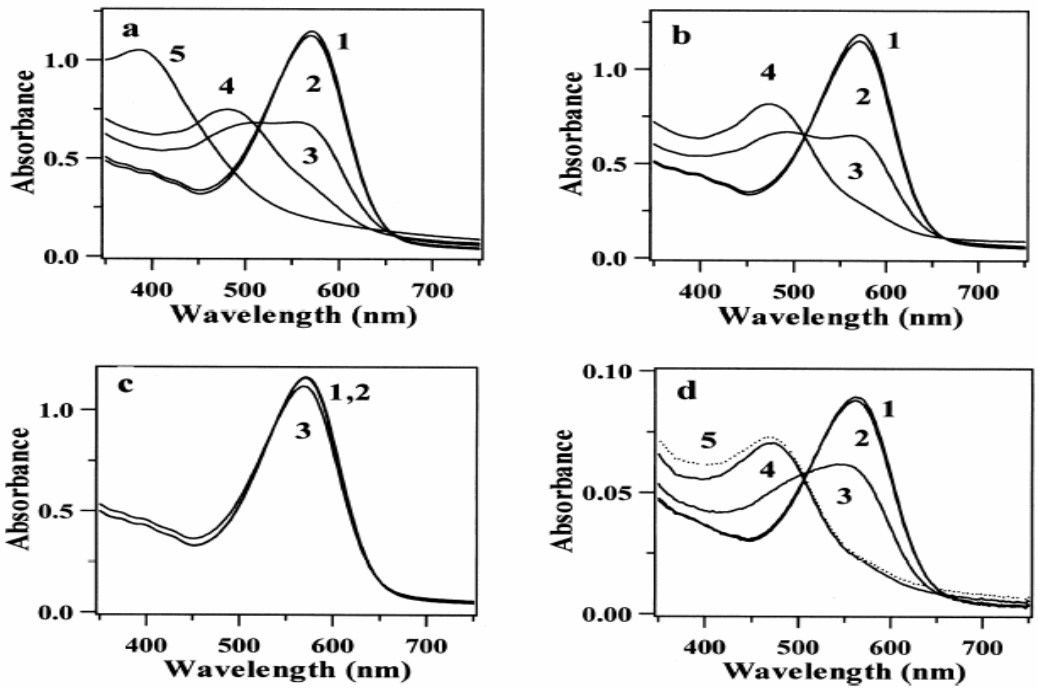

Figure 1.26: Dependence of the absorption spectra of bR on the concentrations of four kinds of volatile anesthetics: a, chloroform: line 1, 0 mM; line 2, 5 mM; line 3, 15 mM; line 4, 30 mM; line 5, 40 mM; b, methoxyflurane: line 1, 0 mM; line 2, 2 mM; line 3, 5 mM; line 4, 20 mM; c, sevoflurane: line 1, 0 mM; line 2, 1 mM; line 3, 10 mM; d, trifluoroethyl iodide: line 1, 0 mM; line 2, 5.6 mM; line 3, 14 mM; line 4, 32 mM; line 5, 32 mM after exposure to room light [118].

The influence of the volatile anaesthetics on the optical properties of bR solution and self-assembled bR thin films showed that increasing of the concentration of anaesthetics leads to the decreasing of absorption at 570 nm. At the concentration of 7.5% of volatile anaesthetics the absorption at 480 nm of the bR in solution increases with the isosbestic point at 510 nm and the new absorption band near 400 nm appears, Figure 1.27a and b [119].

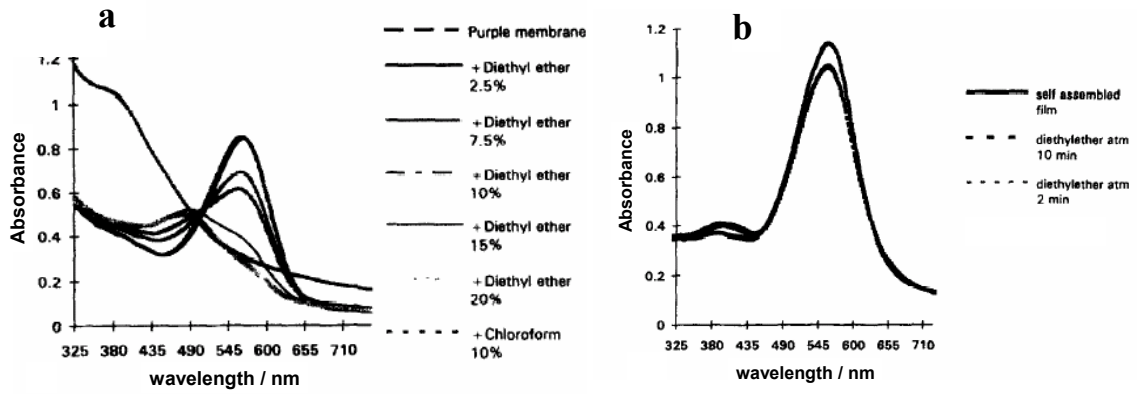

Figure 1.27: Influence of the diethylether and chloroform on absorption spectra of bR a, in suspension 0.3%; and b, in the self-assembled film [119].

The optical response of the bR film monitored at 570 nm to the successive increasing and decreasing of the concentration of volatile anaesthetics is demonstrated in Figure 1.28.

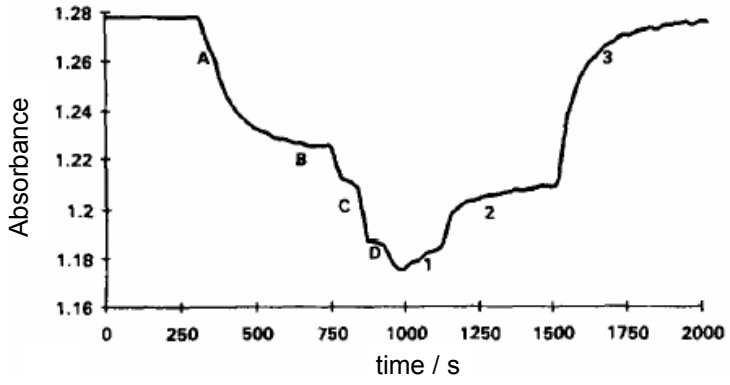

Figure 1.28*:* Optical response of the bR thin film monitored at 570 nm upon exposure to the diethyl ether by increasing concentration (A, B, C, D) and upon exposition to a compressed air stream for the desorption of the anesthetic (regions 1, 2 and 3) [119].

The good reversibility of the optical properties at 570 nm when the bR is exposed to the two types of anaesthetics: ether and a hydrocarbon such as

chloroform, allows a bR thin film to be used as a sensitive layer for optical anaesthetic sensors [119].

D96N mutant bR together with the enzymes was immobilized into sol-gel glass for the detection of urea, acetylcholine and penicillin as the first step of a biosensor development [120]. The absorption spectra (Figure 1.29) of the bR incorporated into sol-gel glass placed in 1 mL cuvette were recorded after incubating it in a phosphate buffer (0.01 M, pH 7.0) for 2 hours and in the substrate solutions of varying concentrations for 30 min.

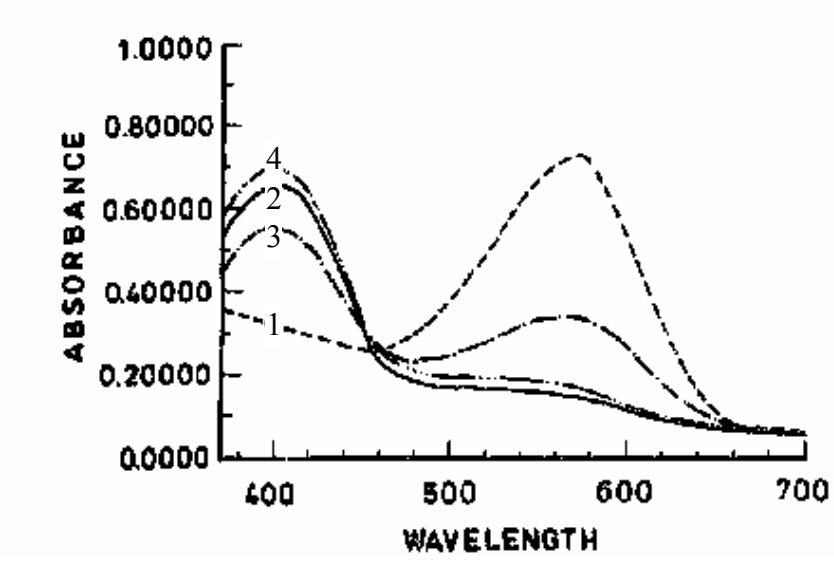

Figure 1.29: Absorption spectra of the D96N mutant bR; line 1, in the absence of the actinic light; other curves under the presence of actinic light; line 2, in working buffer; line 3, in ammonium chloride (0.02 M in working buffer); and line 4, in benzylamine (0.04 M); (bR=0.28 mg mL^{-1}) [120].

When exposed to actinic light the presence of the chemical species leads to a decrease in the absorption maxima at 570 nm whereas an increase occurs at 410 nm that shows the presence of bR in the M state. In the presence of

ammonium ions (curve 3), less absorbance was observed, whereas the presence of benzylamine (curve 4) resulted in an increase in absorbance, as compared to the absorbance in working buffer (curve 2). Additionally in the presence of ammonium ion both the 410 nm and 570 nm components are seen (curve 3) [120]. The decay rate of the intermediate M state was recorded at 410 nm after sample illumination for 5 sec with the optical filter that eliminated all light from the projector below 520 nm. Depending on the concentration of the ammonium chloride and benzylamine different behaviours of the lifetime changes of the M state occur, as demonstrated in Figure 1.30 [120]. The variations of the lifetime of the M state in the presence of different enzymatic reactions are shown at the Figure 1.31.

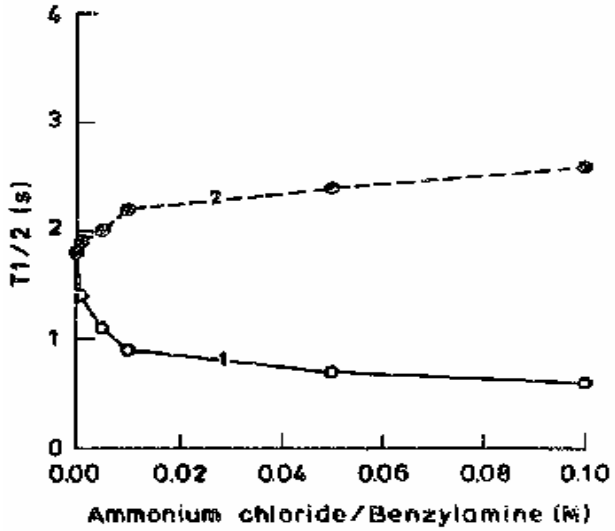

Figure 1.30: Half time of M state of D96N mutant bR in the sol-gel glass in the presence of different concentrations of line 1, ammonium chloride; and line 2, benzylamine in 0.0l M phosphate buffer (pH 7.0); (bR=0.31 mg mL^{-1}) [120].

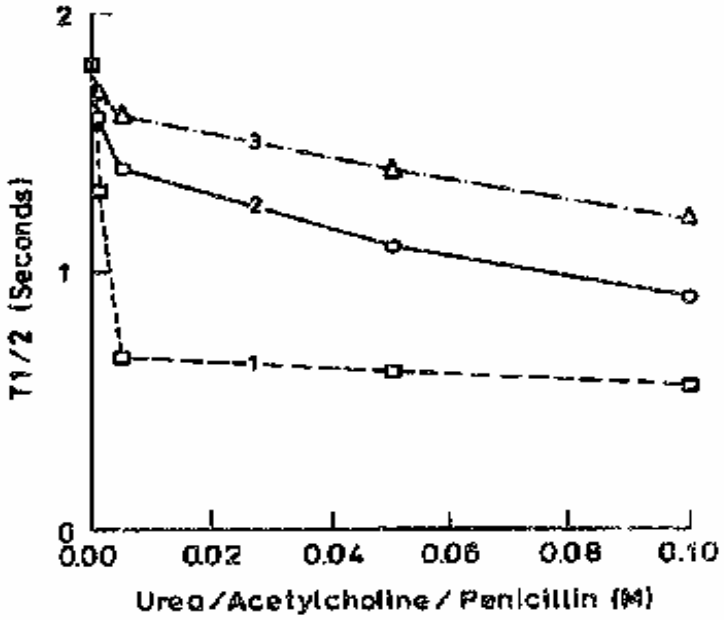

Figure 1.31: Variation of the half time of M state decay of D96N mutant bR in the sol-gel glass in the presence of three enzymatic systems: line 1, urea; line 2, acetylcholine; and line 3, penicillin [120].

For all three enzymatic systems a decrease of the lifetime of the M state with increasing concentration was observed. The results showed that it was possible to employ bR immobilized in the sol-gel glass as a probe for monitoring enzymatic reactions [120].

In order to better understand the transition of the M state back to the bR ground state the same authors [121] studied the dependence of the kinetics of decay for the M, N and O states of the D96N bR on the presence of (i) ammonium ions and (ii) an aromatic amine. The measurement of the absorbance and kinetics changes at the 410 nm, 530 nm and 640 nm which corresponds to the absorption maxima of the M, N and O intermediates respectively was undertaken. The presence of amino compounds led to a decrease of the lifetime for the all M, N and O intermediates, whereas the

presence of amine caused an increase of lifetime for all intermediates, Figure 1.32.

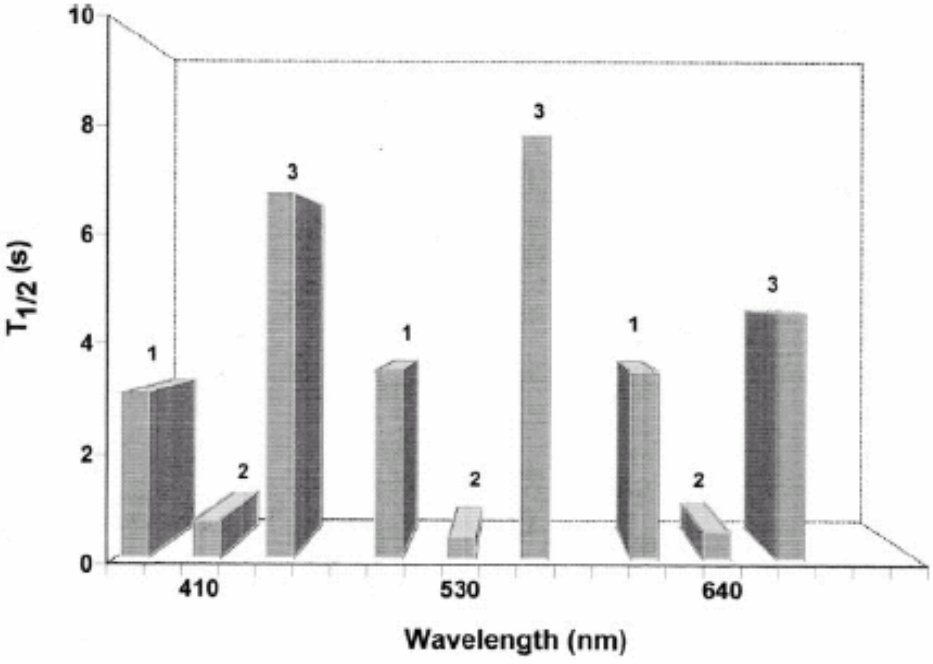

Figure 1.32: Dependence of the lifetime of M, N and O intermediate of the D96N mutant bR in the sol-gel glass on the presence of ammonium ions and benzylamine; column 1, control (taken in 0.01 M phosphate buffer pH 7.0); column 2, ammonium ion (0.003 M); column 3, benzylamine (0.04 M) [121].

Different results were observed when the absorption changes were measured. The absorption changes and the effect of ammonium ions and amine on the decay kinetics of D96N bR are more apparent at 530 nm than at 410 nm and 640 nm Figure 1.33.

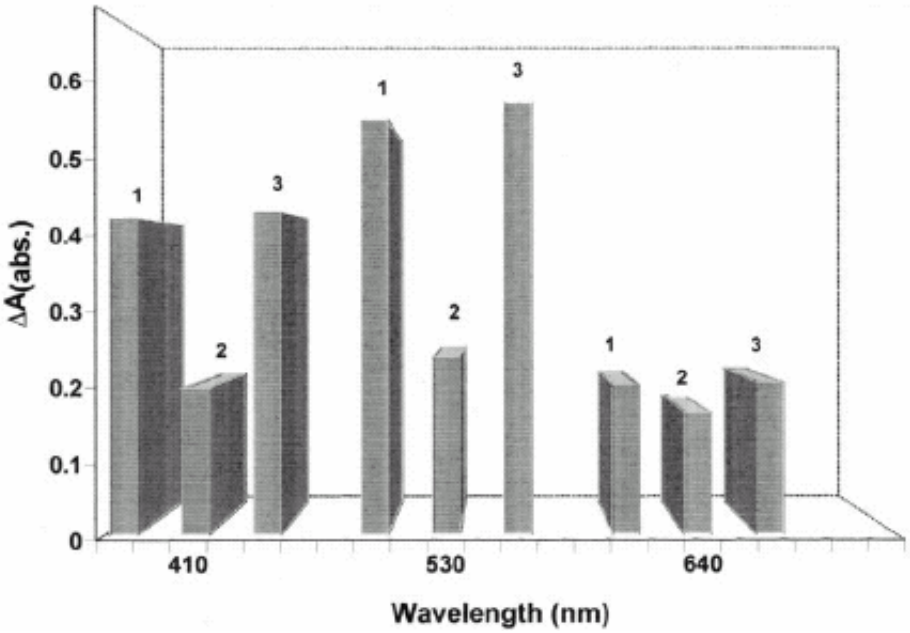

Figure 1.33: Dependence of the absorption changes of M, N and O intermediate of the D96N mutant bR in the sol-gel glass on the presence of ammonium ions and benzylamine; column 1, control (taken in 0.01 M phosphate buffer pH 7.0); column 2, ammonium ion (0.003 M); column 3, benzylamine (0.04 M) [121].

The measurements were repeated 15 times and a good reproducibility of the results was achieved with the experimental error less than 2% [121].

Conclusions and Summary:

Reported results of the reversible and sensitive response of the photochromic properties of the bR films to the presence of different chemical species can be employed for the development of the sensitive elements for optical sensors. For practical sensing applications, one can monitor the changes under the presence of chemical species of the spectral and kinetic parameters of bR films that are incorporated into a matrix.

The main topic of this thesis is to study the possibility of using a bR film for the construction of fibre-optic sensors for monitoring ammonia and humidity. The possibility to control the sensitivity and selectivity of the sensor element to the presence of ammonia and changes of relative humidity based on the use of bR by using chemical additives and by employing the different materials as a matrix for the creation of bR films is reported in the thesis. The example based on ammonia and relative humidity is used to show how using a broad range of the different chemical additives bR can be sensitized as a sensitive element to a wide spectrum of species, and thus possesses the potential to be a universal film material for optical sensors.

Chapter 2: Film characterization techniques

In this Chapter the film characterization techniques used in this thesis for the investigation of the impact of structural characteristics of bR-based films in the matrix on the sensitive element and some typical results will be introduced. The measurement method used for the investigation of the influences of ammonia gas and relative humidity changes on the optical properties of the bR films of different composition will be described. The gas generation system used for the generation of the desired range of ammonia concentrations will be described. The principle of operation and design of the fibre-optic sensors will be explained. The sensor sensitivity and equations used for the calculation of the sensors response will be discussed. The gas generation system and measurements chamber used for the calibration of the sensor response and design of the proposed fibre-optic sensor will be described.

2.1 Structural characterization

The morphology of the surface, cross-sections and distribution of the purple membranes within the bR films was studied using a Hitachi S–5200 field emission scanning electron microscope (FE-SEM) equipped with the energy dispersive spectroscopy (EDS) microanalyses function. Surface morphology of the films based on bR in the sol-gel matrix was studied with the help of a Jeol JSPM-5210 atomic force microscope (AFM). The porosity of the matrix used for the film preparation was measured with the help of the surface area and pore size analyzer – Sorptomatic 1990.

2.1.1 Scanning electron microscopy (FE-SEM and EDS)

The principle of operation of a scanning electron microscope is based on the scanning of a focused beam of high energy electrons across a sample surface. The beam specimen interaction produces a number of signals including; secondary electrons, back scattered electrons and X-rays.

When the primary electron beam bombards the object, secondary electrons are emitted from the object surface with a certain velocity that is determined by the levels and angles at the surface of the object. The secondary electrons strike the scintillator (fluorescing screen) that produces photons. The location and intensity of the illumination of the screen depends on the properties of the secondary electrons, and contrast of the real time image reflects the structure of the surface of the object [122].

X-rays are produced and emitted by the interaction of the electron beam with atoms in the specimen. These X-rays are characteristic of the chemical elements present and they may be separated out in an energy spectrum to

allow the identification of the elemental composition of the specimen. The emitted X-rays can also be mapped back to their original position in the sample to provide a map of the distribution of the elements in the sample. Energy dispersive spectroscopy (EDS) is the measurement of X-rays emitted during electron bombardment in an electron microscope to determine the chemical composition of materials and distribution of elements on the micro- and nano- scales.

The Hitachi S–5200 field emission scanning electron microscope (FE-SEM) with a high resolution of the 1.8nm at 1kV equipped with the EDS system was used to study the surface morphology, cross section and element distribution of the bR films.

For SEM measurements the bR films were deposited onto 5 mm^2 glass substrates in order to fit the sample holder of the FE-SEM. Before measurements the films were vacuum dried for 6 hours in order to remove all water from the samples and then were coated with thin (5 nm) platinum film to allow a discharge of the sample surface during interaction with the electronic beam.

Typical examples of the surface morphology and cross section of a bR film are shown in Chapter 3, Figure 3.11a and b respectively.

2.1.2 Atomic force microscopy (AFM)

Atomic force microscopy (AFM) belongs to the family of the scanning probes microscopes and employs a small probe that is a raster and which scans over a sample using a piezoelectric device to produce an image of the sample surface.

A sharp tip (radius of few nm) usually made in 4-sided pyramidal form is attached to a fixed substrate on a cantilever with a very low spring constant

(typically 0.1 N/m) and a constant small force (typically 10^{-9} N) is applied to the tip by mean of the piezoelectric positioning element [123]. The interaction force between the tip and sample surface and contouring surface is measured (Figure 2.1). The solid surface is continuously scanned under the tip by means of an XYZ piezoelectric tube with the recording of approximately 400x400 points or greater. As the probe tip experiences attractive or repulsive forces, the cantilever will bend, which can be detected by a laser beam reflected off of the cantilever towards a position sensitive photodiode. The AFM can measure sample topography in two ways: by recording the feedback output ("Z" signal) or the cantilever deviation from the preset deflection ("error" signal; see Figure 2.1) at discrete intervals. The sum of these two signals always yields the actual topography, but given a well-adjusted feedback loop, the error signal should be negligible. The deflexion (x, y) position of the tip and the feedback signal are electronically recorded to produce with the help of the software a three dimensional map of the surface or other information depending on the type of tip used [124].

In general AFM can operate in three different modes: *contact mode* (Figure 2.2a), when the tip is placed in contact with the sample surface and the repulsive forces dominate the tip-sample interaction of the force measured directly from the deflexion of the cantilever; in the *non-contact mode* (Figure 2.2b), the tip is oscillated close to the sample surface (distance in order of ten to hundreds ängströms); the frequency (typically from 100 to 400 kHz) of the oscillations is influenced by the van der Waals attraction force between the tip and the surface and the force is measured by comparing the frequency and/or amplitude of the cantilever oscillation relative to the driving signal (piezoelectric crystal); and *tapping mode* in which the cantilever is excited using the piezoelectric crystal to oscillate

near its resonance frequency (50–500 kHz) and the AFM operates in the repulsive force region, but the tip touches the sample only for short periods of time, which reduces the possibility of sample damage when measuring fragile objects [125].

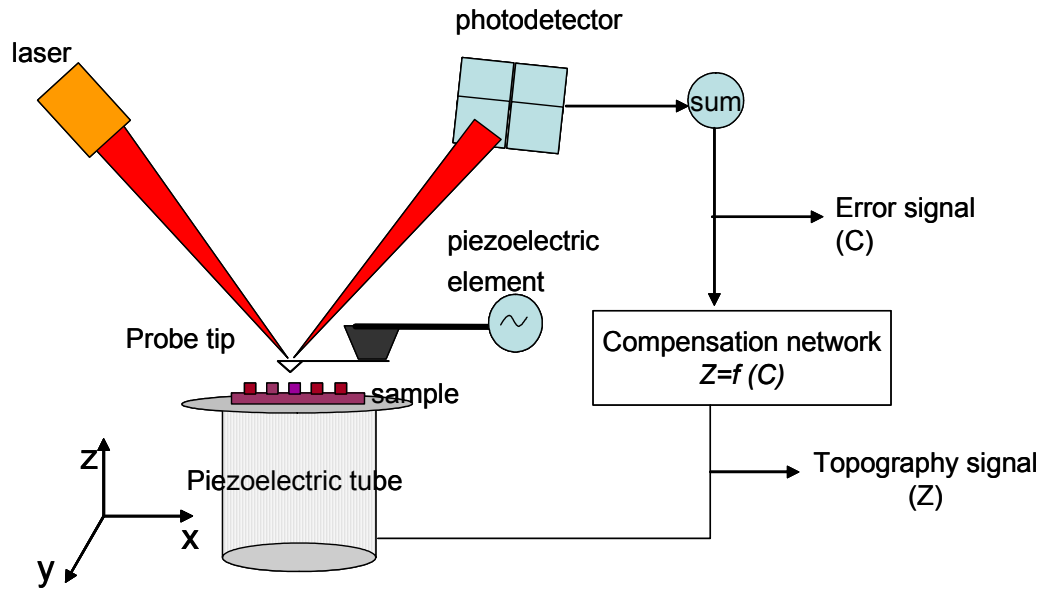

Figure 2.1: Simple schematic diagram of the AFM instrument.

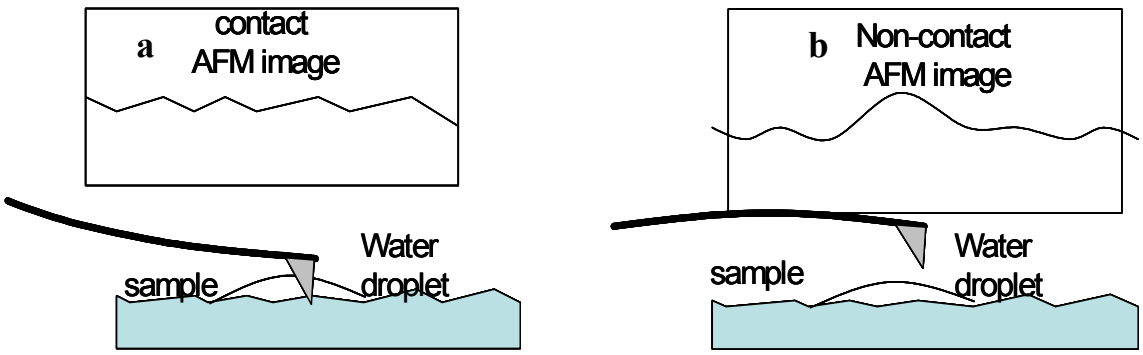

Figure 2.2: Modes of the AFM operations: a, contact mode; b, non-contact mode.

Surface morphology of the films based on bR in different matrices deposited onto glass substrates was studied in non-contact mode with the help of a Jeol JSPM–5210 atomic force microscope, typical examples of the AFM image of the surface morphology of films based on bR in a gelatin matrix and a PVA matrix are shown on Figure 3.12a and b (Chapter 3), respectively.

The SEM and AFM are complementary techniques that use different principles of surface scanning and can provide similar information about surface features of the sample [126]. However, in contrast to electronic microscopy, the main drawback of which is that rather drastic sample preparation is required, with the help of AFM the surface morphology of biological objects can be easily observed, *in situ*, in their native environments by applying a small force (typically of pN) to the cantilever that depends on the origin of the sample [127, 79], see for example Chapter 1, Figure 1.17.

2.1.3 Porosity measurements

Porosity is an important parameter that can define the efficiency of film sensitive elements for gas sensors. A matrix with a high proportion of open pores allows a large surface area of the sensitive element to be constructed throughout the matrix. Consequently, the chemical analytes penetrate and interact with the bR inside the entire film volume, thus increasing the effectiveness of the sensor response. Knowledge of the pore structure is an important step towards the determination of a material's characteristics when predicting its behaviours under the influence of external stimuli.

Accordingly, measurements of the porosities of the materials to be used as matrices for bR films were carried out.

The total sum of the ratio of the void volume to the total volume of a given sample of material is called porosity. There are two main and important typologies of pores:

(i) Closed pores that are completely isolated from the external surface because no path exists between them. Consequently, access to the internal pores of external substances in both liquid or gaseous phase is not possible, and

(ii) Open pores that are interconnected with paths existing from the interior to the external surface and so the internal pore spaces are accessible to fluids, depending on the nature and size of the pores and the nature of the fluid.

Consequently, the porosity characterization of the materials used as a matrix for the manufacturing bR-based films was undertaken considering only the open pores.

The characterization of the materials in terms of porosity consists of determining the following parameters:

- pore size in terms of nominal diameter (micropores – less than 2 nm; mesopores – between 2 and 50 nm; macropores – larger than 50 nm)
- specific pore volume
- porosity
- pore size distribution
- bulk density
- percentage porosity

- specific surface area, which is the total surface area of the sample that is in contact with external environment, expressed in square meters per gram of dry sample (m^2/g)

The pore size distribution and specific surface area were measured by means of the static volumetric principle used to characterize films samples by the technique of gas adsorption [128]. The principle of operation is based on introducing consecutive known amounts of adsorbate to the sample holder, which is kept at liquid nitrogen temperature (77 K). A schematic diagram of the principle of operation of the static volumetric gas adsorption is shown in Figure 2.3.

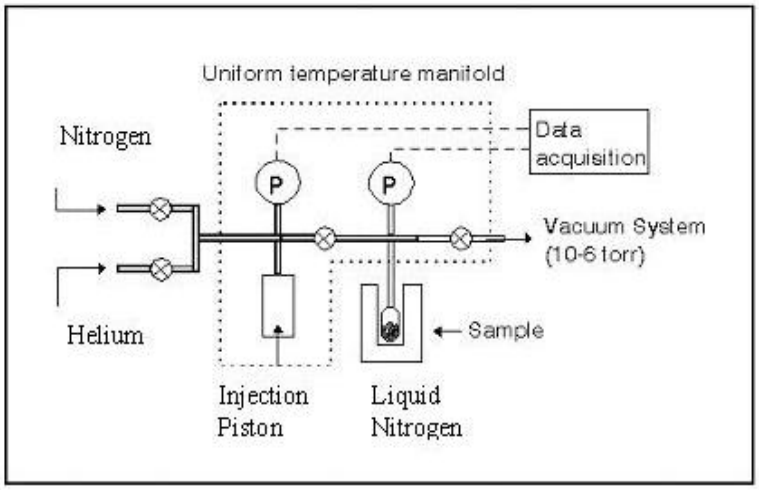

Figure 2.3: Measurement scheme of the instrument "Sorptomatic –1990" used for porosity measurements.

Adsorption of the injected gas onto the sample causes the pressure to slowly decrease until an equilibrium pressure is established in the manifold (Figure 2.4).

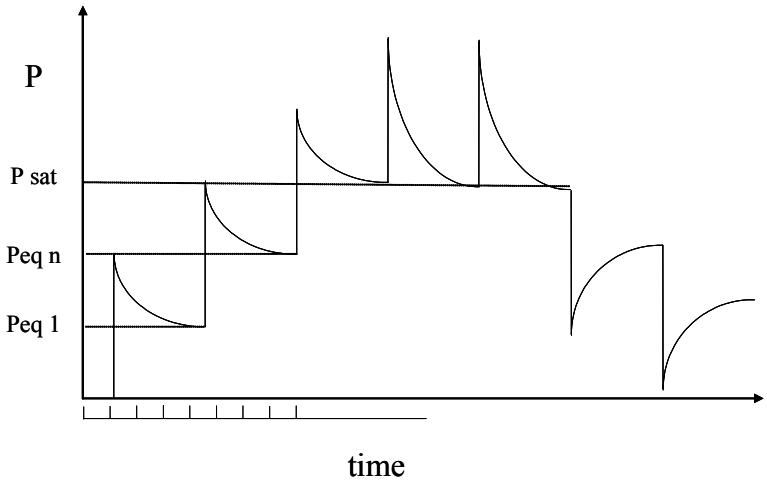

Figure 2.4: Measurement of the equilibrium pressure, $P_{eq\ n}$, equilibrium pressure, P_{sat}, saturation pressure using static volumetric gas adsorption.

The raw experimental data are the equilibrium pressures and the amount of gas adsorbed for each step. The complete adsorption/desorption analysis is called an *adsorption isotherm*. There are six standard isotherms (Figure 2.5), which differ because the systems demonstrate different gas/solid interactions.

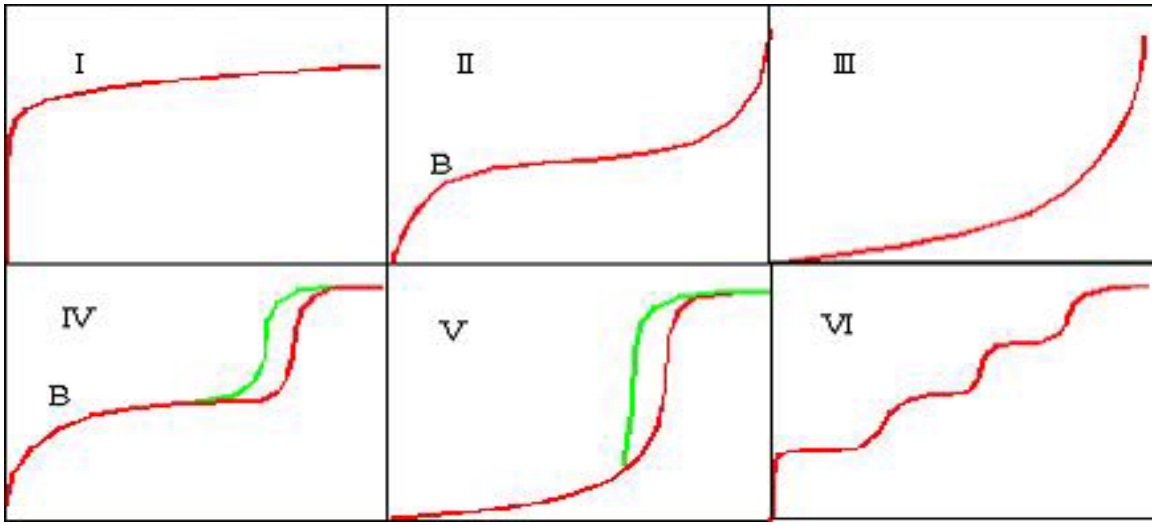

Figure 2.5: Adsorption isotherms classified according to IUPAC [129]: I, typical for microporous solids and chemisorption isotherms; II, finely divided nonporous solids; III and V, typical of vapours (water on hydrophobic solids); IV, feature a hysteresis loop generated by the capillary condensation in mesopores; VI, steps-like isotherm (nitrogen on special carbons).

Once the isotherm is obtained, a number of calculation theories can be applied to the adsorption isotherm to evaluate the specific surface area (i.e. Brunauer- Emmet-Teller (BET), Dubinin, Langmuir, etc.) or the micro and mesopore volume and size distributions (i.e. Barret-Joyner-Halenda (BJH), Dollimore-Heal (DH), Horvath-Kavazoe (HK), etc.). The BET [130] theory and BJH [131] were used in this work for calculations of the specific surface areas and pore size distributions respectively. The main state of BET theory is that gases form an unlimited number of layers over surfaces and it is a generalized Langmuir theory. Forces active in the condensation of gases are responsible for multi-molecular layer formation and this theory is applicable to isotherms type II, IV, VI [130]. The BJH model is based on the Kelvin equation correcting the Kelvin radius with the thickness of the still adsorbed gas and it is applicable to isotherms type IV, V [131].

The experiments were undertaken using “Sorptomatic 1990” which is a completely computerized instrument. The typical adsorption isotherm of the gelatin film that was used for the calculation of the surface area and pore size distribution is shown on the Figure 2.6.

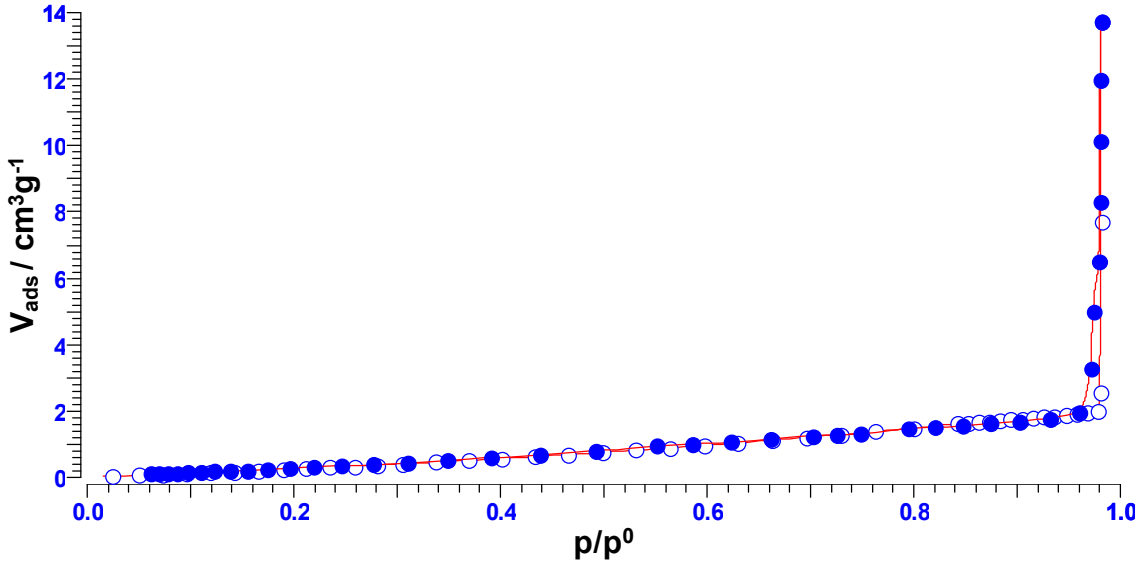

Figure 2.6: Adsorption isotherm of the gelatin film; open symbols, adsorption isotherm; close symbols, desorption isotherm.

2.2 Optical characterization

For the purposes of determining the original parameters of the film samples the spectral static and temporal characteristics were measured at room temperature using an HR2000 Ocean Optics fibre-optic spectrophotometer and a double beam Jasco V-550 UV-VIS spectrophotometer.

2.2.1 Optical spectra

A double beam spectrophotometer (SF) Jasco V-550 was used for the high resolution measurements of the static spectral characteristics of the prepared bR films. The SF uses a single monochromator with a plane grating of 1200 grooves/mm and a photomultiplier is used as a detector. Converging light enters the monochromator where it is dispersed by the grating and subsequently passes through an exit slit. The sector mirror splits the light into two beams: one incident on the sample to be measured; the other incident on the reference. After passing through the sample or the reference the light reaches the photomultiplier Figure 2.7.

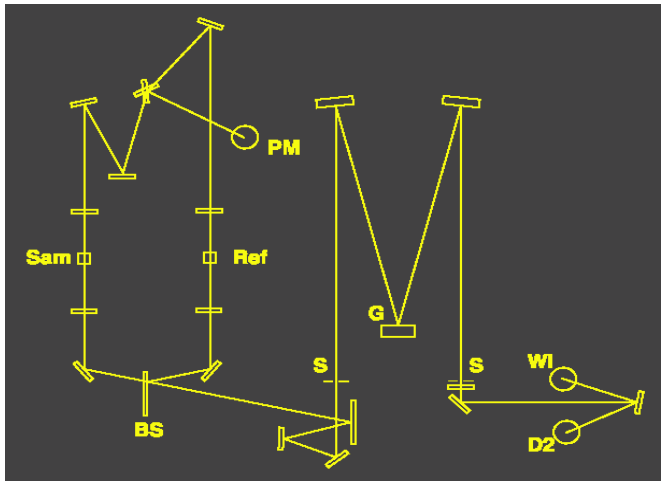

Figure 2.7: Schematic diagram of the Jasco V-550 SF. WI, halogen lamp; D2, deuterium lamp; G, grating; S, slit; BS, beam splitter; REF, reference beam; SAM, sample beam; PM, photomultiplier tube.

The Ocean Optics HR2000 (OO HR2000) spectrophotometer with a charge-coupled device (CCD) detector was used for the measurements of the dynamic changes of the bR films spectra before and after exposing them to the ammonia and environments of varying relative humidity. The

OO HR 2000 consists of an SMA connector for easy connection of the optical fibre; a slit and filter for the regulation of the light intensity; collimating mirror to focus light towards the SF grating; grating to diffract the light onto the focusing mirror; focusing mirror to focus the light onto the CCD detector; and CCD detector that converts the optical signal to the digital, see Figure 2.8.

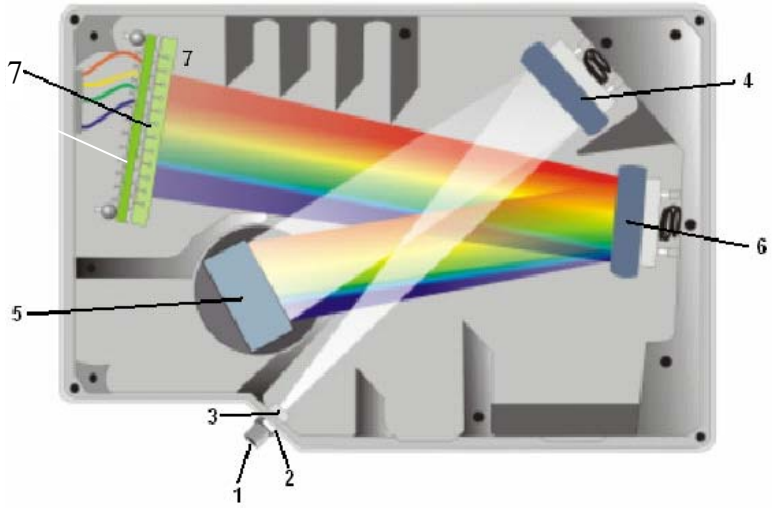

Figure 2.8: Schematic diagram of the OO HR200 CCD spectrophotometer [132]. 1, SMA connector; 2, slit; 3, filter; 4, collimating mirror; 5, grating; 6, focusing mirror; 7, CCD detector.

The Ocean Optic tungsten halogen lamp HL-2000 VIS-NIR (360 nm-2 000 nm) was used as the probe light source (LS) for spectral measurements with the OO SF HR2000. Optical fibres of varying diameters were used to connect the sample holder (SH), LS and spectrophotometer.

Absorbance spectra were obtained using the OOIBase32 software that calculates absorbance (A) using the following equation 2.1:

$$A = -\log_{10}\left(\frac{S_\lambda - D_\lambda}{R_\lambda - D_\lambda}\right), \qquad (2.1)$$

where S_λ, the intensity transmitted through the sample at wavelength λ, D_λ, the dark intensity at wavelength λ, R_λ, the reference intensity at wavelength λ.

2.2.2 Measurement set up

A specially designed and laboratory-built sensor chamber (Figure 2.9) was used for measuring the effects of the presence of ammonia on the optical properties of the bR films. The sample holder with the bR film was placed inside the chamber and connected (using SMA connectors) to the light source (LS) and spectrophotometer (SF) by means of multimode quartz optical fibres (Ocean Optics, QP1000-2-UV-VIS) with an external diameter of 2 mm (diameter of the core, 1 mm; cladding (doped fused-silica) thickness, 25 μm; and protection cladding thickness, 0.9 mm, see inset in Figure 2.9). Optical fibres located inside chamber and LS and SF placed outside chamber were connected through the vacuum feed-through connectors (Ocean Optics VFT-600-UV-275). Gas cylinders containing nitrogen together with calibrated ammonia concentrations (100 ppm, 1 000 ppm, 0.1% and 10%) were connected to the gas chamber in order to provide known concentrations of ammonia within the chamber. Pressure gauges were used to control the gas flow into the chamber (Figure 2.9). To obtain ammonia concentrations of less then 100 ppm, that mixture was admitted to the chamber to give a pressure increase of e.g. 0.1 atmospheres (giving a concentration of 10 ppm). This took about 20 s. It was verified that the 10% pressure increase did not affect the optical absorbance of the bR (Figure 2.9).

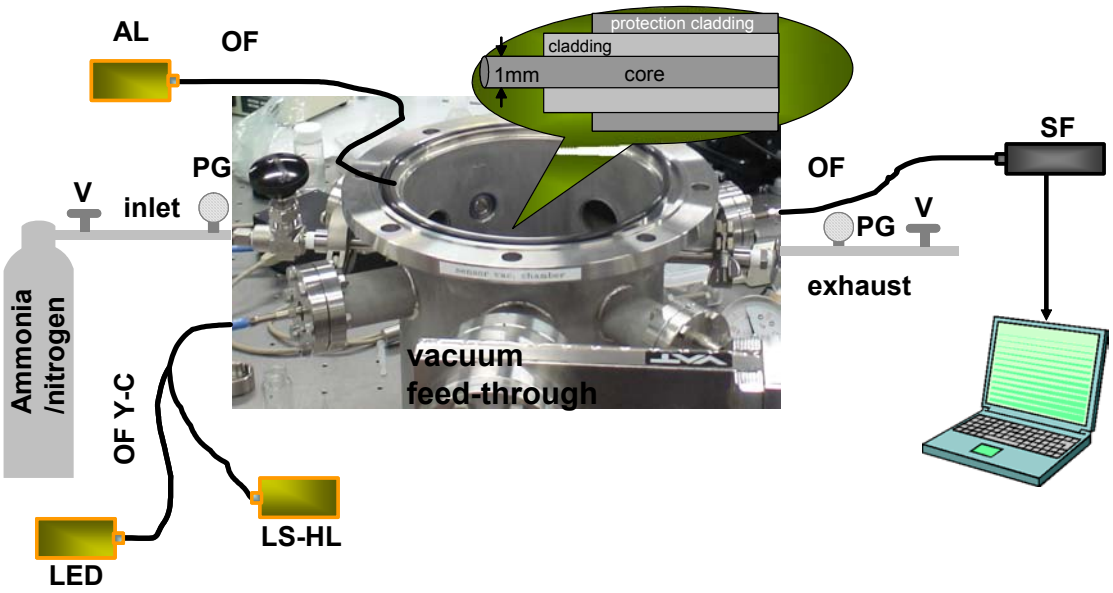

Figure 2.9: Measurement set up (see text). The chamber volume was 7 L. OF, optical fibre; SF, spectrophotometer; as the light source (LS) a halogen lamp (HL) was used; AL, actinic light source used for the photo-excitation of the bR photocycle; LED, light emitting diode; OF Y-C, optical fibre Y-type coupling; PG, pressure gauge; V, valves. The inset shows the structure of the optical fibre.

A gas generation system was used to measure the effects of ammonia at lower concentrations (i.e. below 100 ppm), see Figure 2.10. An aqueous ammonium solution 30 percent by weight (wt. %) placed in a balloon flask was used for the creation of a saturated concentration of ammonia gas (Figure 2.10). In this flow system compressed humidified air was used as a carrier gas which was passed through a bubbler containing the analytes to be detected, the analyte vapour being in equilibrium with its liquid. The concentration of ammonia gas in the flask head space was calculated from the difference in flask weight before and after flowing the humidified air through the flask for 10 min at a flow rate of 1 L/min, and making allowance for water evaporation.

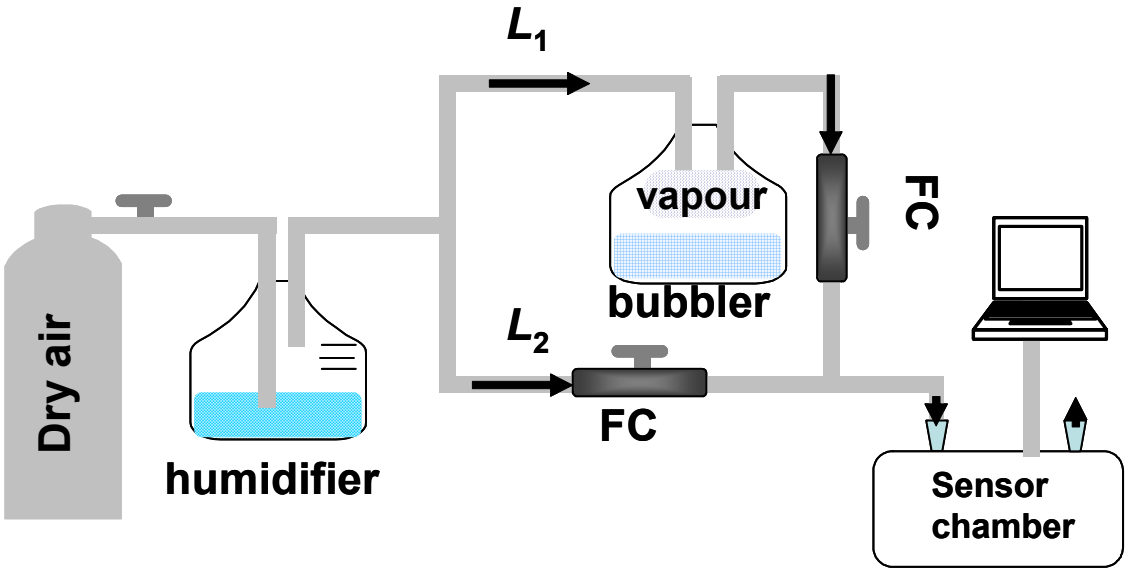

Figure 2.10: Set up of gas generation system.

The concentration of the analyte gas in the air can be calculated by using the following equation:

$$C = \frac{L_1}{L_1(1+z)+L_2}, \tag{2.2}$$

where C, the concentration of the analyte; z, molar fraction of the analyte in the flask (ratio of the partial pressure of the solution p_s at the given temperature to the atmospheric pressure P; $z = p_s/P$); L_1 and L_2, the flow rates of the air passed through flask and carrier gas respectively.

L_1 was kept constant at 1 L/min flow rate whereas by changing the ratio between L_1 and L_2 different gas concentration of analyte could be obtained. The base line of each experiment was recorded by flowing ammonia-free air through the chamber. Ammonia concentrations in the range 10–1 000 ppm were used for the measurements.

Continuous changes of relative humidities (rH) from values of 30% up to 90% was achieved by placing the open volume with water inside the closed chamber and the influence of the rH changes on the bR optical properties were measured. rH inside the sensor chamber was monitored in real time using a relative humidity Gemini Data Logger "Tinytalk" device with a capacitance sensor that is able to measure the change of rH in the range of 0–95% with the accuracy of ± 3% at 25 ^{o}C and with a reading resolution of 0.5% rH.

2.2.3 Kinetics measurements

For measurements of photoinduced absorption changes an Ocean Optics LS-450 Blue LED Pulsed Light Source with the light emitting diodes (LED) of different emission wavelengths (LED_{518}, LED_{640}, LED_{470}, LED_{595}, LED_{380}) or a tungsten halogen lump with Ocean Optics high-pass filter OF2-OG515 and with a cut off wavelength λ= 530 nm (transmit only light with the $\lambda > 530$ nm) were used for photo excitation of the bR photocycle. The actinic light was transported by means of a multimode quartz optical fibre (Ocean Optics, QP1000-2-UV-VIS) with an external diameter of 2 mm (diameter of the core, 1 mm; doped fused-silica cladding thickness, 25 μm; and protection cladding thickness, 0.9 mm) to the film fixed in the sample holder. The structure of the optical fibre is shown in the inset of Figure 2.9. The measurements were made at the wavelengths 410 and 570 nm, which correspond to the absorption maxima of the main intermediate M_{410} state of the bR photocycle and the ground state bR_{570} respectively. For the difference spectra, the spectrum of the illuminated sample was measured 5 min after start of the exposure to the actinic light.

The photoinduced absorption changes ΔA were calculated as the normalized ratio of the maximum absorbance of the unbleached sample Equation 2.3:

$$\Delta A = \frac{A_{m\lambda} - A_{m\lambda a}}{A_{m\lambda}}, \tag{2.3}$$

where, $A_{m\lambda}$ (unbleached sample), the absorbance of the bR film at the probed wavelength (410 or 570 nm) without actinic light; $A_{m\lambda a}$, the absorbance of the bR film at the presence of the actinic light.

Additionally, the half-time of the M state decay ($\tau_{1/2}$) was measured, i.e. the time to achieve a change of absorbance of 0.5 after turning off the actinic illumination. The kinetics measurements of the absorbance changes were performed using Ocean Optics spectrophotometer HR-2000 which allows the absorbance changes to be measured with milliseconds resolution. This time resolution was enough for measuring the half-time of the M state decay. The decay curve of M_{410} state of the bR film in a gelatin (GE) matrix without chemical additives was fitted into an equation of the form:

$$\Delta A(t) = C + A_0 \exp(-\frac{t}{\tau_1}) + A_1 \exp(-\frac{t}{\tau_2}), \tag{2.4}$$

where A_0, A_1, the relative amplitudes of the time constants τ_0, τ_1, respectively.

The typical kinetics of the decay of the light-induced absorbance changes of the bR film in GE matrix are shown in Figure 2.11. The decay was measured after bR film was illuminated by actinic light for the 100 seconds

in order to achieve a maximum population of the intermediate M_{410} state in the bR-based film.

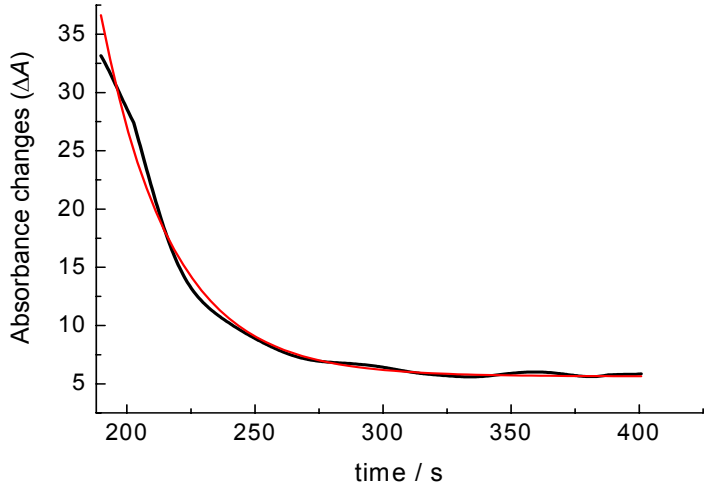

Figure 2.11: black line, typical kinetics of the decay of the light-induced absorbance changes of the bR film, the fluctuations of the signal are caused by noise of the SF and LS; and red line, double exponential fitting.

The measurement of the effects of ammonia concentration on the kinetics properties of bR films was accomplished by introducing inside the sensor chamber an additional optical fibre connected to an actinic light source (LS); or by using a Y-type optical fibre coupler, one channel of which was connected to the probe LS and second was connected to the actinic LS as it is shown in Figure 2.9.

Sensor response (S.R.) was calculated using Equation 2.5:

$$\text{S.R.} = \frac{(A_0 - A)}{A_0} \cdot 100\%, \qquad (2.5)$$

where A_0, the absorbance of the bR film without ammonia and A, the absorbance in the presence of ammonia.

2.2.4 Fibre-optic sensor

In order to examine the possibility of employing bR films as sensitive elements for the fibre-optic sensor (FOS), the bR film was deposited onto the distal end of multimode fibre-optic Y-type couplers (Ocean Optics SPLIT200- UV-VIS) of different core diameters (200 μm, 400 μm and 600 μm). The structure of the optical fibre used in the Y-type coupler is shown in the inset of the Figure 2.12; the core diameter and cladding thickness were 200 μm and 10 μm respectively. The responses of the FOS coated with bR film to variations of ammonia concentration or changes of relative humidity were measured by introducing the distal end of the FOS into the sensor chamber while the other two ends were connected to the LS and SF respectively (Figure 2.12). The principle of operation of this FOS is based on the measurement of the changes induced by the presence of chemical species on reflected light from the bR film. Light from the LS travels along the input fibre to the bR coated distal end, reflects from the fibre-end-film interface and then is transported by the output fibre to the SF. According to the Fresnel's equation (Equation 2.6) any change of the refractive index of film will change the light reflected from the distal end - film interface.

$$R = \left(\frac{n_2 - n_1}{n_2 + n_1}\right)^2, \qquad 2.6$$

where, n_2, refractive index of the fibre; n_1, refractive index of the film; R, reflectance.

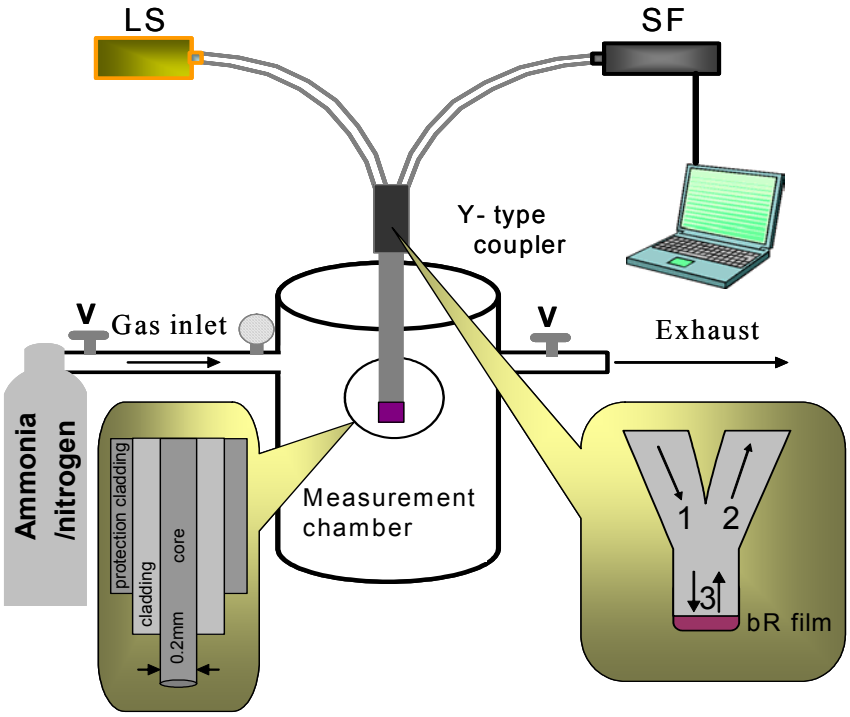

Figure 2.12: Fibre optic sensor coated with bR film. SF, spectrophotometer; LS, light source; 1, input fibre-opic channel; 2, output fibre-optic channel; 3, distal end (optical fibre-bR film interface).

This type of sensor design allows measurements to be performed with the sensitivy given by Equation 2.7.

$$\frac{dR}{dn_1} = -2\frac{n_2 - n_1}{(n_2 + n_1)^2}\left(1 + \frac{n_2 - n_1}{n_2 + n_1}\right), \qquad (2.7)$$

where n_2, refractive index of the fibre; n_1, refractive index of the film; R, reflectance.

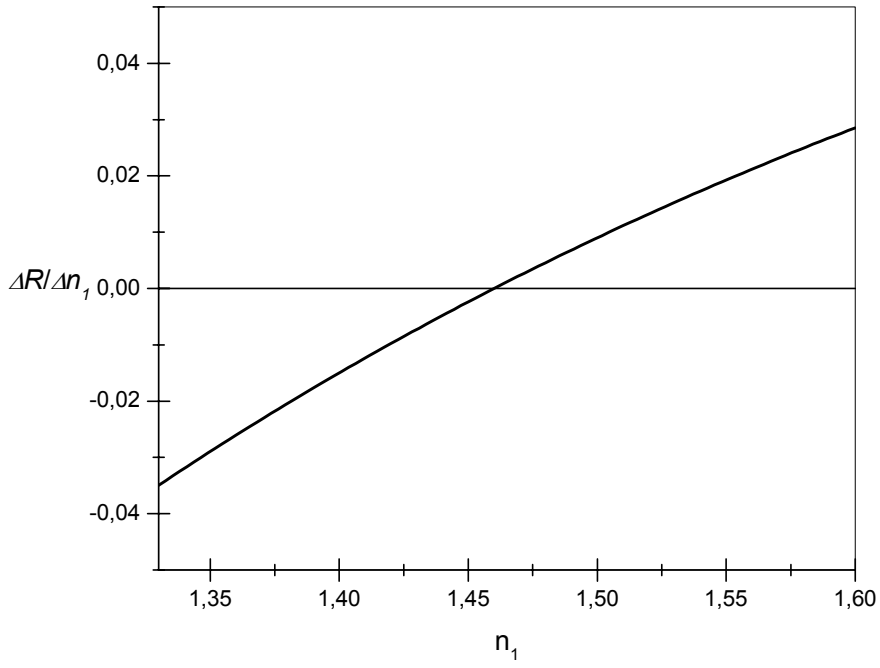

Figure 2.13: Sensor sensitivity; n_1, refractive index of the bR film; R, reflectance.

The concentration of ammonia or relative humidity inside the chamber were varied as described above in section 2.2.1.

As reflected light travels to the photodetector there are two classes of parameter that will influence the signal detected from the sensor. The first includes the parameters of the experimental set-up, associated with light propagation in the optical fibre and light source intensity, which are insensitive to the analyte, but might vary during measurements. Changes of these parameters can be easily accounted, for example, by undertaking a reference measurement.

The second class concerns the parameters associated with the light reflected at the interfaces of the optical fibre and sensitive element and the

sensitive element and surrounding medium. As a rather thick film was deposited on the end of the optical fibre, the detected light will be the sum of the reflections at two interfaces: optical fibre-sensitive element (of-s) and sensitive element-environment (f-e), Figure 2.14.

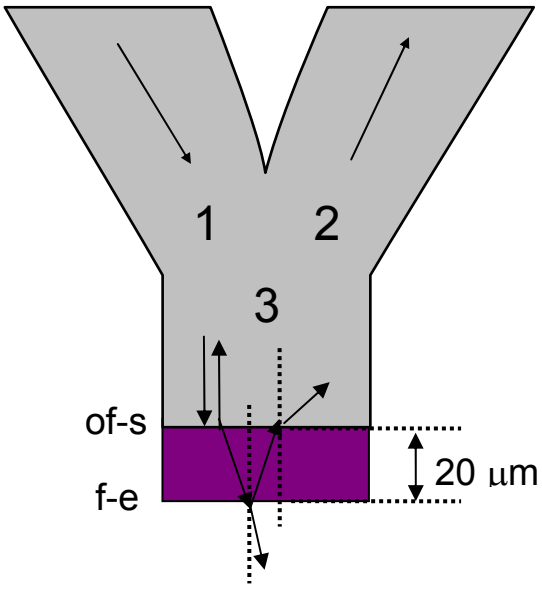

Figure 2.14: Schematic illustration of the light reflections at the optical fibre-sensitive film interface; 1, input fibre-opic channel; 2, output fibre-optic channel; 3, distal end of the fibre-optc sensor coated with bR film; of-s, optical fibre and sensitive element inteface; f-e, film and enviroment interface.

Consequently, the signal received at the detector light will also be influenced by the absorption of the sensitive element. The reflectivity in Equation 2.6 can be written taking into account the complexity of the refractive index, Equation 2.7.

$$\hat{n} = n_0 - ik\,, \tag{2.7}$$

where, n_0, real part of the refractive index; k, imaginary part of the refractive index (coefficient of extinction, shows how much light is absorbed by material).

Thus the sensor response of the fibre-optic sensor is influenced by both refractive index and absorption, with absorption dominating.

Using the techniques described in Chapter 2 allows the creation of bR films with predictable optical and structural properties and this was employed for the development of the sensitive elements based on the bR film for the fibre-optic sensor element. The detailed results of the structural and optical investigations and sensor performances are shown in the next part of this thesis. The results of the influence of the structural parameters on the sensitivity, selectivity and response time of the sensitive element based on bR film will be introduced and discussed in the following part of this thesis.

Chapter 3: Preparation and characterization of the bacteriorhodopsin films

In order to study the possibility of using bR as a sensitive element for optical sensors the film samples were prepared using different techniques and film forming materials. For practical applications, bR embedded into films has been used because it is easy to work with thin materials. Although there is a tendency for the purple membrane fragments to aggregate in the matrix, which can increase the light scattering, this can be decreased through careful fabrication. In this chapter the technological features of the preparation of bR films of different composition are discussed. The influence of the film forming material on the structural properties of the films is studied. Polymer bR films using gelatin (GE) and polyvinyl alcohol (PVA) as a matrix and organic-inorganic composites using the sol-gel method were manufactured. Different conventional techniques for the deposition of the bR films were employed and their impact on the structural parameters of the bR films was studied. Results of the morphological studies and porosity measurements of the different materials used as matrices for the creation of bR based films are shown. Deposition of the bR film onto the distal end of an optical fibre is discussed and demonstrated.

3.1 Preparation of the bR films

3.1.1 Materials

Polymer film samples based on bacteriorhodopsin were prepared using hide gelatin (Sigma) and PVA (Sigma) polymer matrices. Wild-type bacteriorhodopsin (bR) was extracted as purple membrane fragments (pmf) according to standard procedures [133] from *Halobacterium salinarum* strain S9 with the protein/lipid ratio in purple membranes of a 3:1 (molecular weight) and 1:10 (number of molecules) and the lyophilized powder of pmf (WTL025) was purchased from Munich Innovative Biomaterials GmbH (MIB). The chemical additives triethanolamine (TEA) and dodecyltrimethylammonium bromide (DTMAB) were purchased form Sigma and used without further purification.

3.1.2 Preparation of the polymer bR based films

Bacteriorhodopsin films in polymer matrices were prepared using the standard procedures [134–136]. A suspension of pmf (14 mg lyophilized powder / mL) was prepared by soaking it for 20 minutes and then stirring for 6 hours in tri-distilled water. Solutions of the polymers of PVA and GE were obtained by soaking GE and PVA powder in the tri-distilled water for 20 minutes before heating and stirring the mixtures at 60 ^{o}C for 40 minutes to obtain the GE and PVA solutions of 6% weight/volume (w/v). The film-forming solution, a mixture of bR and GE or PVA was prepared from 0.168 mL of the bR suspension, of 14 mg/mL; and 0.248 mL of the 6% w/v GE

or PVA and tri-distilled water solutions to give a final volume of the film-forming solution of 0.5 mL.

Using PVA and GE as the base materials for the incorporation of bR into a polymer film allowed the creation of uniform bR films with high quality optical properties, defined and determined in terms of the ratio of the absorbance at 280 nm to the absorbance value at 570 nm which should have a value < 2.5 [137]. This ratio signifies that the film displays high transparency and low light scattering, see Chapter 4, Figure 4.1.

The inclusion of some chemical additives, in various combinations, into the films was used to modify the photosensitivities and temporal characteristics of the photocycle of the sensitive elements over wide ranges of values. The additives provided the possibility to enhance the chemical sensitivity and selectivity of the bR films. The amine-containing substances triethanolamine (TEA) (Sigma) and dodecyltrimethylammonium bromide (DTMAB) (Sigma) in combination with halogen containing organic compounds were used as photosensitizing chemical additives. The halogen-containing organic compounds comprised the ethyl and methyl functional groups along with chlorine, bromine and iodine. A 0.4 M aqueous solution of TEA was added to the film-forming suspension to give a TEA : bR molar ratio of 250:1 (which previously had been found to give maximal photosensitivity [115]). The concentration of the DTMAB was of the order of 0.01 M.

The mixtures of purple membrane fragments suspension, GE and chemical additives solutions in the appropriate ratio were stirred for 20–30 minutes using a magnetic stirrer, while placed in a desiccator from which the air was exhausted.

After the preparation of a film-forming solution, the different coating techniques were employed for the deposition of films onto glass substrates

and optical fibre distal ends. The casting, formation and spin coating methods were used for the deposition of the films onto glass substrates in order to obtain films with different thickness and optical properties.

3.1.3 Casting method

Casting provides a simple method of bR film preparation, while allowing the creation of uniform films of high optical quality. The casting method is based on the placing of a drop of the film-forming solution onto a horizontally fixed cleaned glass substrate (Figure 3.1). After deposition of a drop of solution the film that was formed was dried through evaporation of water for 24 hours using a desiccator to increase the evaporation rate of water from the sample.

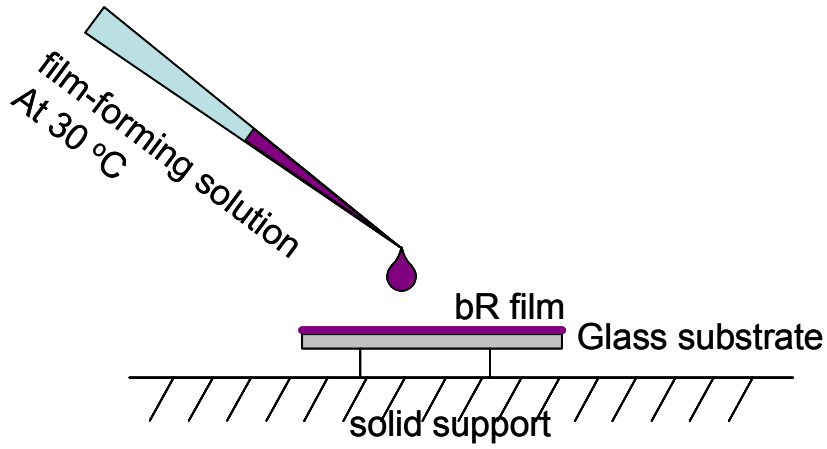

Figure 3.1: Schematic diagram of the casting method of bR film preparation.

The thickness of the film deposited when using this method can be controlled by volume of the drop that is placed on the glass substrate. For example, 0.225 mL of film-forming solution deposited onto a 6.25 cm^2

glass substrates produce a film of approximately 20 μm thickness. Similarly, 10 μL deposited onto the distal end of a 200 μm diameter optical fibres produce a film of approximately the same thickness. In general, the thickness of the bR films prepared by this method occurred in the range of 20–40 μm. The thickness of the individual films can then be measured accurately using SEM and optical interferometric method. The concentration of bR in such dry films occur within the range of 12–20% by weight.

For the SEM and AFM measurements samples of the bR films in the polymeric matrix were deposited onto 25 mm^2 glass substrate that fit the sample holder of the AFM and SEM instruments. Before SEM measurements the bR samples were coated with thin (5 nm) platinum film to allow a discharge of the sample surface during interaction with the electronic beam.

3.1.4 Formation method

The deposition of the bR films by the so-called "formation" method was accomplished by introducing the heated (up to 30 ^oC) film-forming solution between two glass plates separated by small gap (Figure 3.2) [135]. The gap between glass plates was set by using metallic rods of the known diameter as spacers. The surface of one of the glass plates was made hydrophobic by soaking it in a 50% solution of the dimethyldichlorsilane in benzol, followed by drying in the oven at 100 ^oC for 1 hour. This was to ensure that the film forming solution would not adhere to the glass plate with the hydrophobic surface. The heated film-forming solution easily filled the gap between the plates due to capillary forces. After drying for 1

hour the glass cover plate with the hydrophobic surface was removed and the film was then dried in a desiccator for 24 hours at room temperature.

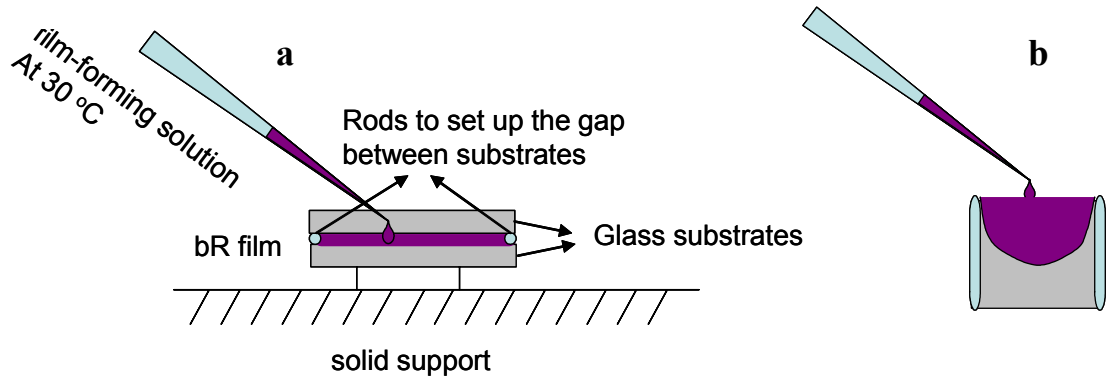

Figure 3.2: Schematic diagram of the preparation of bR film by formation method in the gap between two glass substrates; a, elevation; b, plan.

The thicknesses of the bR films produced by this method were in the range of 50–100 μm, which depended on the diameter of the metallic rods used to separate the glass plates.

Uniform and smooth bR films with well controlled thicknesses and high optical qualities were manufactured using this method.

3.1.5 Spin coating method

The spin coating technique is an alternative and versatile method for producing thin film samples with thicknesses ranging in the micrometer dimensions. The film thickness deposited by means of spin coating methods depends on the spinning speed, and the viscosity and volume of the solution applied. The spin coating method starts with the deposition of a

small drop of the solution onto the substrate and then the substrate is spun with the solution at a high rate (Figure 3.3).

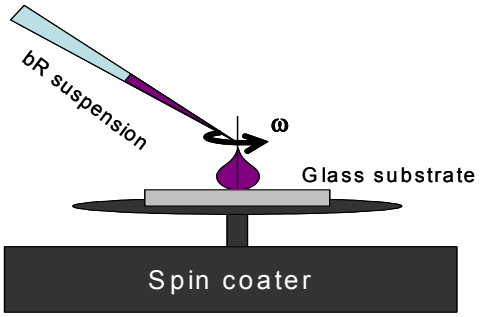

Figure 3.3: Basic principle of the spin-coating method of the bR film deposition onto glass substrate.

Bacteriorhodopsin films were obtained by the deposition of 10 μL of the prepared film-forming solution onto a glass substrate and spinning it at different rates. Films of different thicknesses were manufactured by spinning the substrate at the 750, 1 000 and 1 500 rpm (revolutions per minute). The film thicknesses were determined from SEM measurements by studying the bR film cross sections (Figure 3.4). Films with thickness of 619 nm, 538 nm and 524 nm were produced using the spinning rates of 750, 1 000 and 1 500 rpm respectively, by placing the same volume of the film-forming solution onto the spinning substrate in each case. For the purposes of illustration typical optical spectra of the bR films in a gelatin matrix are presented in Figure 3.5. It can be observed that different film thicknesses cause different optical absorbance of the bR at the 570 nm wavelength. This will be discussed in more details in Chapter 4.

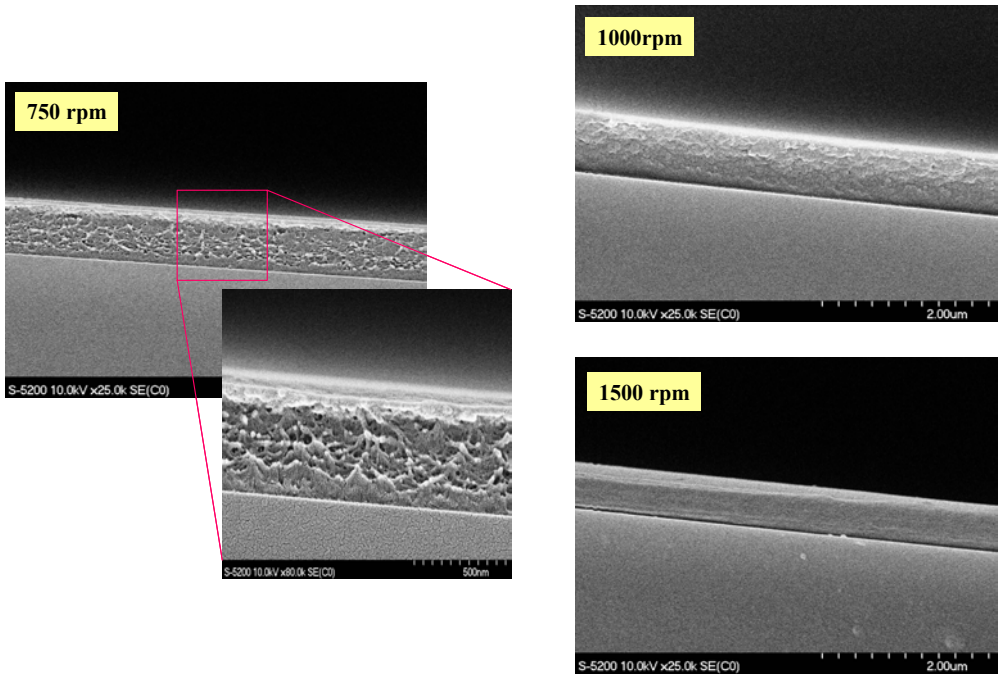

Figure 3.4: Cross-section of the bR films deposited onto glass substrate by spin coating method at different spinning rate.

Employing the casting and formation methods of film deposition as described in this Chapter allows films with uniform thickness distributions over the entire area of the samples to be manufactured; see Figure 3.11. Thin bR films prepared by the spin-coating method have a slightly greater thickness at the edges of the glass substrate. However, this thickness heterogeneity can be neglected in the optical measurements because the diameters of the probe and actinic light beam were smaller then the area of the thickness heterogeneity.

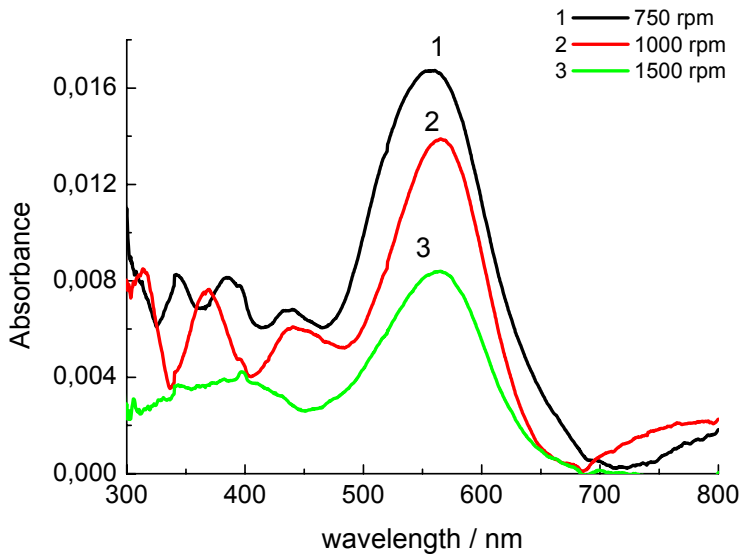

Figure 3.5: Optical spectra of the bR films deposited onto glass substrate by spin coating method at different spin rate; black line 1, 750 rpm; red line 2, 1 000 rpm; green line 3, 1 500 rpm (mass ratio bR : GE = 12.5 : 87.5).

3.2 Incorporation of bacteriorhodopsin into sol-gel matrix

A drawback of using certain polymer matrices is their solubility in water, which makes it impossible to use such sensing elements for the monitoring of aqueous media. The encapsulation of bR into a transparent, water insoluble matrix should overcome this disadvantage, provided a bR-compatible material of adequate optical quality can be found.

The sol-gel process is a convenient and versatile method for the preparation of optically transparent and water insoluble matrices at moderate temperatures [138]. Ambient processing conditions enable composite optical materials to be created with numerous organic, organometallic and biological molecules embedded within a porous matrix of sol-gel glass [139]. Most sol-gel techniques use water and low molecular weight

alkoxides such as tetraethoxysilane (TEOS) and tetramethoxysilane (TMOS) as sol-gel precursors.

The chemical reaction of the sol-gel process can be described as follows:

Hydrolysis: $M(OR)_n + nH_2O \longrightarrow M(OH)_n + nR(OH)$ (1)

and polycondensation: $pM(OH)_n \longrightarrow pMO_{n/2} + (pn/2)H_2O$, (2)

where M, a metal and R, an alkyl radical

When a silicon oxide is used as a precursor a catalyst is required because SiO_2 is not very reactive and the unaided polymerization process can take weeks to complete. The hydrolysis reaction can be promoted by acid catalysis while the condensation reaction can be accelerated by basic catalysis [140].

Hydrolysis and condensation of tetra-alkoxysilanes during the sol-gel process help to form a solid silicate matrix around the sensing molecules which are dissolved in the liquid phase [141].

Bacteriorhodopsin retains its characteristic optical properties when entrapped in a silicate glass by the sol-gel process [142, 143], and therefore this process could be used for the manufacture of sensing elements for the envisaged biosensor application [120]. The preparation of dry films based on bR of high optical quality will considerably enhance the application of bR for producing sensitive elements of integrated optic and fibre-optic sensors.

3.2.1 Sample preparation

Different bR films embedded into sol-gel matrices were manufactured in order to investigate the effect of the film chemical composition, thickness and structure on the sensitivity and selectivity of these films towards ammonia and relative humidity.

Tetraethoxysilane (TEOS) (Fluka Company, Switzerland) was used as a precursor for the sol-gel glass. The sol-gel glass was prepared using slightly modified methods described by Weetall et al. [142]. Utilising this method, 7 mL TEOS, 3.0 mL of distilled water and 0.1 mL of 0.04 M HCl were mixed together and sonicated for 20 minutes. The resulting product was diluted with an equal volume of distilled water. A 0.5 mL sample of this solution was mixed with 0.25 mL sodium borate buffer solution (pH 9) and 0.1 mL or 0.2 mL bR solution (14 pmf mg/mL) in turn to create film-forming solutions with different bR concentrations.

For the preparation of chemically modified films, bR solution was mixed with TEA and DTMAB, before mixing with the sol-gel mixture, and afterwards 0.02 mL of the bR-chemical additives mixture was added to 0.12 mL of the sol-gel mixture.

The creation of 20 μm thick pure sol-gel films and films of bR in the sol-gel matrix was accomplished by depositing a 0.1 mL of the film-forming mixture onto 5 cm^2 glass substrates. The films were dried in a refrigerator at 4 ^oC for 24 hours.

Additionally, thin films, with thicknesses < 1 μm, were prepared by the spin-coating methods, by depositing a drop of the film-forming mixture, with a volume of approximately 10 μL, onto a glass substrate that was rotating at 2 500 rpm.

3.2.2 Structural and optical features of the bR films in sol-gel matrix

The surfaces of the pure TEOS films prepared by the casting method are uniform and possess a low roughness of 0.586 nm (Figure 3.6), for details see Appendix A, Figure A1. Incorporation of bR into the TEOS sol-gel matrix considerably increases the film surface roughness up to 37.3 nm (Figure 3.7), for details see Appendix A, Figure A2. It has been assumed that the increase in roughness is due to the aggregation of fragments of bR purple membranes to form bR conglomerates. The deposition of sol-gel films onto the glass substrate by the spin-coating method could improve the optical quality of the films.

Cross-sectional study of the sol-gel films showed that they have the grain structure suggesting the strongly developed micro- and mesoporosity (Figure 3.8 and 3.9). This was later confirmed with the porosity measurements (Table 3.1, section 3.4). This suggests that during the adsorption of detected vapours of chemical species not only the surface but the entire film volume of the sensing element will be involved, thereby considerably enhancing the efficacy of the sensor operation. The thickness of films deposited by formation and drying was 10–20 μm (Figure 3.8 and 3.9), and of films deposited by spin-coating < 1 μm (not shown).

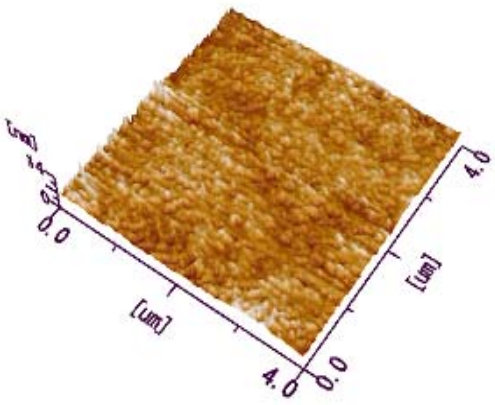

Figure 3.6: AFM image of the surface morphology of a pure TEOS sol-gel matrix, prepared by the casting method and drying.

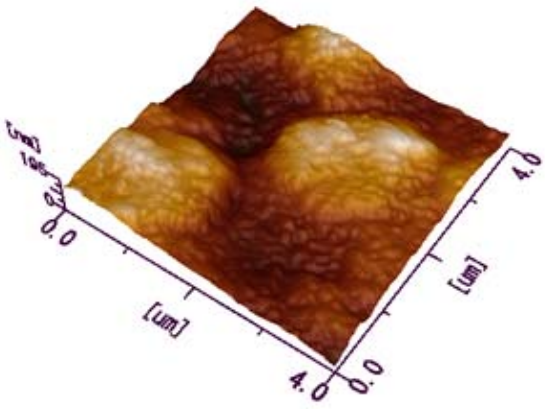

Figure 3.7: AFM image of the surface morphology of films incorporating bacteriorhodopsin in a TEOS sol-gel matrix, prepared by the casting method and drying (mass ratio bR : TEOS = 5.5 : 94.5).

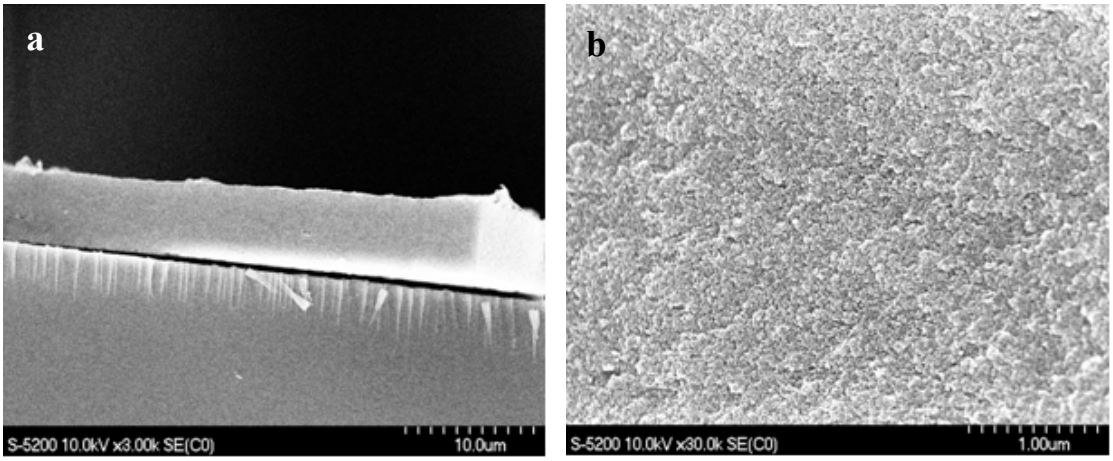

Figure 3.8: SEM images of the cross section of a TEOS sol-gel matrix, prepared by casting method; a, scale 10μm; b, scale 1 μm.

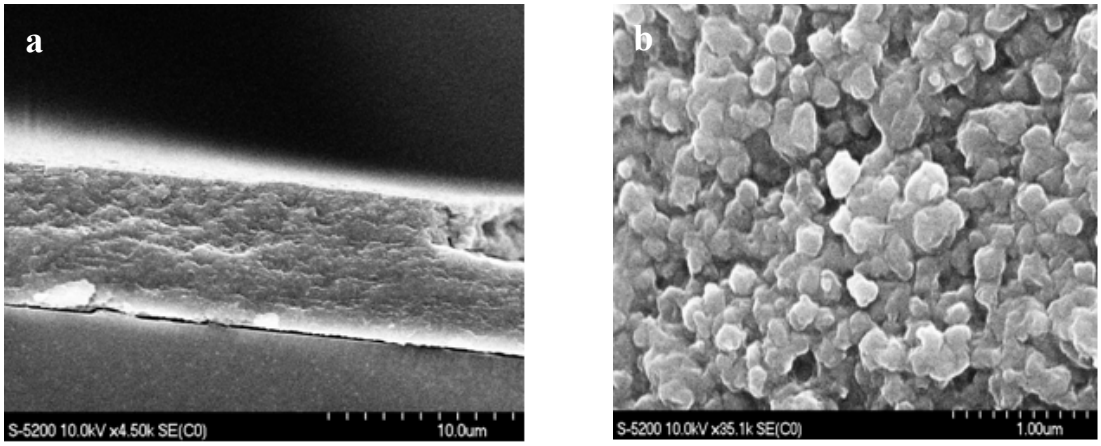

Figure 3.9: SEM images of the cross section of films based on bR in a TEOS sol-gel matrix, prepared by casting method; a, scale 10 μm; b, scale 1 μm (mass ratio bR : TEOS = 5.5 : 94.5).

The optical absorption spectra of films based on bR in a sol-gel matrix with different bR concentrations is shown in Figure 3.10. The characteristic absorption maxima proved that in the dry sol-gel film the bR retains its optical properties and its structure and is not denatured.

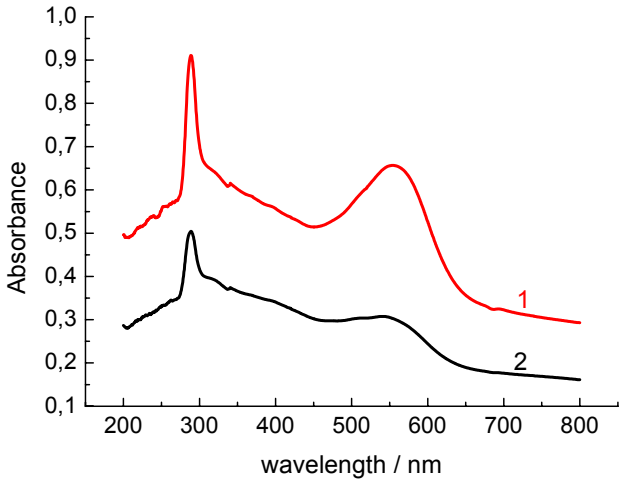

Figure 3.10: Absorption spectra of films based on bR in sol-gel matrix; line 1, mass ratio bR : TEOS = 5.5 : 94.5; line 2, bR : TEOS = 2.25 : 97.75.

The line 1 of Figure 3.10 indicates that preparing films with higher bR concentration still provides a film with sufficient optical quality; i.e. light scattering is relatively low as indicated by the high absorbance.

3.3 Morphologic and cross-section study of the bR films

The morphology of the surface and cross-sections of the bacteriorhodopsin-based films in polymer matrices were studied using a Hitachi S-5200 scanning electron microscope and Jeol JSPM-5210 atomic force microscope. The bacteriorhodopsin films in gelatin matrix (Figure 3.11a, b) obtained by the casting method have a uniform structure characterized by purple membrane fragments with an average diameter of 0.5 μm and a thickness of 5 nm evenly stacked practically parallel to the substrate surface.

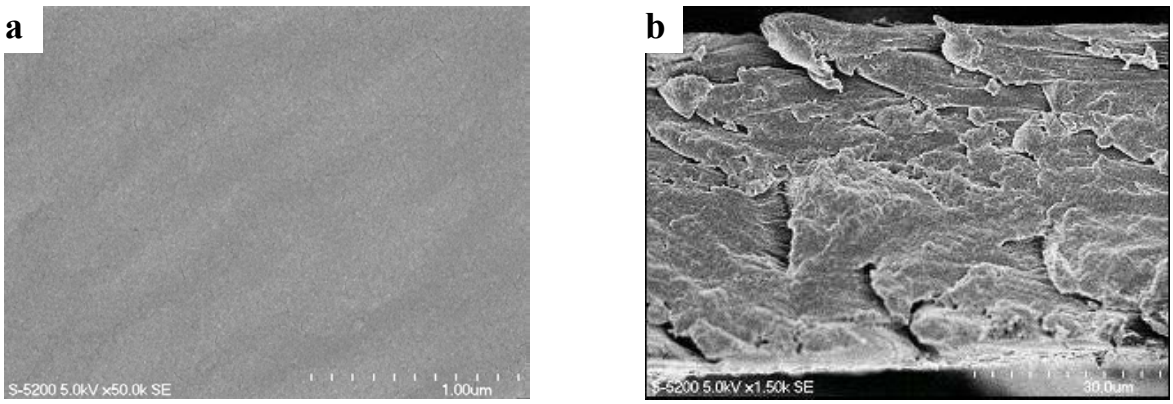

Figure 3.11: SEM pictures of: a, surface morphology; and b, cross section of films based on bR in a gelatin matrix prepared by casting method (mass ratio bR : GE = 12.5 : 87.5).

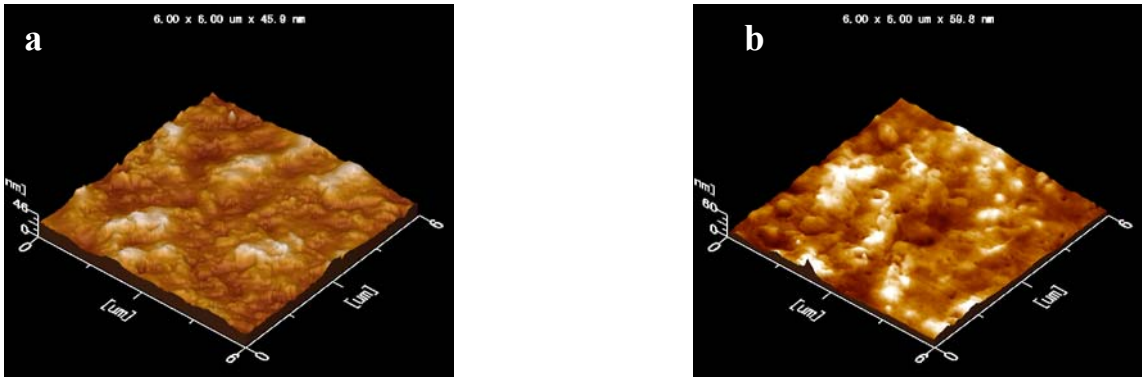

Figure 3.12: AFM images surface morphology of: a, films based on bacteriorhodopsin in: a, a GE matrix; and b, a PVA matrix (mass ratio bR : GE (PVA) = 12.5 : 87.5).

Morphology of the bR films in GE and PVA matrices are shown in Figure 3.12. The surface roughness of films based on bacteriorhodopsin is 3.46 nm and 3.10 nm for the GE (Figure 3.12a) and PVA (Figure 3.12b) matrices, respectively, for details see Appendix A, Figures A3, A4.

Morphological features of the GE film and bR embedded into GE matrix deposited by spin coating technique are shown in Figure 3.13a, b.

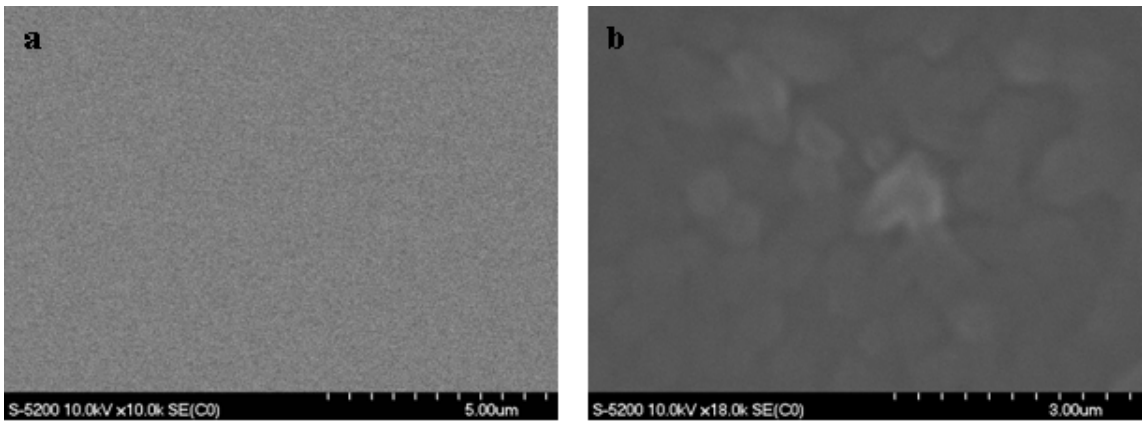

Figure 3.13: SEM images of the surface morphology of the GE and bR film in GE matrix deposited by spin coating at 750 rpm; a, GE film; b, bR embedded into GE matrix (mass ratio bR : GE (PVA) = 12.5 : 87.5).

Bacteriorhodopsin is uniformly distributed in the gelatin matrix (Figure 3.13). The uniform distribution of the bR in the GE matrix was confirmed by measurements of the distribution of the chemical elements using EDS. Figure 3.14 shows the distribution of the chemical elements in the bR film in gelatin matrix with the chemical additives containing bromine (Br) manufactured using the formation method.

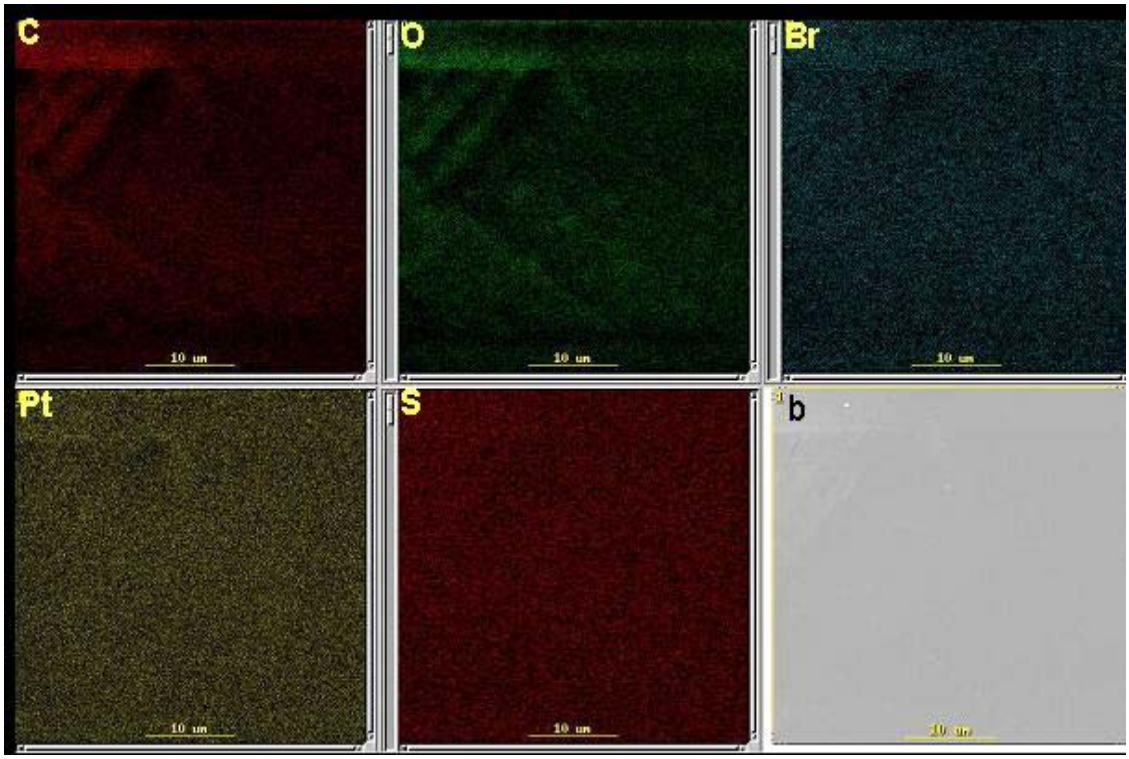

Figure 3.14: Elemental distribution image (mapping) (25 kV, 512x512, 20 s) of the bR film in the GE matrix with the chemical additives containing bromine (Br) (DTMAB - $C_{15}H_{34}N^{-}Br^{+}$) manufactured using the formation method (thickness ca. 50–100 μm); The elemental distribution in the bR film was acquired using the acceleration voltage of 25 kV in raster mode and with magnification of 3 000, from the film surface of 150 μm^2; Along with the bromine (Br), carbon (C), oxygen (O), platinum (PT) and sulphur (S) have been detected; b, SEM image of the bR film surface.

The elemental distribution in the bR film was acquired using an acceleration voltage of 25 kV in raster mode and with a magnification of 3 000, from the film surface of 150 μm^2. The distribution of the bromine was used for the determination of the distribution of the bR in the film. Along with the bromine, carbon, oxygen, platinum and sulphur have been detected. Before the EDS and SEM measurements the film was coated with the 5 nm thin film of Pt in order to reduce the surface charge. These results confirmed that the formation method provides films with a uniform distribution of bR and chemical additives in the GE matrix.

On the other hand, when bR is incorporated into GE matrix the surface roughness increases from a 0.383 nm up to 8.40 nm (Figure 3.15), for details see Appendix A, Figures A5 and A6.

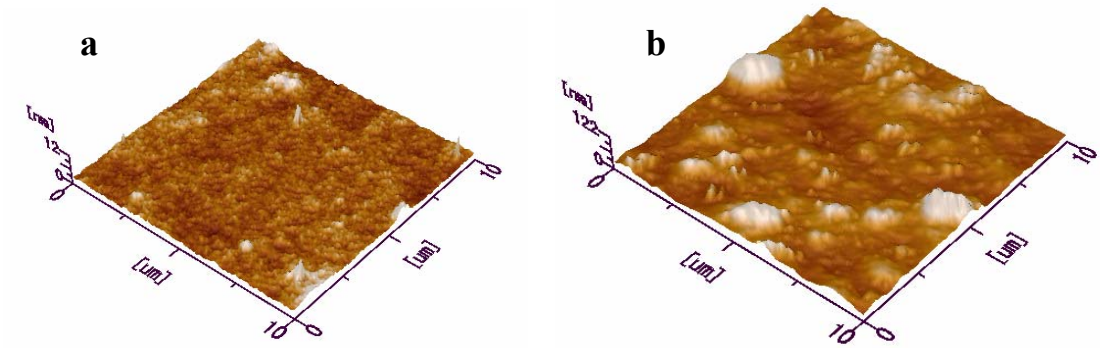

Figure 3.15: AFM images of the surface roughness of the GE and bR film in GE matrix deposited by spin coating at 750 rpm; a, a pure GE film; b, bR embedded into GE matrix, for details see Appendix A, Figures A5 and A6 (mass ratio bR : GE = 12.5 : 87.5).

Cross-section of the GE films and bR in GE matrix are shown in Figure 3.16. The film based on bR in a GE matrix shows a higher porosity

compared to the GE film. This is because of incorporation of big fragments of the purple membranes into gelatin polymer structure during the deposition.

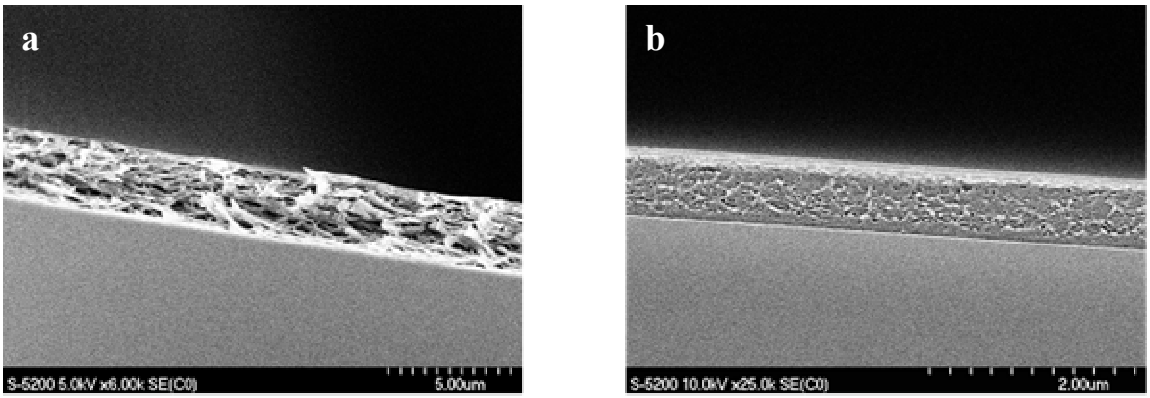

Figure 3.16: SEM images of the cross section of the GE and bR film in GE matrix deposited by spin coating at 750 rpm; a, bR embedded into GE matrix (mass ratio bR : GE = 12.5 : 87.5); b, GE film.

Results of the morphological and cross-sectional studies of the bR polymer films showed that bR is uniformly distributed within the films and that the films have some degree of porosity. The surface roughness is bigger for the films deposited by means of spin coating when compared to the films obtained by casting method. There are no significant differences in the film's structure when comparing the GE or PVA matrices. Both of these polymers produce uniform films with the possibility of precise thickness control.

3.4 Matrix porosity of the bR films

Porosities of the materials used as matrices for the creation of the bR based films were measured using a "Sorptomatic 1990". The PVA, GE films were

prepared by the casting method, described in section 3.1.1 in order to obtain a sufficient quantity of film samples. Briefly, the film-forming solution of the PVA and GE were placed onto a glass substrate treated to produce a hydrophobic surface (81 cm^2). After drying in a desiccator for 24 hours the film was removed from the hydrophobic glass substrate and cut into pieces of 0.25 cm^2 in order to fit the "Sorptomatic 1990" sample holder. At least two grams mass of the films were used for the porosity measurements by the gas adsorption technique.

It is known [140] that using different conditions for the sol-gel process can influence the porosity of the resulting glass; e.g. temperature, pressure and the catalyst utilized for the sol-gel reaction. Sol-gel glass samples were prepared using different catalyst in order to ascertain which catalyst produced the sample with the highest porosity.

The film samples were weighed and pre-treated by degassing to produce a completely clean sample surface and so provide reliable and reproducible measurements. The cleaned samples were then placed inside the sample holder. Degassing was accomplished under conditions of high vacuum and a temperature of 50 ^oC for 24 hours. Helium was used for the base readings and calibration of the dead volume within the "Sorptomatic 1990".

The typical adsorption isotherm of the sol-gel glass measured by adsorption and desorption of the nitrogen is shown in the Figure 3.17. The behaviour of this adsorption isotherm is well described by the BET model. The small hysteresis that is observed in the process of the gas adsorption and desorption can be explained by the capillary condensation of the adsorbate in the mesopores of the sol-glass.

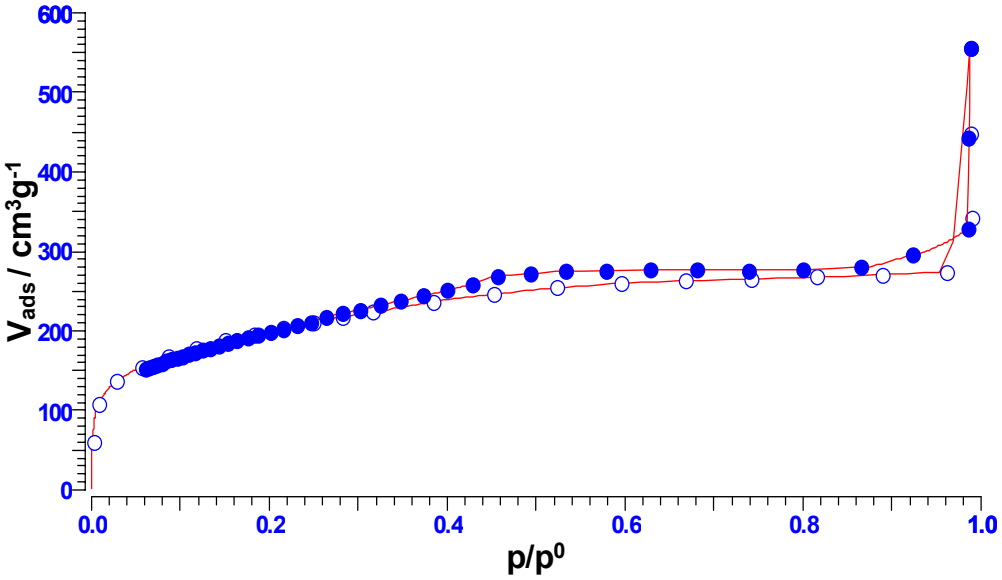

Figure 3.17: Adsorption isotherm of the sol-gel (TEOS) glass with acid catalyst; closed symbols, adsorption part of the adsorption isotherm; open symbols, desorption part of the adsorption isotherm.

The values of specific surface area calculated by the B.E.T method, for the sol-gel samples prepared at the same external conditions using the (i) HCl, (ii) H_2O and (iii) HCl+Na_2B_4 as a catalysts were 584.4, 676.6 and 544,8 m^2/g respectively.

The pore sizes distribution was determined by the method of nitrogen desorption using the B.J.H model. The spectrum of the pores sizes in the sol-gel glass sample is shown in Figure 3.18. The pore sizes are in the range of the 0–1.5 nm and 1.5–5 nm, indicating that the sol-gel glass possesses a well developed micro- and mesoporosity structure.

The summary of the results of the surface area and pore size distributions in the polymeric films and the sol-gel glass are shown in the Table 3.1. The porosities of the sol-gel glass films are greater than for the polymeric films. Additionally, the specific surface areas of the sol-gel glass and GE films are greater than for PVA films. Consequently, using the sol-gel and gelatin

matrices for the incorporation of the bR is preferable due to their higher porosities. This higher porosity allows chemical analytes to penetrate and interact with the bR inside the entire film volume, thus increasing the effectiveness of the sensor response.

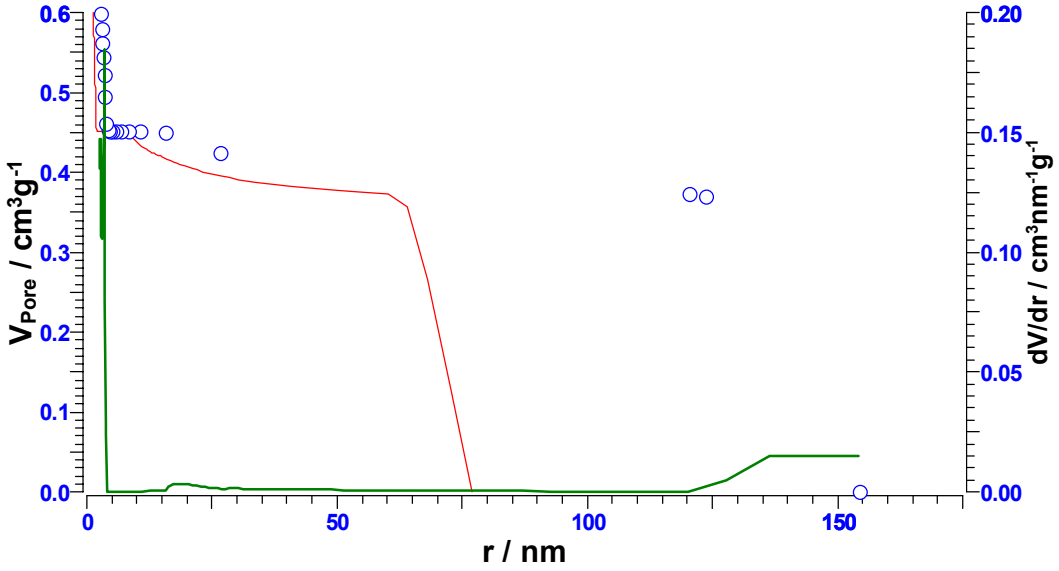

Figure 3.18: Pore size distribution in the (TEOS) sol-gel glass.

Table 3.1: Specific surface area value and pore size distribution.

Sample name	Specific surface area, m^2/g, BET	Pore specific volume, cm^3/g	Specific surface area, m^2/g, BJH	Pore classes		
				From (nm)	To (nm)	A (%)
Gelatin film	2.6	0.003	3.45	0	1.5	13.9
				1.5	3	41.9
				3	5	8.9
				10	50	32.0
PVA film	1.7	0.001	2.93	0	1.5	15.5
				1.5	3	44.5
				3	5	13.9
				10	50	22.1
Sol-gel films	676.6	0.519	—	0	1.5	17.9
				1.5	3	58.9
				3	5	13.9

3.5 Deposition of the bR films on the optical fibre end face

It was confirmed from the structural investigations that the casting method provided the most convenient method for the creation of the bR films with both a uniform bR distribution within the matrix and a high optical quality. Consequently, this method was employed for the coating of the distal ends of the fibre-optic sensors with the bR film in gelatin matrix. Optical spectra were monitored in real time during the deposition of the bR film-forming solution onto the optical fibre distal end. Figures 3.19a and b show the dynamic changes of the optical absorbance monitored at 410 and 570 nm when a 10 μL drop of the bR film-forming solution was placed onto distal end of 600 μm in diameter of a Y-type coupler. The optical spectra were recorded every second using an Ocean Optics HR-2000 spectrophotometer (SF). Deposition of the bR film was accomplished at temperature of 25 ^{o}C and relative humidity of 50%.

A 10 μL quantity of the film-forming solution of the bR and gelatin was placed onto optical fibre at a time 261 second after the start of the measurement process and so the signal from 0 sec to 261 seconds corresponds to the contact of the fibre end face with air, see Figure 3.19a.

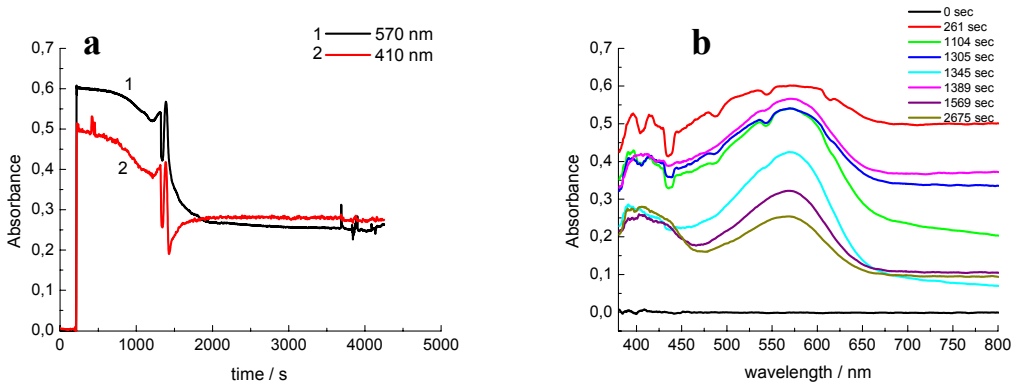

Figure 3.19: Deposition of the bR onto optical fibre distal end; a, recorded in real time: black line 1, 570; and red line 2, 410 nm; and b, spectral changes during drying of the film-forming solution (for explanation see text).

When the bR film-forming solution was placed onto the fibre end the signal changed dramatically as the drop of the film-forming solution is formed on the optical fibre end. During drying, the geometry of the drop changed which corresponds to the change of absorbance signal at both wavelengths 570 and 410 nm. Finally, at the time 1 300 seconds sudden sequential changes are observed, which are associated with the complete evaporation of the water contained within the drop and the formation of the dry bR film. The further change in absorbance signal corresponds to the photoinduced transition of the bR molecules from the bR_{570} ground state to the M_{410} state (light adaptation, see Chapter 4, section 4.1). This can be confirmed from the decreasing absorbance signal at 570 nm after about 1 300 seconds and the formation of an absorbance band at 410 nm. As the final step, the dry uniform bR film is created on the optical fibre distal end. In Figure 3.20 the optical image of the bR film coated optical fibre is demonstrated.

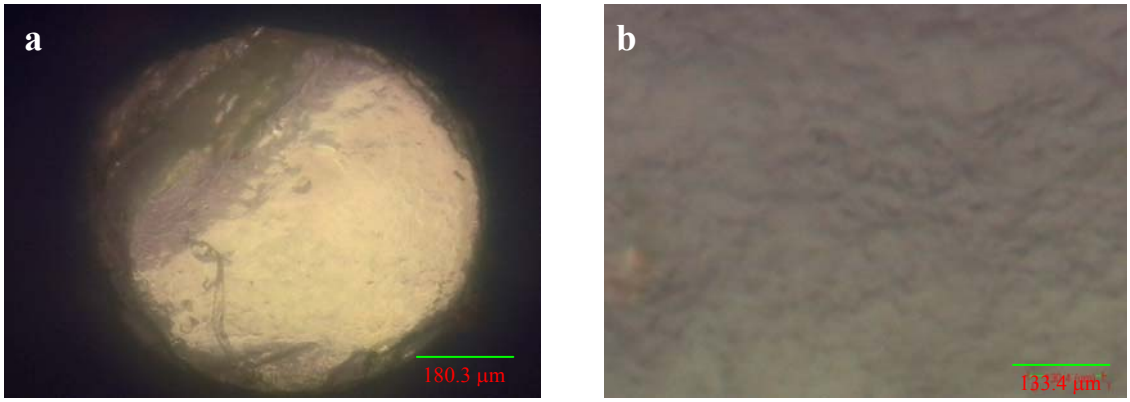

Figure 3.20: Optical images of the optical fibre of 600 µm in diameter coated with bR film by the casting method: a, magnification 10 times; b, magnification 200 times.

In order to assess the dependence of the sensitivity of the bR films on the concentration of bR in the gelatin matrix, bR films with different concentrations of bR were deposited onto fibre optic distal ends. Figure 3.21 shows the absorbance spectra of bR films with different concentrations of bR. Additionally, the spectra of a GE film without bR and bR film without GE matrix are shown. The concentration of the bR was changed by changing the bR concentration in the film-forming solution and was calculated as a weight % of bR and GE in the dry film.

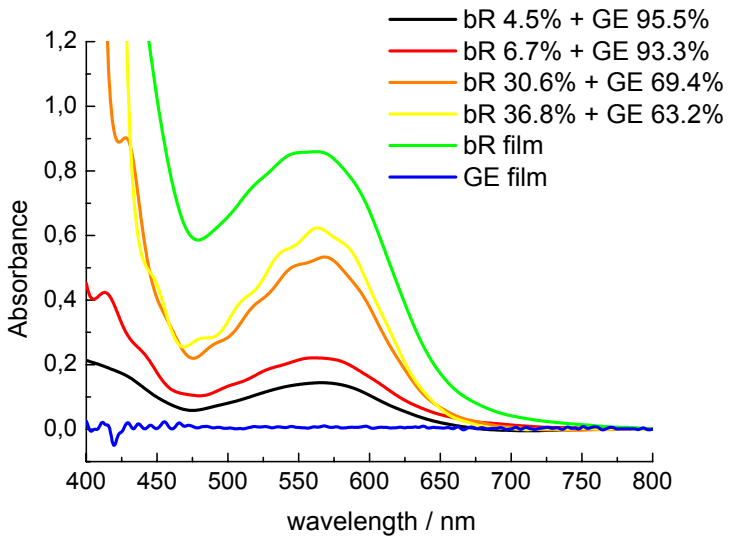

Figures 3.21: Absorbance spectra of the bR films with different concentration of bR deposited onto fibre optic distal end (concentration of the bR is in a weight % of the bR and GE in the dry film).

Dependence of the drying time (time needed for the complete formation of the dry film) on the bR concentration was also investigated. Regardless of the bR concentration in the GE, the drying time at the room conditions 25^{o}C and 50% rH was within 2 000 seconds.

Conclusions and Summary:

In this Chapter the methods used for the preparation of the bR based films were introduced. The impact of the technological features and film-forming material used for the film preparation were investigated. Samples with different chemical compositions were prepared for application as sensitive elements for the development of fibre-optic sensors. Results of the morphological studies and porosity measurements of the different materials used as matrices for the creation of bR based films showed that:

- films prepared from the sol-gel glass had the highest porosity;
- films prepared employing the casting method and GE as a film-forming material created uniform bR based films of high optical quality;
- film structures for the GE or PVA matrices were similar but the porosity of the GE films was slightly bigger;
- using the polymer materials (GE and PVA) allowed the manufacture of bR films with high optical quality ($A_{280}/A_{570} < 2.5$) to be obtained, on the other hand using the sol-gel matrix due to aggregation of the purple membrane fragments with silica particles produced film with high light scattering ($2.5 < A_{280}/A_{570} < 4.2$);

Bacteriorhodopsin films in a gelatin matrix with different bR concentration were deposited onto the distal ends of the optical fibres as a first step for the creation the fibre-optic sensor.

In the next Chapter the optical features of the created bR films will be investigated and discussed. The effects of the matrix materials and the chemical additives used for the bR film manufacturing on the optical properties of the bR photocycle will be demonstrated.

Chapter 4: Optical parameters of the bacteriorhodopsin films

In this chapter the optical parameters: photo-induced absorbance changes (ΔA) and half-life ($\tau_{1/2}$) of the intermediate M_{410} state of the bR films will be introduced and discussed. Differences in the photocycle behaviours between bR aqueous solution and bR films will be explained and analyzed. The kinetic models which simulate the behaviours of the bR photocycle in the bR aqueous solution and bR films will be demonstrated. The influence of the sensor element matrix and chemical additives on the optical parameters of the bR photocycle will be shown. The dependence of the kinetics of the photo-induced changes in the bR photocycle on the intensity of the actinic light source will be demonstrated.

4.1 Optical characteristics of the photocycle of the bR films

Bacteriorhodopsin has a characteristic absorbance peak at 570 nm which is attributed to the retinal chromophore covalently bound to the apoprotein of the bR molecule through a protonated Schiff base linkage. Incorporation of the bR into the polymeric matrix of the sensor element does not change the wavelength of the absorption maxima, implying retention of the bR photo-activity in the polymeric matrix. The optical absorption spectra of the bR solutions and films based on the bR in the polymer matrices are shown in Figure 4.1. In the dry bR films a small shift of the absorbance peak into the blue region is observed as compared to the bR solution. This shift of the absorbance peak is attributed to the removal of the water molecule which is located close to the Schiff base linkage and which plays a very important role in the bR function. The proton covalently bounded at the Schiff base of the chromophore due to dehydration of the bR molecule is removed and the configuration of the retinal moiety is changed [144, 145].

In the unexcited state (unbleached state, i.e. without actinic light) bR can exist in two states, dark adapted (bR_{550}) and light adapted (bR_{570}), distinguished by their absorption maxima [146]. In the dark adapted state 50 to 60% of the bR molecules have there retinal in the 13-*cis* form; while in the light adapted state 100% have the all-*trans* form [147–149].

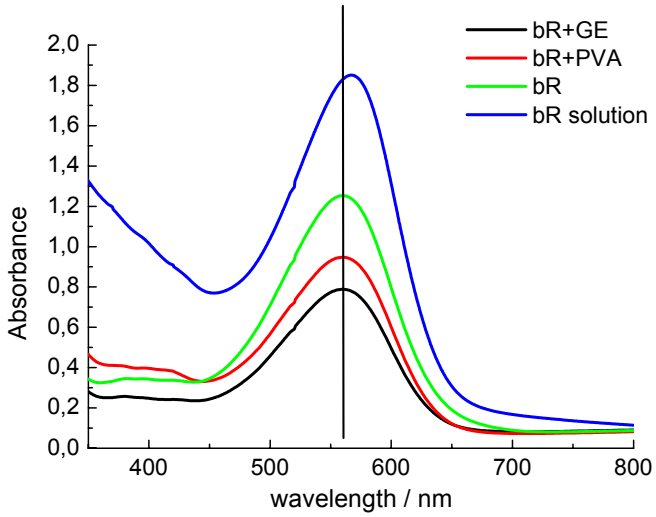

Figure 4.1: Optical absorption spectra of the bR aqueous solution (14 mg/mL) and bR film in polymer matrices (mass ratio bR : GE (PVA) = 12.5 : 84.5) manufactured by casting method.

In this thesis all measurements were conducted with the light adapted bR films. Light adaptation of the bR film samples deposited on the glass plates was performed by exposing them to the ambient light for 5 minutes. The bR films deposited on the optical fibre were light adapted by turning on the probe light source connected to the input fibre optic channel of the fibre optic Y-type coupler, for more details see Chapter 2 section 2.2. The measurements of the ammonia and relative humidity effect were carried out after recording the base line, i.e. when the bR molecules were in steady state and no more absorbance changes in the bR film were observed through light adaptation.

Upon exposure to the light from the actinic light source the proton transport in the bR molecule in its native environment commences and this is accompanied with the series of the conformational changes of the retinal chromophore by passing through spectroscopically distinct intermediates.

The series of these photochemical reactions is called a photocycle. After adsorption of the light quantum bR is in an excited state and thermally reverts to its initial state. Figure 4.2 shows the generally accepted scheme of the photocycle of the bR molecule indicating the absorption maxima of the bR intermediates and branched pathway [74, 85].

During the one cycle of the photochemical reactions the energy absorbed by the bR retinal chromophore is transferred to the protein and one proton is transported from the intercellular to the extracellular membrane side [81].

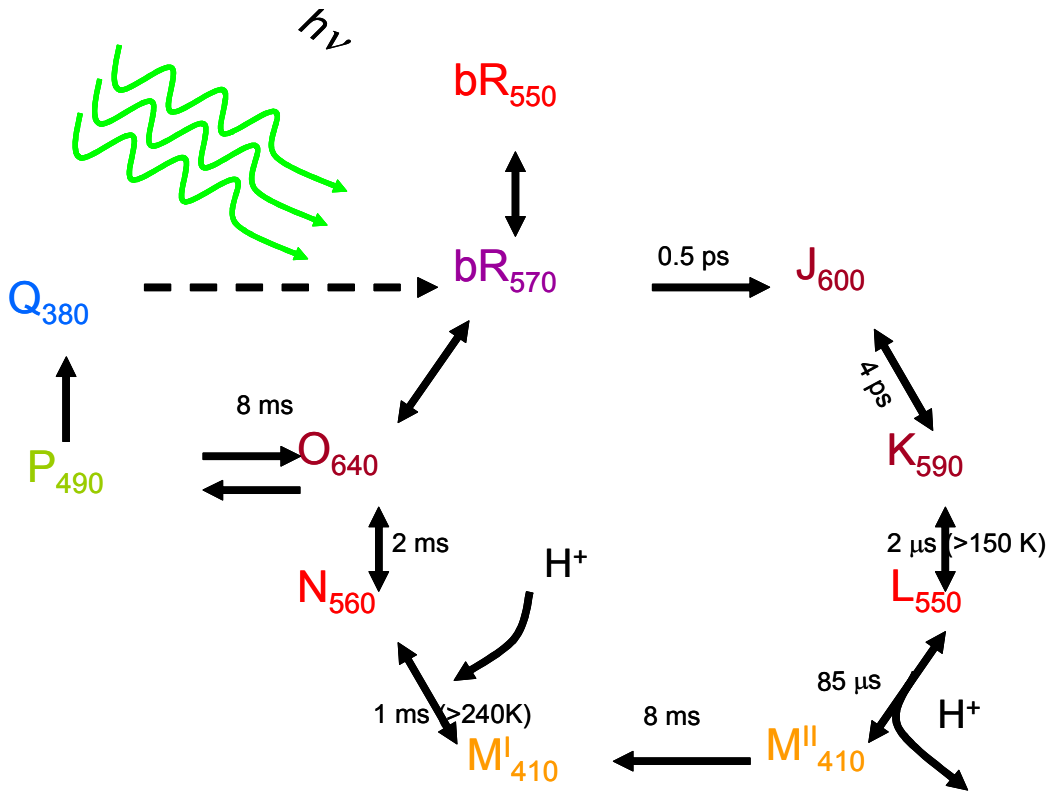

Figure 4.2: Photocycle of the bR molecule. The main intermediate states are shown with their commonly used letter abbreviation and the pertinent absorption maxima of the intermediate states as subscripts. The steps at which Schiff base is released and takes up a proton are indicated. The primary and branched photocycle and the lifetime of the intermediates are shown [74, 85, 155–164].

Many approaches and models for the description of the bR photocycle exist because the photocycle is very dependent on external conditions, and some researchers in order to simplify the photocycle process are omitting some of the branched intermediates [150–152]. Additionally, in order to fully describe the bR photocycle simultaneously with visible absorption data the other structural features of the molecule, such as the protonation states of individual residues and/or protein conformational states must be studied [153].

Consequently, particular models related to particular conditions are used. All of these models at certain conditions can be used to describe the bR photocycle. Based on data from currently available literature the series of the photochemical reactions can be described as follows [154]:

After absorption of a quantum of light within a time interval of 0.5 ps the J intermediate with an absorption wavelength at 600 nm is formed, retinal is in 13-*cis* configuration. After a further period of 4 ps the bR in the J state thermally relaxes to form the K_{590} intermediate state, configuration of the retinal is the 13-*cis* and Schiff base is protonated at this stage [154–156]. The chromophore exists in the K_{590} state for 2 μs and due to further thermal reactions transforms to the L_{550} state. This is followed after 85 μs by the formation of the M_{410} state and deprotonation of the Schiff base [157–159]. At this step the Schiff base loses its proton and exists in deprotonated form, while the *Asp–85* becomes protonated and retinal is in 13-*cis* configuration form [160]. *Asp* is the amino acid residue and is part of the structure of the bR molecule which is involved in proton transport and serves as a proton acceptor, see Figure 1.18. The absorbance maximum of the M_{410} intermediate is shifted as compare with the bR_{570} because the Schiff base is in the deprotonated form. Reprotonation of the Schiff base occurs after 8 ms at the M_{410} state and then transition to the N_{560} intermediate state occurs

[161, 162]. Upon the formation of the O_{640} intermediate the retinal chromophore returns to the *all-trans* isomerization form and finally the protein returns to the ground state bR_{570} [163].

This example is given as an illustration of the bR photocycle and the time intervals may change in response to temperature and chemical environment but it does give an indication of the stages involved and approximate time intervals.

In the dry film matrix the proton transport is different as compared with a solution because the position of the bR molecule is strongly physically fixed and the intermediate states shown in Figure 4.2 are less pronounced. Accordingly, the model of the photocycle can be simplified to the description of the two main intermediate states: ground bR_{570} state in which the retinal is in *all-trans* configuration and M_{410} state, the retinal exists in the *13-cis* form, see Figure 4.3 [74, 164].

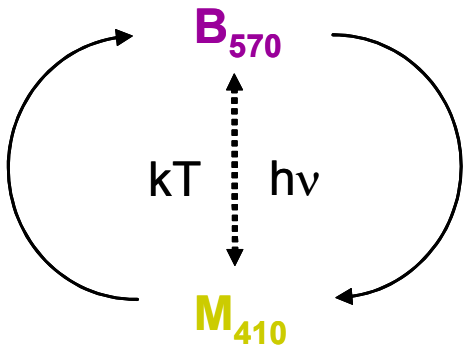

Figure 4.3: Simplified photocycle model of the bR molecule embedded into solid matrix [74].

Exposure of the bR film to the actinic light leads to the photo-induced changes and causes a decrease of the absorbance at the 570 nm, and a new absorbance maximum is observed at 410 nm, see Figure 4.4.

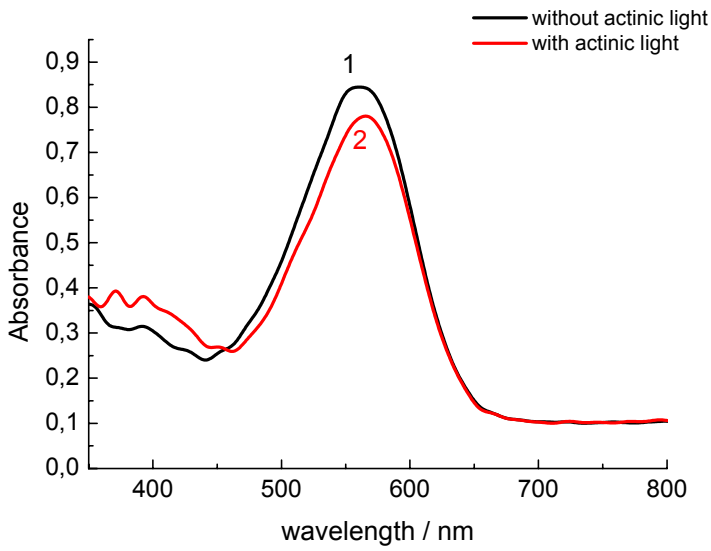

Figure 4.4: Absorbance spectra of the bR film in GE matrix manufactured by casting method (the ratio of bR in the GE films is bR : GE = 12.5 : 84.5); black line 1, taken at the absence of the actinic light; red line 2, recorded at the presence of the actinic light; light-emitting diode (LED) with the emission wavelength 518 nm was used as an actinic light source.

Figure 4.5a and b shows the "difference" absorbance spectra and time dependence of the photo-induced absorbance changes monitored at 412 and 570 nm, respectively. Difference absorbance spectra are calculated by subtraction of the spectrum recorded in the absence of the actinic light (dark) from the spectrum recorded in the presence of the actinic light (light) (light minus dark). Time dependence of the photo-induced absorbance changes (Figure 4.5b) were normalized using Equation 2.3, see Chapter 2.

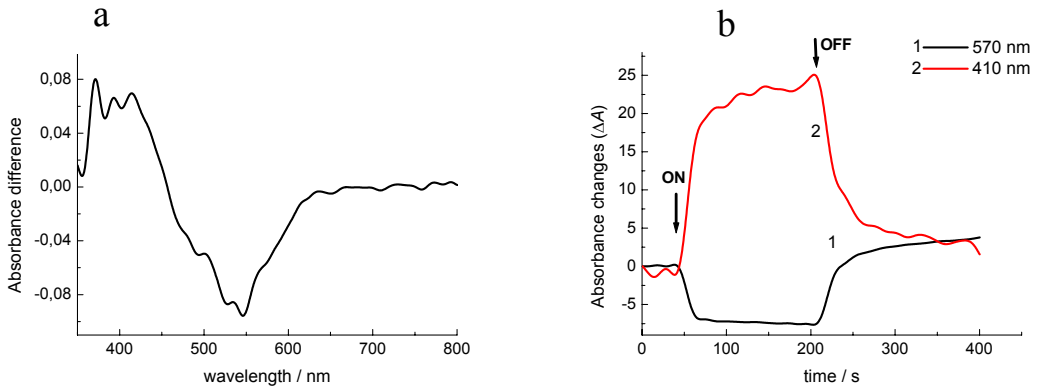

Figure 4.5: a, difference absorbance spectra (light minus dark); and b, time dependence of the photo-induced absorbance changes (calculated using Equation 2.3) monitored at black line 1, 570 nm; and red line 2, 410 during and after actinic light (LED_{518}) (for explanation see text) of the bR film in GE matrix (measured at 25 ^{o}C and rH 50%; mass ratio bR : GE = 12.5 : 84.5).

The functional forms of the rise and decay kinetics of the photo-induced absorption changes of the M_{410} state monitored at 410 nm (Figure 4.5b) are double exponential, see Figure 4.10b and are described by the Equations 2.4, see Chapter 2.

In this thesis the photo-induced absorbance changes at the wavelengths 570 and 410 nm (ΔA_{570}; ΔA_{410}) and half-life of the decay kinetics of the M_{410} state were chosen as the controlled optical parameters for the investigation of the effects of the presence of ammonia gas and changes in relative humidity on the behaviours of the bR films. The half-life ($\tau_{1/2}$) of the M_{410} intermediate was determined as the time required for the decaying absorbance changes to fall to one half of its initial value.

Measurements of the influences of ammonia and relative humidity on these parameters were employed for the development of selectively sensitive elements for fibre-optic sensors.

Tittor et al. [165] in their work demonstrated that the quantum yield of the bR photoreaction is independent from the bR concentration in the sample and from the wavelength of the actinic light in the range from 500 to 600 nm, and that only the intensity of the actinic light plays significant role in the magnitude of the photo-induced absorbance changes. In order to choose the optimal (i.e. at which the maximal amplitude of the photo-induced absorbance changes will be observed) wavelength and intensity of the actinic light source, a study of the effects of the wavelengths and intensities of the actinic light sources on the photo-induced absorbance changes and half-life was carried out. Figure 4.6 shows the emission spectrum of the actinic light sources used for the excitation of the photocycle in the bR films and the absorbance spectrum of the bR film in a GE matrix.

The emission spectra of the LED light sources were measured using the CCD spectrophotometer (Ocean Optics HR2000) connected to the LED using an optical fibre with the diameter of 100 μm. The integration time was 5 milliseconds or lower to avoid the light saturation of the CCD detector for all measurements; the intensity in Figure 4.6 is shown in arbitrary units and corresponds to the voltage (in mV) value of the photodetector.

The largest photo-induced absorbance changes (ΔA,%) were observed when the LED_{518} with emission wavelength peaking at 518 nm, see Figure 4.6, and a halogen lamp with the high pass filter (> 530 nm) were used as actinic light sources (Figure 4.7a and b). These absorbance changes correspond to the different intensities of the chosen light sources, see Figure 4.6. Consequently, an LED_{518} and a halogen lamp were used as actinic light sources for studying the effects of the ammonia and relative humidity on the absorbance characteristics of the bR films.

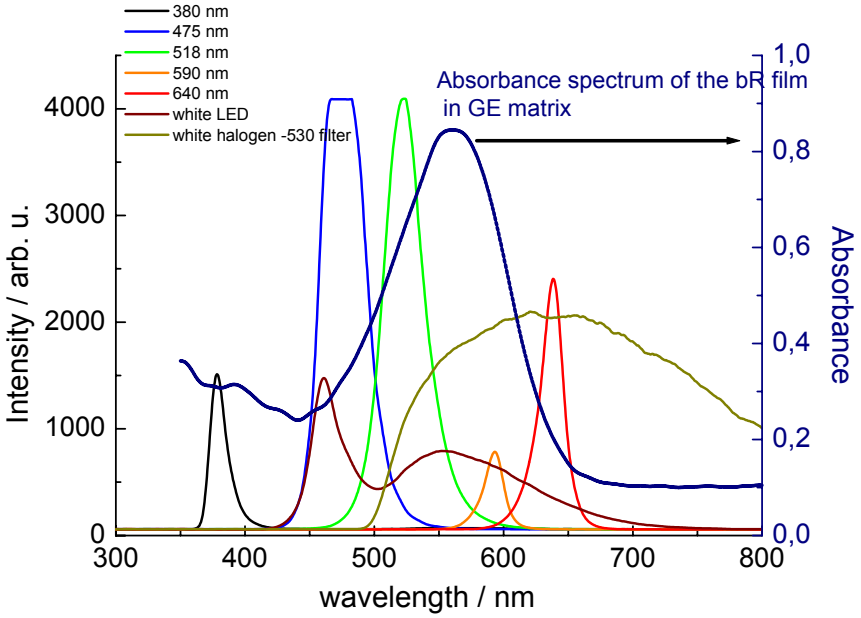

Figure 4.6: Emission spectra of the light sources used as actinic light and absorbance spectrum of the bR film in the GE matrix.

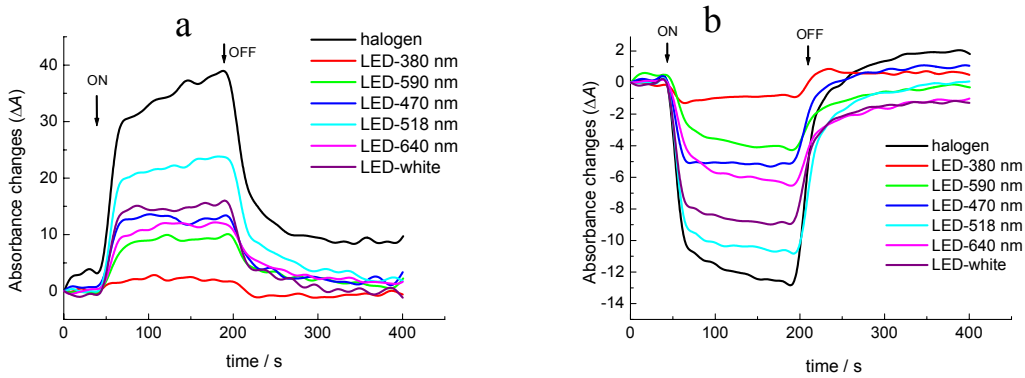

Figure 4.7: Time dependence of the photo-induced absorbance changes (calculated using Equation 2.3) of the bR film in GE matrix manufactured by formation method, when different actinic light sources were used; a, monitored at 410 nm; b, monitored at 570 nm (measured at 25 ^{o}C and rH 50%; mass ratio bR : GE = 12.5 : 84.5).

In the Table 4.1 the dependences of the photo-induced absorbance changes and half-life of the bR films in the GE matrix on the source of actinic light used for the excitation of the bR photocycle are shown.

Table 4.1: Dependence of the photo-induced absorbance changes of the bR film in GE matrix (manufactured by formation method) on the actinic light.

Sample	Actinic light wavelength, nm	λ / nm [a]	ΔA [b,c]	$\tau_{1/2}$ / s [d]
bR+GE	470	410	13.0 ± 0.1	26.0 ± 0.5
		570	5.0 ± 0.1	
	518	410	23.7 ± 0.1	32.0 ± 0.6
		570	10.0 ± 0.1	
	590	410	10.0 ± 0.1	32.0 ± 0.8
		570	4.2 ± 0.1	
	640	410	11.8 ± 0.1	38.0 ± 0.5
		570	6.5 ± 0.1	
	White LED	410	15.9 ± 0.1	28.0 ± 0.6
		570	8.2 ± 0.1	
	Halogen lamp (> 530 nm)	410	38.9 ± 0.1	23.0 ± 0.2
		570	12.8 ± 0.1	

[a] Wavelengths of the probe light (corresponds to the absorption peaks M_{410} and bR_{570})
[b] Percentage of photo-induced absorbance changes, calculated using Equation 2.3;
[c] Uncertainties are representing the accuracy of the measurement equipment.
[d] Uncertainties are representing the fitting of individual curves to the double exponential decay. Uncertainties for the measurement of different samples ca. = 0.58 (standard deviation derived from 4 measurements); Uncertainties for the 8 measurement of the one sample ca. = 0.12 (standard deviation derived from 8 measurements).

Measurements were undertaken at room conditions and these data were used as the initial data for the estimation of the parameters measured at different ammonia contractions and relative humidities. All measurements were undertaken at the same conditions.

4.2 Matrix effects on the optical parameters of the bR films

Interfacial water plays a very important role in the activity of biological species [166]. Different materials used as a matrix for the manufacturing of the bR-based films will have a different interaction with the available water [96, 97, 167]. In the polyvinyl alcohol water is strongly bonded within the polymer chains (via numerous hydrogen bonds with the hydroxyl groups of the polyvinyl alcohol) and consequently it will not be accessible to the bR chromophore [97]. Additionally, different matrices possess different porosities. Consequently, they will contain different amounts of water in the vicinity of the bR molecule, which will influence the properties of bR photocycle [144]. In order to check the effect of the matrix materials on the photo-induced bR optical properties, the parameters of films based on bR in polymeric matrices and in a sol-gel glass matrix manufactured by the casting method were compared. The difference absorption spectra of the films based on bR in different matrices are shown in Figure 4.8. The photo-induced absorption changes were measured after illumination of the bR film using LED_{518} with emission wavelength 518 nm, for 5 minutes.

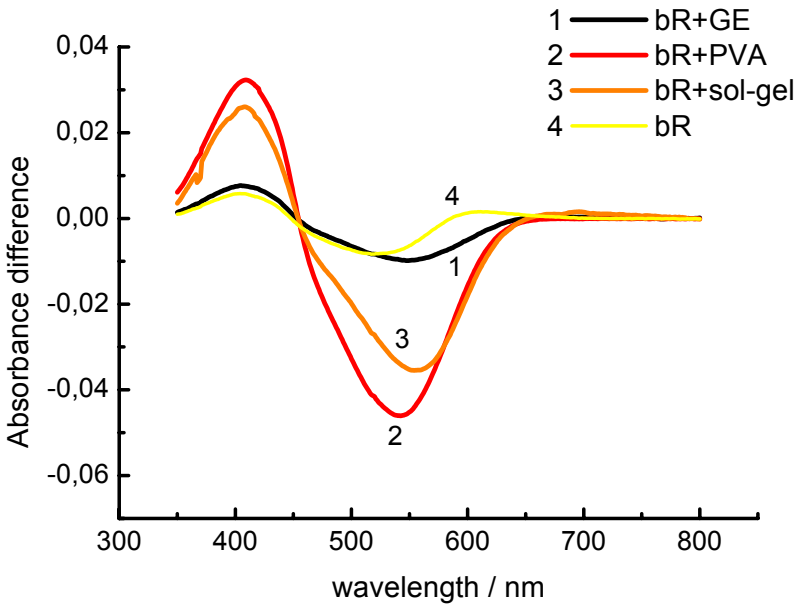

Figure 4.8: Difference absorption spectra (light minus dark) of the bR films in different matrices; line 1, bR in GE matrix; line 2, bR in PVA matrix; line 3, bR in sol-gel matrix; and line 4, bR without matrix (mass ratio: line 1, bR : GE (PVA) = 12.5 : 85.5; line 3, bR : TMOS = 5.5 : 94.5; line 4, film produced by drying of the bR suspension (14 mg/mL), all films were produced by casting method; measured at 25 ^{o}C and rH 50%), for experimental results see Appendix B, Figure B1–B4.

Comparing three different films types: bR in polyvinyl alcohol, in gelatin and in sol-gel glass, from the difference absorbance spectra, Figure 4.8, we can conclude that the gelatin film contains the largest amount of available water and the polyvinyl alcohol film the least [167]. Table 4.2 summarises the results of the effect of the different materials used as a matrix on the optical parameters of the photocycle of bR films.

These results demonstrate the possibility to control and modify the bR photocycle properties by choosing the matrix type.

Table 4.2: Dependence of the optical parameters of the films based on bR on the different matrices, manufactured by casting method (LED_{518} was used as an actinic light source), for experimental results see Appendix B, Figure B7, B9.

Sample	λ / nm [a]	ΔA [b,c]	$\tau_{1/2}$ / s [d]
bR+GE	410	0.5± 0.1	9.0 ± 0.6
bR+PVA	410	2.0 ± 0.1	20.0 ± 0.4
bR+sol-gel	410	2.3 ± 0.1	18.0 ± 0.5

[a] Wavelengths of the probe light (corresponds to the absorption peak M_{410})
[b] Percentage of photo-induced absorbance changes, calculated using Equation 2.3;
[c] Uncertainties are representing the accuracy of the measurement equipment.
[d] Uncertainties are representing the fitting of individual curves to the double exponential decay. Uncertainties for the measurement of different samples ca. = 0.58 (standard deviation derived from 4 measurements); Uncertainties for the 8 measurement of the one sample ca. = 0.12 (standard deviation derived from 8 measurements).

The half-life and photo-induced absorbance changes can be controlled by choosing different materials for manufacturing the bR film.

4.3 Effect of the chemical additives on the optical parameters of the bR films

Inclusion of chemical additives in various combinations into a bR film is a means to permanently modify the photosensitivity and temporal characteristics of the photocycle over a wide range, with the possibility of enhancing the chemical sensitivity and selectivity of the films [168]. Figure 4.9 shows the difference absorption spectra of the bR films in a GE matrix with different chemical additives.

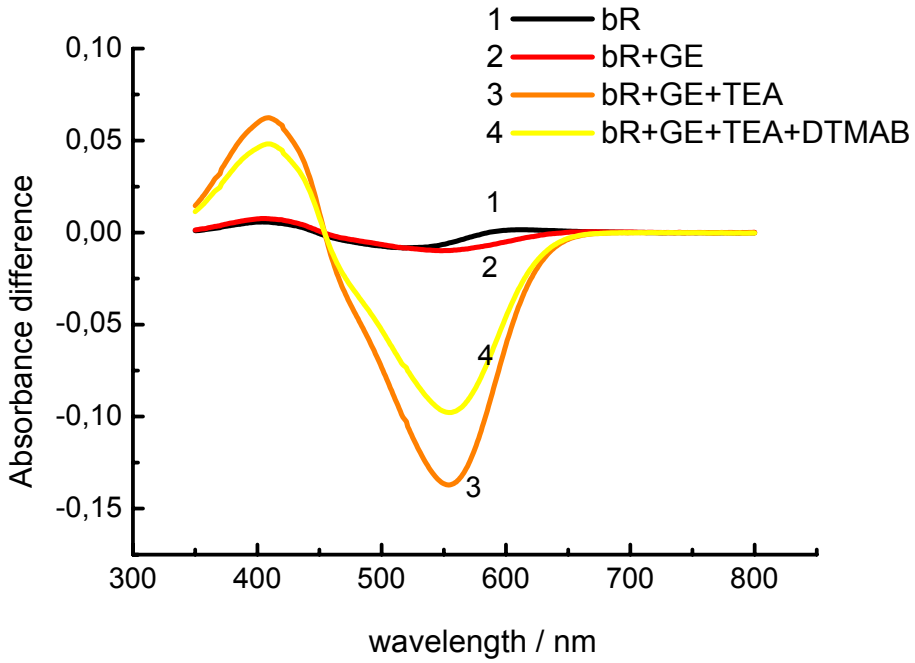

Figure 4.9: Difference absorption spectra of the bR films in GE with chemical additives; line 1, bR self-assembled film; line 2, bR in GE matrix; line 3, bR in GE matrix with TEA added; line 4, bR in GE matrix with TEA and DTMAB added; (mass ratio bR : GE = 12.5 : 87.5; bR : GE : TEA = 12.4 : 73.54 : 13.8; bR : GE : TEA : DTMAB = 12.4 : 73.54 : 12.8 : 1.16; (films manufactured by casting method, measured at 25 ^{o}C and rH 50%), for experimental results see Appendix B, Figure B4–B6.

Inclusion of the triethanolamine (TEA) and dodecyltrimethylammonium bromide (DTMAB) increases the amplitudes of the photo-induced changes in the bR films by 2 times at 410 nm and by 4 times at 570 nm (Figure 4.10, Table 4.3). The half-life of the M_{410} increases almost 10 times when the combination of the TEA and DTMAB is added to the bR film in GE matrix, see Figure 4.10.

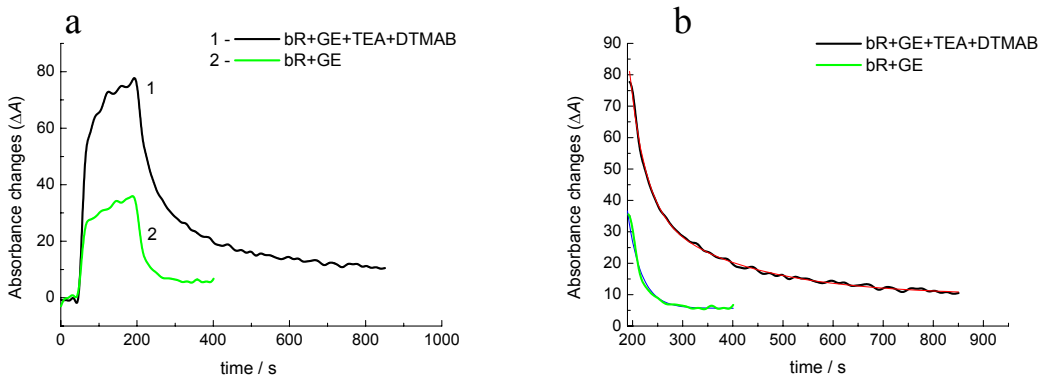

Figure 4.10: a, time dependence of the photo-induced (actinic light source halogen lamp with filter (>530 nm)) absorption changes monitored at 410 nm; line 1, bR film TEA+DTMAB added; line 2, bR film without chemicals added; b, double exponential fitting of the M_{410} decay curve of the: black line, chemically modified bR film; green line, bR+GE; red and blue lines are double exponential fitting of the bR film TEA+DTMAB added and bR film without chemicals added respectively (films were manufactured by formation method) (measured at 25 ^{o}C and rH 50%); normalization was carried out using Equation 2.3.

Table 4.3 summarises the effect of the chemical additives on the optical parameters of the bR films in GE matrix.

Table 4.3: Effect of the chemical additives on the optical parameters of the bR films in GE matrix (manufactured by formation method) (data from Figure 4.10)

Sample	λ / nm [a]	$\Delta A^{b,c}$	$\tau_{1/2}$ / s[d]
bR+GE	570	12.0 ± 0.1	
	412	39.0 ± 0.1	23.0 ± 0.3
bR+GE+TEA+DTMAB	570	58.0 ± 0.1	
	410	76.0 ± 0.1	201 ± 1

[a] Wavelengths of the probe light (corresponds to the absorption peak M_{410})
[b] Percentage of photo-induced absorbance changes, calculated using Equation 2.3;
[c] Uncertainties are representing the accuracy of the measurement equipment.
[d] Uncertainties are representing the fitting of individual curves to the double exponential decay.

Similar effects caused by the chemical additives are observed when other matrices were used. Tables 4.4 and 4.5 summarise the data for the sol-gel matrix and PVA matrix respectively.

Table 4.4: Optical characteristics of the bR films in the sol-gel matrix with chemical additives [169], for experimental results see Appendix B, Figure B7.

Sample	λ / nm [a]	$\Delta A^{b,c}$	$\tau_{1/2}$ / s[d]
bR+TEOS	570	4.2 ± 0.1	
	410	2.3 ± 0.1	12.0 ± 0.5
bR+TEOS+TEA	570	4.6 ± 0.1	
	410	2.8 ± 0.1	21.0 ± 0.2
bR+TEOS+TEA+ DTMAB	570	4.2 ± 0.1	
	410	2.5 ± 0.1	13.0 ± 0.4

[a] Wavelengths of the probe light (corresponds to the absorption peak M_{410})
[b] Percentage of photo-induced absorbance changes, calculated using Equation 2.3;
[c] Uncertainties are representing the accuracy of the measurement equipment.
[d] Uncertainties are representing the fitting of individual curves to the double exponential decay. Uncertainties for the measurement of different samples ca. = 0.58 (standard deviation derived from 4 measurements); Uncertainties for the 8 measurement of the one sample ca. = 0.12 (standard deviation derived from 8 measurements).

Table 4.5: Optical characteristics of the bR films in PVA matrix with chemical additives (actinic light source halogen lamp with long pas filter > 530 nm), for experimental results see Appendix B, Figure B8.

Sample	λ / nm [a]	$\Delta A^{b,c}$	$\tau_{1/2}$ / s[d]
bR+PVA	570	6.7 ± 0.1	
	410	8.2 ± 0.1	9.0 ± 0.8
bR+PVA+TEA+DTMAB	570	16.8 ± 0.1	
	410	10.6 ± 0.1	18.0 ± 0.3

[a] Wavelengths of the probe light (corresponds to the absorption peak M_{410})
[b] Percentage of photo-induced absorbance changes, calculated using Equation 2.3;
[c] Uncertainties are representing the accuracy of the measurement equipment.
[d] Uncertainties are representing the fitting of individual curves to the double exponential decay.

The experimental results of the investigation of the effects of the chemical additives in the bR films with GE used as a matrix demonstrated that bR optical properties can be modulated in a wider range as compared with the films with the PVA and sol-gel matrices. Consequently, bR films with a GE matrix and chemical additives were considered as a prime candidates for the development of the sensitive element for fibre-optic sensors.

The effect of the chemical additives on the optical parameters of the bR films can be employed for the creation of the sensitive elements of the optical sensors. Measurement of the half-life and amplitude of the photo-induced absorption changes can be used for the determination of the chemical species which will induce the modulation of the optical parameters of the bR film.

The possible mechanism of the chemical additives effect was suggested by Batory-Tarcy et al. [154]. By additional investigation of the chemical additives' effects on the optical properties of both the wild-type bR and the bR mutants it was suggested that chemical additives are acting on the extracellular side of the purple membrane. Electronegative functional groups that are present in the chemical species used as additives can capture the proton which is released on the extracellular side of the membrane. Consequently, in this thesis it is suggested that bR could be used for the detection of the chemical species that can induce changes in the proton pathway in the bR photocycle.

Conclusions and Summary:

In this Chapter the optical parameters of the bR films and features of the bR photocycle in the aqueous solution and solid film were introduced. The model of the bR photocycle was shown. The influence of the matrix on the bR photo-induced absorbance changes and half-life of the M_{410} state allowed the manufacture of bR films with the different optical properties when different matrices were used. The most pronounced matrix effect was observed when PVA was used as a matrix.

The effect of the chemical additives on the optical properties of the bR films was demonstrated. Inclusions of the TEA and DTMAB can increase the half-life of the M_{410} intermediate almost in 10 times, and photo-induced absorbance changes in 4 times when monitored at 570 nm as compared with bR films without chemical additives. Explanations of the suggested mechanism of the chemical additives acting have been discussed. The biggest modulation induced by chemical additives of the optical properties of the bR films was observed when GE matrix was used as compared with the PVA matrix.

The main ***hypothesis*** of this thesis is that the particular chemical species present in the environment can modulate the amplitude of the photo-induced absorbance changes and half-life of the bR in a similar way to the chemical additives, and this could be employed for the development of the sensitive elements for the optical chemical sensors. The next Chapters of this thesis will be devoted to prove the state of this *hypothesis*.

Consequently, in the Chapter 5 the effect of the presence of ammonia and changes in relative humidity on the half-life and amplitude of the photo-

induced absorption changes of the bR films will be demonstrated. The impact of the matrix and chemical additives on the response of the bR films to the ammonia and relative humidity will be discussed. The influence of the matrix and chemical additives on the selectivities, sensitivities and limits of detections of the bR films towards ammonia and rH will be shown.

Chapter 5: The influences of chemical species on the optical parameters of bR films - results, discussion and conclusions

The influence of the presence of ammonia gas and changes in relative humidity on the half-life and amplitude of the photo-induced absorption changes of the bR films will be described in this Chapter. The time dependence of the absorbance changes induced by the presence of ammonia gas at different concentrations will be studied mainly in terms of the time response and sensitivity of the sensitive element based on the bR films. The limit of detection (*LOD*) to ammonia of the sensitive element of the optical sensors based on the bR films will be calculated from the experimentally derived calibration curves. The impact of the matrix structure and the chemical additives on the response of the bR films to ammonia and relative humidity changes will be shown and discussed.

5.1 The effect of ammonia

It was demonstrated in Chapter 4 that chemical species containing amine with an electronegative function group can alter the optical parameters of bR when present in its environment. The ammonia has a similar chemistry to amine compounds and function groups and so was chosen as the target chemical species in order to study the possibility of using bR films as the sensitive elements for optical chemical sensors. Both the ammonia and amines contain the $–NH_2$ amino electronegative function group, therefore suggesting that ammonia will influence the optical properties of the bR in similar way.

Additionally, ammonia belongs to the group of so called nitrogen air pollutants; and when ammonia exceeds some critical level it has a high potential health risk [170]. Sensitive detection of ammonia gas is desired but not yet effectively achieved in the environmental, automotive, chemical and medical areas of human activity. The application areas for ammonia gas sensors are summarized in the Table 5.1 [171]. The key sensor parameters of the existing sensor and sensor systems for the detection ammonia are summarized in the Table 5.2 [171].

Briefly, the principles of operation of the sensors summarized in Table 5.2 are based on [171]:

(i) metal-oxide sensors, the conductance change induced by the chemisorption of the gas molecules on the metal-oxide film, which has a large number grains, contacting at their boundaries. The main disadvantage is the selectivity of metal-oxide sensors.

(ii) catalytic sensors, the charge carrier concentration in the catalytic metal is changed when the concentration of analyte gas is changed. This can be monitored by employing field effect devices,

transistors or capacitors. Selectivity depends on the parameters of the metal layer used.

(iii) optical sensors can employ two methods for the ammonia detection: (1), detection of the reagent colour changes induced by ammonia; (2), by detecting the absorption of the light passed through the ammonia gas. The main disadvantages of this method are the cost of the equipment and the large amount of sample that is needed for the accurate analysis.

Table 5.1: Application areas for the ammonia sensors (reproduced from [171]) (ppm, part per million —10^{-6}; ppb, part per billion — 10^{-9}; ppt, part per trillion — 10^{-12}).

Application		Detection limit	Required response time	Temperature range
Environmental	Monitoring ambient conditions	20–40 ppb to >200 ppm	Minutes	0–40 ^{o}C
	Measure in stables	1 to >25 ppm	<1 min	10–40 ^{o}C
Automotive	Measure NH_3 emission from vehicles	4–2 000 g/min (concentration unknown)	Seconds	Up to 300 ^{o}C
	Passenger cabinet air control	50 ppm	<1 s	0–40 ^{o}C
	Detect ammonia slip	1–100 ppm	Seconds	Up to 600 ^{o}C
Chemical	Leakage alarm	20–1 000 ppm	Minutes	Up to 500 ^{o}C
Medical	Breath analysis	50–2 000 ppb	<1 min	20–40 ^{o}C

Table 5.2: Parameters of the ammonia sensors and systems (reproduced from [171]).

Principle		Lower detection limit	Response time	Temperature range
Metal-oxide	WO_3	1 ppm	<5 min	400 ^{o}C
Catalytic metal	Palladium	1 ppm	<1 min	Up to 600 ^{o}C
	Conducting polymer Polyaniline	1 ppm	<3 min	Up to 150 ^{o}C (regeneration)
Optical gas sensors	Nessler	50 μM (90 ppb)	<1 min	37 ^{o}C
	Colorimetric	1 ppt	<5 min	–
	Absorption spectroscopy	1 ppb	<5 min	
	pH-transition and EC detectors	100 ppt	<20 min	0–40 ^{o}C

In spite of sensor techniques available for the detection of the ammonia gas [171–175], it is still a task of current importance and relates to many aspects of human activities.

Consequently, bR films of different compositions were deposited onto a glass substrate and onto the distal end of optical fibres to create sensors. These sensing elements were exposed to ammonia gas of different concentrations. The sensor parameters of the bR films employed as sensitive elements of the fibre-optic sensors such as sensitivity, response time and selectivity to the presence of ammonia were studied.

5.1.1 Ammonia-induced absorbance changes

The absorbance spectra of a bR film in a GE matrix were measured without the presence of ammonia and in ammonia atmosphere with a concentration of 10 000 ppm and these are compared in Figure 5.1. The detailed experimental method can be found in section 2.2.2. of Chapter 2. It can be

observed that the presence of the ammonia gas leads to a decrease of the absorbance at the wavelength of 570 nm and small absorbance increase at 410 nm. As well as the decrease of the absorbance at 570 nm, a shift of the wavelength of the absorbance maximum from 565 nm to 550 nm was observed. The difference absorbance spectrum (i.e. the spectrum taken in the presence of ammonia subtracted from the spectrum taken without ammonia) is shown in Figure 5.2.

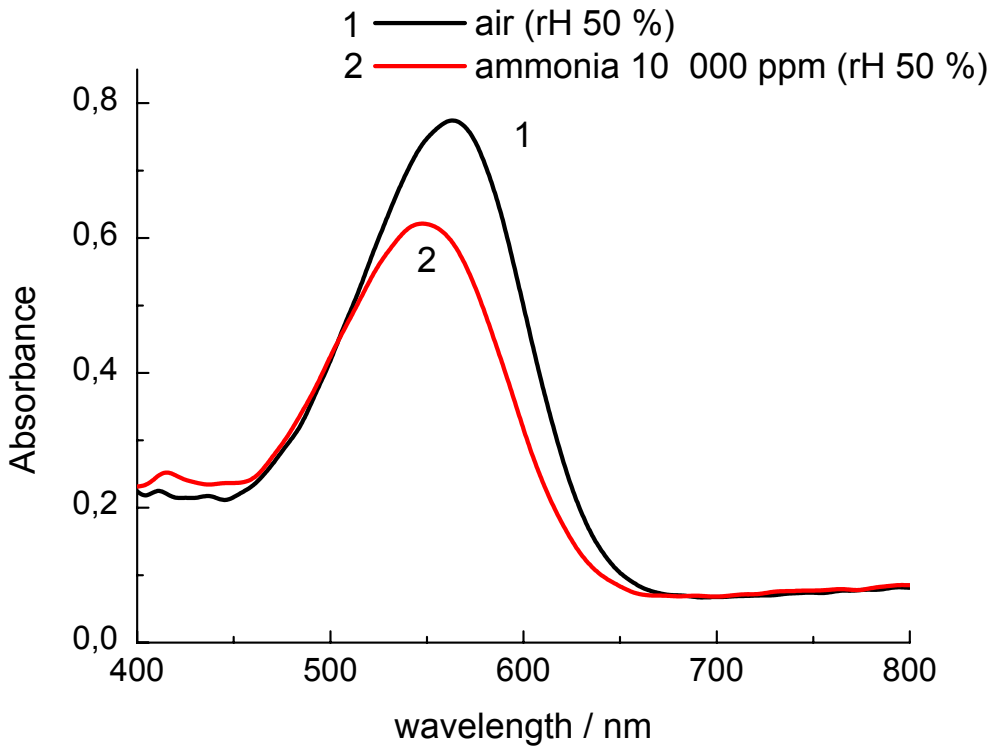

Figure 5.1: Absorbance spectra of the bR film in the GE matrix (mass ratio bR : GE = 12.5 : 87.5) measured at 25 ^{o}C and rH 50%: black line 1, without ammonia; and red line 2, in an ammonia atmosphere with the concentration of 10 000 ppm.

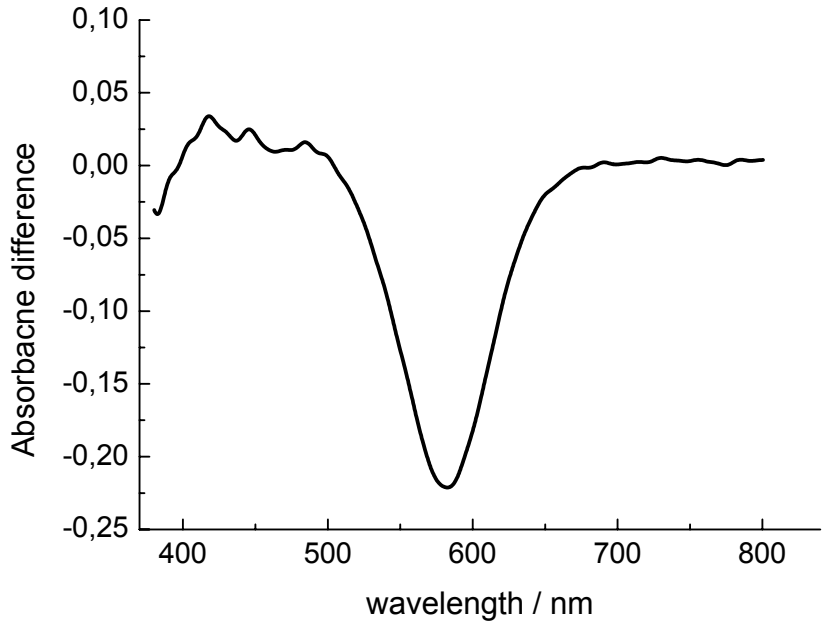

Figure 5.2: Difference absorbance spectrum (ammonia minus air) of the bR film in the GE matrix (mass ratio bR : GE = 12.5 : 87.5) measured at 25 ^{o}C and rH 50%.

The difference absorbance spectrum indicates that the largest absorbance changes in the bR film in the GE matrix occur at the wavelength of 580 nm. The time dependence of the normalized absorbance changes (S.R.) of the bR film in the GE matrix induced by the presence of ammonia gas monitored at 570 nm, 580 nm and 410 nm are shown in Figure 5.3.

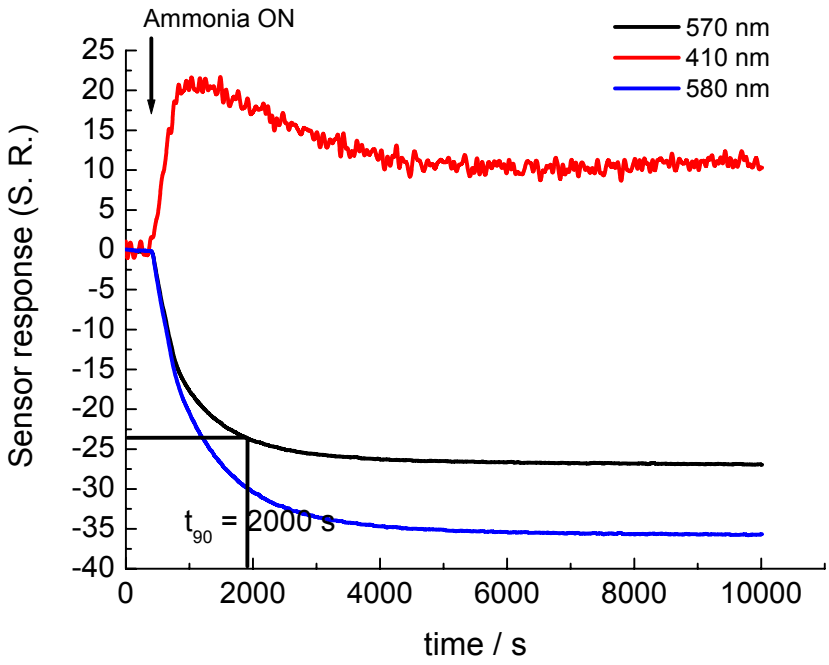

Figure 5.3: Time dependence of the sensor response (S.R.) of the bR film in the GE matrix (mass ratio bR : GE = 12.5 : 87.5 measured at 25 ^{o}C and rH 50%) induced by presence of ammonia monitored at: black line, 570 nm; blue line, 580 nm; and red line, 410 nm. Normalization was undertaken using Equation 2. 5. The t_{90} represents the response time that was determined as the time needed for signal to achieve 90% of its maximum value at 570 nm.

The sensor response (S.R.) was calculated using Equation 2.5, see Chapter 2.

In Figure 5.3 the t_{90} represents the time response of the sensitive element and was determined as the time interval needed for the signal to achieve 90% of its saturation value. For the bR film in the GE matrix the t_{90} value was about 2 000 s after the sensor film was exposed to the ammonia concentration of 10 000 ppm.

The results showed that the effect of ammonia leads to a 36% decrease of the absorbance at 580 when exposed to the ammonia concentration of 10

000 ppm, while at the wavelength of 410 nm the ammonia induced absorbance changes were 20%.

Figure 5.4 shows the sensor response of the bR film in the GE matrix to increasing the ammonia concentration from 10 to 10 000 ppm. From the results of the ammonia-induced absorbance changes a calibration curve was plotted which shows a linear response in the ammonia concentration range of 0–200 ppm when monitored at the wavelengths of 570 nm and 580 nm, see Figure 5.5 a.

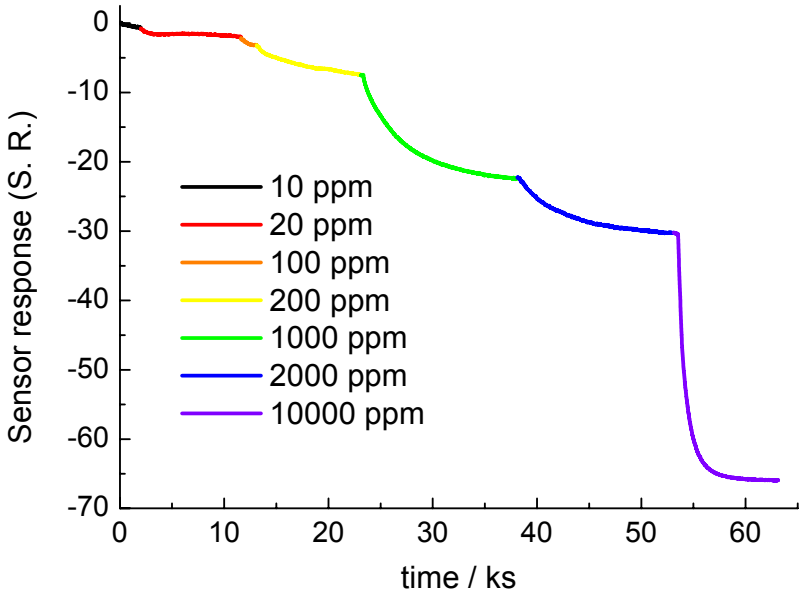

Figure 5.4: Response of the bR film in GE matrix to increasing the concentration of ammonia from 10 to 10 000 ppm monitored at the wavelength 580 nm (mass ratio bR : GE = 12.5 : 87.5 measured at 25 ^{o}C and rH 50%). The measurements were done by admitting the ammonia gas of the desired concentration balanced with nitrogen into the measurement chamber (for details see section 2.2.2).

The slope diminishes at higher concentrations, but from 1 000 ppm up to 10 000 ppm the response can be approximated as linear (Figure 5.5 b). The response times t_{50} and t_{90} of the bR film in the GE matrix to the given ammonia concentration are summarized in Table 5.3.

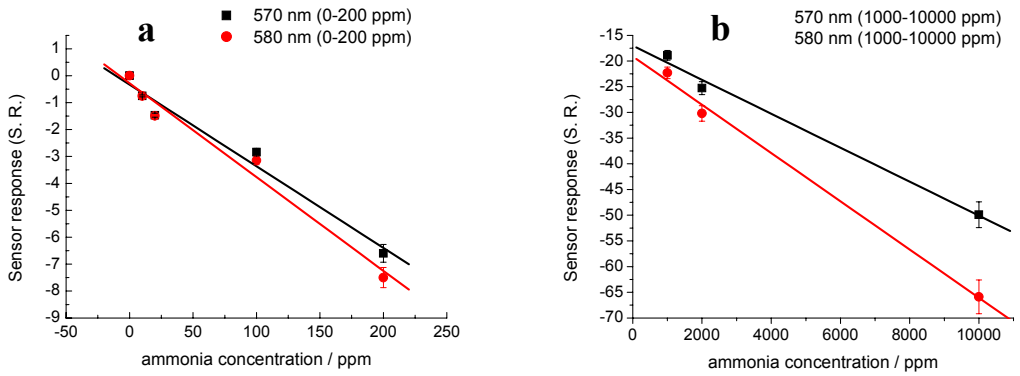

Figure 5.5: Calibration curves constructed from the results of ammonia-induced absorbance changes in the bR film in the GE matrix: a, in the range of ammonia concentration, 0–200 ppm: squares, slope: –0.030 ± 0.003 at 570 nm; circles, slope –0.035 ± 0.003 at 580 nm; b, ammonia concentration range 1 000–10 000 ppm: squares, slope: –0.0030 ± 0.0003 at 570 nm; circles, slope: –0.0050 ± 0.0003 at 580 nm (see Figure 5.4).

The limit of detection (*LOD*) for the bR film in GE matrix was 5 ppm and was calculated using Equation 5.1 [176]:

$$LOD = 3\frac{\sigma}{m}, \tag{5.1}$$

where σ, the standard deviation derived from the 220 blank measurements; and *m*, the slope of the calibration curve, see legend to the Figure 5.5.

Table 5.3: The response time values t_{50} and t_{90} for the bR film in the GE matrix (mass ratio bR : GE = 12.5 : 87.5 measured at 25 ^{o}C and rH 50%) when exposed to ammonia gas atmospheres of different concentrations constructed from the results shown in Figure 5.4.

Sample	Concentration / ppm	Response time, t_{90} [a]	Response time, t_{50} [a]
bR+GE	10	30 ± 0.1min	8 ± 0.1 min
	20	8 ± 0.1min	6 ± 0.1min
	100	10 ± 0.1 min	3 ± 0.1 min
	200	73 ± 0.1 min	21 ± 0.1
	1 000	120 ± 0.1 min	67 ± 0.1min
	2 000	143 ± 0.1 min	42 ± 0.1 min
	10 000	33 ± 0.1 min	10 ± 0.1 min

[a] Uncertainties represents the accuracy of the measurement equipment

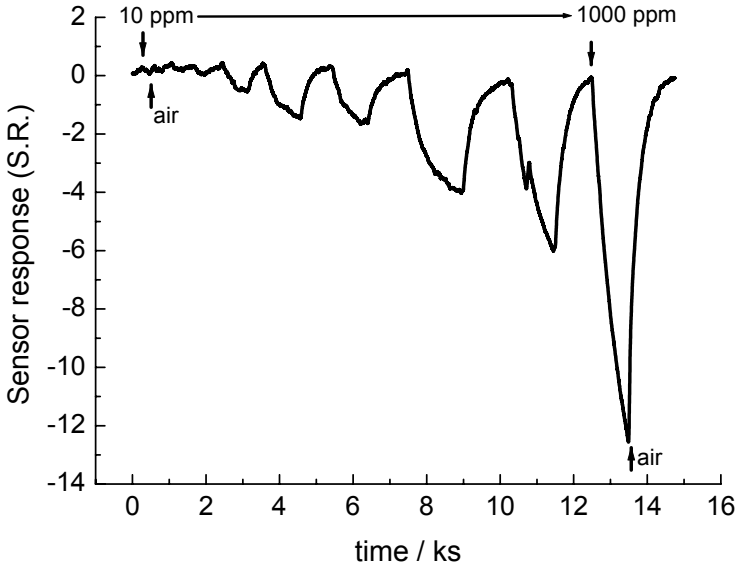

Figure 5.6: Time dependence of the sensors response of the bR film deposited onto the distal end of the fibre-optic Y-type coupler of 200 μm. (mass ratio bR : GE = 12.5 : 87.5 measured at 25 ^{o}C and rH 50%; probe light LED_{590} emission wavelength 590 nm). Measurements were undertaken in flow mode. Initially the ammonia concentration was increased and then the system was flushed with clean air at a flow rate of 1 L/min until the full recovery of the S.R..

Reversal of the ammonia response was investigated by flushing the ammonia gas at the desired concentration through the measurement chamber with a flow rate of 1 L/min, followed by flushing ammonia-free humidified air at a flow rate of 1 L/min until the full recovery of the sensor response (S.R.) was achieved. The response of the sensing element is shown in Figure 5.6. For the lower ammonia concentrations (up to 100 ppm) the response was completely reversible with the recovery time of 100 seconds, at higher concentrations (> 100 ppm) the longer flushing time (1000 s) was applied in order to achieve complete recovery of the S.R.

5.1.1.1 Phenomenology (mechanism of the ammonia influence on the bR optical properties)

The results of the ammonia-induced changes of the bR film optical properties, suggest the following alternative mechanisms of ammonia action on the bR:

(i) decreasing absorbance at 570 nm and increasing absorbance at 410 nm suggests that ammonia shifts the equilibrium between the ground state bR_{570} and the intermediate M_{410} state, which is similar to the action of actinic light;

$$bR + NH_3 \rightleftharpoons bR^*$$

where bR^* represents a modified form of bR

(ii) the shift of the absorption maximum into blue spectral range suggests that ammonia interacts with the water in the vicinity of the retinal chromophore, generally hydroxyl ions:

$$NH_3 + H_2O \rightleftharpoons NH_4^+ + OH^-$$

This effect is similar to dehydration of the bR film [116], which causes the absorbance decrease at 570 nm and increase at 410 nm, along with a blue shift of the absorbance maximum. It has been proposed that it is due to dissociation of water molecules specifically bound to the retinal chromophore [116].

As it was demonstrated by Hildebrandt et al. [144] the effect of ammonia on the hydrated bR film leads to insignificant changes in the chromophoric structure. Thus, there is no structural disruption of the bR molecule and this suggests that ammonia effect will have the reversible influence on the bR optical parameters (Figure 5.6).

5.1.2 Effect of ammonia on the photocycle parameters of the bR film

The photo-induced absorbance changes of the bR film in the GE matrix measured at 25 ^{o}C and rH 50% without ammonia and in ammonia in nitrogen atmosphere with the concentration of 10 000 ppm are shown in Figure 5.7.

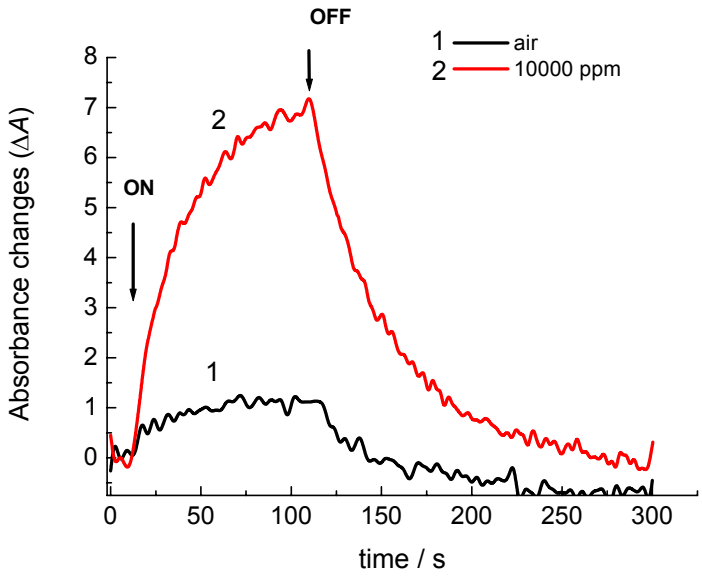

Figure 5.7: Time dependence of photo-induced absorbance (ΔA) changes of bR film in GE matrix (mass ratio bR : GE = 12.5 : 87.5 measured at 25 ^{o}C and rH 50%) monitored at 410 nm during and after actinic illumination (halogen light source with a high pass filter (> 530 nm)) (arrows indicates the turning ON and OFF the actinic light source); 1, without ammonia; 2, with ammonia concentration of 10 000 ppm. Normalization was carried out using Equation 2.3, see Chapter 2.

The measurements utilised an LED light source with maximum emission at a wavelength near 410 nm used as the probe light and a halogen light source with a high pass filter (> 530 nm) employed as an actinic light. The probe light and actinic light were transported to the sample by means of fibre-optic Y- type coupler as was shown in Chapter 2, Figure 2.9.

The kinetic changes occurring at 410 nm confirmed that the presence of the ammonia gas causes the bR photocycle to change in a similar way as with other chemical additives, previously reported in Chapter 4. The amplitude of the photo-induced absorbance changes increased by almost 6 times and the half-life of the intermediate M_{410} state increased by 2 times when bR

film in the GE matrix was exposed to ammonia concentration of 10 000 ppm.

Figure 5.8 shows the kinetic changes measured at 410 nm in the presence of ammonia gas atmospheres of different concentrations.

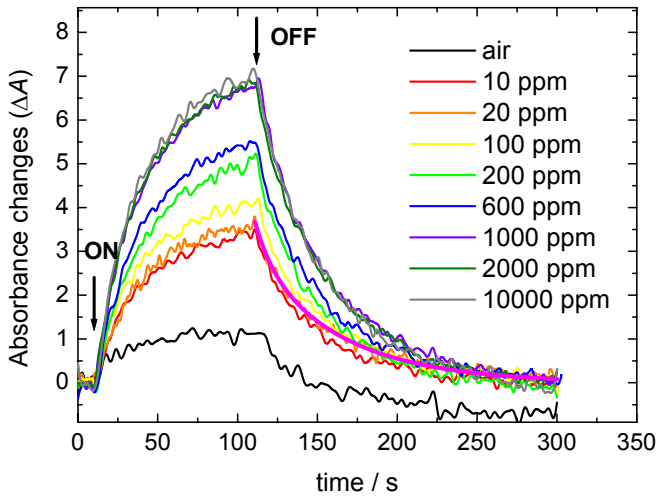

Figure 5.8: Time dependence of photo-induced absorbance (ΔA) changes of bR in GE matrix film (mass ratio bR : GE = 12.5 : 87.5 measured at 25 ^{o}C and rH 50%) monitored at 410 nm during and after actinic illumination (halogen light source with a high pass filter (> 530 nm)) in the presence of ammonia gas of different concentrations (arrows indicate the turning ON and OFF the actinic light source). Normalization was carried out using Equation 2.3, see Chapter 2.

The presence of ammonia gas at the low concentration (10 ppm) caused noticeable changes in the photocycle parameters of the bR film.

The decay kinetics curves (Figure 5.8) of the photo-induced absorbance changes measured when exposed to the ammonia gas atmospheres of different concentrations fit equation 2.4, see Chapter 2.

Results of the double exponential fitting are summarized in the Table 5.4.

Table 5.4: M_{410} decay time constant of the bR film in the GE matrix (mass ratio bR : GE = 12.5 : 87.5 measured at 25 °C and rH 50%) monitored at different concentration of the ammonia atmospheres.

Sample name	Ammonia concentration / ppm	$\Delta A^{a,b}$	$\tau_{1/2}$ / s[c]
bR+GE	0	1.4 ± 0.1	15.0 ± 1.4
	10	3.6 ± 0.1	19.0 ± 0.5
	20	3.8 ± 0.1	20.0 ± 0.7
	100	4.2 ± 0.1	23.0 ± 0.2
	200	5.2 ± 0.1	25.0 ± 0.1
	1 000	6.8 ± 0.1	27.0 ± 0.1
	2 000	7.0 ± 0.1	28.0 ± 0.1
	10 000	7.2 ± 0.1	31.0 ± 0.1

[a] Percentage of photo-induced absorbance changes, calculated using Equation 2.3;
[b] Uncertainties are representing the accuracy of the measurement equipment.
[c] Uncertainties are representing the fitting of individual curves to the double exponential decay, see Figure 4.10. Uncertainties for the measurement of different samples ca. = 0.58 (standard deviation derived from 4 measurements); Uncertainties for the 8 measurement of the one sample ca. = 0.12 (standard deviation derived from 8 measurements).

This measurement methodology allows two parameters to be measured: the amplitude of the photo-induced absorbance changes (ΔA), calculated using the Equation 2.3 and the half-life of the intermediate M_{410}, calculated using Equation 2.4, see Chapter 2.

The ammonia-induced changes of the photocycle parameters of the bR in the GE matrix were reversible. The initial parameters of the bR photocycle were regenerated after measurement of each ammonia gas concentration by flushing the sensor with an air atmosphere. The regeneration time was very long (> 1000 sec) when the bR film in GE matrix was exposed to the ammonia concentrations that exceeded 1 000 ppm compared with the low ammonia concentration.

The results obtained for the ammonia gas shows the possibility of employing a bR film as the sensitive element for optical sensors.

5.2 Humidity effect

Water molecules play a very important role in the bR function. Consequently, changes of the relative humidity experienced will change the optical parameters of the bR film which suggests that it could be employed for the development of the optical humidity sensor.

5.2.1 Humidity effect on the absorbance of the bR film

The absorbance spectra of the bR film in GE matrix recorded at the different relative humidities (rH) are shown in Figure 5.9.

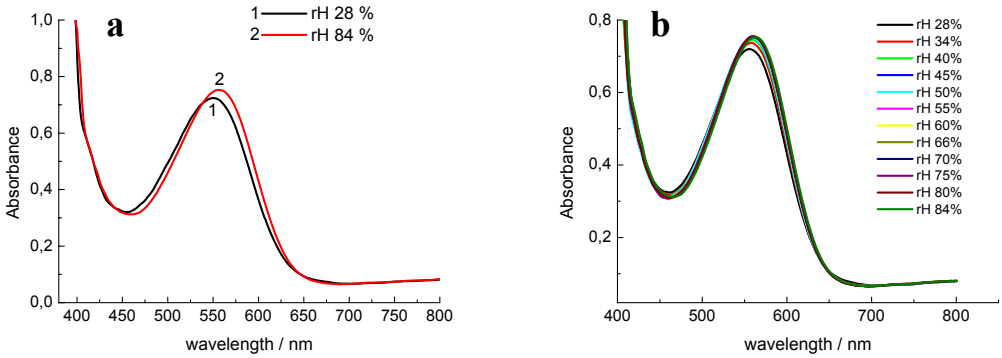

Figure 5.9: a, absorbance spectra of the bR film in GE matrix (mass ratio bR : GE = 12.5 : 84.5) measured at different relative humidities, utilizing a white light source without an actinic light: black line, rH = 28%; and red line 2, rH = 84%; b, absorbance spectra taken at different values of the rH.

The result shows that increasing the rH caused changes of the optical absorbance spectrum of the bR film in the GE matrix; the absorbance increased at the higher relative humidity at both wavelengths – 410 and 570 nm. The difference absorbance spectrum (rH 84% minus rH 28%) shown in

Figure 5.10 indicates that the greatest difference was observed at the wavelength of 587 nm. Additionally, increasing the rH caused a shift of the absorbance maximum from 550 nm to the 561 nm, see Figure 5.9.

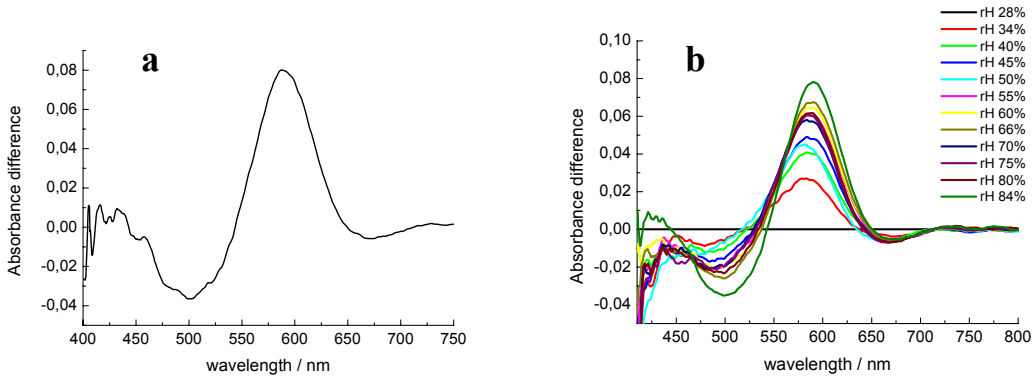

Figure 5.10: a, difference absorbance spectrum as derived from Fig 5.9a (rH 84% minus rH 28%) of the bR film in GE matrix (mass ratio bR : GE = 12.5 : 87.5), measured utilizing a white light source without an actinic light; b, difference spectra constructed from Figure 5. 9b by subtracting the rH 28% from higher values of the rH.

Figure 5.11 shows the time dependence of the normalized absorbance changes induced by the change of the relative humidity measured at the wavelengths of 410 nm and 570 nm. Normalization was carried out using the Equation 5.2 and represents the sensor response (S.R.):

$$S.R. = \frac{A_0 - A_{RH}}{A_0} \cdot 100\% , \qquad (5.2)$$

where, A_0, the absorbance of the bR film at rH=28%,; A_{RH}, the absorbance of the bR film at the given rH.

The results show that increasing the rH from the 28% to 50% led to a decrease of absorbance at 410 nm, while at 570 nm the absorbance was increased. In the range of rH 50–84% the absorbance at 410 nm started to increase.

The relative humidity was varied by placing a Petri dish containing water inside the closed measurement chamber where the sample was fixed and was monitored in the real time using the relative humidity Gemini Data Logger "Tinytalk", see chapter 2.2.2.

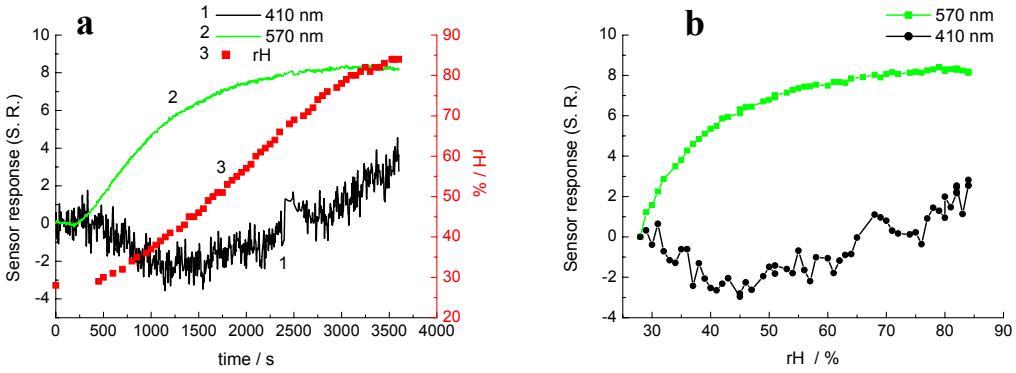

Figure 5.11: a, time dependence of the sensor response of the bR film in GE matrix (mass ratio bR : GE = 12.5 : 87.5) induced by the change of the relative humidity monitored at: black line 1, 410 nm and green line 2, 570 nm; red line 3, shows the changes of the relative humidity in time measured with the humidity meter; b, dependence of the sensor response on rH derived from the graph (a); sensor response was calculated using Equation 5.2.

The bR film in GE matrix showed a low sensitivity towards rH changes when compared to its sensitivity towards the presence of ammonia gas. The absorbance is changed only by 8% of the initial absorbance value at 570 nm and 3% of the initial absorbance value at 410 nm when the rH was changed from 28% to 84%. In contrast, the presence of ammonia changed

the absorbance by 70% of the initial absorbance at 570nm when the ammonia concentration was changed from 0 up to 10 000 ppm.

5.2.2 Humidity effect on the photocycle parameters of the bR film

Figure 5.12 shows the dependence of the decay half-life of the M_{412} state on relative humidity [168]. The relative humidity in measurement cell was set at fixed values by utilizing saturated solutions of LiCl, $MgCl_2$, $Ca(NO_3)$, $CoCl_2$ or KCl, to create equilibrium values of relative humidity of 0.12, 0.33, 0.5, 0.65 and 0.85 respectively [168]. Using this technique the calibrated values of relative humidity could be achieved for the purpose of testing the sensor element.

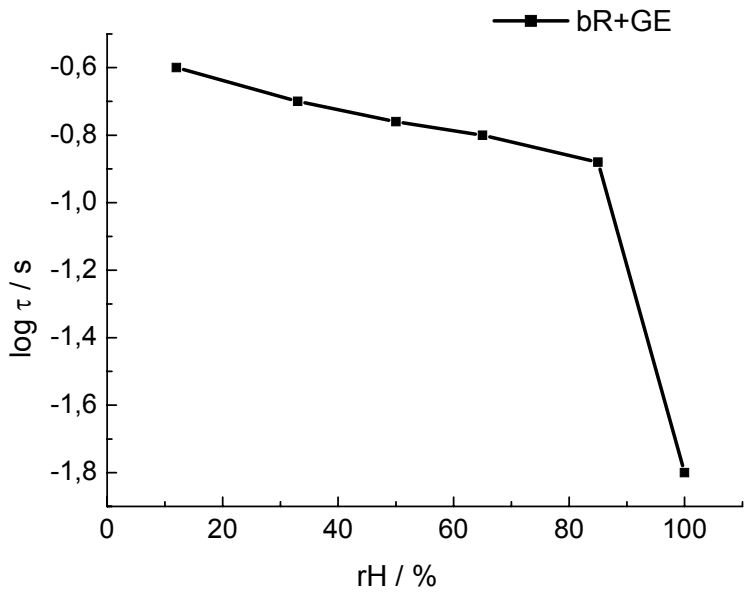

Figure 5.12: Dependence of the decay half-life of the M_{410} state for bR film in GE matrix on relative humidity (mass ratio bR : GE = 12.5 : 87.5), see Appendix C, Figure C1.

For films based on bR without chemical additives the half-life does not vary significantly for a wide range of the rH values (10–80%). At the high level of the rH (80–100%) the half-life of the M_{410} state of the bR becomes faster and is almost equal to the half-life in the aqueous solution.

5.3 Matrix and chemical additives: effects on the responses of the bR films to ammonia and humidity

The construction material, the structure of the matrix and the use of chemical additives can have strong influences on the optical properties of the bR films. Consequently, it was suggested that the response time, sensitivity and selectivity of the bR films towards the presence of either ammonia or changes in relative humidities can be optimized by using the appropriate combinations of matrices and chemical additives.

5.3.1 Effect of the chemical additives

5.3.1.1 Ammonia response

The ammonia induced absorbance changes spectra for atmospheres containing various concentrations of ammonia compared to that of air of the bR film in GE matrix and bR film in GE matrix with the triethanolamine added are compared in Figure 5.13.

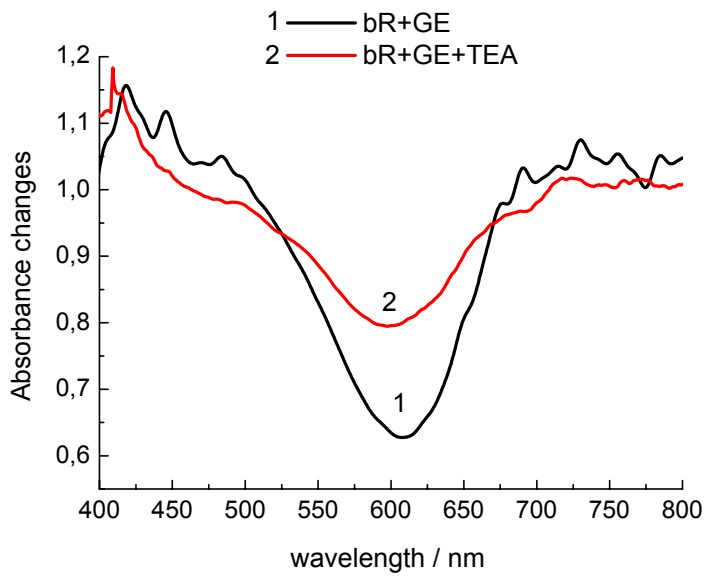

Figure 5.13: Ammonia induced absorbance changes spectra (ratio of spectrum taken at ammonia 10 000 ppm to spectrum taken with air only) of the: black line 1, bR film in GE matrix; and red line 2, bR film in GE matrix with the TEA added, for an optimal concentration of the TEA, see chapter 4 and Appendix C, Figure C12 (dried at rH 50%) (mass ratio bR : GE = 12.5 : 87.5; bR : GE : TEA = 12.4 : 73.54 : 13.8, measured at 25 ^{o}C and rH 50%), see Figures 5.2 and Appendix C Figure C2.

In order to represent a comparison between two different films in a more quantitative way the ratio of the spectra of the bR film without added TEA and with added TEA (taken at ammonia 10 000 ppm to spectrum taken at air) is plotted in Figure 5.13 instead of spectrum difference. This allows the difference in bR concentrations and thicknesses between different bR films to be eliminated.

According to Beer-Lambert law, absorbance spectra can be described using Equation 5.3:

$$A(\lambda) = \varepsilon(\lambda) \cdot C \cdot L\,, \tag{5.3}$$

where $A(\lambda)$, the absorbance of the bR film at the wavelength λ; $\varepsilon(\lambda)$, extinction coefficient at the wavelength λ; C, bR concentration in the bR films; L, thickness of the bR film

Hence, only optical properties ($\varepsilon(\lambda)$) of the bR are dependent on the ammonia effect while concentration of the bR and thickness of the bR film parameters are independent of the ammonia influence. Consequently, the ratio of the spectra of one film measured at different conditions, i.e. in the presence of ammonia gas and without it, will eliminate the C and L from the equation, according to:

$$\frac{A(\lambda, NH_3[10000\,ppm])}{A(\lambda, NH_3[0\%])} = \frac{\varepsilon(\lambda, NH_3[10000\,ppm]) \cdot \cancel{C} \cdot \cancel{L}}{\varepsilon(\lambda, NH_3[0\%]) \cdot \cancel{C} \cdot \cancel{L}}, \qquad (5.4)$$

where $A(\lambda, NH_3[10000ppm])$, $A(\lambda, NH_3[0\%])$, the absorbance of the bR film at the presence of the ammonia gas of 10 000 ppm and without ammonia, respectively at wavelength λ; $\varepsilon(\lambda, NH_3[10000ppm])$, λ; $\varepsilon(\lambda, NH_3[0\%])$, extinction coefficient at the presence of the ammonia gas of 10 000 ppm and without ammonia, respectively at wavelength λ, ; C, is bR concentration in the bR films; L, thickness of the bR film

The ratio of the spectra measured at different conditions are plotted when the bR films of different composition and thicknesses are compared.

The results demonstrated that the sensitivity of the bR film in GE matrix without chemical additives is higher than that of the bR film with the TEA added. It is proposed that the amine groups of the TEA additive suppress the effect of the ammonia gas on the bR and leads to the reduced magnitude of the optical responses of the bR film, as compared to the bR film without chemical additives.

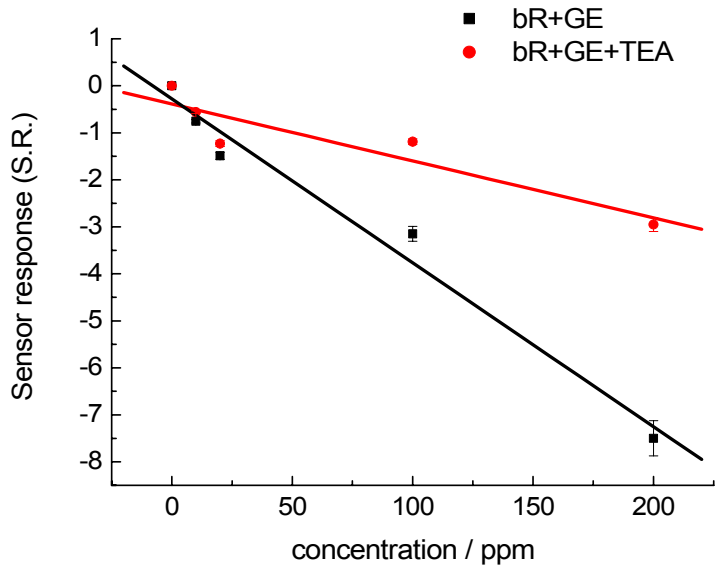

Figure 5.14: Calibration curves plotted from the results of ammonia-induced absorbance changes monitored at 580 nm in the: black line (squares), bR film in the GE matrix, slope: –0.035 ± 0.003; and, red line (circles), bR film in GE matrix with TEA added, slope: –0.012± 0.003 matrix (film composition mass ratio bR : GE = 12.5 : 87.5; bR : GE : TEA = 12.4: 73.54 : 13.8, measured at 25 ^{o}C and rH 50%), for details see Figure 5.4 and Appendix C, Figure C3.

The calibration curves for the bR film in GE matrix without and with TEA added, plotted from the ammonia-induced absorbance changes at different ammonia concentrations are demonstrated in Figure 5.14. The bR film in GE matrix without chemical additives demonstrates the higher sensitivity and faster response time towards ammonia as compared to the bR film with chemical additive. The *LOD* for the bR film with TEA added was 18 ppm that is 3 times higher then for the bR film without chemical additives.

Ammonia gas has a negligible influence on the photocycle parameters of the bR film in the GE matrix with TEA. Figure 5.15 shows time

dependence of the photo-induced absorbance changes measured in the presence of ammonia gas of the different concentrations.

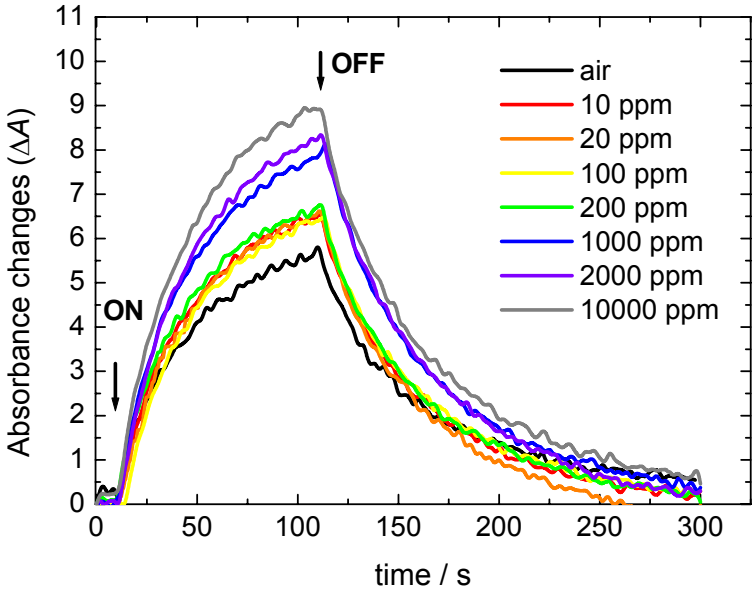

Figure 5.15: Time dependence of photo-induced absorbance (ΔA) changes of bR film in the GE matrix with TEA added measured at 25 ^{o}C and rH 50% monitored at 410 nm during and after actinic illumination (halogen light source with a high pass filter (> 530 nm)) in the presence of ammonia gas of different concentration (arrows indicate the turning ON and OFF the actinic light source) (film composition mass ratio bR : GE = 12.5 : 87.5; bR : GE : TEA = 12.4 : 73.54 : 13.8).

The calibration curves plotted for bR+GE and bR+GE+TEA using data of the double exponential fitting (Equation 2.4) are compared in Figure 5.16. The half-life of the decay of the M_{410} state of the bR film in the GE matrix with TEA added became dependent on the presence of ammonia only when film was exposed to the high ammonia concentration (> 2 000 ppm).

The *LOD*, calculated using Equation 5.1 for the bR film in GE matrix without added TEA was 0.8 ppm and 10 ppm for the lifetime of the M_{410} state decay and photo-induced absorbance changes, respectively.

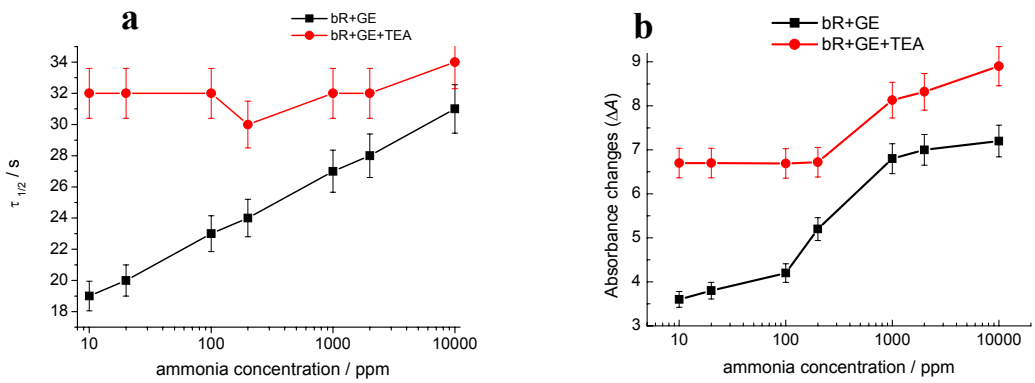

Figure 5.16: Calibrations curves were plotted using the data of the double exponential fitting (Equation 2.4) and represent: a, the half-life ($\tau_{1/2}$) of the M_{410} state; b, the photo-induced absorbance changes (ΔA); squares, bR film in GE matrix; circles, bR+GE+TEA (measured at 25 ^{o}C and rH 50%, mass ratio bR : GE = 12.5 : 87.5; bR : GE : TEA = 12.4 : 73.54 : 13.8).

5.3.1.2 Humidity response

The absorbance spectra of the bR film in GE matrix with TEA added recorded at the different values of rH are shown in Figure 5.17.

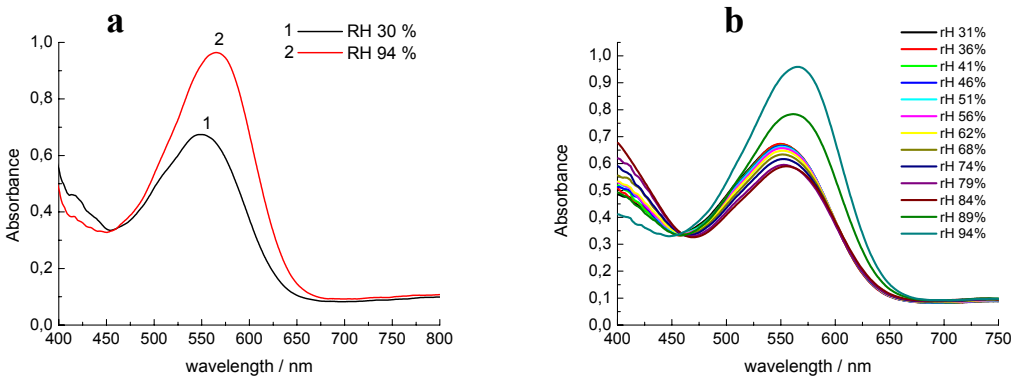

Figure 5.17: a, absorbance spectra of the bR film in GE matrix with TEA added measured at: black line 1, rH = 30%; and red line 2, rH = 94% (mass ratio bR : GE = 12.5 : 87.5; bR : GE : TEA = 12.4 : 73.54 : 13.8); b, absorbance spectra measured at different values of rH.

The comparison of the difference spectra of the bR film in GE matrix with and without the chemical additive TEA is shown in Figure 5.18. In contrast to ammonia, the largest absorbance differences in response to changes in rH were observed in the film with TEA added. Moreover, the absorbance linearly decreased at 535 nm and increased at 410 nm, when rH increased from 31% to 84% (Figure 5.18b). At higher rH (84–94%) the biggest absorbance difference was observed at 580 nm. The time dependence of the S.R. of the bR film in GE matrix with TEA to the change of the rH is shown in Figure 5.19a, b. Contrary to the bR film without TEA additive, in bR film with added TEA the absorbance changes of 30% and 50% induced

by changes of rH from 31% to 84% and from 84% to 95% respectively are observed at 410 nm (Figure 5.19b).

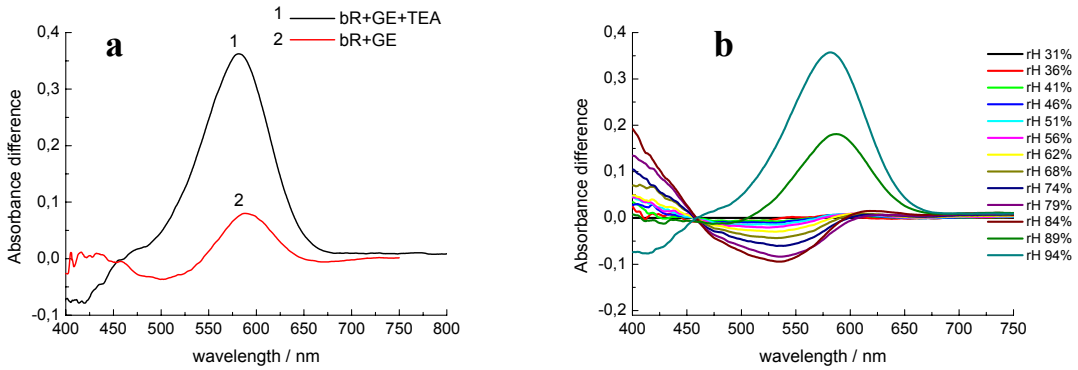

Figure 5.18: a, comparison of the difference absorbance spectra (high rH minus low rH) of the: black line 1, bR+GE+TEA; and red line 2, bR +GE (mass ratio bR : GE = 12.5 : 87.5; bR : GE : TEA = 12.4 : 73.54 : 13.8); b, difference spectra constructed from Figure 5.17b by subtracting the rH 31% from higher values of the rH.

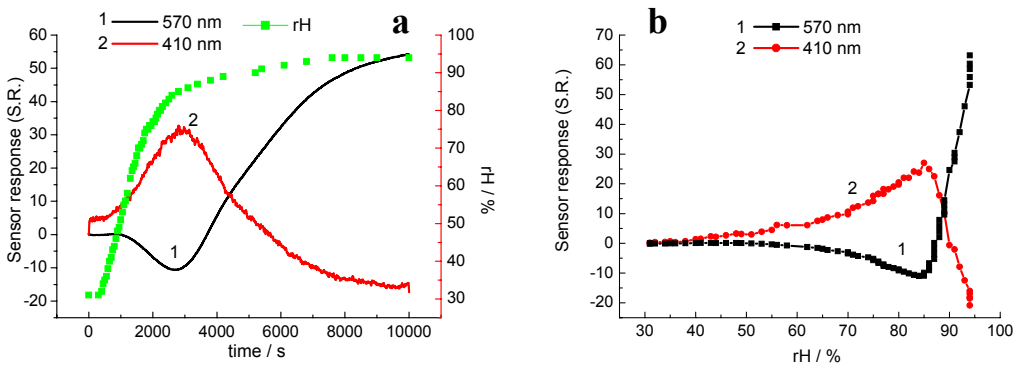

Figure 5.19: a, time dependence of the sensor response of the bR film in GE matrix with TEA (mass ratio bR : GE : TEA =12.4 : 73.54 : 13.8) to the change of the relative humidity monitored at: black line 1, 570 nm and red line 2, 410 nm; green line, shows the changes of the relative humidity in time measured with the humidity meter; b, dependence of the sensor response on rH derived from the graph (a); sensor response was calculated using Equation 5.2.

The dependences of the half-life of the intermediate M_{410} state on the humidity for the bR+GE+TEA film and bR+GE film are shown in Figure 5.20.

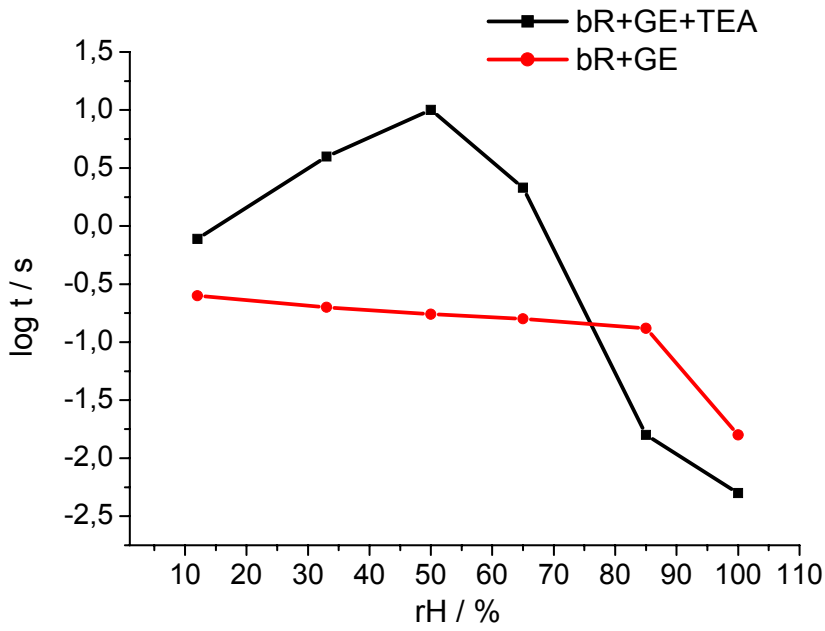

Figure 5.20: Dependence of the decay half-life of the M_{410} state on relative humidity for: black line 1 (squares), bR+GE+TEA; red line 2 (circles), bR film in GE matrix; [168] (mass ratio bR : GE = 12.5 : 87.5; bR : GE : TEA = 12.4 : 73.54 : 13.8), for experimental results see Appendix C, Figure C1.

Results of the effects of changes of ammonia concentration and of the rH on the optical properties of the bR films with and without chemical additive demonstrate that the sensitivity of the detection system can be tailored towards rH by the addition of the chemical additive (TEA).

The presence of ammonia in the atmosphere surrounding the film resulted in changes of the optical absorbance and the photocycle parameters for both bacteriorhodopsin in the GE matrix and bR in the GE matrix with

added TEA. The magnitudes of these changes were significantly different, however. The kinetic changes at 410 nm confirmed that the presence of ammonia modulates the parameters of the bacteriorhodopsin photocycle for all the films investigated, but the sensitivity depends on film composition; in contrast to the humidity result, films without the chemical additives TEA are more sensitive to ammonia.

5.3.2 Matrix effect

5.3.2.1 Ammonia response

In order to study the effect of the matrix on the response time and sensitivity of the bR films towards ammonia the bR in different matrices and bR self-assembled film were exposed to atmospheres containing ammonia gas at different concentrations. Bacteriorhodopsin self-assembled films were produced by the casting method described in Chapter 3. Briefly, a 0.5 mL of the bR aqueous solution (14 mg lyophilized powder /mL) was placed on a glass substrate and dried for 24 hours in a desiccator. The difference absorbance spectra (ammonia atmosphere minus air) of the bR self-assembled film without matrix, with the matrix constructed from gelatin, bR+GE, a matrix constructed from polyvinyl alcohol, bR+PVA and bR+sol-gel films are compared in Figure 5.21a.

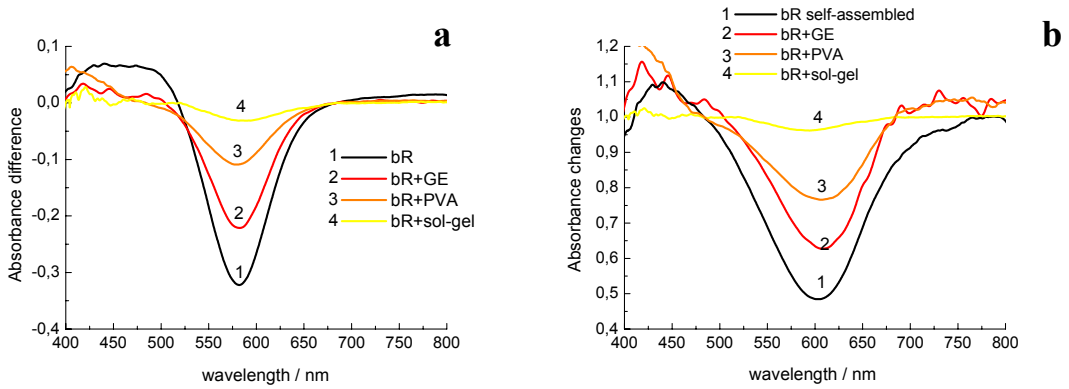

Figure 5.21: a, difference absorbance spectra (ammonia 10 000 ppm minus air) of the: line 1, bR self-assembled; line 2, bR+GE; line 3, bR+PVA; and line 4, bR+sol-gel films (measured at 25 ^{o}C and rH 50%, mass ratio bR : GE (PVA) = 12.5 : 87.5; bR : TEOS = 5.5 : 94.5), for experimental results, see Appendix C, Figures C4–C6; b, absorbance changes normalized to the bR concentration by dividing the spectra taken and ammonia concentration 10 000 ppm to the spectra taken at air, i.e. NH_3[10 000 ppm]/NH_3[%].

The highest sensitivity towards ammonia gas was shown by the self-assembled bR film and bR film in GE matrix. Bacteriorhodopsin incorporated into a sol-gel glass demonstrated the lowest sensitivity among all films. This can be attributed to the low concentration of the bR in the sol-gel glass. During the manufacturing process of the bR sol-gel film it was difficult to obtain a sample with a high concentration of bR in the sol-gel glass. Presumably, it was due to aggregation between the fragment of the purple membranes and silica gel particles. The light scattering was high and sol-gel samples were practically opaque when a high concentration of the bR was used.

On the other hand, the response time t_{90} of the bR film in the sol-gel matrix was 10 times and 3 times faster compared to the bR film in the GE matrix and bR self-assembled film, respectively (Table 5.5). This can be explained when considering the porosities of the matrices used for the film

production; the porosity of the sol-gel glass is 200 times greater than the porosity of the polymeric films, see chapter 3.4 (Table 3.1). This phenomenon can be explained if we consider that highest porosity of the matrix allows the fastest diffusion of the ammonia gas into the bR film structure, hence providing the faster reaction to occur between bR and the analyte gas.

Increasing the concentration of the bR in the sol-gel glass possibly will overcome the disadvantage of the low ammonia sensitivity this film demonstrated. However, when this work was undertaken no techniques were available to achieve this. Recently it was demonstrated that a bacteriorhodopsin film in a sol-gel matrix with the high concentration of the bR and low light scattering could be manufactured using the method proposed by Pandey et al. [177]. In this approach the bR was sandwiched between two layers of the organically modified silica glass and showed high stability and photoactivity [177].

Figure 5.22 and Table 5.5 summarize the results of the ammonia effect on the bR films of the different compositions indicating the limits of detection and response times to ammonia gas with a concentration of 1 000 ppm.

Table 5.5: Response times (concentration 1 000 ppm) and limits of detections of the bR films in different matrices to the presence of ammonia gas (measurements were undertaken at 25 °C and rH 50%), for experimental results, see Appendix C, Figures C7, C8.

Sample	Response times		*LOD* (ppm)	Linear range (ppm)	Sensitivity $\Delta A/\Delta C$, (%/ppm)	bR : matrix mass ratio	Specific surface area, m^2/g, B.E.T
	t_{90}	t_{50}					
bR+sol-gel	10 min	113 sec	8	10–200	–0.017± 0.002	5.5 : 94.5	676.6
bR	28 min	5.8 min	3	10–200	–0.040± 0.004	Self-assembled (no matrix) prepared from the bR aqueous solution of 14 mg/mL	—
bR+GE	120 min	67 min	5	10–200	–0.035 ± 0.003	12.5 : 87.5	2.6

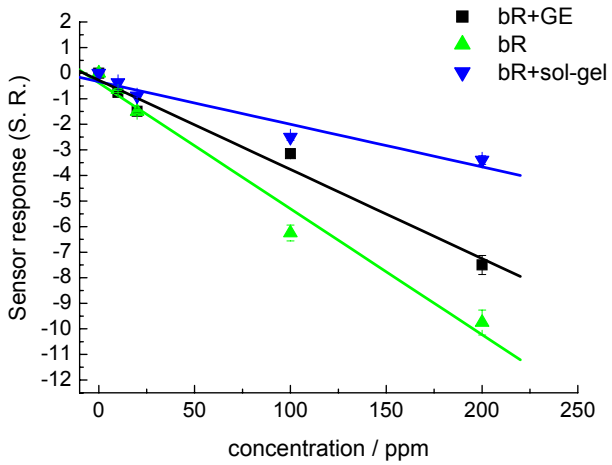

Figure 5.22: Calibration curves plotted from the results of ammonia-induced absorbance changes (measured at 25 °C and rH 50%, mass ratio bR : GE = 12.5 : 87.5; bR : TEOS = 5.5 : 94.5) monitored at 580 nm in the: black line (squares), bR film in the GE matrix, slope: –0.035 ± 0.003; blue line (triangles), bR film in sol-gel matrix added, slope: –0.017± 0.002; green line (triangles), bR self-assembled film, slope: –0.040± 0.004), for experimental results see Figure 5.14 and Appendix C, Figures C7, C8.

The presence of ammonia modulates the optical parameters of the bR films in a similar way regardless of the matrices used for the film manufacturing. The magnitudes of the changes were different, however. The sensitivity and response time of these changes depend on the structural parameters of the material used as a matrix. Bacteriorhodopsin embedded into the sol-gel glass demonstrated the fastest response time, and at the same time possessed the lowest sensitivity.

The photo-induced absorbance changes of the bR photocycle and half-life were influenced by the presence of ammonia gas. The largest changes of the half-life of the M_{410} state were observed in the bR film in the GE matrix. The measurement of the photo-induced absorbance changes of the bR incorporated into the sol-gel glass was difficult to accomplish because of the high light scattering in this sample.

5.3.2.2 Relative humidity effect

The differential absorbance spectra (rH=90% minus rH=30%) of the bR films in the different matrices are compared in Figure 5.23.

The results indicate that the changes of the rH from 30% up to 90% lead to similar changes of the absorbance features of the bR films incorporated into different matrix materials. The largest changes of the absorbance were observed in the bR self-assembled film at the wavelength of 580 nm. Bacteriorhodopsin incorporated into GE and PVA polymeric matrices showed a similar response to the change of the relative humidity.

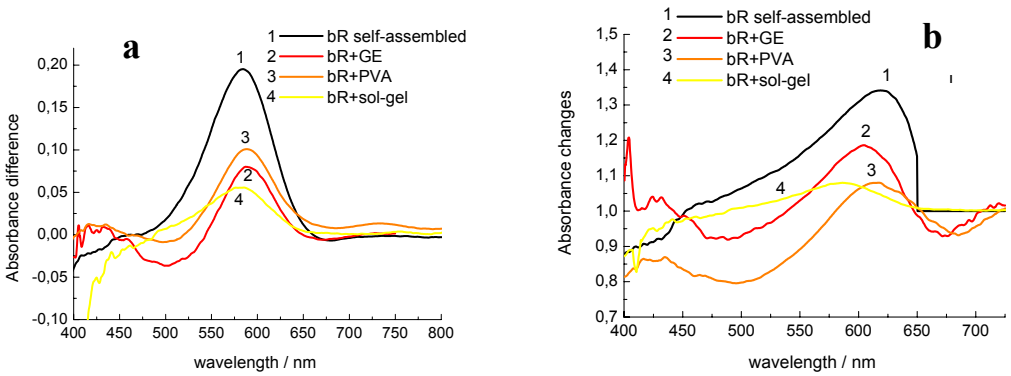

Figure 5.23: a, difference absorbance spectra (rH=90% minus rH=30%) of the line 1, bR self-assembled; line 2, bR+GE; line 3, bR+PVA; and line 4, bR+sol-gel films (mass ratio bR : GE (PVA) = 12.5 : 87.5; bR : TEOS = 5.5 : 94.5); b, normalized to the bR concentration by dividing the spectra taken and rH = 30% to the spectra taken at rH= 90%, i.e. rH[30%]/rH[90%], for experimental results see Appendix C, Figures C9–C11.

Figure 5.24 shows the sensor response of the bR films in the different matrices to the relative humidity changes monitored at 570 nm.

The response to the rH changes of the bR incorporated into different matrices has a different behaviour (Figure 5.24). The absorbance of bR film in the GE matrix increased from the 30% up to 90%, while in the film of bR in PVA matrix the absorbance was almost constant at the rH range of 40–75%, followed by linear changes of the absorbance at the high rH (80–90%). The response of the bR film incorporated into sol-gel matrix decreased linearly in the rH range of 40–60% went through a maximum at 65% and showed the linear increasing response in the rH range of 70–90%.

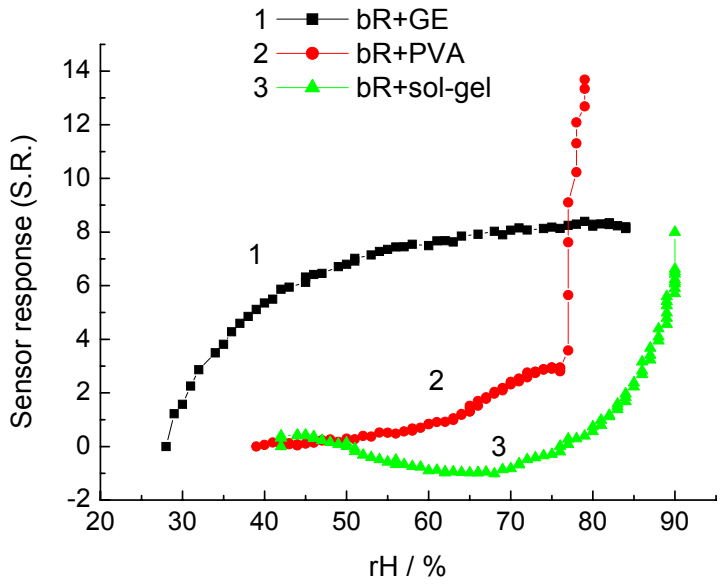

Figure 5.24: Dependences of the sensor response of the bR film in different matrices to the change of the relative humidity from 30% up to 90% monitored at 570 nm; black line (squares), bR in GE matrix; red line (circles), bR in PVA matrix; green line (triangles), bR in sol-gel matrix (mass ratio bR : GE (PVA) = 12.5 : 87.5; bR : TEOS = 5.5 : 94.5).

The results of the effect of ammonia gas and rH changes on the bR films in the different matrices indicate that sensitivity, selectivity (towards ammonia and rH changes) and response time can be varied by using the different matrices. The bR self-assembled film shows the highest sensitivity towards ammonia, but the poor adhesion of this film to the substrate (glass plate or quartz optical fibre) is a question which needs to be studied carefully. On the other hand, the bR film in GE matrix shows a similar sensitivity and *LOD* towards ammonia as the bR self-assembled films, which provides the potential for the manufacturing of these films with good adhesion and optical quality.

5.3.3 Selectivity to other chemical species

In order to study the selectivity of bR films bR was exposed to hydrogen peroxide vapour (H_2O_2), chlorine (Cl_2) gas and ethanol vapour. When the bR film was exposed to the Cl_2 gas and H_2O_2 vapours no significant changes were observed in the optical properties of the bR films in a GE matrix. The presence of the ethanol vapour at high concentration caused irreversible absorbance changes at the wavelength of 570 nm, indicating the denaturation of the bR [178].

5.3.4 Effect of the light source intensity

Different light sources intensities were used in order to investigate the influence of the light intensity on the response of the bR film in GE matrix to rH changes, see Appendix C, Figures C13, C14. The results demonstrated that at high light intensity the absorbance changes induced by the changes of rH were two times bigger when compared to the light source with relatively low intensity of units of mW/cm^2.

Conclusions and Summary:

The effect of the ammonia gas and relative humidity changes on the optical properties of the bR films was investigated in this Chapter. The presence of the ammonia gas modulated the bR optical properties in a similar manner to the chemical additive. The results obtained from the experiments indicated the possibility of the employing bR as a sensitive element for the development of a fibre-optic ammonia sensor.

Additionally, it was demonstrated that inclusion of the chemical additives (such as TEA) into the bR film increased the sensitivity towards relative humidity not only via optical absorption, but also via the half-life of the M_{410} state of the photocycle. On the other hand, it suppressed the ammonia response. This illustrates a very important feature of bR films, namely that for a given additive, the sensitivities towards different substances can vary very considerably, thus minimizing the influence of possibly interfering substances on a given measurement, so selectivity is readily achievable.

Accordingly, bR film without chemical additives is suitable for the creation of an ammonia sensitive element for the fibre-optic sensor, while the bR film with TEA added can be employed as a relative humidity sensitive element.

Employing the bR films with the different matrices can vary the sensitivity, response time and *LOD* of the sensitive element, thus enhancing the possible application areas of the bR films in fibre-optic sensor development. The highest sensitivity demonstrated was for the self-assembled bR film with the *LOD* = 3 ppm and linear response to the ammonia in the range of concentrations (0–10 000 ppm). On the other hand, the fastest response time (t_{90}) was achieved when bR was incorporated into the sol-gel glass.

The half-life of the M_{410} state of the bR photocycle varied when the bR film was exposed to ammonia gas.

The presence of other chemical species within the matrix, such as chlorine and hydrogen peroxide, did not influence the optical parameters of the bR films. The presence of ethanol vapours at high concentrations led to the bleaching of the absorbance maximum at 570 nm and to the denaturation of the bR.

In the next Chapter 6, different measurement schemes for the development of the fibre-optic sensors will be discussed. The features of the measurements of the amplitude changes and time characteristics will be demonstrated. The optimal fibre-optic sensor design, in terms of sensitivity and applicability, will be suggested.

Chapter 6: Choosing the optimal design of the optical sensor - discussion

The results demonstrated in the previous Chapter 5, both for humidity and for ammonia vapour, indicated that bR films could be applied as a sensitive element for the fabrication of fibre-optic sensors.

In this Chapter, two possible designs of the fibre-optic sensors utilising bR film as a sensitive element are presented: (i) based on the amplitude and (ii) half-life time measurements. The sensitivities, advantages and disadvantages of these proposed designs will be compared and discussed. The optimal solution in terms of sensitivity and usefulness as a sensor scheme will be proposed. The features of the measurements of the amplitude absorbance changes and time characteristics will be discussed.

6.1 Measurement of the amplitude changes induced by ammonia and relative humidity

Bacteriorhodopsin film shows the biggest absorbance amplitude changes at the wavelength 580 nm when exposed to ammonia gas or when the relative humidity is changed, see Figure 5.2 and 5.10, respectively. Consequently, the simplest method to create the fibre-optic sensor would be to measure the reflectance of films based on bR with appropriate chemical additives at the wavelengths of a 580 nm. The research results suggest that the best design solution would be to develop an amplitude type fibre-optic sensor with a sensitive film element deposited on the optical fibre distal end face. The typical response of the sensor to a change of relative humidity inside the chamber is shown in Figure 6.1.

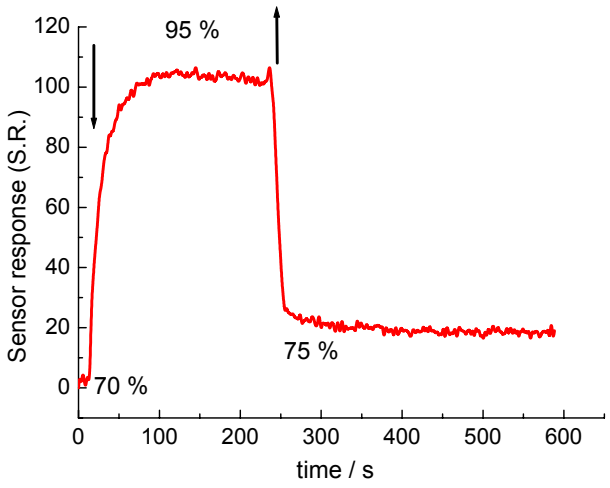

Figure 6.1: Response to the change of humidity inside a chamber of the bR film with added TEA deposited onto the optical fibre of a fibre optic Y-type coupler, probed at 410 nm. The arrows denote placing a drop of water inside the closed chamber; at 250 s the chamber was opened.

The scheme of the fibre-optic sensors used for the measurements of the amplitude changes induced by the ammonia gas and relative humidity is shown in Chapter 2, see Figure 2.15.

However, the key disadvantage of this measurement method is that changes of both the value of the relative humidity and the concentrations of the ammonia gas concurrently cause changes in the optical absorbance of the bR films. The inclusion of the chemical additives to some degree enhanced the selectivity of the bR film; increasing the sensitivity towards relative humidity and suppressing the sensitivity towards ammonia gas. At the same time, the bR film without chemical additives shows a response to both changes of the relative humidity and the concentrations of the ammonia gas when measured at 580 nm. The magnitudes of these changes were different, however, but at low concentrations of the ammonia gas it is impossible to distinguish between these two effects (Figure 6.2).

Additionally, the response of the bR film to the ammonia gas was humidity-dependent; at the low range of rH value 3–30% the bR film shows no response to the low concentration of ammonia gas and very little ammonia-induced effect on the bR absorbance was observed when bR film was exposed to high ammonia concentrations (>2 000 ppm) at low rH value. For the detection of the ammonia the optimal relative humidity range was within of 30–80% rH.

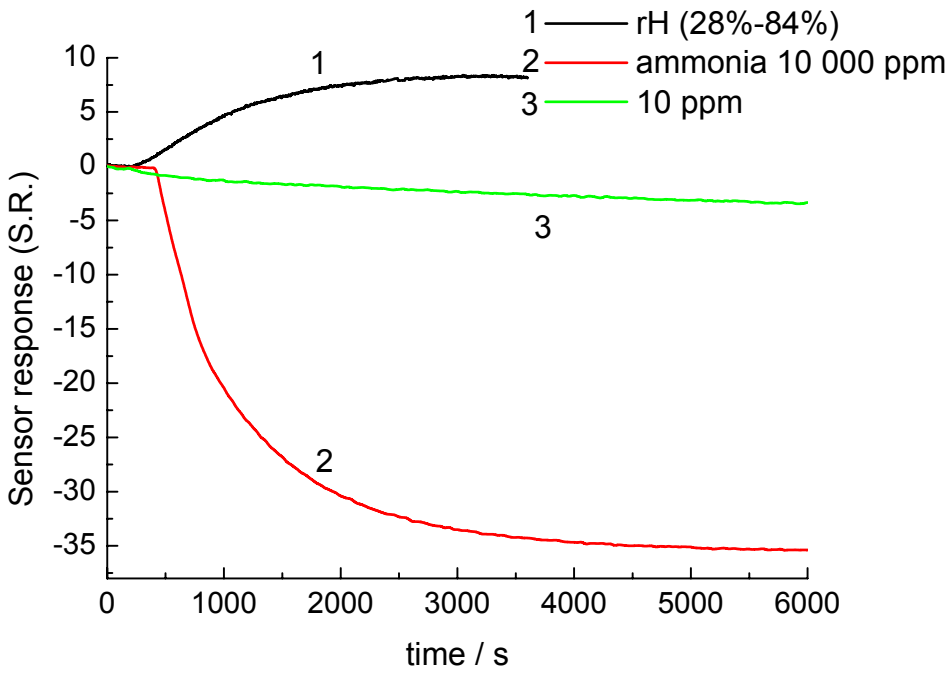

Figure 6.2: Comparison of the sensor response of the bR film in GE matrix: black line 1, to the changes of the rH from 28% to 84%; red 2 and green line 3, to the presence of ammonia gas of 10 000 ppm and 200 ppm, respectively.

One possible solution of this problem would be to develop a sensor system consisting of two sensors, one of which will be coated by the bR film containing chemical additives to serve as a reference sensor for the evaluation of the rH value; while the second sensor would be used for the measurement of the ammonia gas concentration, taking into account the signal from the reference sensor (rH value).

This can be accomplished by simultaneous interrogation of both sensors coated by the bR films with and without added TEA. Sensor response (S.R.) of the bR film with chemical additives could be represented according to Equation 6.1:

$$S.R.^{TEA} = \frac{\Delta S.R._{rH}^{TEA}}{\Delta rH} + \frac{\Delta S.R._{NH_3}^{TEA}}{\Delta NH_3}, \quad (6.1)$$

where, S.R.^{TEA}, the sensor response of the bR film with added TEA; $\frac{\Delta S.R._{rH}^{TEA}}{\Delta rH}$, the response of the bR film with added TEA to the rH changes; $\frac{\Delta S.R._{NH_3}^{TEA}}{\Delta NH_3}$, the sensor response of the bR film with added TEA to the presence of the NH_3.

On the other hand, sensor response of the bR film without added TEA can be given using Equation 6.2:

$$S.R.^{bR} = \frac{\Delta S.R._{rH}^{bR}}{\Delta rH} + \frac{\Delta S.R._{NH_3}^{bR}}{\Delta NH_3}, \quad (6.2)$$

where, S.R.^{bR}, the sensor response of the bR film without added TEA; $\frac{\Delta S.R._{rH}^{bR}}{\Delta rH}$, the sensor response of the bR film with added TEA to the rH changes; $\frac{\Delta S.R._{NH_3}^{bR}}{\Delta NH_3}$, the response of the bR film with added TEA to the presence of the NH_3.

Knowing the dependence of the sensor response S.R. of the bR film with and without added TEA on the rH changes and using the software that will solve the combined equations (6.1 and 6.2), it could be possible to measure simultaneously both parameters rH changes and ammonia concentration.

6.2 Life-time measurements

The other possible option of the creation of fibre-optic sensor is to measure the half-life times ($\tau_{1/2}$) of the M_{410} intermediate in response to switching the exposure to actinic illumination on and off. The experimental results showed that the half-life time of this intermediate displays the highest changes when exposed to chemical analytes. A sensor design could be based on a variant of the fibre-optic sensor by including an additional illumination channel and a timer recording the change of time of the maximum (or minimum) signal up to a certain level (Figure 6.3) [179].

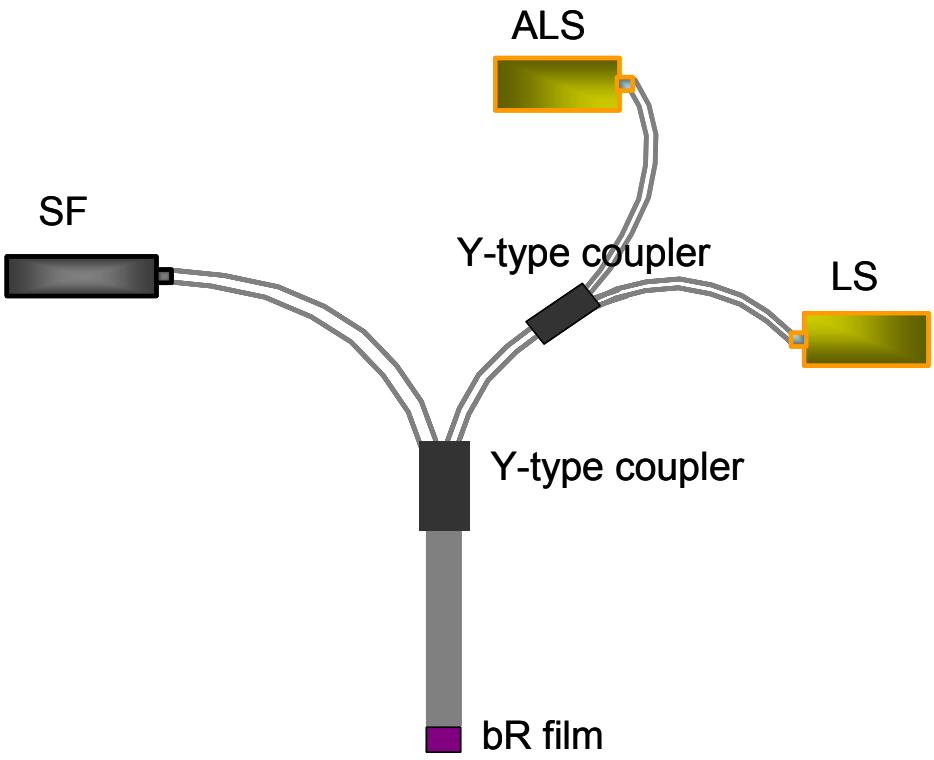

Figure 6.3: Schematic diagram of the fibre-optic sensor with additional channel for the measurements of the half-life time of the M_{410} state; LS, probe light source; SF, spectrophotometer; ALS, actinic light source.

Recording would start at the instant of switching off the actinic light, and the interval τ required for the output signal to reach a certain fraction of the starting condition (conveniently 1/e (or 36.8%) of the initial amplitude) would be recorded, see Figure 6.4.

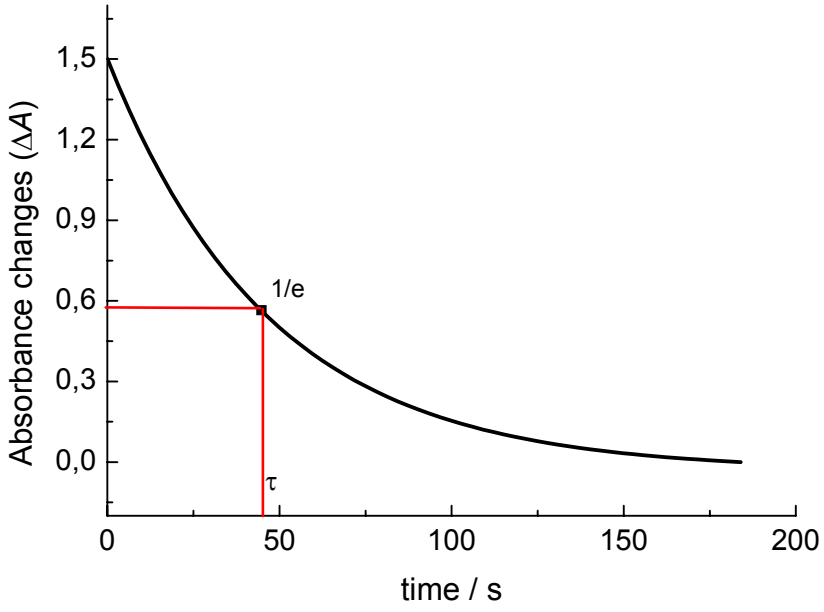

Figure 6.4: Time dependence of the photo-induced absorbance changes (Δ*A*) of the bR film in GE matrix monitored at 410 nm after switching off the actinic light indicating the time interval τ required for the signal to achieve the value of 1/e of the initial amplitude (normalization was carried out using Equation 2.3).

The influences of the ammonia gas and changes of the rH on the half-life time of the M_{410} of the bR film in GE matrix without TEA added were different as was demonstrated from the experimental results, see Chapter 5, Figures 5.12 and 5.16 (squares line). These results displayed that negligible changes occur for the half-life time in bR film without chemical additive

over a wide range of relative humidity values. However, the presence of ammonia gas changes the magnitude of the half-life by a factor of 2.

When the chemical additive (TEA) was added, the opposite effect was displayed. Changes of the value of the relative humidity in the range of 30–100% modulated the half-life time of the bR film by 3 orders of magnitude, while the presence of ammonia gas did not change a half-life time of the M_{410} state at all (Figure 5.16a).

These results suggest that using measurements of the half-life time will enhance the selectivity and performance of the fibre-optic sensor with the sensitive element based on the bR film. The implementation of the measurement scheme, however, requires the use of an additional Y-type fibre optic coupler and is more complicated and expensive when compared to the measurement technique which employs amplitude changes.

However, the sensitivity on terms of limit of detection (*LOD*) to ammonia gas of the bR film without TEA added is higher (*LOD*=0.8 ppm) when the half-life time measurements are measured as compared to the amplitude absorbance changes measurements (*LOD*=5 ppm). The choice of the appropriate scheme, either measurement of the amplitude of the absorbance changes or the half-life time of the M_{410} state of the bR, will depend on the required areas and targets of the application.

When high sensitivity of the control of changes of rH is required the fibre-optic sensor based on the measurement of the half-life time of the bR film with TEA added would be the best measurement system to employ.

For high sensitive and cheap detection of the ammonia gas, the bR film without chemical additives deposited on the distal end of the fibre-optic sensor based on the measurements of the amplitude changes would be the most appropriate measurements scheme.

It was demonstrated that inclusions of chemical additives led to the modulation of the optical properties and sensitivity of the bR films to the analytes ammonia and the moisture content of the air; Chapter 4, Figure 4.9 and Chapter 5, Figures 5.14 and 5.18. The optimal concentration of the chemical additive triethanolamine in the bR films was found by Z. Batory-Tartsi [154] to be 13.8%; at this concentration the bR films possessed the highest photosensitivity and longest half-life time of the M_{410} state that is very important for application bR films as an optical storage medium. For the sensor application of bR, increasing the TEA concentration in the bR film beyond this value possibly could completely suppress the response of the bR film to the presence of the ammonia gas; at the same time it could increase the sensitivity to the changes of rH.

It would be useful for future work to study the effect of the concentration of chemical additives in bR films on their selectivity and sensitivity. The effects of other chemical additives that can tailor the sensitivity and specificity of the bR films to other chemical species should be studied. This would create the possibility of using bR films as universal sensitive elements for fibre-optic sensor systems. In this sensor system the individual fibre-optic sensor would be coated with the appropriate bR film selectively sensitive to a particular chemical species.

Different materials used as a matrix for the manufacturing of bR based films showed a little effect on the selectivity towards ammonia and rH; all films showed the similar responses. However, the response time and sensitivity of the sensing element were changed dramatically when different matrices were used. The response time of the bR based film when exposed to ammonia was faster by 2 orders of magnitude, when the inorganic sol-gel film was used as a matrix, as compared with the gelatin and polyvinyl alcohol bR based films. Bacteriorhodopsin film in GE matrix

demonstrated the highest sensitivity to the presence of ammonia gas. The sensitivity of the bR film in silica sol-gel matrix can be increased by optimizing the manufacturing technology and by increasing the concentration of the bR in the silica matrix.
Moreover, as it was demonstrated, two different measurement schemes, depending on either the amplitude or half-life of the signal, can be employed using the bR films as a sensitive element of the fibre-optic sensors that can enhance the performance of the sensor system.

Summarizing, in this work the possibility of creating a universal sensitive element for fibre-optic sensors for the measurement of ammonia concentration and relative humidity based on bR films was demonstrated. The sensor parameters, namely sensitivity, response time, selectivity and limit of detection can be controlled simply by changing the chemical composition of the bR films.

References

1. Snyder, A. and Love, J. *Optical waveguide theory*, Bristol: J. W. Arrowsmith Ltd., 1983.
2. Mehrvar, M., Bis, C., Scharer, J. M., Moo-Young, M., Luong, J. H. Fibre-optic biosensors-trends and advances. *Analytical sciences*, 16, 2000, p. 677–692.
3. Seitz, W. R. Chemical sensors based on fibre optics. *Analytical chemistry*, 56, 1984, p. 16–34.
4. Arnold, M. A. Fibre optic chemical sensors. *Analytical chemistry*, 64, 1992, p. 1015–1025.
5. Grattan, K. T. V. and Meggitt, B. T. *Chemical and environmental sensing*, Boston: Kluwer Academic Publisher, 1999.
6. Medlock, R. S. Fibre-optic intensity modulation sensors. In: *Optical Fiber Sensors Proc. of the NATO Advanced Study Institute*, Erice, Italy, May 10–20, 1986, *NATO Science Series E: Applied Sciences,* Vol. 132, 1987, p. 123–124.
7. Spooncer, R. Fibre optic in instrumentation. In: *Handbook of Measurement Science*, edited by P.H. Sydenham & R. Thorn, 1992, p. 1691–1720.
8. Spenner, K., Singth, M. D., Schulte, H., Boehnel, H. J. Experimental investigation on fibre optic liquid level sensors and refractometer. In: *Proc. 1st international conference on optical sensors* (Ed) IEE, London, 1983, p. 96–99.
9. Galbarra, D., Arregui, F. J., Matias, I. R., Claus, R. O. Ammonia optical fibre sensor based on self-assembled zirconia thin films. *Smart materials and structures*, 14, 2005, p. 739–744.

10. Wolthuis, R. A., Mitchell, G. L., Suaski, E., Hartl, J. C., Afromowitz, M. A. Development of medical pressure and temperature sensors employing optical spectrum modulation. *IEEE, Transaction on biomedical engineering*, 38, 1991, p. 974–981.
11. Oberg, K. I., Hodyss, R., Beauchamp, J. L. Simple optical sensor for amine vapors based on dyed silica microspheres. *Sensors & Actuators B: Chemical*, 115, 2006, p. 79–85.
12. Zhang, K., Butler, C., Yang, Q., Lu, Y. A fibre optic sensor for the measurement of surface roughness and displacement using artificial neural networks. *IEEE, Transaction on instrumentation and measurement*, 46, 1997, p. 899–102.
13. Christie, S., Scorsone, E., Persaud, K., Kvasnik, F. Remote detection of gaseous ammonia using the near infrared transmission properties of polyaniline. *Sensors & Actuators B: Chemical*, 90, 2003, p. 163–169.
14. Giordano, M., Russo, M., Cusano, A. An high sensitivity optical sensor for chloroform vapours detection based on nanometric film of δ-form syndiotactic polystyrene. *Sensors & Actuators B: Chemical*, 107, 2005, p. 140–147.
15. Cusano, A., Persiano, G. V., Russo, M., Giordano, M. Novel optoelectronic sensing system for thin polymer films glass transition investigation. *IEEE Sensors Journal*, 4, 2004, p. 837–844.
16. Zalvidea, D., Diez, A., Cruz, J. L., Andres, M. V. Palladium-coated fibre-taper hydrogen sensor: temperature response. *Proc. of SPIE*, 5855, 2005, p. 447–450.
17. Ming Tan, K., Tjin, S. C., Chan, C. C., Mohanty, L., Tay, C. M. High relative humidity sensing using gelatin-coated long period grating. *Proc. of SPIE*, 5855, 2005, p. 375–378.

18. Cusano, A., Cutolo, A., Giordano, M., Nicolais, L. Optoelectronic refractive index measurements: application to smart processing. *IEEE Sensors Journal*, 3, 2003, p. 781–787.
19. Stanley, M. A., Maxwell, J., Forrestal, M., Doherty, A. P., MacCraith, B. D., Diamond, D., Vos, J. G. Comparison of the analytical capabilities of an amperometric and an optical sensor for the determination of nitrate in river and well water. *Analytica Chimica Acta*, 299, 1994, p. 81–90.
20. Le Coq, D., Boussard- Plédel, C., Fonteneau, G., Pain, T., Bureau, B., Adam, J.L. Chalcogenide double index fibres: fabrication, design, and application as a chemical sensor. *Materials Research Bulletin*, 38, 2003, p. 1745–1754.
21. Munkholm, C., Walt, D. R., Milanovich, F. P. A fibre-optic sensor for CO_2 measurement. *Talanta*, 35, 1988, p. 100–112.
22. Bariani, C., Matias, I. R., Romeo, I., Garrido, J., Laguna, M. Behavioural experimental studies of a novel vapochromic material towards development of optical fibre organic compound sensor. *Sensors & Actuators B: Chemical*, 76, 2001, p. 25–31.
23. Lee, Y.-S., Joo, B.-S., Choi, N.-J., Lim, J.-O., Huh, J.-S., Lee, D.-D. Visible optical sensing of ammonia based on polyanilin film. *Sensors & Actuators B: Chemical*, 93, 2003, p. 148–152.
24. Malins, C., Landl, M., Simon, P., MacCraith, B.D. Fibre optic ammonia sensing employing novel near infrared dyes. *Sensors & Actuators B: Chemical*, 51, 1998, p. 359–367.
25. Grady, T., Butler, T., MacCraith, B. D., Diamond, D., McKervey, M. A. Optical sensor for gaseous ammonia with tunable sensitivity. *Analyst*, 122, 1997, p. 803–806.

26. Malins, C., Doyle, A., MacCraith, D. B., Kvasnik, F., Landl, M., Šimon, P., Kalvoda, L., Lukaš, R., Puflere, K., Babusík, I. Personal ammonia sensor for industrial environments. *The Journal of Environmental Monitoring*, 1, 1999, p. 417–422.

27. Moreno, J., Arregui, F. J., Matias, I. R. Fibre optic ammonia sensing employing novel thermoplastic polyurethane membranes. *Sensors & Actuators B: Chemical*, 105, 2005, p. 419–424.

28. Nivens, D. A., Schiza, M. V., Angel, S. M. Multilayer sol-gel membranes for optical sensing applications: single layer pH and dual layer CO_2 and NH_3 sensors. *Talanta*, 58, 2002, p. 543–550.

29. Kondratowicz, B., Narayanaswamy, R., Persaud, K. C. An investigation into the use of electrochromic polymers in optical fibre gas sensors. *Sensors & Actuators B: Chemical*, 74, 2001, p. 138–144.

30. James, S. W., Tatam, R. P. Fibre optic sensors with nano-structured coatings. *Journal of Optics A: Pure and Applied Optics*, 8, 2006, p. S430–S440.

31. Giordano, M., Russo, M., Cusano, A., Mensitieri, G., Guerra, G. Syndiotactic polystyrene thin film as sensitive layer for an optoelectronic chemical sensing device. *Sensors & Actuators B: Chemical*, 109, 2005, p. 177–184.

32. Consales, M., Campopiano, S., Cutolo, A., Penza, M., Aversa, P., Cassano, G., Giordano, M., Cusano, A. Carbon nanotubes thin films fibre optic and acoustic VOCs sensors: performances analysis. *Sensors & Actuators B: Chemical*, 118(1–2), 2006, p. 232–242.

33. Tao, S., Jayaprakash, A. A fibre optic temperature sensor with an epoxy-glue membrane as a temperature indicator. *Sensors & Actuators B: Chemical*, 119(2), 2006, p. 615–620.

34. Sloan, W. D., Uttamlal, M. A fibre-optic calcium ion sensor using a calcein derivative. *Luminescence*, 16, 2001, p. 179–186.
35. Zhao, Z., Carpenter, M., Xia, A. H., Welch, D. All-optical hydrogen sensor based on a high alloy content palladium thin film. *Sensors & Actuators B: Chemical*, 113, 2006, p. 532–553.
36. Dybko, A., Wroblewski, W., Rozniecka, E., Pozniak, K., Maciejewski, J., Romaniuk, R., Brzozka, Z. Assessment of water quality based on multiparameter fibre optic probe. *Sensors & Actuators B: Chemical*, 51, 1998, p. 208–213.
37. Elosúa, C., Bariáin, C., Matías, I. R., Arregui, F. J., Luquin, A., Laguna, M. Volatile alcoholic compounds fibre optic nanosensor. *Sensors & Actuators B: Chemical*, 115, 2006, p. 444–449.
38. Vohra, S. T., Todd, M. D., Johnson, G. A., Chang, C. C., Danver, B. A. Fibre Bragg grating sensor system for civil structure monitoring: applications and field tests. *Proc. of SPIE*, 3746, 1999, p. 32–37.
39. Schroeder, R. J., Yamate, T., Udd, E. High pressure and temperature sensing for the oil industry using fiber Bragg gratings written onto side hole single mode fiber. *Proc. of SPIE*, 3746, 1999, p. 42–45.
40. Bucholtz, F., Dagenais, D. M., Koo, K. P. High frequency fibre-optic magnetometer with 70 fT per square root hertz resolution. *Electronics Letters*, 25, 1989, p. 1719–1721.
41. Dandridge, A. Fibre optic sensors based on the Mach-Zehnder and Michelson interferometers, In: *Fiber Optic Sensors: An Introduction for Engineers and Scientists*, edited by E. Udd. New York: Wiley, 1991.
42. Yuan, L., Yang, J. Two-loop based low-coherence multiplexing fibre optic sensors network with Michelson optical path demodulator. *Proc. of SPIE*, 5855, 2005, p. 595–598.

43. Udd, E., Corones, J., Laylor, H. M. Fibre optic sensors for infrastructure applications. *Technical Report Form DOT F 1700.7 (8–72)*, 1998.
44. Russell, S. J., Dakin, J. P. Location of time-varying strain disturbances over a 40 km fibre section, using a dual-Sagnac interferometer with a single source and detector. *Proc. of SPIE*, 3746, 1999, p. 580–584.
45. Burns, W. K. *Optical fibre rotation sensing*, San Diego: Academic Press, 1994.
46. Udd, E., Michal, R. J., Theriault, J. P., Cahill, R. F. High accuracy light source wavelength and optical fibre dispersion measurements using the Sagnac interferometer. In: *Proc. 7th Optical Fibre Sensors Conference*, IREE Australia, 1990, p. 329–332.
47. Udd, E. Sagnac distributed sensor concepts. *Proc. of SPIE*, 1586, 1991, p. 46–52.
48. Rao, Y. J., Cooper, M. R., Jackson, D. A., Pannell, C. N., Reekie, L. High resolution static strain measurement using an in-fibre-Bragg-grating-based Fabry Perot sensor. *Proc. of SPIE*, 4185, 2000, p. 284–287.
49. Cibu1a, E., Donlagic, D. All-fibre Fabry-Perot strain sensor. *Proc. of SPIE*, 5502, 2004, p. 180–183.
50. Lin, C.-J., Tseng, Y.-T., Lin, S.-C., Yang, C.-S., Tseng, F.-G. A novel in-vitro and in-situ immunoassay biosensor based on fibre-optic Fabry-Perot interferometry. *Proc. of SPIE*, 5502, 2004, p. 304–307.
51. Leung, A., Rijal, K., Shankar, P. M., Mutharasan, R. Effects of geometry on transmission and sensing potential of tapered fibre sensors. *Biosensors and Bioelectronics*, 21(12), 2006, p. 2202–2209.

52. Monzón-Hernández, D., Villatoro, J. High-resolution refractive index sensing by means of a multiple-peak surface plasmon resonance optical fibre sensor. *Sensors & Actuators B: Chemical*, 115, 2006, p. 227–231.
53. Gupta, B. D., Sharma, A. K. Sensitivity evaluation of a multi-layered surface plasmon resonance-based fibre optic sensor: a theoretical study. *Sensors & Actuators B: Chemical*, 107, 2005, p. 40–46.
54. Rajan, Chand, S., Gupta, B. D. Fabrication and characterization of a surface plasmon resonance based fibre-optic sensor for bittering component—Naringin. *Sensors & Actuators B: Chemical*, 115, 2005, p. 344–348.
55. Rayss, J., Sudolski, G. Ion adsorption in the porous sol-gel silica layer in the fibre optic pH sensor. *Sensors & Actuators B: Chemical*, 87, 2002, p. 397–405.
56. Beltrán-Pérez, G., López-Huerta, F., Muñoz-Aguirre, S., Castillo-Mixcóatl, J., Palomino-Merino, R., Lozada-Morales, R., Portillo-Moreno, O. Fabrication and characterization of an optical fibre pH sensor using sol-gel deposited TiO_2 film doped with organic dyes. *Sensors & Actuators B: Chemical*, 120, 2006, p. 74–78.
57. Gupta, B. D., Sharma, D. K. Evanescent wave absorption based fibre optic pH sensor prepared by dye doped sol-gel immobilization technique. *Optics Communications*, 140, 1997, p. 32–35.
58. Gupta, B. D., Sharma, S. A long-range fibre optic pH sensor prepared by dye doped sol-gel immobilization technique. *Optics Communications*, 154, 1998, p. 282–284.
59. Bansal, L., El-Sherif, M., Intrinsic optical-fibre sensor for nerve agent sensing. *IEEE Sensors Journal*, 5, 2005, p. 648–655.
60. Lucas, P., Solis, M. A., Le Coq, D., Juncker, C., Riley, M. R., Collier, J., Boesewetter, D. E., Boussard-Plédel, C., Bureau, B. Infrared

biosensors using hydrophobic chalcogenide fibres sensitized with live cells. *Sensors & Actuators B: Chemical*, 119(2), 2006, p. 355–362.

61. Walsh, J. E., MacCraith, B. D., Meaney, M., Vos, J. G., Regan, F., Lancia, A., Artioushenko, S. Midinfrared fiber sensor for the in-situ detection of chlorinated hydrocarbons. *Proc. of SPIE*, 2508, 1995, p. 233–237.
62. Le Coq, D., Michel, K., Keirss, J., Boussard- Plédel, C., Fonteneau, G., Bureau, B., Le Quéré, J.-M., Sire, O., Lucas, J. Infrared glass fibres for in-situ sensing, chemical and biochemical reactions. *Comptes Rendus Chimie*, 5, 2002, p. 907–913.
63. Beyer, T., Hahn, P., Hartwig, S., Konz, W., Scharring, S., Katzir, A., Steiner, H., Jakusch, M., Kraft, M., Mizaikoff, B. Mini spectrometer with silver halide sensor fibre for in situ detection of chlorinated hydrocarbons. *Sensors & Actuators B: Chemical,* 90, 2003, p. 319–323.
64. Abdelghani, A., Chovelon, J. M., Jaffrezic-Renault, N., Lacroix, M., Gagnaire, H., Veillas, C., Berkova, B., Chomat, M., Matejec, V. Optical fibre sensor coated with porous silica layers for gas and chemical vapour detection. *Sensors & Actuators B: Chemical*, 44, 1997, p. 495–498.
65. Ogita, M., Nagai, Y., Mehta, M. A., Fujinami, T. Application of the adsorption effect of optical fibres for the determination of critical micelle concentration. *Sensors & Actuators B: Chemical*, 64, 2000, p. 147–151.
66. Kawahara, F. K., Fuitem, R. A., Silvus, H. S., Newman, F. M., Frazar, J. H. Development of a novel method for monitoring oils in water. *Analytica Chimica Acta*, 151, 1983, p. 315–327.

67. Sharma, A. K., Gupta, B. D. Fibre optic sensor based on surface plasmon resonance with nanoparticle films. *Photonics and Nanostructures - Fundamentals and Applications*, 3, 2005, p. 30–37.
68. Ronot, C., Gagnalre, H., Goure, J. P., Jaffrezic-Renault, N., Plchery, T. Optimization and performance of a specifically coated intrinsic optical-fibre sensor for the detection of alkane compounds. *Sensors & Actuators A: Physical*, 41–42, 1994, p. 529–534.
69. Abdelghani, A., Chovelon, J. M., Jaffrezic-Renault, N., Ronot-Trioli, C., Veillas, C., Gagnaire, H. Surface plasmon resonance fibre-optic sensor for gas detection. *Sensors & Actuators B: Chemical*, 38–39, 1997, p. 407–410.
70. Trouillet, A., Ronot-Trioli, C., Veillas, C., Gagnaire, H. Chemical sensing by surface plasmon resonance in a multimode optical fibre. *Pure and Applied Optics: Journal of the European Optical Society Part A*, 5, 1996, p. 227–237.
71. Villatoro, J., Luna-Moreno, D., Monzón-Hernández, D. Optical fibre hydrogen sensor for concentrations below the lower explosive limit. *Sensors & Actuators B: Chemical*, 110, 2005, p. 23–27.
72. Bevenot, X., Trouillet, A., Veillas, C., Gagnaire, H., Clement, M. Surface plasmon resonance hydrogen sensor using an optical fibre. *Measurement Science and Technology*, 13, 2002, p. 118–124.
73. Abdelghania, A., Chovelon, J. M., Jaffrezic-Renault, N., Veilla, C., Gagnaire, H. Chemical vapour sensing by surface plasmon resonance optical fibre sensor coated with fluoropolymer. *Analytica Chimica Acta*, 337, 1997, p. 225–232.
74. Hampp, N. Bacteriorhodopsin as a photochromic retinal protein for optical memories. *Chemical Reviews*, 100, 2000, p. 1755–1776.

75. Ermolina, I., Lewis, A., Feldman, Y. Dielectric properties of the bR membrane. *Journal of Physical Chemistry*, 107, 2003, p.14537–14544.
76. Oesterhelt, D., Stoeckenius, W. Rhodopsin-like protein from the purple membrane of *Halobacterium halobium*. *Nature: New biology*, 233, 1971, p. 149–152.
77. Henderson, R., Baldwin, R. J. M., Zemlin, T. A. J., Beckmann, E. K., Downing, H. Model for the structure of bacteriorhodopsin based on high-resolution electron cryo-microscopy. *Journal of Molecular Biology*, 213, 1990, p. 899–929.
78. Subramaniam, S., Gerstein, M., Oesterhelt, D., Henderson, R. Electron diffraction analysis of structural changes in the photocycle of bacteriorhodopsin, *The EMBO Journal,* 12, 1993, p. 1–8.
79. Müller, D. J., Büldt, G., Engel, A. Force-induced conformational change of bacteriorhodopsin. *Journal of Molecular Biology*, 249, 1995, p. 239–243.
80. Lanyi, J. K. Bacteriorhodopsin. *Previously published in Biophysics Textbook Online*, 2001.
81. Lozier, R. H., Bogomolni, R. A., Stoeckenius, W. Bacteriorhodopsin: a light-driven proton pump in *Halobacterium halobium. Biophysical journal*, 15, 1975, p. 955–962.
82. Dér, A., Keszthelyi, L. Charge motion during the photocycle of bacteriorhodopsin. *Biochemistry (Moscow),* 66, 2001, p. 1234–1248. *Translated from Biokhimiya*, 66, 2001, p. 1527–1545. Original Russian Text Copyright © 2001 by Dér, Keszthelyi.
83. Lee, Y.-S., Krauss, M., Dynamics of proton transfer in bacteriorhodopsin. *Journal of the American Chemical Society*, 126, 2004, p. 2225–2230.

84. Váró, G., Lanyi, J. K., Thermodynamics and energy coupling in the bacteriorhodopsin photocycle. *Biochemistry*, 30, 1991, p. 5008–5015.
85. Birge, R. R., Gillespie, N. B., Izaguirre, E. W., Kusnetzow, A., Lawrence, A. F., Singh, D., Wang Song, Q., Schmidt, E., Stuart, J. A., Seetharaman, S., Wise, K. J. Biomolecular electronics: protein-based associative processors and volumetric memories. *The Journal of Physical Chemistry B*, 103, 1999, p. 10746–10766.
86. Marwan, W., Hegemann, P., Oesterhelt, D. Single photon detection by an archaebacterium. *Journal of Molecular Biology*, 199(4), 1988, p. 663–664.
87. Xu, J., Stickrath, A. B., Bhattacharya, P., Nees, J., Váró, G., Hillebrecht, J. R., Ren, L., Birge, R. R. Direct measurement of the photoelectric response time of bacteriorhodopsin via electro-optic sampling. *Biophysical Journal*, 85, 2003, p. 1128–1134.
88. Miyasaka, T., Koyama, K., Itoh, I. Quantum conversion and image detection by a bacteriorhodopsin-based artificial photoreceptor. *Science*, 255, 1992, p. 342.
89. Saga, Y., Watanabe, T., Koyama, K., Miyasaka, T. Mechanism of photocurrent generation from bacteriorhodopsin on gold electrodes. *The Journal of Physical Chemistry B*, 103, 1999, p. 234–238.
90. Sasabe, H., Furuno, T., Takimoto, K., Photovoltaics of photoactive protein/polypeptide LB films. *Synthetic Metals*, 28, 1989, p. 787–792.
91. Hong, F. T., Retinal proteins in photovoltaic devices. In: *Molecular and Biomolecular Electronics,* edited by Birge, R. R. ed., ACS Advances in Chemistry Series No. 240, American Chemical Society, Washington, DC, 1994, p. 527–559.
92. Birge, R. R., Fleitz, P. A., Gross, R. B., Izgi, J. C., Lawrence, A. F., Stuart, J. A., Tallent, J. R. Spatial light modulators and optical

associative memories based on bacteriorhodopsin. In: *12th AIC of the IEEE Engineering in Medicine and Biology Society*. Piscataway, N.J.: Institute of Electrical and Electronics Engineers, 12, 1990, p. 1788–1789.

93. Song, Q. W., Zhang, C., Gross, R., Birge, R. R. Optical limiting by chemically enhanced bacteriorhodopsin films. *Optics Letters*, 18, 1993, p. 775–777.

94. Opto & Laser Europe Apr 1, 2001, Photonics finds a natural solution. (WWW document) http://optics.org/optics/Articles.do?channel=technology&type=ole&volume=6&issue=4&article=4&page=1 (accessed 2nd November 2006).

95. Heeg, B., Needleman, R., Khizhnyak, A., L'Esperance, D. M., Scott, E., Markov, V. B., Trolinger, J. D. Bacteriorhodopsin as a chemical and biological sensor. *Proc. of SPIE*, 5085, 2003, p. 109–118.

96. Dyukova, T., Vsevolodov, N., Chekulaeva, L. Change in the photochemical activity of bacteriorhodopsin in polymer matrices on its dehydration. *Biophysical Journal*, (Moscow), 30, 1985, p. 668–672.

97. Dyukova, T., Robertson, B., Weetall, H., Optical and electrical characterization of bacteriorhodopsin films. *Biosystems*, 41, 1997, p. 91–98.

98. Wu, S., Ellerby, M. L., Cohan, J. S., Dunn, B., El-Sayed, M. A., Valentine, J. S., Zink, J. I. Bacteriorhodopsin encapsulated in transparent sol-gel glass: a new biomaterial. *Chemistry of Materials*, 5, 1993, p. 115–120.

99. Weetall, H. H. D96N mutant bacteriorhodopsin immobilized in sol-gel glass characterization. *Applied Biochemistry and Biotechnology*, 49, 1994, p. 241–256.

100. Eroglu, I., Aydemif, A., Tiirkerb, L., Meral Yiicel, A. Photoresponse of bacteriorhodopsin immobilized in polyacrylamide gel membranes. *Journal of Membrane Science*, 86, 1994, p. 171–179.

101. Weetall, H. H., Druzhko, A. B., Samuelson, L. A., de Lera, A. R., Alvarez, R. Optical and electrical properties of bacteriorhodopsin Langmuir-Blodgett films: II. D96N mutant and its 4-keto and 9-demethyl retinal analogs. *Bioelectrochemistry and Bioenergetics*, 44, 1997, p. 37–43.

102. He, J.-A., Samuelson, L., Li, L., Kumar, J., Tripathy, S. K. Oriented bacteriorhodopsin/polycation multilayers by electrostatic layer-by-layer assembly. *Langmuir*, 14, 1998, p. 1674–1679.

103. Frydryh, M., Lensu, L., Aschi, C., Parkkinen, S., Perkkinen, J., Jaaskelainen, T. Model of photovoltage response of bacteriorhodopsin in PVA films. In: *Technical Proceedings of the 2001 International Conference on Computational Nanoscience, ICCN'2001*, Hilton Head Island, South Carolina, U.S.A., March 19–21, 2001, p. 17–20.

104. Druzhko, A. B., Chamorovsky, S. K., Lukashev, E. P., Kononenko, A. A., Vsevolodov, N. N. 4-Keto-bacteriorhodopsin films as a promising photochromic and electrochromic biological material. *Biosystems*, 35, 1995, p. 129–132.

105. Zingoni, J., Or, Y. S., Crouch, R. K., Chang, C.-H., Govindjee, R., Ebrey, T. G. Effect of variation of retinal polyene side-chain length on formation and function of bacteriorhodopsin analogue pigments. *Biochemistry*, 25, 1986, p. 2022–2027.

106. Nakasako, M., Kataoka, M., Tokunaga, F. Arginine remarkably prolongs the lifetime of the M-intermediate in the bacteriorhodopsin photocycle at room temperature. *FEBS Letters*, 254, 1989, p. 211–214.

107. Batori-Tartsi, Z., Ludman, K., Váró, G. The effect of chemical additives on the bacteriorhodopsin photocycle. *Journal of Photochemistry and Photobiology B: Biology,* 49, 1999, p. 192–197.

108. Wang Song, Q., Zhang, C., Gross, R. B., Birge, R. R. The intensity-dependent refractive index of chemically enhanced bacteriorhodopsin. *Optics Communications*, 112, 1994, p. 296–301.

109. Liang, B., Li, B., Jiang, L. Study on the long lifetime of the M sate in chemically modified bacteriorhodopsin film. *Chemistry of Materials*, 13, 2001, p. 2746–2748.

110. Dér, A., Ramsden, J. J. Evidence for loosening of a protein mechanism. *Naturwissenschaften*, 85, 1998, p. 353–355.

111. Zhang, G., Li, B., Zhang, J. A study on the fabrication of chemically modified bacteriorhodopsin film and its photochemical properties. *Biochemical and Biophysical Research Communications*, 313, 2004, p. 733–737.

112. Gross, R. B., Izgi, K. C., Birge, R. R. Holographic thin films, spatial light modulators, and optical associative memories based on bacteriorhodopsin. *Proc. of SPIE*, 1662, 1992, p. 186–196.

113. Ovchinnikov, Yu. A., Abdulaev, N. G., Dergachev, A. E. Photoelectric and spectral responses of bacteriorhodopsin modified by carbodiimide and amine derivatives. *European Journal of Biochemistry*, 127, 1982, p. 325–332.

114. Ormos, P., Dér, A., Gergely, C., Kruska, S., Száraz, S., Tokaji, Z. The effect of azide on the photocycle of bacteriorhodopsin. *Journal of Photochemist and Photobiology B: Biology*, 40, 1997, p. 111–119.

115. Batori-Tartsi, Z., Ludmann, K., Chemically modified bacteriorhodopsin based photosensitive material for optoelectronic application. In: *Bioelectronic applications of photochromic pigments*,

edited by A. Dér and L. Keszthelyi. Amsterdam: IOS Press, 2001, p. 137–148.

116. Dyukova, T. V., Lukashev, E. P. Dehydration effects on D96N bacteriorhodopsin films. *Thin solid Films*, 283, 1996, p. 1–4.

117. Korenstein, R., Hess, B. Hydration effects on *cis-trans* isomerization of bacteriorhodopsin. *FEBS Letters*, 82, 1977, p. 7–11.

118. Nakagawa, T., Hamanaka, T., Nishimura, S., Uchida, I., Mashimo, T., Kito, Y. The quantitative analysis of three action modes of volatile anesthetics on purple membrane. *Biochimica et Biophysica Acta*, 1467, 2000, p. 1390–149.

119. Maccioni, E., Radicchi, G., Erokhin, V., Paddeu, S., Facci, P., Nicoloni, C. Bacteriorhodopsin thin film as a sensitive layer for an anaesthetic sensor. *Thin Solid Films*, 284–285, 1996, p. 898–900.

120. Pandey, P. C., Singh, S., Upadhyay, B., Weetall, H. H., Chen, P. K. Reversal in the kinetics of the M state decay of D96N bacteriorhodopsin: probing of enzyme catalyzed reactions. *Sensors & Actuators B: Chemical*, 35–36, 1996, p. 470–474.

121. Pandey, P. C., Upadhyay, B. C., Pandey, C. M. D., Pathak, H. C. Dependence of M, N and O states decay kinetics of D96N bacteriorhodopsin on amine and amino compounds and its application in chemical sensing. *Sensors & Actuators B: Chemical*, 46, 1998, p. 80–86.

122. Goldstein, J. I., Newbury, D. E., Echlin, P., Joy, D. C., Lyman, C. E., Lifshin, E., Sawyer, L., Michael, J. R. *Scanning electron microscopy and X-ray microanalysis*, 3rd ed. New York: Kluwer Academic/Plenum Publishers, 2003.

123. Kaupp, G., Schmeyers, J., Haak, M., Herrmann, A. Kraftmikroskopie (AFM) zur Aufklärung abfallfreier Festkörpersynthesen, *Labo-Trend*

95, 1995, p. 57–63; (WWW document). http://kaupp.chemie.uni-oldenburg.de/~haak/hyper/kraftmikroskopie.html (accessed 2nd November 2006) Atomic Force Microscopy for the Elucidation of Waste-Free Solid-State Syntheses, (WWW document) http://kaupp.chemie.uni-oldenburg.de/~haak/hyper/afm.html (accessed 2nd November 2006).

124. PhotoMetrics Inc., The Material Characterization Laboratory. (WWW document). http://www.photometrics.net/AFM.html (accessed 2nd November 2006).
125. Binning, G., Quate, C., Gerber, C. Atomic force microscope. *Physical Review Letters,* 56, 1986, p. 930–933.
126. Russell, P., Batchelor, D. SEM and AFM: Complementary techniques for surface investigations. *Microscopy and Analysis*, 15(4), 2001, p. 9–12.
127. Müller, D. J., Schoenenberger, C.-A., Schabert, F., Engel, A. Structural changes in native membrane proteins monitored at subnanometer resolution with the atomic force microscope: A Review. *Journal of structural biology*, 119, 1997, p. 149–157.
128. Basic operating principles of the Sorptomatic 1990. (WWW document). http://saf.chem.ox.ac.uk/Instruments/BET/sorpoptprin.html (accessed 2nd November 2006).
129. International Union of Pure and Applied Chemistry (IUPAC) Reporting physisorption data for gas/solid system. *Pure and Applied Chemistry*, 57, 1985, p. 603–619.
130. Brunauer, S., Emmet, P. H., Teller, E. Adsorption of gases in multimolecular layers. *Journal of the American Chemical Society*, 60, 1938, p. 309–319.

131. Barrett, E. P., Joyner, L. G., Halenda, P. P. The determination of pore volume and area distributions in porous substances. I. Computations from Nitrogen Isotherms. *Journal of the American Chemical Society*, 73, 1951, p. 373–380.

132. HR2000 series high-resolution fibre optic spectrometer, operating instructions, Ocean Optics, Dunedin, Fla., USA.

133. Munich Innovative Biomaterials GmbH (WWW document). http://www.mib-biotech.de/ (accessed 2nd November 2006).

134. Báthori-Tárczy, Z., Sárkany, J., Bandrovszkaja, I., Sersun, J., Korposh, O., Jaros, V. Bakteriorodopszin-alapanyagú fotochrom rétegek. *Tudományos találkozó*, 1992, p. 110–112.

135. Kikineshy, A., Batori-Tartsi, Z., Sharkany, Y. Materials and devices for fibre optic sensors. *Multichip Modules with Integrated Sensors. NATO ASI Series. High Technology*, 3, 1995, p.181–184.

136. Lensu, L., Frydrych, M., Parkkinen, J., Parkkinen, S., Jaaskelainen, T. Photoelectric properties of bacteriorhodopsin analogs for colour-sensitive optoelectronic devices. *Optical Materials*, 27, 2004, p. 57–62.

137. Ikonen, M. Bacteriorhodopsin in Langmuir-Blodgett films—preparation, structure and photoinduced optical and electrical properties. *Commentat. Physico-Mat. Chemico-Med*, 149, 1993, p. 1–27.

138. Dorothy, C. L., Bruce, D., Jeffrey, I. Z. Room temperature luminescence of silicate sol-gel materials containing trisodium Tris(dipicolinato) neodymate (III). *Inorganic Chemistry*, 35, 1996, p. 2152–2154.

139. Gupta, R., Mozumdar, S., Chaughury, N. K. Fluroscence spectroskopic studies to characterize the internal environment of

tetraethyl-orthosilicate derived sol-gel bulk and thin films with aging. *Biosensors and Bioelectronics*, 20, 2005, p. 1358–1365.

140. Ponton, A., Griesmar, P., Barboux-Doeuff, S., Sanchez, C. Rheological investigation of the sol-gel transition: effect of hydrolysis variation in silicon oxide and titanium oxide based matrices. *Journal of Materials Chemistry*, 11, 2001, p. 3125–3129.

141. Lev, O., Tsionsky, M., Rabinovich, L., Glezer, V., Sampath, S., Pankratov, I., Gun, J. Organically modified sol-gel sensors. *Analytical Chemistry*, 67, 1995, p. 22A–30A.

142. Weetall, H. Retention of bacteriorhodopsin activity in dried sol-gel glass. *Biosensors & Bioelectronics*, 11, 1996, p. 325–333.

143. Shuguang, W.U., Ellerby, L. M., Cohan, J. S., Dunn, B., El-Sayed, M. A., Selverstone, J., Zink, J. I. Bacteriorhodopsin encapsulated in transparent sol-gel glass: A new biomaterial. *Chemistry of Materials*, 5, 1993, p. 115–120.

144. Hildebrandt, P., Stockburger, M. Role of water in bacteriorhodopsin's chromophore: resonance Raman study. *Biochemistry*, 23, 1984, p. 5539–5548.

145. Shibata, M., Tanimoto, T., Kandori, H. Water molecules in the Schiff base region of bacteriorhodopsin. *Journal of the American Chemical Society*, 125, 2003, p. 13312–13313.

146. Harbison, G. S., Smith, S. O., Pardoen, J. A., Winkel, C., Lugtenburg, J., Herzfeld, J., Mathies, R., Griffin, R. G. Dark-adapted bacteriorhodopsin contains 13-*cis*, 15-*syn* and all-*trans*, 15-*anti* retinal Schiff bases. In: *Proc. of the National Academy of Sciences of the United States of America*, 81, 1984, p. 1706–1709.

147. Oesterhelt, D., Meentzen, M., Schulmann, L. Reversible dissociation of the purple complex in bacteriorhodopsin and identification of *13-cis*

and *all-trans*-retinal as its chromophores. *European Journal of Biochemistry*, 40, 1973, p. 453–463.

148. Sperling, W., Carl, P., Rafferty, Ch. N., Dencher, N. A. Photochemistry and dark equilibrium of retinal isomers and bacteriorhodopsin isomers. *European Biophysics Journal*, 3, 1977, p. 79–94.

149. Pettei, M. J., Yudd, A. P., Nakanishi, K., Henselman, R., Stoeckenius, W. Identification of retinal isomers isolated from bacteriorhodopsin. *Biochemistry*, 16, 1977, p. 1955–1959.

150. Marcus, M. A., Lewis, A. Resonance Raman spectroscopy of the retinylidene chromophore in bacteriorhodopsin (bR570), bR560, M412, and other intermediates: structural conclusions based on kinetics, analogs, models, and isotopically labeled membranes. *Biochemistry*, 17, 1978, p. 4722–4735.

151. Korenstein, R., Hess, B., Kuschmitz, D. Branching reactions in the photocycle of bacteriorhodopsin. *FEBS Letters*, 93, 1978, p. 266–270.

152. Nagle, J. F., Parodi, L. A., Lozier, R. H. Procedure for testing kinetic models of the photocycle of bacteriorhodopsin. *Biophysical Journal*, 38, 1982, p. 161–174.

153. Lozier, R. H., Xie, A., Hofrichter, J., Clore, G. M. Reversible steps in the bacteriorhodopsin photocycle. In: *Proc. of the National Academy of Sciences of the United States of America*, 89, 1992, p. 3610–3614.

154. Batori-Tartsi, Z. I. Modification of optical property of film structures on the base of bacteriorhodopsin. *Thesis for Candidate of science degree in physics and mathematics in speciality of physics of semiconductors and insulators,* Uzhgorod National University, Ukraine, Uzhgorod (2002), (in Ukrainian).

155. Sharkov, A. V., Pakulev, A. V., Chekalin, S. V., Matveetz, Y. A. Primary events in bacteriorhodopsin probed by subpicosecond spectroscopy. *Biochimica et Biophysica Acta*, 808, 1985, p. 94–98.

156. Van den Berg, R., Jang, D. J., Bitting, H. C., El Sayed, M. A. Subpicosecond resonance Raman spectra of the early intermediates in the photocycle of bacteriorhodopsin. *Biophysical Joutnal*, 58, 1990, p. 135–141.

157. Braiman, M. S., Bousche, A., Rotschild, K. J. Protein dynamics in the bacteriorhodopsin photocycle: Submillisecond Fourier transform infrared spectra of the L, M and N photointermediates. In: *Proc. of the National Academy of Sciences of the United States of America*, 88, 1991, p. 2388–2392.

158. Gerwert, K., Souvignier, G., Hess, B. Simultaneous monitoring of light-induced changes in protein side-group protonation, chromophore isomerization, and backbone motion of bacteriorhodopsin by time-resolved Fourier-transform infrared spectroscopy. In: *Proc. of the National Academy of Sciences of the United States of America*, 87, 1990, p. 9774–9778.

159. Seibert, F., Mantele, W., Kreutz, W. Evidence for the protonation of two internal carboxylic groups during the photocycle of bacteriorhodopsin. *FEBS Letters*, 141, 1982, p. 82–87.

160. Butt, H. J., Fendler, K., Bamberg, E., Tittor, J., Oesterhelt, D. Aspartic acids 96 and 85 play a central role in the function of bacteriorhodopsin as a proton pump. *The EMBO Journal*, 8, 1989, p. 1657–1663.

161. Gerwert, K., Hess, B., Soppa, J., Oesterhelt, D. Role of aspartate - 96 in proton translocation by bacteriorhodopsin. In: *Proc. of the National*

Academy of Sciences of the United States of America, 86, 1989, p. 4943–4947.

162. Otto, H., Marti, T., Holtz, M., Mogi, T., Lindau, M., Khorana, H. G., Heyn, M. P. Aspartic acid-96 is the internal proton donor in the reprotonation of the Schiff base of bacteriorhodopsin. In: *Proc. of the National Academy of Sciences of the United States of America*, 86, 1989, p. 9228–9232.

163. Pfefferle, J.-M., Maeda, A., Sasaki, J., Yoshizawa, T. Fourier transform infrared study of the N intermediate of bacteriorhodopsin, *Biochemistry*, 30, 1991, p. 6548–6556.

164. Batori-Tartsi, Z., Ludmann, K. Effect of TEA on the kinetic properties of bR. *Research Workshop*, Szeged, Hungary, September 20–21, 2000. (12 pages).

165. Tittor, J., Oesterhelt, D. The quantum yield of bacteriorhodopsin. *FEBS Letters*, 263, 1990, p. 269–273.

166. Mentr, P. Interfacial water: modulator of biological activity. *Journal of Biological Physics and Chemistry*, 4, 2004, p. 115–123.

167. Vsevolodov, N. N. *Biomolecular Electronics. An introduction via Photosensitive Proteins*, Boston: Birkhäuser, 1998.

168. Sharkany, J. P., Korposh, S. O., Batori-Tartsi, Z. I., Trikur, I. I., Ramsden, J. J. Bacteriorhodopsin-based biochromic films for chemical sensors. *Sensors & Actuators B: Chemical*, 107, 2005, p. 77–81.

169. Korposh, S. O., Sichka, M. Y., Trikur, I. I., Sharkany, Y. P., Yang, D. H., Lee, S. W., Ramsden, J. J. Films based on bacteriorhodopsin in sol-gel matrices. *Proc. SPIE*, 5956, 2005, p. 312–320.

170. *Air Quality Guidelines for Europe*, Second Edition, WHO Regional Publications, Copenhagen, Denmark, European Series, No. 91, WHO, 2000.

171. Timmer, B., Olthuis, W., Van den Berg, A. Ammonia sensors and their applications—a review. *Sensors & Actuators B: Chemical*, 107, 2005, p. 666–677.

172. Srivastava, R. K., Lal, P., Dwivedi, R., Srivastatva, S. K. Sensing mechanism in tin oxide-based thick film gas sensors. *Sensors & Actuators B: Chemical*, 21, 1994, p. 213–218.

173. Mayo, N., Harth, R., Mor, U., Marouani, D., Hayon, J., Bettelheim, A. Electrochemical response to H_2, O_2, CO_2 and NH_3 of a solidstate cell based on a cation- or anion-exchange membrane serving as a polymer electrolyte. *Analytica Chimica Acta*, 310, 1995, p. 139–144.

174. Nicolas-Debarnot, D., Poncin-Epaillard, F. Polyaniline as a new sensitive layer for gas sensors, Review. *Analytica Chimica Acta*, 475, 2003, p. 1–15.

175. Ghauch, A., Rima, J., Charef, A., Suptil, J., Fachinger, C., Martin-Bouyer, M. Quantative measurements of ammonium, hydrogenophosphate and Cu(II) by diffuse reflectance spectroscopy. *Talanta,* 48, 1999, p. 385–392.

176. Swartz, M. E., Krull, I. S. *Analytical method development and validation*, New York: Marcel Dekker, Inc., USA, 1997.

177. Pandey, P. C., Upadhyay, S., Upadhyay, B. C. Photo-electrochemistry of ormosil sandwiched D-96N bacteriorhodopsin. *Journal of Sol-Gel Science and Technology*, 33, 2005, p. 51–58.

178. Sharkany, J. P., Trikur, I. I., Korposh, S. O., Ramsden, J. J. Sensitive elements based on bacteriorhodopsin for fibre-optic sensors of chemical components. *Proc. SPIE*, 5855, 2005, p. 411–414.

179. Ramsden, J. J., Sharkan, Y. P., Zhitov, N. B., Korposh, S. O. Sensors for spacecraft cabin environment monitoring. In: *Proc. 56th*

International Astronautical Congress, Paper–№–IAC–05–1.6.03, Fukuoka, 17–21 October, 2005.

Research publications bibliography

1. Sharkany, J. P., Korposh, S. O., Zhytov, N. B., Sichka, M. Y. Fibre optical pH meter. p. 361–362, *Presented at 4th Euspen International Conference, Glasgow, 30th May – 2nd June, 2004*.

2. Sharkany, J. P., Korposh, S. O., Zhytov, N. B., Sichka, M. Y. Fiber-optic device for the parameters measurement of microdoses of the physiological solutions. p. 290–291, *Presented at 4th Euspen International Conference, Glasgow, 30th May – 2nd June, 2004.*

3. Sharkany, J. P., Korposh, S. O., Batori-Tartsi, Z. I., Trikur, I. I., Ramsden, J. J. Bacteriorhodopsin–based biochromic films for chemical sensors. *Sensors & Actuators B: Chemical*, 107, 2005, p. 77–81.

4. Sharkany, J. P., Trikur, I. I., Korposh, S. O., Ramsden, J. J. Sensitive elements based on bacteriorhodopsin for fibre-optic sensors of chemical components. *Proc. SPIE*, 5855, 2005, p. 411–414, *Presented at 17th International Conference on Optical Fibre Sensors, Bruges, Belgium, May 23–27, 2005*.

5. Korposh, S. O., Sichka, M. Y., Trikur, I. I., Sharkany, Y. P., Yang, D. H., Lee, S. W., Ramsden, J. J. Films based on bacteriorhodopsin in sol-gel matrices. *Proc. SPIE*, 5956, 2005, p. 312–320, *Presented at International Congress on Optics and Optoelectronics, Warsaw, Poland, 28 August–2 September, 2005*.

6. Sharkany, Y., Jytov, N., Sichka, M., Korposh, S., Ramsden, J. Rapid fibre-optic sensor for the control of chemical composition of solutions. p. 176–178, *Presented at 3rd International Symposium on Sensor Science (I3S), Julich, 18–21 July, 2005*.

7. Ramsden, J. J., Sharkany, Y. P., Zhitov, N. B., Korposh, S. O. Sensors for spacecraft cabin environment monitoring. Paper–№ – IAC–05– 1.6.03, *Presented at 56th International Astronautical Congress, Fukuoka, 17–21 October, 2005*.

8. Sharkany, Y. P., Korposh, S. O., Zhitov, N. B., Ramsden, J. J., Popovich, I. I. Optical pH sensor of microdoses of the Biological mediums. p. 46, *Presented at 2nd International Meeting on Microsensors and Microsystems,15–18 January, 2006*.

9. Korposh, S. O., Takahara, N., Ramsden, J. J., Lee, S-W., Kunitake, T. Nano-assembled thin film gas sensors. I. Ammonia detection by a porphyrin-based multilayer film. *Journal of Biological Physics and Chemistry*, 6, 2006, p. 125–133.

Appendices

Appendix A

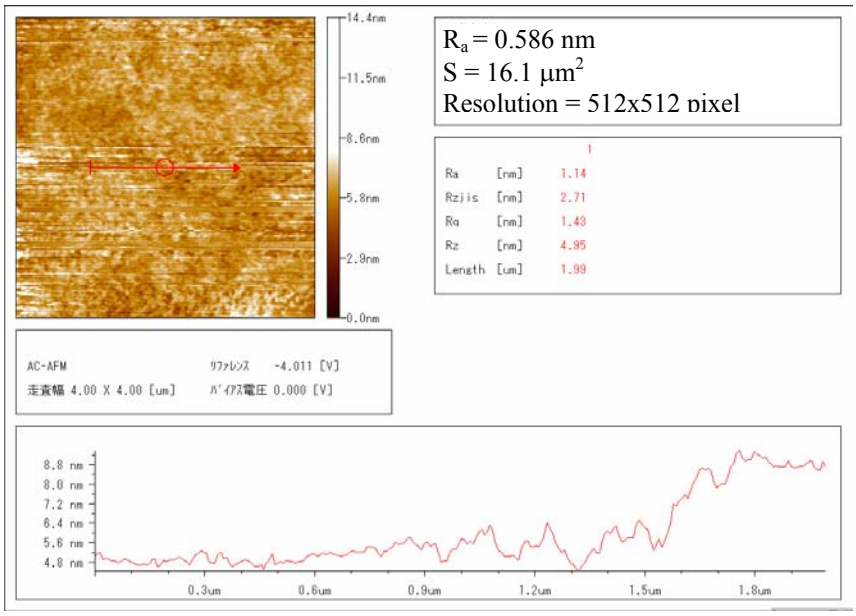

Figure A1: Roughness of a pure TEOS sol-gel matrix, prepared by the casting method and drying, measured from the surface area of a 16.1 µm^2.

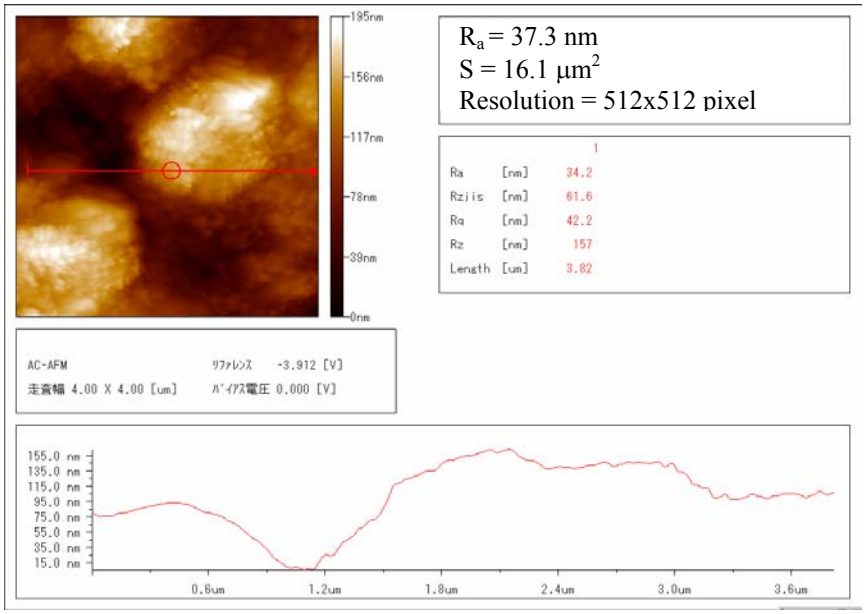

Figure A2: Roughness of films incorporating bacteriorhodopsin in a TEOS sol-gel matrix, prepared by the casting method and drying (mass ratio bR : TEOS = 5.5 : 94.5), measured from the surface area of a 16.1 µm^2.

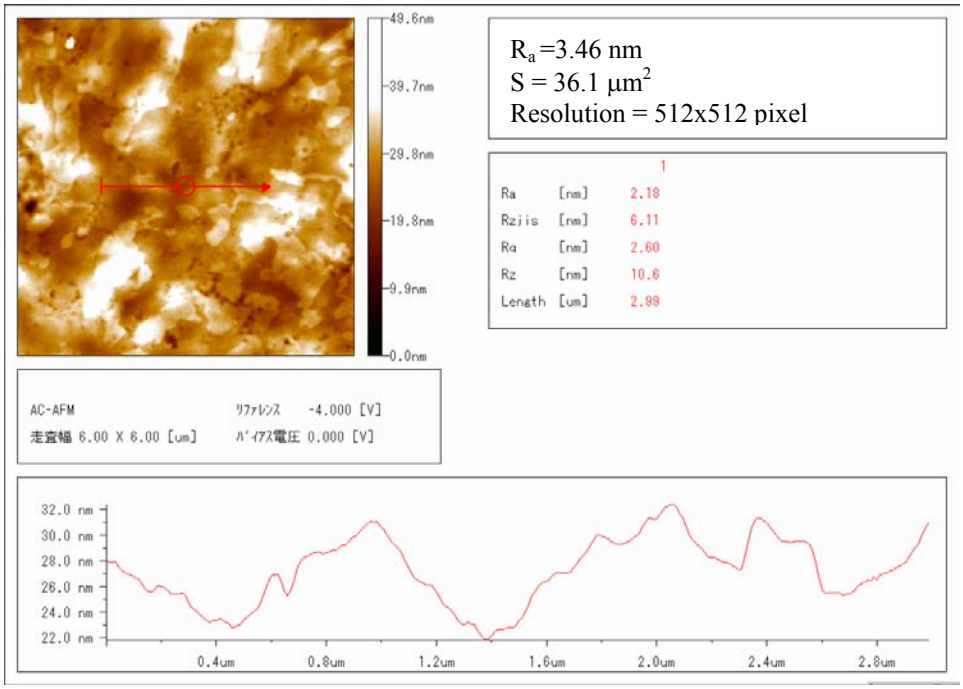

Figure A3: Roughness of film based on bacteriorhodopsin in a gelatin matrix (mass ratio bR : GE = 12.5 : 87.5), measured from the surface area of a 36.1 µm^2.

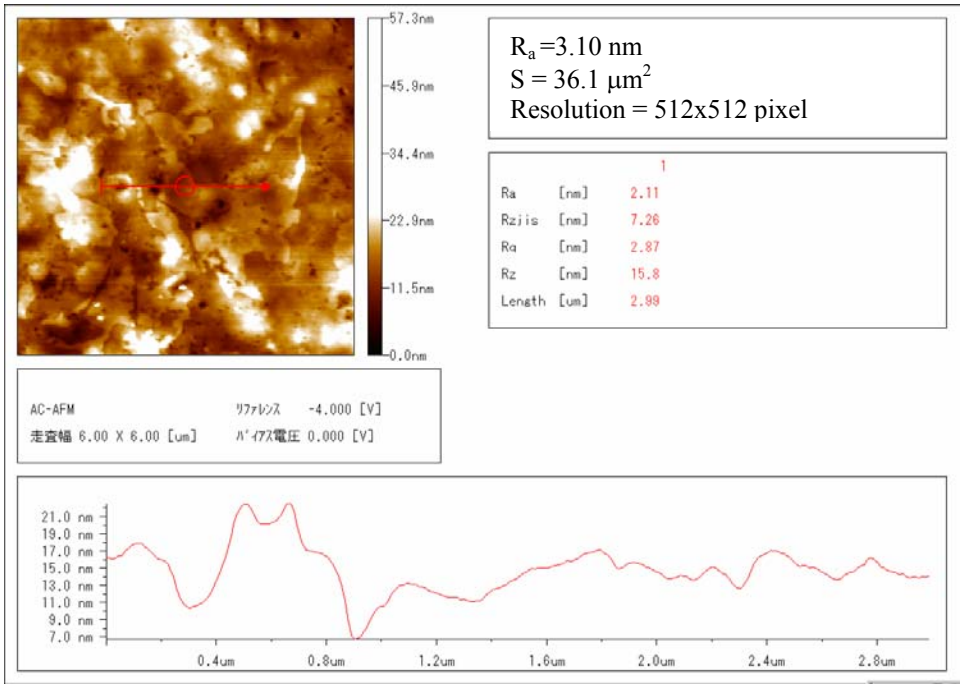

Figure A4: Roughness of film based on bacteriorhodopsin in a PVA matrix (mass ratio bR : PVA = 12.5 : 87.5), measured from the surface area of a 36.1 μm^2.

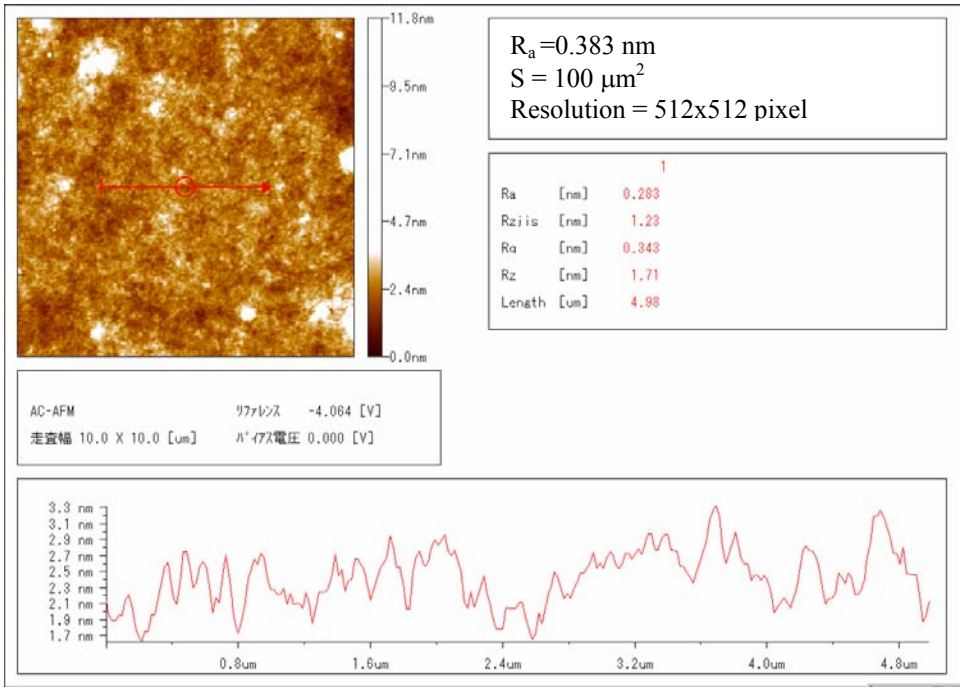

Figure A5: Roughness of the pure GE film deposited by spin coating at 750 rpm, measured from the surface area of a 100 μm^2.

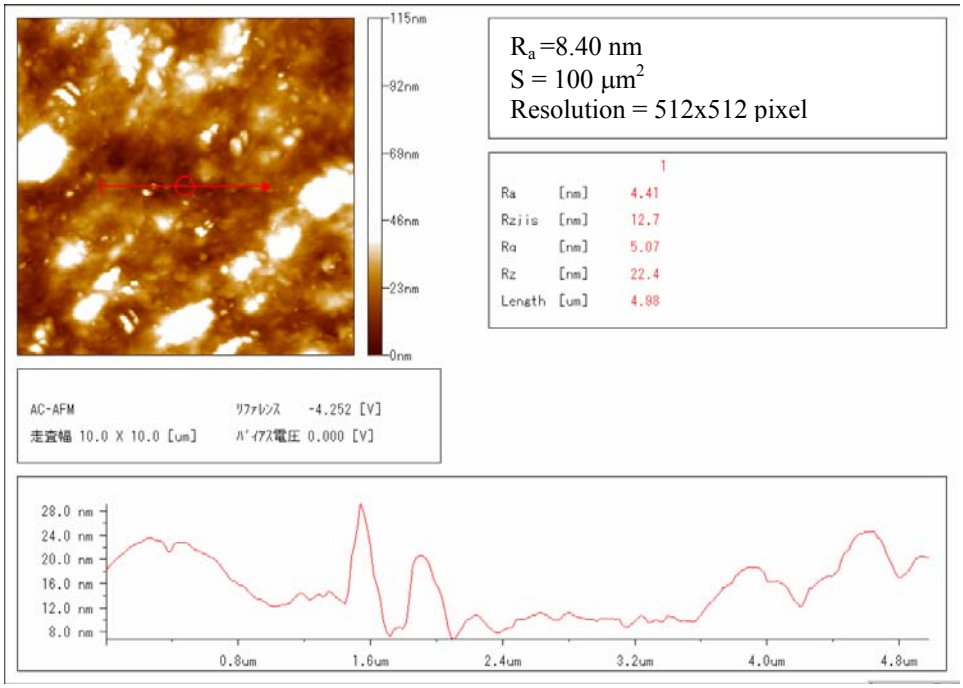

Figure A6: Roughness of the bR embedded into GE matrix deposited by spin coating at 750 rpm, measured from the surface area of a 100 μm^2.

Appendix B

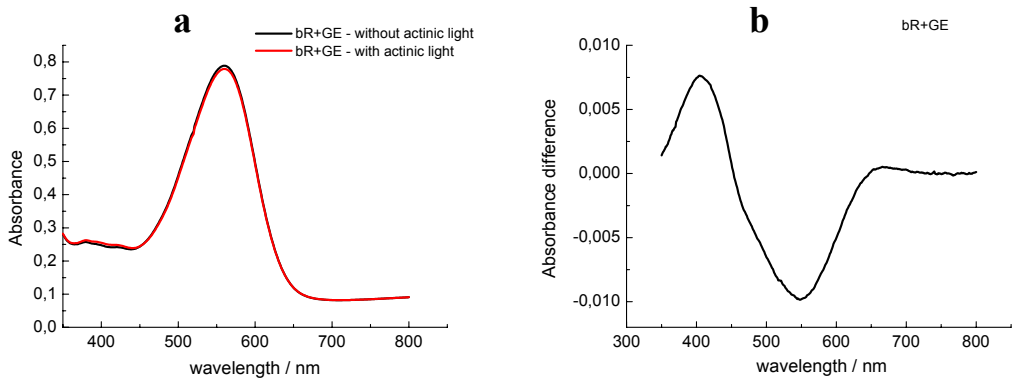

Figure B1: a, absorption spectra of the bR film in GE matrix produced by casting method; black line, without actinic light; red line, with the presence of the actinic light (LED = 518 nm); b, difference spectrum (light minus dark). Mass ratio in the dry film bR : GE = 12.5 : 87.5 (measured at 25 ^{o}C and rH 50%).

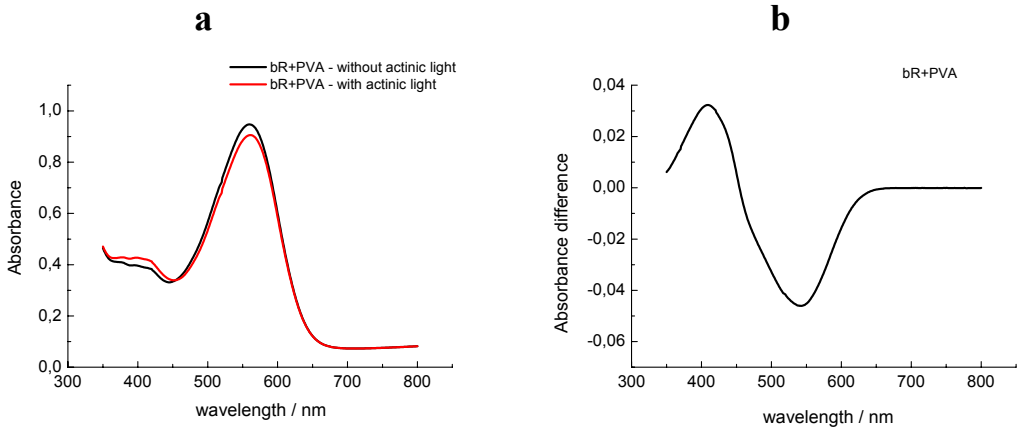

Figure B2: a, absorption spectra of the bR film in PVA matrix produced by casting method; black line, without actinic light; red line, with the presence of the actinic light (LED = 518 nm); b, difference spectrum (light minus dark). Mass ratio in the dry film bR : PVA = 12.5 : 87.5 (measured at 25 ^{o}C and rH 50%).

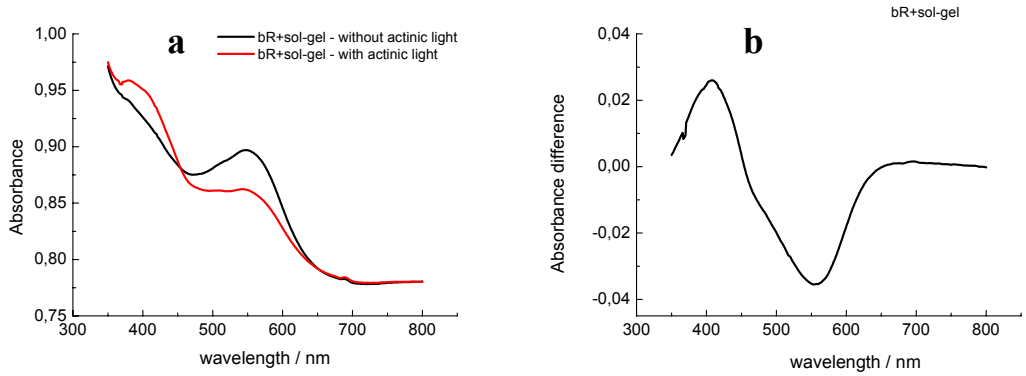

Figure B3: a, absorption spectra of the bR film in sol-gel matrix produced by casting method; black line, without actinic light; red line, with the presence of the actinic light (LED_{518} = 518 nm); b, difference spectrum (light minus dark). Mass ratio in the dry film bR : TMOS = 5.5 : 94.5 (measured at 25 ^{o}C and rH 50%).

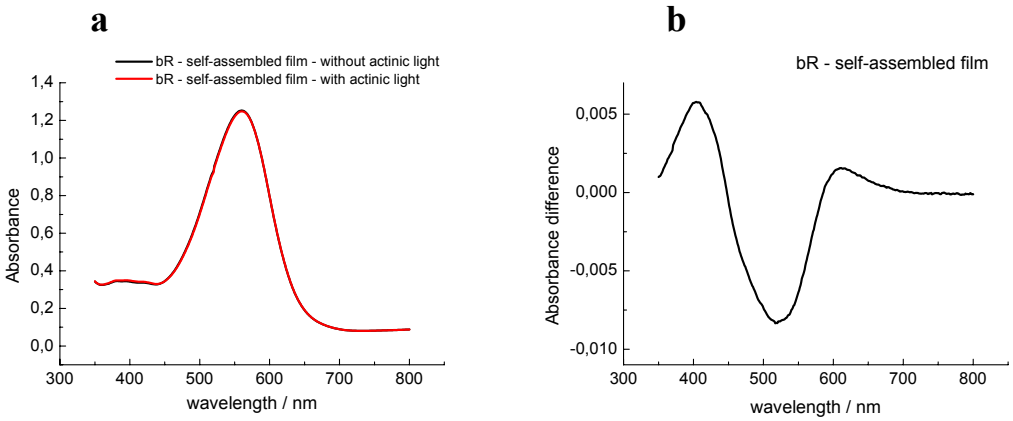

Figure B4: a, absorption spectra of the bR self-assembled film produced by drying of the bR suspension (14 mg/mL); black line, without actinic light; red line, with the presence of the actinic light (LED = 518 nm); b, difference spectrum (light minus dark) (measured at 25 ^{o}C and rH 50%).

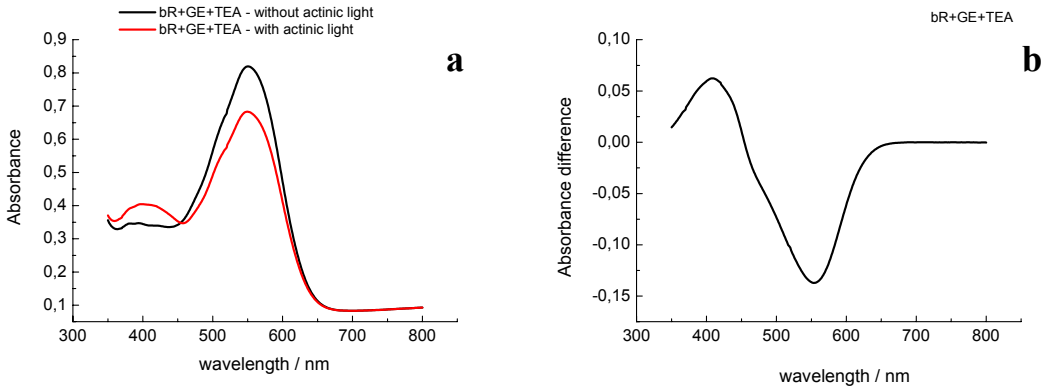

Figure B5: a, absorption spectra of the bR film in GE matrix with TEA added produced by casting method; black line, without actinic light; red line, with the presence of the actinic light (LED_{518} = 518 nm); b, difference spectrum (light minus dark). Mass ratio in the dry film bR : GE : TEA = 12.4 : 73.54 : 12.8 (measured at 25 ^{o}C and rH 50%).

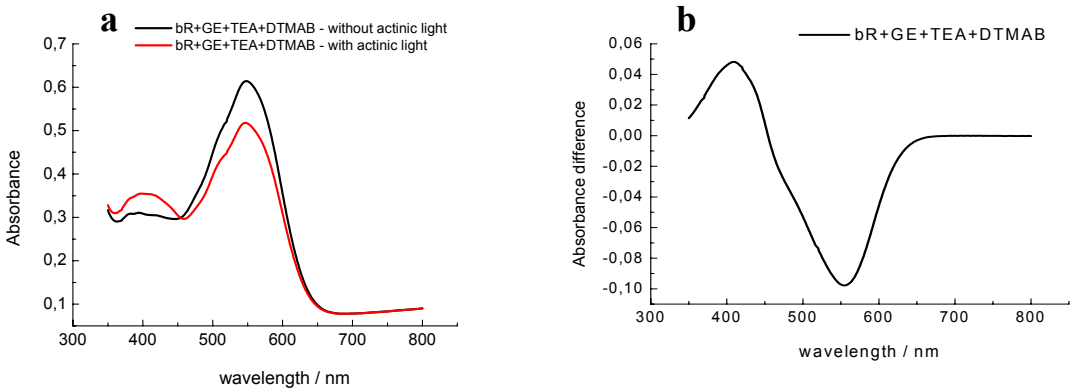

Figure B6: a, absorption spectra of the bR film in GE matrix with TEA and DTMAB added produced by casting method; black line, without actinic light; red line, with the presence of the actinic light (LED_{518} = 518 nm); b, difference spectrum (light minus dark). Mass ratio in the dry film bR : GE : TEA : DTMAB = 12.4 : 73.54 : 12.8 : 1.16 (measured at 25 ^{o}C and rH 50%).

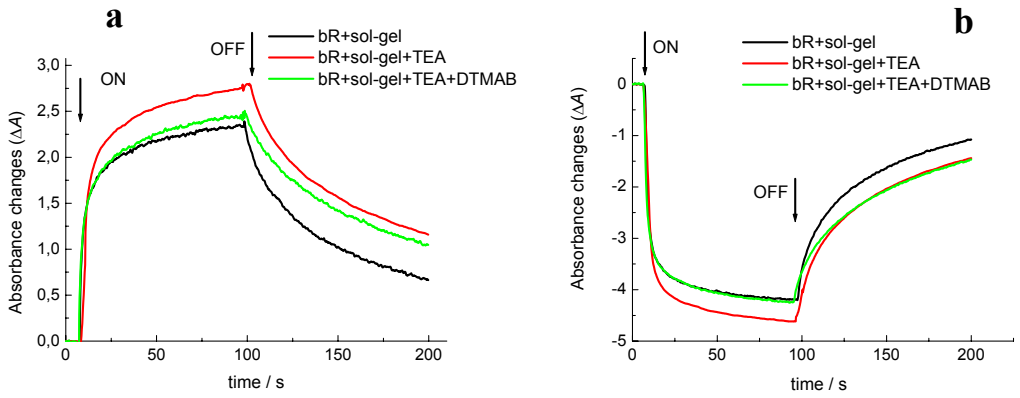

Figure B7: Time dependence of photo-induced absorbance changes (ΔA) (measured at 25 ^{o}C and rH 50%) monitored at: a, 410 nm and b, 570 nm during and after actinic illumination (actinic light source LED_{518}) (arrows indicate the turning ON and OFF the actinic light source); black line, bR film in sol-gel matrix without chemical additives; red line, bR in sol-gel matrix with TEA added; green line, bR film in sol-gel matrix with TEA and DTMAB added; normalization was carried out using Equation 2.3, see Chapter 2.

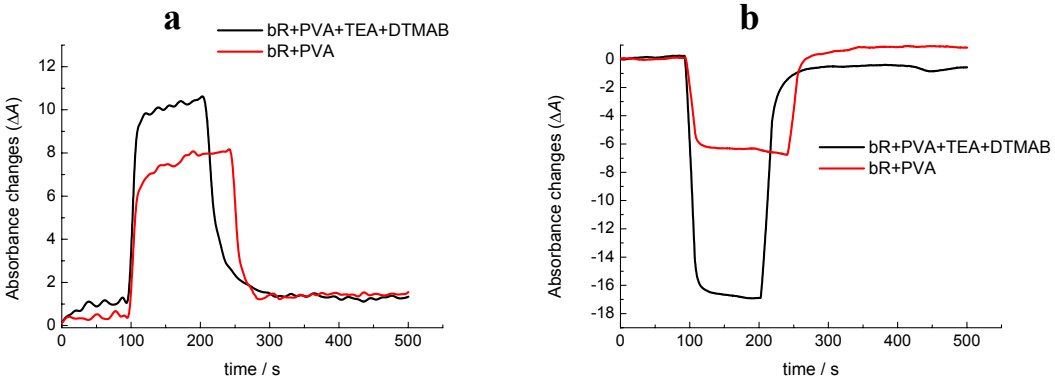

Figure B8: Time dependence of the photo-induced (actinic light source halogen lamp with long pas filter > 530 nm) absorption changes monitored at: a, 410 nm and b, 570 nm; black line, bR film in PVA matrix with added TEA and DTMAB; red line, bR in PVA matrix without added chemicals (measured at 25 ^{o}C and rH 50%); normalization was carried out using Equation 2.3, see Chapter 2.

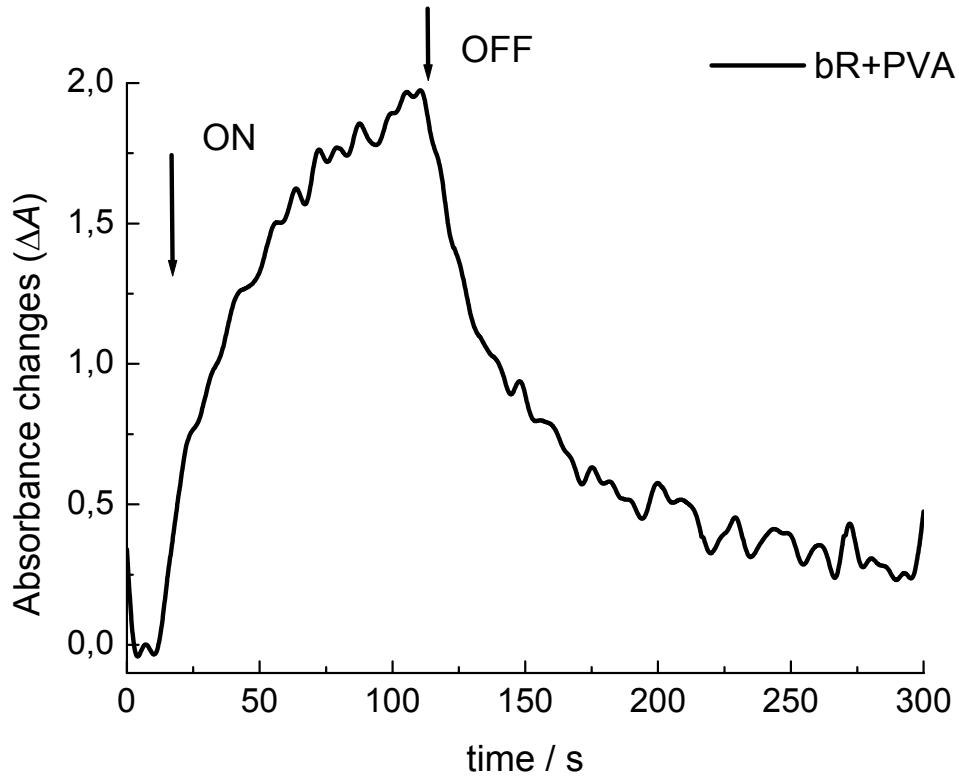

Figure B9: Time dependence of photo-induced absorbance (ΔA) changes of bR in PVA matrix film (mass ratio bR : PVA = 12.5 : 87.5 measured at 25 ^{o}C and rH 50%) monitored at 410 nm during and after actinic illumination (actinic light source LED_{518}) (arrows indicates the turning ON and OFF the actinic light source); normalization was carried out using Equation 2.3, see Chapter 2.

Appendix C

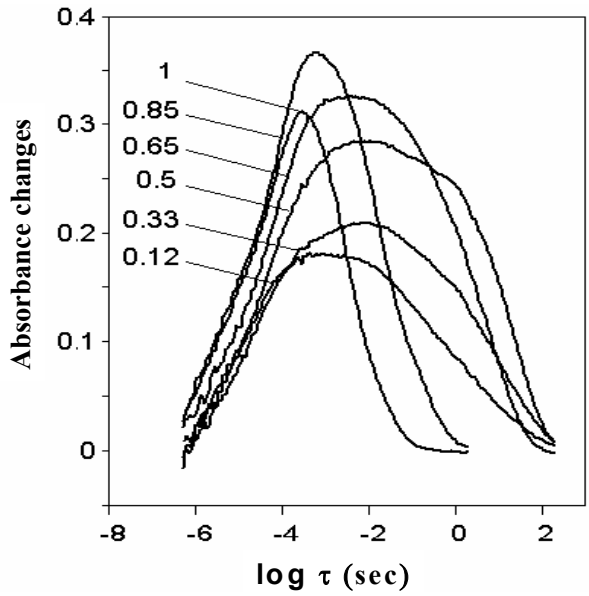

Figure C1: Dependence of the decay half-life of the M_{410} state for bR film in the GE matrix with TEA added on relative humidity (mass ratio bR : GE : TEA = 12.4 : 73.54 : 13.8) [154].

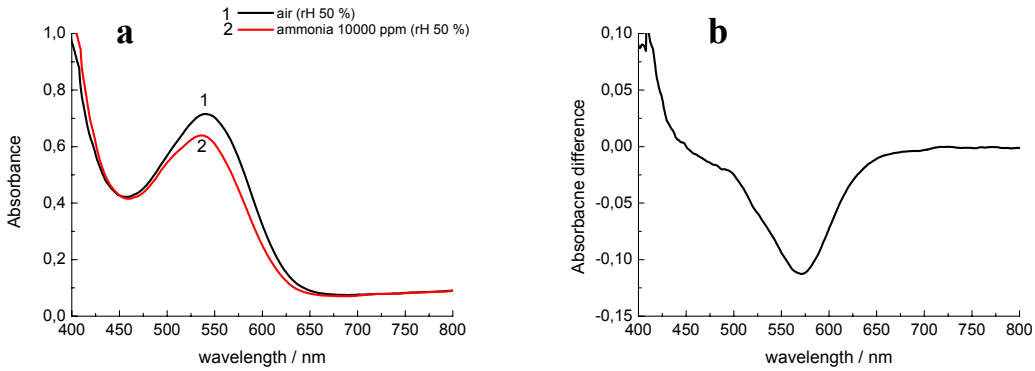

Figure C2: a, absorbance spectra of the bR film in the GE matrix with TEA added (mass ratio bR : GE : TEA = 12.4 : 73.54 : 13.8) measured at 25 ^{o}C and rH 50%: black line 1, without ammonia; and red line 2, in an ammonia atmosphere with the concentration of 10 000 ppm; b, difference absorbance spectra (ammonia 10 000 ppm minus air).

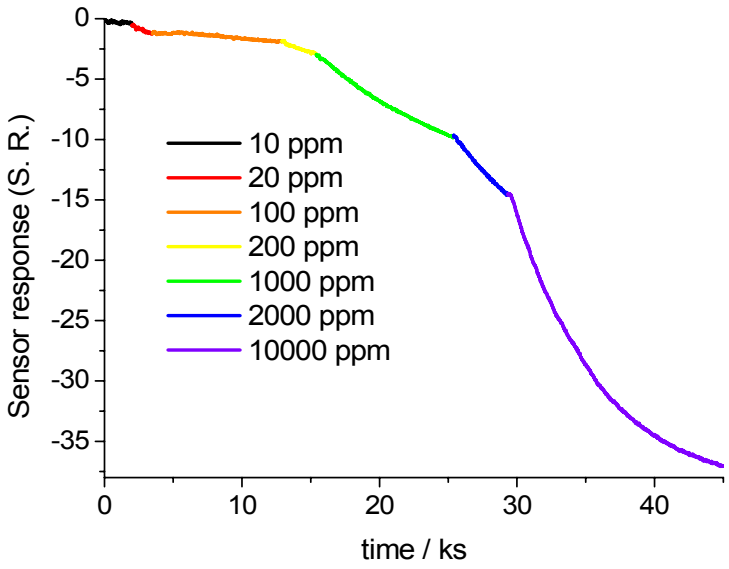

Figure C3: Response of the bR film in GE matrix with added TEA to increasing the concentration of ammonia from 10 to 10 000 ppm monitored at the wavelength 580 nm (mass ratio bR : GE : TEA = 12.4 : 73.54 : 13.8 measured at 25 ^{o}C and rH 50%). The measurements were done by filling the measurement chamber with the ammonia gas of the desired concentration balanced with nitrogen (for details see section 2.2.2).

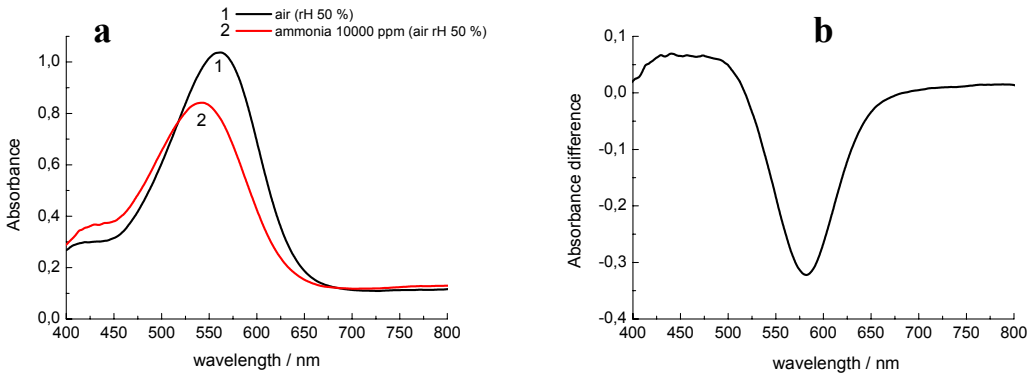

Figure C4: a, absorbance spectra of the bR self-assembled film measured at 25 ^{o}C and rH 50%: black line 1, without ammonia; and red line 2, in ammonia atmosphere with the concentration of 10 000 ppm; b, difference absorbance spectra (ammonia 10 000 ppm minus air).

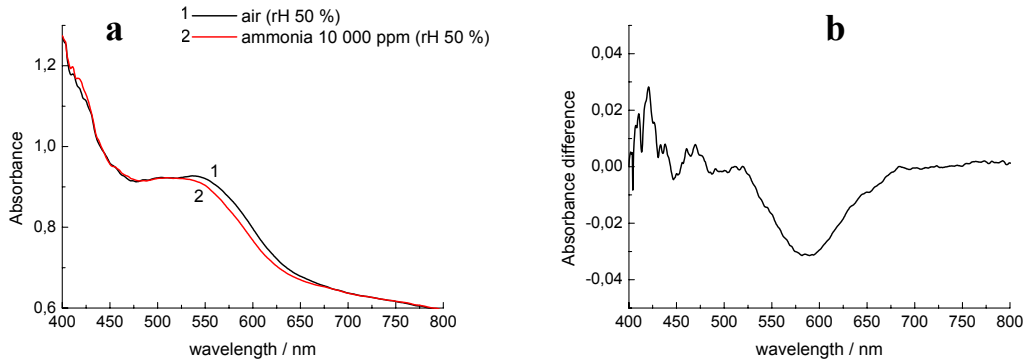

Figure C5: a, absorbance spectra of the bR film in the sol-gel matrix (mass ratio bR : sol-gel = 5.5 : 94.5) measured at 25 ^{o}C and rH 50%: black line 1, without ammonia; and red line 2, in an ammonia atmosphere with the concentration of 10 000 ppm; b, difference absorbance spectra (ammonia 10 000 ppm minus air).

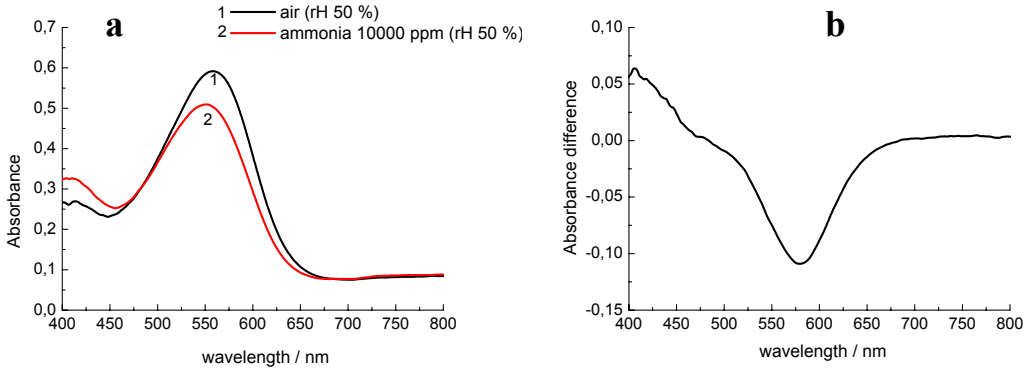

Figure C6: a, absorbance spectra of the bR film in the PVA matrix (mass ratio bR :PVA = 12.5 : 87.5) measured at 25 ^{o}C and rH 50%: black line 1, without ammonia; and red line 2, in an ammonia atmosphere with the concentration of 10 000 ppm; b, difference absorbance spectra (ammonia 10 000 ppm minus air).

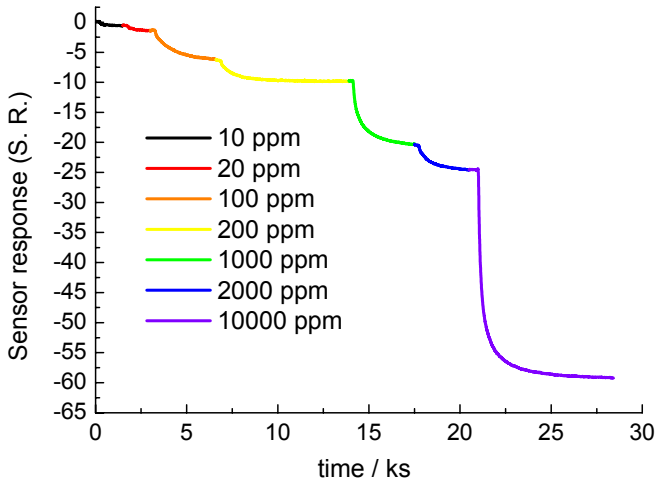

Figure C7: Response of the bR self-assembled film to increasing the concentration of ammonia from 10 to 10 000 ppm monitored at the wavelength 580 nm (measured at 25 ^{o}C and rH 50%). The measurements were done by filling the measurement chamber with the ammonia gas of the desired concentration balanced with nitrogen (for details see section 2.2.2).

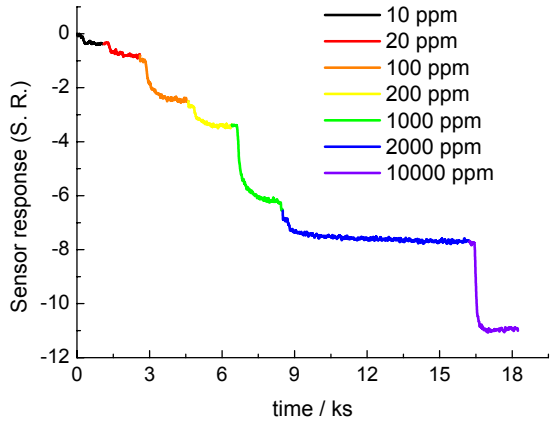

Figure C8: Response of the bR film in sol-gel silica matrix to increasing the concentration of ammonia from 10 to 10 000 ppm monitored at the wavelength 580 nm (mass ratio bR : sol-gel = 5.5 : 94.5 measured at 25 ^{o}C and rH 50%). The measurements were done by filling the measurement chamber with the ammonia gas of the desired concentration balanced with nitrogen (for details see section 2.2.2).

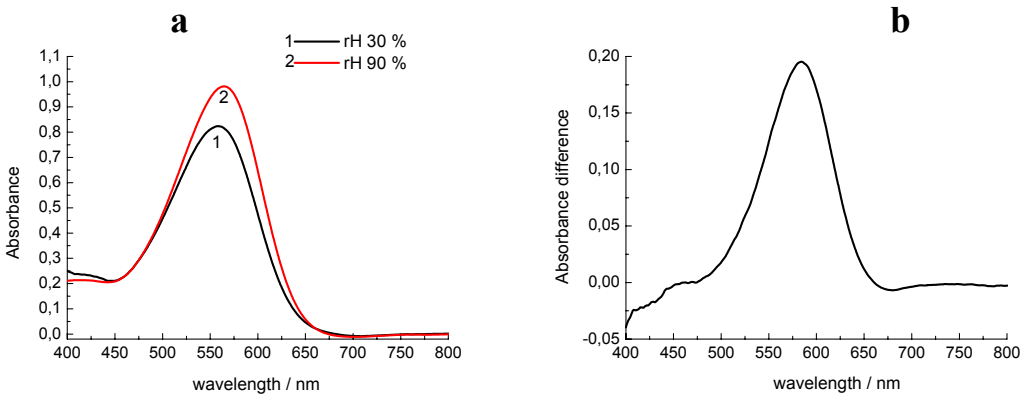

Figure C9: a, absorbance spectra of the bR self-assembled film measured at different relative humidities: black line 1, rH = 30%; and red line 2, rH = 90%; b, difference absorbance spectra (rH 90% minus rH 30%).

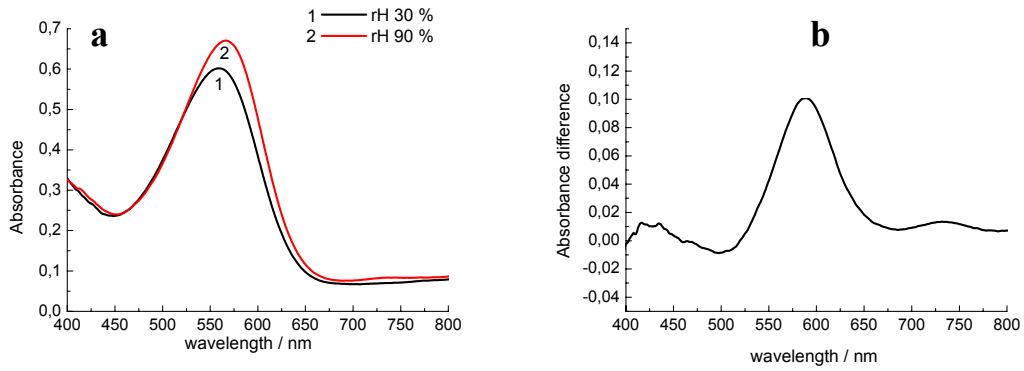

Figure C10: a, absorbance spectra of the bR film in PVA matrix (mass ratio bR : PVA = 12.5 : 87.5) measured at different relative humidities: black line 1, rH = 30%; and red line 2, rH = 90%; b, difference absorbance spectra (rH 90% minus rH 30%).

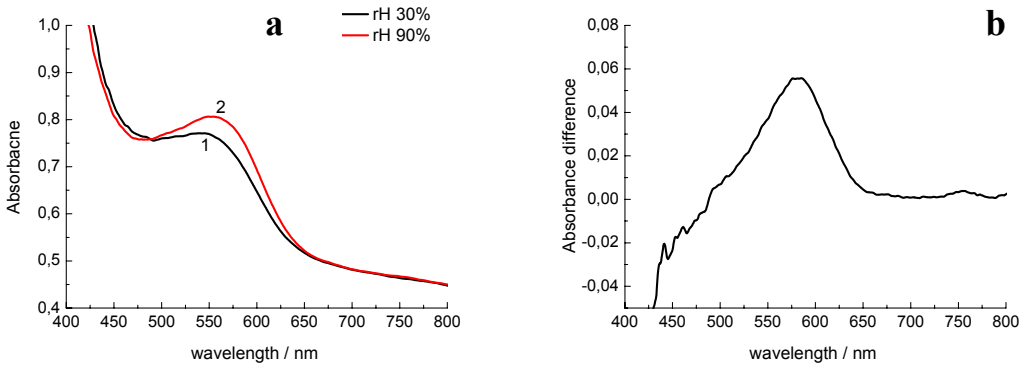

Figure C11: a, absorbance spectra of the bR film in sol-gel matrix (mass ratio bR : sol-gel = 5.5 : 94.5) measured at different relative humidities: black line 1, rH = 30%; and red line 2, rH = 90%; b, difference absorbance spectra (rH 90% minus rH 30%).

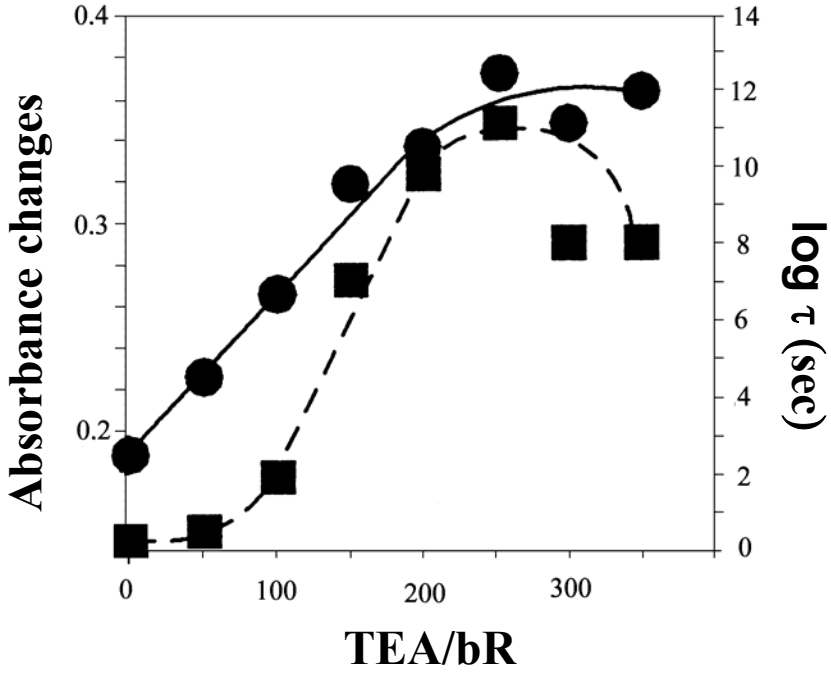

Figure C12: circles, absorbance changes and squares, half-life as a function of a TEA content in the bR film. TEA/bR ratio in the range of 0 up to 300 corresponds to the mass concentration of 0–18% in the dry bR film with GE matrix [154].

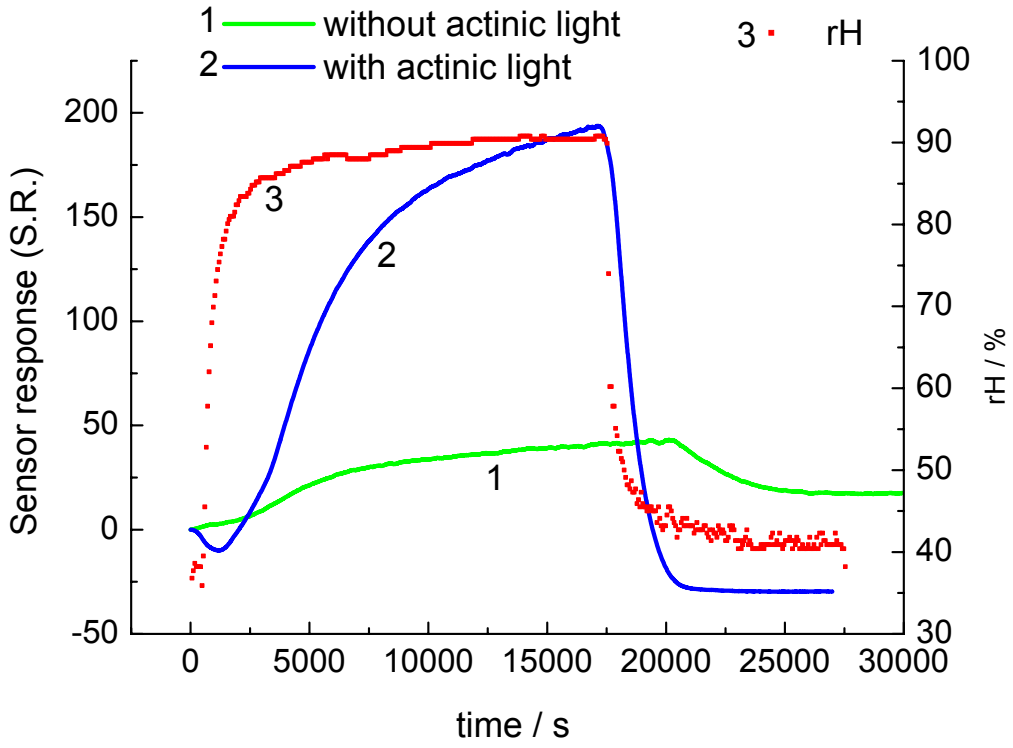

Figure C13: Time dependence of the sensor response (calculated using Equation 5.2, see Chapter 5) of the bR film in the GE matrix with added TEA (mass ratio bR : GE : TEA = 12.4 : 73.54 : 13.8 manufactured by formation method) to the relative humidity changes monitored at 570 nm; green line 1, without actinic light; blue line 2, with the presence of the actinic light (halogen light source with a high pass filter (> 530 nm) was used as an actinic light source); red line 3, shows the changes of the relative humidity measured using the humidity meter.

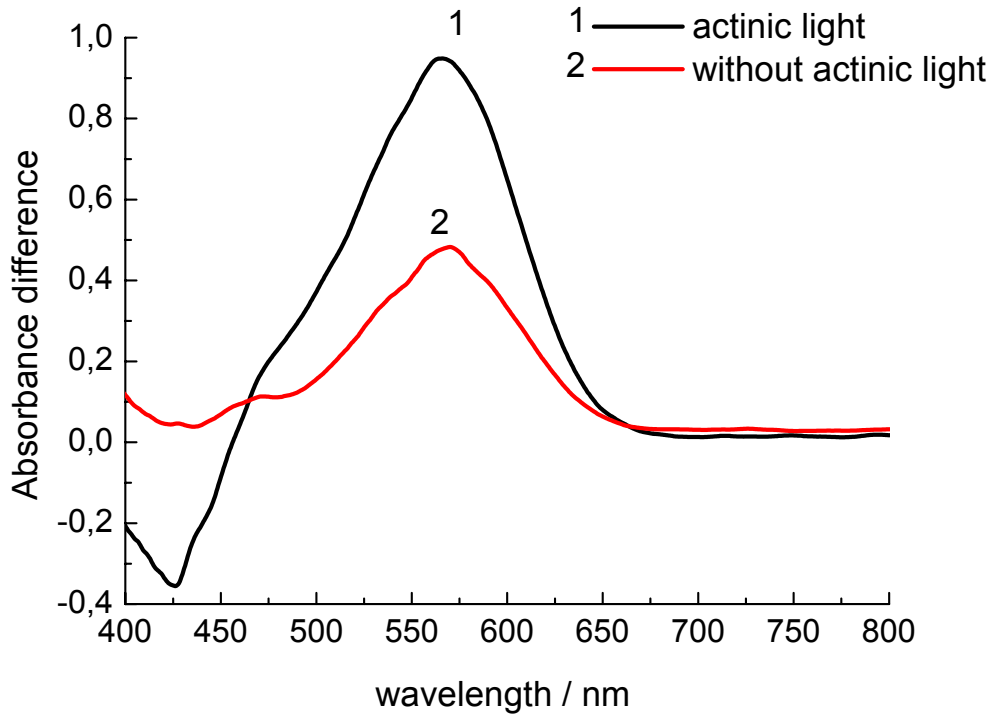

Figure C14: Difference absorbance spectra (high rH minus low rH) of the bR+GE+TEA (mass ratio bR : GE : TEA = 12.4 : 73.54 : 13.8); black line 1, with the presence of actinic light; red line 2, without actinic light source (halogen light source with a high pass filter (> 530 nm) was used as an actinic light source).

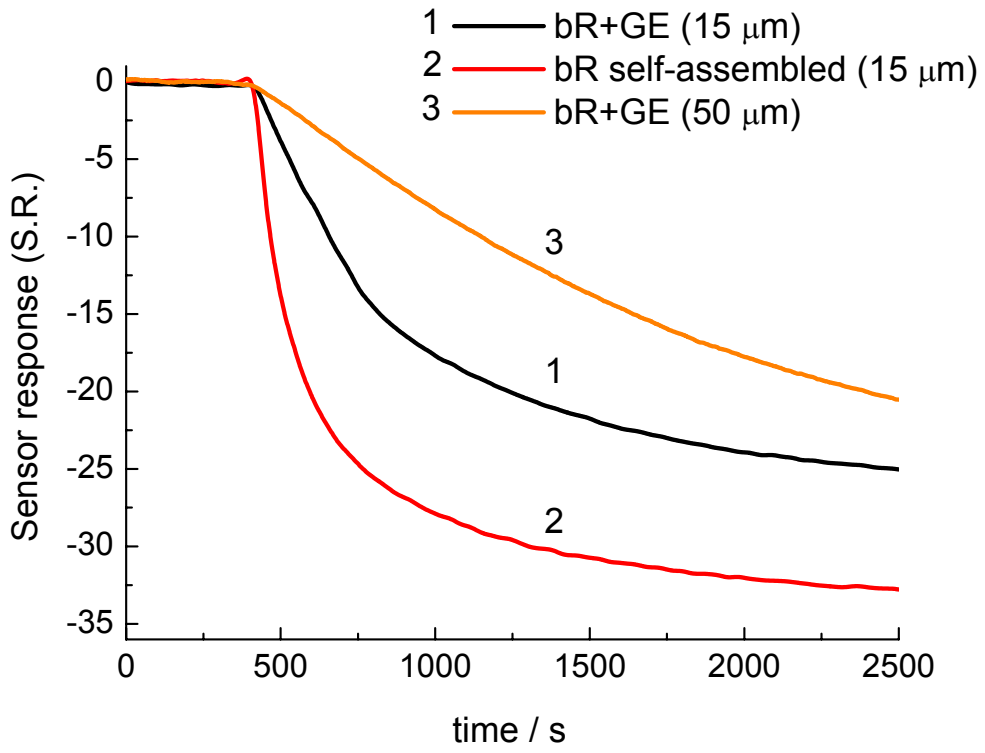

Figure C15: Comparison of the sensor response of the bR film in the GE matrix of the different thicknesses to the ammonia gas with the concentration of 10 000 ppm (measured at 25 ^{o}C and rH 50% by filling the measurement chamber with the ammonia gas of the desired concentration balanced with nitrogen, for details see section 2.2.2); black line 1, bR+GE of 15 μm thickness manufactured by casting method (see Chapter 3, section 3.1.3); red line 2, bR self-assemble film produced by casting method from the aqueous bR solution (14 mg/mL); orange line 3, bR+GE of 50 μm thickness manufactured by formation method (see Chapter 3, section 3.1.4).